

# **Aspects of Main Group Metal Amido and Carbene Chemistry**

**By**

**Aaron James Davies  
BSc. (Hons.) Cardiff**

**This thesis is presented for the degree of Doctor of Philosophy to the Faculty of  
Science, Cardiff University, October 2004.**

UMI Number: U202197

All rights reserved

INFORMATION TO ALL USERS

The quality of this reproduction is dependent upon the quality of the copy submitted.

In the unlikely event that the author did not send a complete manuscript and there are missing pages, these will be noted. Also, if material had to be removed, a note will indicate the deletion.



UMI U202197

Published by ProQuest LLC 2013. Copyright in the Dissertation held by the Author.  
Microform Edition © ProQuest LLC.

All rights reserved. This work is protected against  
unauthorized copying under Title 17, United States Code.



ProQuest LLC  
789 East Eisenhower Parkway  
P.O. Box 1346  
Ann Arbor, MI 48106-1346

## **Dedication**

**I would like to dedicate this thesis in memory of my grandfather Ron Pritchard, my uncle Howard Pritchard and my aunty Barbara Davies, who are sorely missed.**

## Acknowledgements

I would personally like to thank Cameron Jones for all his guidance, supervision and advice during this research and for providing me the opportunity to study in Australia.

I would also like to thank everyone in my lab and the whole inorganic section in Cardiff especially, Tom for all his banter, making time in the lab an enjoyable experience, Woff for his never ending patience and just being himself, Bob for his time in running the GCMS. Thanks also to Koffy boy, Markus, Anne, Marcus, Matt, Millsy Boy, Rosey and Krisna with whom I shared the lab with. Further thanks is due to Prof. Pete Edwards, Prof. Kingsley Cavell, Dr. Simon Aldrich, Dr. Angelo Amoroso, Dr. Ian Fallis, Sam, Julia, Bex, Adders, Woody, Eli, Ems, Stu, Rhi, Dennis, Hugo, the Tazzies, Coombsey, Andreas, Bres, Nat, Jonesy, Tom Tat, Cerys, Ruth, Dave, Si and Longy. Thanks also to Dr. David Willock and Rajinder Mann for running detailed space group calculations and providing us with graphical images, Dr. Nick Tomkinson for useful discussions involving curly arrows, Trish, John Bo, Robin, Gaz and the girls (Terri and Michelle). A big thanks to Rob Jenkins for all the instrumental and technical support particularly with the NMR and GCMS. Thanks to my flatmates Beanie, Bish, Oj, Readey boy and Bex for a tremendous six years together and the boys Hilly, Hughesy, Hugo, Bill, Iws, Brucey, Adders, Ga, Els, Cat, KathyB, Chez, Bell, Moxy, Dessie, Gump, Jonny Ear-ache and young Coxy. I would also like to thank Peter Junk for his supervision and hospitality during my studies in Monash University, Australia and extend my gratitude to everyone down under for making my time there such a memorable and enjoyable experience including Junky, Vicky, Matze, Kath, and Dave. Thanks also to Marcus for running my crystal structures on the XRD. Thanks to Prof. Glen Deacon and Prof. Keith Murray and their respective groups especially Jen, Cristina and Maureen to name just a few. A huge thanks to the Monash University RFC especially Macca, Laury, Cas, Sheds, Ene and the Queenslanders for playing such a big role in my time down under. Thanks to my Uncle Bob and Joan, Mark and Lisa and families for giving us an "Ozzie Crimbo".

A heart felt thank you to my parents Lynette and Malcolm, my sister Sarah-Jane and Richard for their unquestioning support and love, without you this thesis would not have been possible. Last, but certainly not least, thank you Bluebell for your devotion.



## Abstract

The work presented in this thesis describes the synthesis, structure and stability of a variety of novel main group amido and carbene complexes. We have also prepared a number of novel phosphino-carbene compounds. Chapter 1 provides an introduction to the elements of group 13 and *N*-heterocyclic carbene ligands before describing the complexation of group 13 metal halides and hydrides by *N*-heterocyclic carbenes in the formation of a series of novel complexes. Chapter 1 also highlights the reactivity of *N*-heterocyclic carbene ligands towards the phosphalkyne, PCBu<sup>t</sup>, with the synthesis of two novel phosphino-carbene compounds.

Chapter 2 provides a general introduction to C-C bond forming reactions promoted by group 13 metals, particularly indium and gallium. This chapter reports the results generated from the use of gallium(I) iodide to mediate a range of C-C bond forming reactions.

Chapter 3 details the use of the formamidine and formamidinate ligands *N,N'*-di(2,6-dimethylphenyl)formamidine (HFXyl), *N,N'*-di(2,6-diethylphenyl)formamidine (HFPhEt) and *N,N'*-di(2,6-diisopropylphenyl)formamidine (HDippForm) in the formation of group 1, 2 and 13 metal complexes. We also report the synthesis of a novel bimetallic group 1 formamidinate complex.

## Table of Contents

<b>Title</b>	<b>I</b>
<b>Declaration</b>	<b>II</b>
<b>Dedication</b>	<b>III</b>
<b>Acknowledgements</b>	<b>IV</b>
<b>Abstract</b>	<b>V</b>
<b>Table of Contents</b>	<b>VI</b>
<b>Abbreviations</b>	<b>IX</b>
<b>Notation</b>	<b>X</b>

## Chapter 1

### *N*-Heterocyclic Carbene Complexes of Group 13 Metal Halides and Hydrides

1.1	Introduction	1
1.1.1	<i>N</i> -Heterocyclic Carbenes	1
1.1.2	Preparation	7
1.1.3	Structure and Bonding	9
1.1.4	Reactivity and Application	19
1.1.5	Research Proposal	22
1.2	Results and Discussion	23
1.2.1	Group 13 Carbene Complexes	23
1.2.2	A Chiral Aluminium Trihydride Carbene Complex	29
1.2.3	Reaction of <i>N</i> -heterocyclic carbenes with a phosphalkyne	36
1.3	Conclusions	41
1.4	Experimental	42
1.4.1	Group 13 Carbene Complexes	42
1.4.2	Asymmetric Reductions	47
1.4.3	Phosphalkyne – Carbene Complexes	47
1.5	References	49

## **Chapter 2**

### **The Use of Gallium(I) Iodide in C–C Bond Forming Reactions**

2.1	Introduction	54
2.1.1	Indium Metal in C-C bond forming reactions	54
2.1.2	Indium(III) Halides in C-C bond forming reactions	60
2.1.3	Indium(I) Halides in C-C bond forming reactions	61
2.1.4	Gallium in C-C bond forming reactions	63
2.1.5	Research Proposal	68
2.2	Results and Discussion	69
2.2.1	Reformatsky Reactions with Gallium(I) iodide	69
2.2.2	Barbier-type Allylation	71
2.3	Conclusions	78
2.4	Future Work	78
2.5	Experimental	79
2.5.1	General Synthesis of Gallium(I) Iodide	79
2.5.2.1	General Reformatsky type reaction	79
2.5.3.1	General Aryl ring Allyl Coupling	81
2.6	References	85

## **Chapter 3**

### **Synthesis of s- and p-Block Formamidine Complexes**

3.1	Introduction	87
3.1.1	Group 1 Amides	87
3.1.2	Group 2 Amides	94
3.1.3	Group 13 Amides	97
3.1.4	Amidines	101
3.1.5	Group 1 Amidinates	104
3.1.6	Group 2 Amidinates	111
3.1.7	Group 13 Amidinates	114
3.1.8	Research Proposal	118
3.2	Results and Discussion	119

3.2.1	Lithium Formamidinate Complexes with oxygen donor solvents	119
3.2.2	Sodium Formamidinate Complexes with oxygen donor solvents	124
3.2.3	Potassium Formamidinate Complexes with oxygen donor solvents	133
3.2.4	Lithium Formamidinate Complexes with nitrogen donor solvents	139
3.2.5	Sodium Formamidinate Complexes with nitrogen donor solvents	148
3.2.6	Potassium Formamidinate Complexes with nitrogen donor solvents	153
3.2.7	Formation of a Bimetallic Formamidinate Complex	159
3.2.8	Synthesis of a Group 2 Formamidinate complex	162
3.2.9	Synthesis of Group 13 Formamidinate complexes	165
3.3	Conclusions	173
3.4	Experimental	174
3.4.1	Syntheses of Formamidine ligands	174
3.4.2	Synthesis of Lithium Formamidinate Complexes in DME	175
3.4.3	Synthesis of Sodium Formamidinate Complexes in DME	176
3.4.4	Synthesis of Potassium Formamidinate Complexes in DME and THF	177
3.4.5	Synthesis of Lithium Formamidinate Complexes in TMEDA	179
3.4.6	Synthesis of Lithium Formamidinate Complexes in PMDETA	180
3.4.7	Synthesis of Sodium Formamidinate Complexes in TMEDA	182
3.4.8	Synthesis of Sodium Formamidinate Complexes in PMDETA	183
3.4.9	Synthesis of Potassium Formamidinate Complexes in TMEDA	184
3.4.10	Synthesis of Potassium Formamidinate Complexes in PMEDA	185
3.4.11	Synthesis of a Bimetallic Potassium-Lithium Formamidinate Complexes in THF	187
3.4.12	Synthesis of a Magnesium Formamidinate Complexes in THF	187
3.4.13	Synthesis of Aluminium Formamidinate Complexes in THF	188
3.4.14	Synthesis of Indium Formamidinate and Formamidine Complexes in THF	189
3.5	References	191
<b>Appendix</b>	<b>Publications, Oral Presentations and Conference Papers</b>	<b>196</b>

## Abbreviations

Å	Angstrom, $1 \times 10^{-10}$ metres
APCI MS	Atmospheric Pressure Chemical Ionisation Mass Spectrometry
b.p	Boiling Point
br	Broad
Bu <sup>t</sup>	Tertiary Butyl
Calc.	Calculated value
cm <sup>-1</sup>	Wavenumber
cm <sup>3</sup>	Cubic centimetre
Cp	Cyclopentadiene
Cy	Cyclohexyl
δ	Chemical shift in NMR (ppm)
d	Doublet
DAB	<i>N,N'</i> -1,4-disubstituted diazabutadiene
decomp.	Decomposition Temperature
DippForm	<i>N,N'</i> -di(2,6-diisopropylphenyl)formamidinate
DME	1,2-Dimethoxyethane
Et{IBu <sup>t</sup> } <sub>2</sub>	1-ethyl di(3-butylimidazol-2-ylidene)
Et	Ethyl
FPhEt	<i>N,N'</i> -di(2,6-diethylphenyl)formamidinate
FXyl	<i>N,N'</i> -di(2,6-dimethylphenyl)formamidinate
GCMS	Gas Chromatography with Mass Spectrometry
HDippForm	<i>N,N'</i> -di(2,6-diisopropylphenyl)formamidine
HFPhEt	<i>N,N'</i> -di(2,6-diethylphenyl)formamidine
HFXyl	<i>N,N'</i> -di(2,6-dimethylphenyl)formamidine
Hz	Hertz
IBu <sup>t</sup>	1,3-di- <i>tert</i> -butylimidazol-2-ylidene
IDipp	1,3-bis(2,6-diisopropylphenyl)imidazol-2-ylidene
IMes	1,3-bis(2,4,6-trimethylphenyl)imidazol-2-ylidene
IPhe	1,3-bis(di( <i>R</i> )ethylphenyl)imidazol-2-ylidene
IR	Infrared
ITetMe	1,3,4,5-tetramethylimidazol-2-ylidene

$^nJ_{XY}$	Coupling constant between nuclei X and Y, over $n$ bonds, in Hz
J	Joule, $\text{kg m}^2 \text{s}^{-2}$
kJ	Kilojoule
$\text{kJ mol}^{-1}$	Kilojoule per mole
$\text{LiO}(2,6\text{-Pr}^i\text{Ph})$	Lithium-(2,4,6-trimethyl)phenolate
M	Molar, $\text{mol dm}^{-3}$
m	Medium
$\text{M}^+$	Molecular Ion
Me	Methyl
$m/z$	Mass/charge ratio
Mes	Mesityl (2,4,6-trimethylphenyl)
m.p	Melting Point
mult	Multiplet
NMR	Nuclear Magnetic Resonance
Ph	Phenyl
PMDETA	$N,N,N',N'',N'''$ -pentamethyldiethylenetriamine
Pr	Propyl
$\text{Pr}^i$	Isopropyl
ppm	Parts per million
R	General organic substituent
s	Singlet or strong
sh	Sharp
str	Strong
TetMeThione	1,3,4,5-tetramethylimidazol-2-thione
THF	Tetrahydrofuran
TMEDA	$N,N,N',N'$ -Tetramethylethane-1,2-diammine
t	Triplet
w	Weak
$\nu$	Frequency

#### Notation

))) Ultrasonic waves

## CHAPTER 1

### *N*-Heterocyclic Carbene Complexes of Group 13 Metal Halides and Hydrides

#### 1.1 Introduction

A carbene is an organic compound containing a carbon atom that is co-ordinated to two adjacent groups by covalent bonding while retaining two unshared electrons with no formal charge on the carbon. These unshared electrons can be assigned to two non-bonding orbitals in different ways to give anti-parallel spins (singlet state) or parallel spins (triplet state). Singlet carbenes are achieved from most carbene precursors as a result of spin conservation and can be regarded as electron deficient, similar to carbocations. However, retaining a pair of non-bonding electrons also makes them comparable to carbanions. This gives rise to both electrophilic and nucleophilic characters respectively, which are dictated by the adjacent group's electron withdrawing or electron donating nature to the carbene carbon. The less common triplet carbenes may be considered as diradicals, though the interaction between two unpaired electrons in orbitals of the same carbon transcends its own complications. These compounds originally regarded as "lab curiosities" by Skell<sup>1</sup>, who established much of their early chemistry, were introduced to inorganic and organometallic chemistry by Fischer<sup>2</sup> and co-workers.

##### 1.1.1 *N*-Heterocyclic Carbenes

*N*-Heterocyclic carbenes are compounds where the carbenic centre is stabilised by one or more adjacent electronegative nitrogen atoms in a five membered ring. These donor nitrogen centres force the originally degenerate orbitals on the carbenic carbon into an energy inequivalence, which enhances the nucleophilic behaviour of the carbon atom and increases thermodynamic stability. This stabilisation is effected by the inductive  $\sigma$ -electron withdrawal of electron density from the carbenic carbon and the delocalisation of electron density around the five-membered hetero-cyclic ring, which in-turn moderates the nucleophilicity of the carbene. The synergic electron donation (back bonding) by the N-centre p-orbital lone pairs and the unsaturated N=C=C-N system into the carbene out of plane p-orbital assists this stability, while moderating

the electrophilic reactivity of the carbene. It is these electronic factors that resulted in the formation of the first stable crystalline carbene, 1,3-di-1-adamantylimidazol-2-ylidene, and not the steric influences of the adamantyl groups as initially suggested<sup>3</sup>. These stable carbenes were first synthesised by deprotonation of the corresponding imidazolium chloride with potassium *tert*-butoxide. Although the Arduengo group takes credit for the formation of free, isolable *N*-heterocyclic carbenes<sup>3</sup>, it was work by Wanzlick<sup>4</sup> who recognised the potential amide groups, particularly imidazole rings had in stabilising the carbene centre. However, attempts to isolate these species were neglected. This pioneering research has led to the understanding of carbenes and the effects their substituents have in their reactivity and stability<sup>5, 6, 7</sup>, enabling their implementation into such areas as homogeneous catalysis<sup>8, 9</sup>.

#### 1.1.1.1 *N*-Heterocyclic Carbenes with Unsaturated C–C Backbones

Unsaturated *N*-heterocyclic carbenes have the largest singlet – triplet gap (approx. 85 kcal mol<sup>-1</sup>), outside of isocyanides and carbon monoxide, of any divalent carbon compounds<sup>10</sup>. This is achieved via the stabilising effects imposed by five-centre six-electron  $\pi$  delocalisation. These compounds refrain from dimerisation to form alkenes unlike their saturated analogues. Figure 1.1 displays some examples of these carbenes.

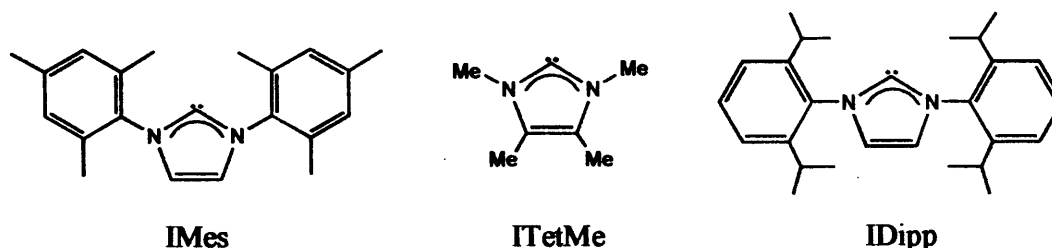


Figure 1.1 – Common *N*-heterocyclic carbenes with unsaturated C–C backbones

#### 1.1.1.2 *N*-Heterocyclic Carbenes with Saturated C–C Backbones

The singlet–triplet gap is reduced upon saturation of the C–C backbone bond providing no impetus for hyperconjugation, encouraging *N*-heterocyclic carbenes with saturated C–C backbones to dimerise. These dimers proved useful as electron rich olefins, used by Lappert *et al.* to prepare metal imidazolidine-carbene complexes<sup>6</sup>. Stable, crystalline *N*-heterocyclic carbenes with saturated C–C backbones were first



prepared by Arduengo in 1995 by the deprotonation of the corresponding cationic conjugate acid<sup>11</sup>.

#### 1.1.1.3 Triazole-Derived Carbenes

The first stable, crystalline triazole-derived carbene, 1,3,4-triphenyl-4,5-dihydro-1*H*-1,2,4-triazol-5-ylidene, was formed in 1995 via the elimination of methanol from the corresponding 5-methoxytriazole<sup>12</sup>. The N(1)-C(1) and N(3)-C(1) bond distances are shorter at 1.351(3) Å and 1.373(4) Å than typical N-C bond lengths<sup>13</sup>. This indicates the strong synergic backbonding via the filled 2p orbitals on both nitrogen atoms with the empty 2p orbital on the carbon, a result confirmed by *ab initio* calculations. Interestingly this is the first carbene to be commercially available (ACROS).

#### 1.1.1.4 Thiazole-Derived Carbenes

The first stable crystalline thiazole carbene, 2,3-dihydrothiazol-2-ylidene, was prepared by Arduengo via the deprotonation of the corresponding thiazolium chloride with potassium hydride in THF<sup>14</sup>.

#### 1.1.1.5 Multidentate Carbenes

The rigid geometry adopted by planar five-membered ring *N*-heterocyclic carbenes means that the number of atoms required to form an appropriate chelate ligand does not match that found with diphosphines or diamines. Methylene-bridged 2,3-dihydro-1*H*-imidazol-2-ylidenes form six membered rings upon metal chelation to transition metals giving bite angles of 78 – 79°. This is a replica of the bite angle generated from the chelation of a transition metal with 1,1'-bis(diphenylphosphino)methane, which yields a four-membered ring<sup>6</sup>. At rhodium centres, however, bis-carbenes have been reported to form dinuclear-bridging complexes<sup>15</sup>. This dinuclear-bridging mode is also favoured by ethylene-bridged bidentate carbenes due to the unfavourable eclipsing of hydrogen atoms experienced by the molecule upon chelation<sup>16</sup>. This preference was confirmed in the report of dinuclear main group metals aluminium, gallium and indium hydrides with bis-carbene 1,2-ethylene-3,3'-di-*tert*-butyl-diimidazole-2,2'-diylidene<sup>17</sup>. However, this ligand has also been reported by Green

and co-workers to form chelating bonding modes with some other main group metals<sup>18, 19</sup>. A stable tridentate free carbene, [1,3,5-{tris(3-tert-butyl-2,3-dihydro-1*H*-imidazol-2-ylidene)methyl}-2,4,6-trimethyl benzene] was isolated in 1994<sup>20</sup>. This molecule displayed no inter or intramolecular interactions between the carbene groups and has not yet been employed as a ligand.

#### 1.1.1.6 Functionalised Carbenes

Free *N*-heterocyclic carbenes with oxygen, nitrogen and diarylalkylphosphino donors in their side chains have been synthesised by the Herrmann group by deprotonating imidazolium salts in a mixture of liquid ammonia and aprotic polar solvents such as THF with mean 30 min reaction times at -40 °C<sup>21</sup>.

#### 1.1.1.7 Chiral Carbenes

In 1996 Herrmann and co-workers successfully synthesised a chiral carbene by deprotonation of the corresponding chiral imidazolium salt. The chiral imidazolium salt was formed from a reaction of the chiral primary amine with glyoxal and formaldehyde<sup>22</sup>. They were able to react this chiral carbene with a rhodium complex to afford a remarkably stable chiral carbene rhodium adduct with great potential in asymmetric synthesis. This potential was confirmed in its application to the hydrosilylation of acetophenone. The newly developed catalyst gave quantitative yields with an enantiomeric excess exceeding 30%<sup>22</sup>. This has serious implications in catalysis since the *N*-heterocyclic carbenes do not appear to dissociate from metal centres, particularly in the case of electron-rich metals such as rhodium and palladium, the catalytic activity of which is well established. This provides an advantage over phosphine ligands where an excess of ligand is required. Nolan and co-workers have been successful in the synthesis of numerous analogous chiral carbene-pentamethyl cyclopentadienyl (Cp\*) ruthenium chloride complexes. However, it is the work undertaken by the Roland group that has provided an alternative to chiral carbene synthesis in the formation of a chiral backbone carbene<sup>23</sup>. These molecules, however, are formed only *in situ* and can only be isolated by coordination to a silver halide. The failure to yield a stable free carbene of this variety is probably due to the loss of stability subjected by their saturated C-C backbones, an

unconditional requirement for the molecule to be chiral. These silver complexes, however, are potent transfer reagent and have been used successfully in the synthesis of palladium and gold complexes<sup>23</sup>. The methodology was reciprocated in early studies by Wang and Lin in 1998<sup>24</sup>, and McGuinness and Cavell in 2000<sup>25</sup>. Figure 1.2 display carbenes exhibiting Hermann and Roland-type optical activity.



Figure 1.2 – (i) Hermann-type chiral carbene; and (ii) Roland-type chiral carbene silver complex

#### 1.1.1.8 Non-classical/Wrong Way Carbenes

As recently as last year Crabtree *et al.* reported an interesting observation in the behaviour of certain carbenes with iridium. It was found that these carbenes were coordinated to the iridium centre through the carbon atoms constituting the backbone of the carbene and not the expected carbenic carbon. These findings are indeed unusual and stand as testament to the delocalisation of electron density in the carbene ring<sup>26</sup>. This non-classical bonding mode is favoured by sterically demanding systems, whereas normal carbene coordination is encouraged by carbenes with less sterically congested substituents. This methodology is demonstrated in figure 1.3<sup>26</sup>.

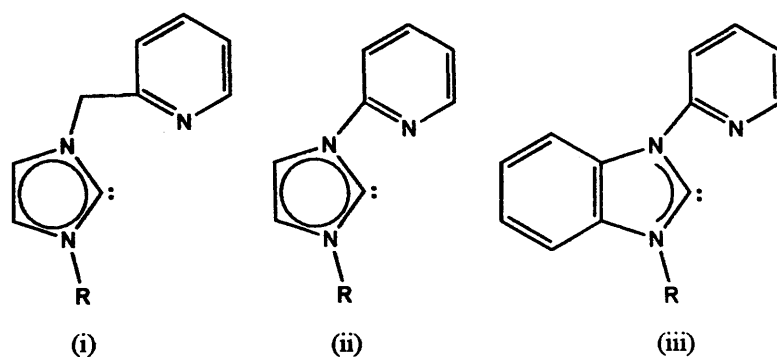


Figure 1.3 Carbenes with an affinity for non-classical Crabtree type bonding and conventional C2 type bonding

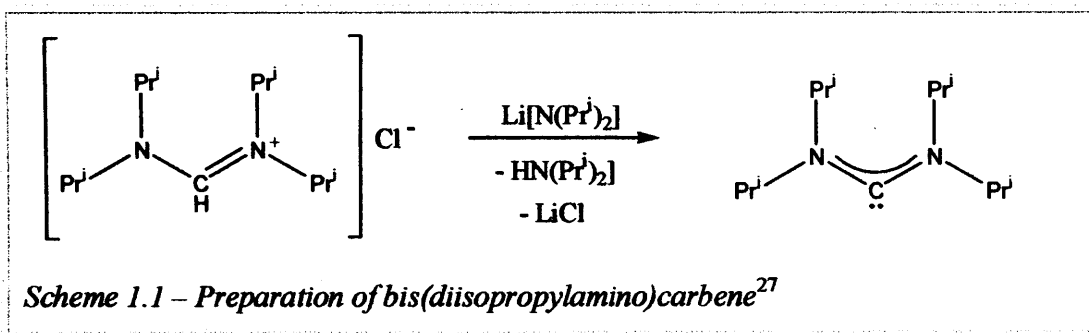
When the R group in (i) and (ii) (Figure 1.3) is large (R = mesityl, Pr<sup>i</sup> or *n*-Bu) reverse carbene ligation is preferred, however in the case where the R substituent is small (R = methyl), both isomers are observed. In carbenes of the type (iii), abnormal binding is impeded affording carbene coordination of the more traditional C2 variety (Figure 1.3)<sup>26</sup>. This conventional way of bonding is illustrated below (Figure 1.4) along with Crabtree's wrong way carbenes:



Figure 1.4 – (i) Conventional C2 bonding and (ii) Crabtree's non-classical carbenes

### 1.1.1.9 Acyclic Carbenes

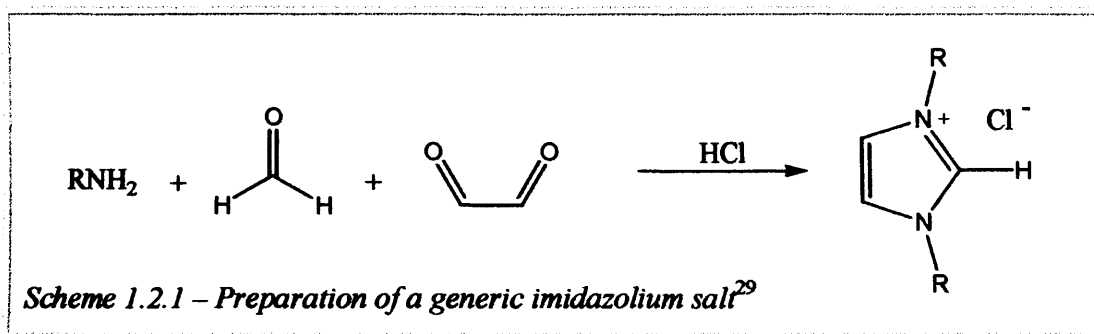
The first stable acyclic carbene was synthesised in 1996 by Alder and co-workers, who were able to prepare bis(diisopropylamino)carbene from the deprotonation of *N,N,N',N'*-tetraisopropylformamidinium chloride with lithium diisopropylamide (LDA) in THF (Scheme 1.1)<sup>27</sup>.



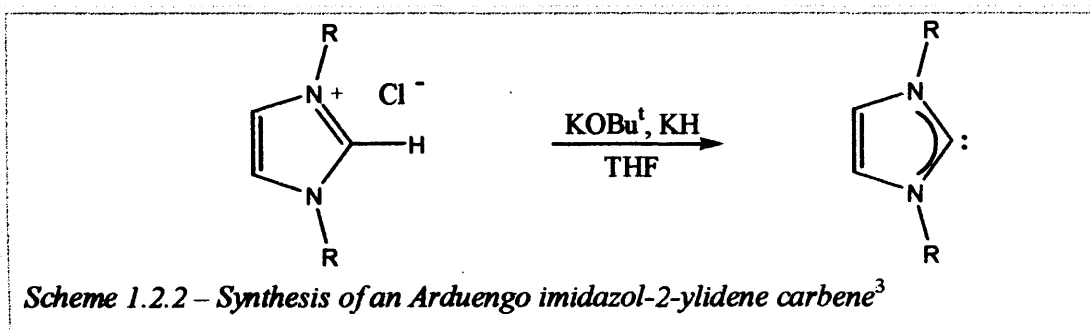
This compound's sensitivity to oxygen and moisture is an implication of the difficulties that arise when dealing with these molecules. It is also reason for their late appearance and chemical development. Importantly, the N-C-N angle (121.0°) is markedly larger than that of its cyclic analogues. The barrier to rotation around the N-C bonds also indicates the double-bond character imposed by the delocalisation of electrons, which is vital to the stability of this molecule<sup>27</sup>.

### 1.1.2 Preparation

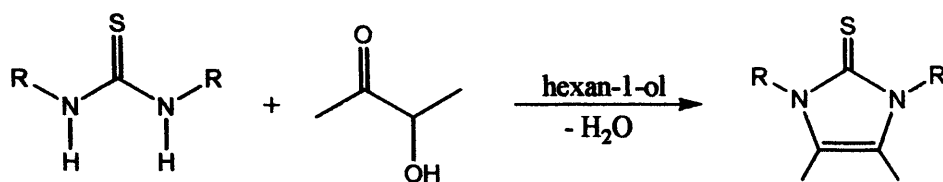
After the failure by Nef<sup>28</sup> to isolate methylene it was assumed that the isolation of carbenes was unlikely. Indeed this idea was believed for nearly a century, with many carbenes synthesised *in situ*, until Arduengo was able to isolate the first stable carbene in 1991<sup>3</sup>. The preparation of this carbene involves a stepwise process with the initial synthesis of the imidazolium salt (Scheme 1.2.1)<sup>29</sup>:



The imidazolium chloride is then deprotonated using catalytic amounts of potassium *tert*-butoxide in the presence of KH to yield the stable carbene (Scheme 1.2.2)<sup>3</sup>.

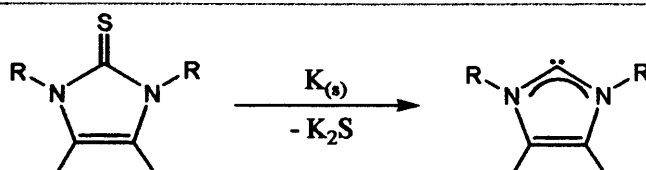


This is a popular, convenient method of forming stable carbenes that is general and has been exploited by Herrmann in the formation of an optically active carbene<sup>22</sup>. The success of this method and stability observed in the carbenes synthesised has encouraged other groups to determine alternative pathways to cyclic carbenes. Kuhn's synthesis of imidazol-2-ylidenes from imidazol-2-thiones<sup>30</sup> is an example of this. The imidazolium thiones are prepared by the condensation reaction of the corresponding thiourea with 3-hydroxy-2-butanone in boiling hexan-1-ol (Scheme 1.3.1)<sup>30</sup>.



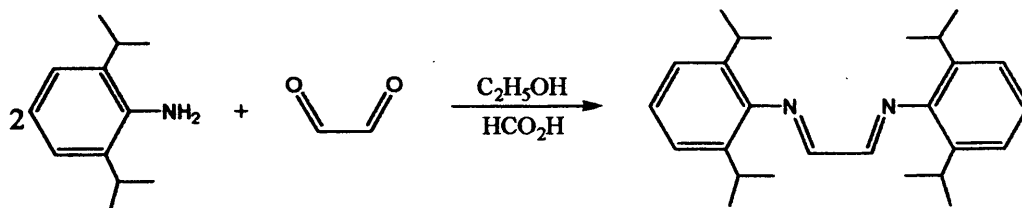
*Scheme 1.3.1 – Preparation of a imidazol-2-thione<sup>30</sup>*

The resulting imidazol-2-thione precursor is purified by crystallisation from diethyl ether/water and reduced with elemental potassium in THF under reflux (*Scheme 1.3.2*)<sup>30</sup>.



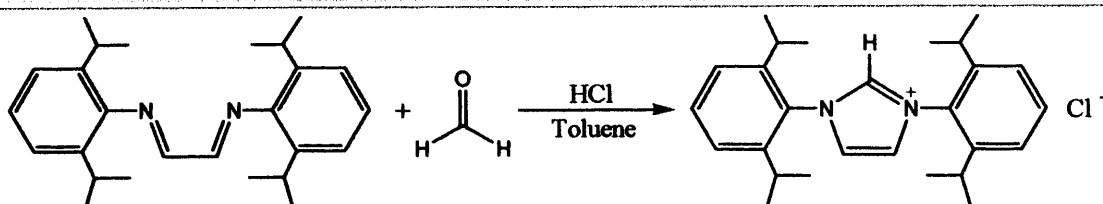
*Scheme 1.3.2 – Synthesis of a imidazol-2-ylidene<sup>30</sup>*

In 2000 Nolan and co-workers contributed to the synthesis of carbenes/imidazolium salts with an alternative route of formation<sup>31</sup>. This method involved the formation of a diazabutadiene (DAB) molecule from a reaction of a 2,6-diisopropyl substituted aniline with glyoxal in ethanol and a catalytic amount of formic acid (*Scheme 1.4.1*).



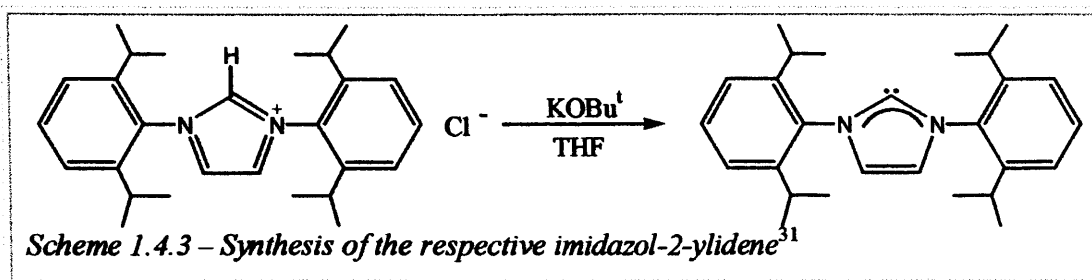
*Scheme 1.4.1 – Preparation of a Diazabutadiene (DAB) molecule<sup>31</sup>*

The imidazolium salt was then formed by the reaction of the DAB molecule with paraformaldehyde and HCl (*Scheme 1.4.2*)<sup>31</sup>:



*Scheme 1.4.2 – Preparation of the respective imidazolium salt<sup>31</sup>*

This can then be reduced, to the carbene using the route initially established by Arduengo<sup>3</sup>:



### 1.1.3 Structure and Bonding

*N*-heterocyclic carbenes are strong neutral Lewis base nucleophiles and hence are prime candidates for ligation in metal complexes. The first *N*-heterocyclic metal – carbene complexes were afforded from the corresponding imidazolium salts in reaction with metal complexes of sufficient basicity to deprotonate the organic substrate, as demonstrated by Öfele (Figure 1.5)<sup>32</sup>

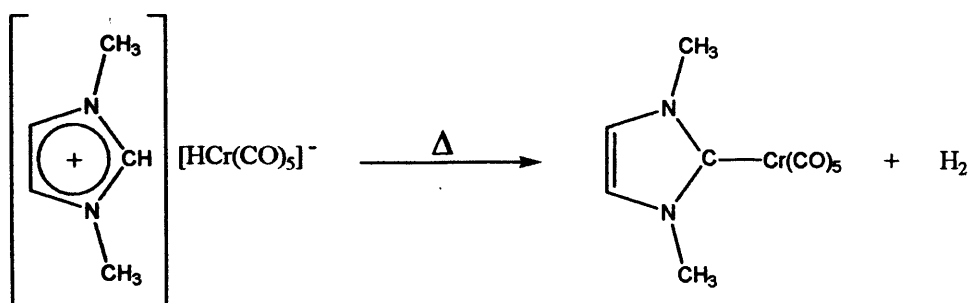


Figure 1.5 Reaction of *N,N'*dimethyl imidazolium with pentacarbonyl chrominate<sup>32</sup>.

Wanzlick *et al*<sup>33</sup> were able to form a related bis carbene mercury complex (Figure 1.6). This was a convenient way of forming the carbene *in situ*, since no attempt was made to isolate the free carbene.

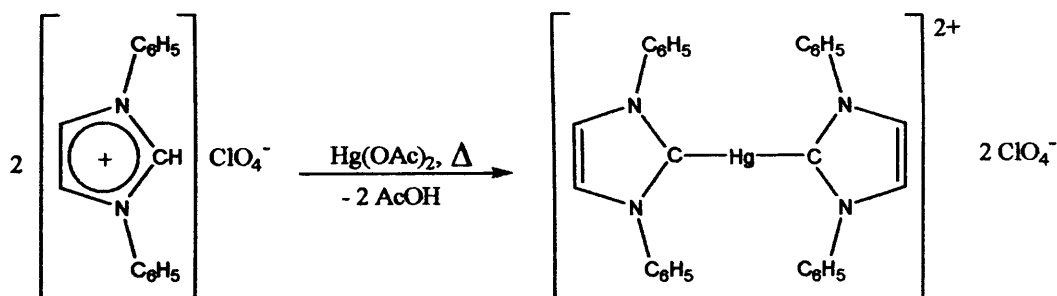


Figure 1.6 – Reaction of *N,N'* diphenyl imadazolium with mercury acetate<sup>33</sup>

Research by Arduengo<sup>3</sup> in 1991 has led to a renaissance in carbene chemistry with the formation of thermodynamically stable, “bottleable” reagents (*Scheme 1.2*). This encouraged the reports of related divalent germanium(II)<sup>34</sup> and silicon<sup>35</sup> congeners and more recently from within our group a gallium(I)<sup>36</sup> congener. More importantly there are similarities in ligand properties between the Arduengo type carbenes and electron rich phosphines, which has encouraged their study and application in catalysis chemistry<sup>37</sup>. Work by Wanzlick<sup>33</sup>, Öfele<sup>32</sup>, Fischer<sup>2</sup>, Doering<sup>38</sup> among others on *N*-heterocyclic carbenes has centred on their complexation to transition metals. Main group metal carbene complexes, however, have also been studied in some detail.

### 1.1.3.1 Group 1 Metal Carbenes Complexes

The carbene 1,3-di-*tert*-butylimidazol-2-ylidene (IBu<sup>t</sup>) was reacted with lithium-(2,4,6-trimethyl)phenolate to yield the dimeric di-nuclear lithium carbene adduct<sup>5</sup>.

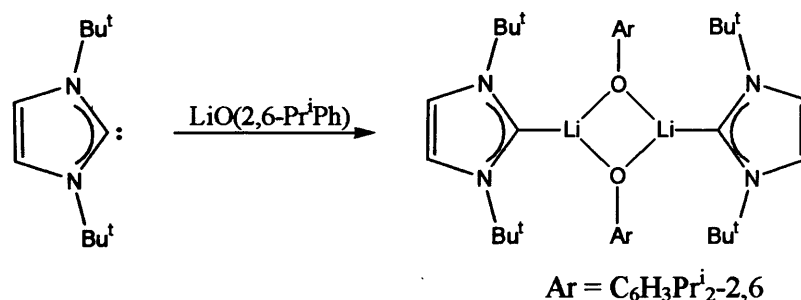


Figure 1.7 Reaction of IBu<sup>t</sup> with lithium-(2,4,6-trimethyl)phenolate<sup>5</sup>

The crystallographic analysis of this complex (Figure 1.7) reveals that the carbenic C-N bond lengths and angles approach those of the free carbene. This suggests a lack of covalence between the co-ordinated lithium metal and the carbene centre. This has been experienced in other related group 1 metal carbene adducts, for example in the bi-dentate carbene lithium dimer ( $n = 2$ )<sup>39</sup> and tetramer ( $n = 4$ )<sup>40</sup> complexes (Figure 1.8).

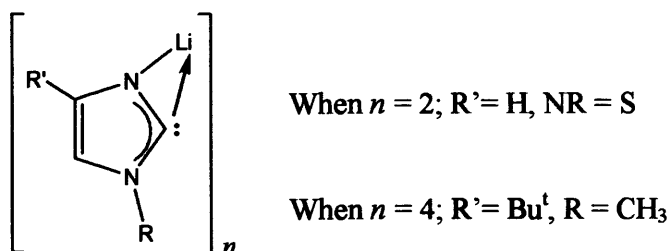


Figure 1.8 – Bi-dentate carbene lithium polymer/integer<sup>39, 40</sup>



These complexes form with co-ordination to the lithium centre from the nitrogen atom and carbenic carbon to afford the chelate complex. They provide evidence that metals incapable of back-bonding can happily co-ordinate to these *N*-heterocyclic carbenes, which function as nucleophilic two-electron donor ligands. This is because *N*-heterocyclic carbenes do not rely on back donation for stability due to the delocalisation of the nitrogen lone pairs into the carbenic p-orbital.

### 1.1.3.2 Group 2 Metal Carbene Complexes

The reaction with two equivalents of the dimethyl carbene,  $\text{CN}(\text{Me})\text{C}_2\text{H}_2\text{N}(\text{Me})$ , with  $\text{BeCl}_2$  afforded a neutral bis carbene beryllium dichloride complex displaying a distorted tetrahedral geometry around the metal. Similarly, a complex with a distorted tetrahedral geometry around the beryllium centre resulted from the treatment of  $\text{BeCl}_2$  with three equivalents of 1,3-dimethyl-2,3-dihydro-1H-imidazol-2-ylidene (Figure 1.9)<sup>41</sup>.

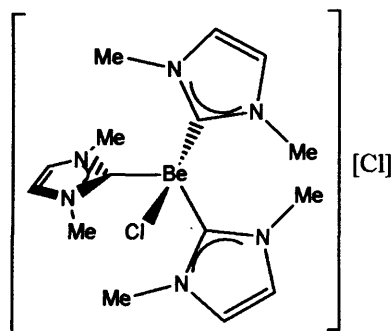


Figure 1.9 –  $\text{BeCl}((\text{CN}(\text{Me})\text{C}_2\text{H}_2\text{N}(\text{Me}))_3)^{41}$

In 1998 Arduengo reported the reactions of 1,2,4,5-tetramethylimidazol-2-ylidene, with the alkaline earth metal decamethyl metallocenes<sup>42</sup>. (Figure 1.10)

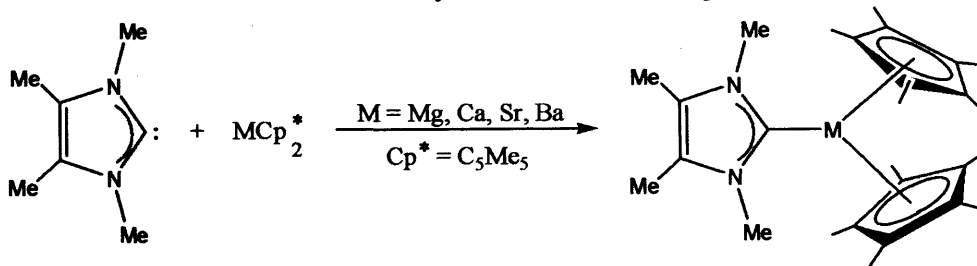


Figure 1.10 – Carbene-Metalloocene complex,  $\text{M}(\text{Cp}^*)_2(\text{ITetMe})^{42}$

All the carbene-metalloocene complexes retained full  $\eta^5$ -hapticity, exclusive of magnesium, which experienced a “slipped” geometry. This “slipped” geometry was

attributed to the smaller radius of magnesium compared to the other group 2 metals. The magnesium centre also experienced a greater degree of nucleophilic  $\sigma$ -donation from the carbene ligand to give a smaller Mg-carbenic carbon bond distance than is normal for magnesium alkyls. This was a trend observed through the entire series of group 2 metallocene-carbene adducts. However, the carbenic-metal bond length increased upon descent of the group. In the case of strontocene and bariocene a second equivalent of the carbene was added to form the bis-carbene adducted metallocene product<sup>42</sup>. This afforded complexes with distorted tetrahedral geometries around the strontium and barium centres (Figure 1.11)<sup>42</sup>.

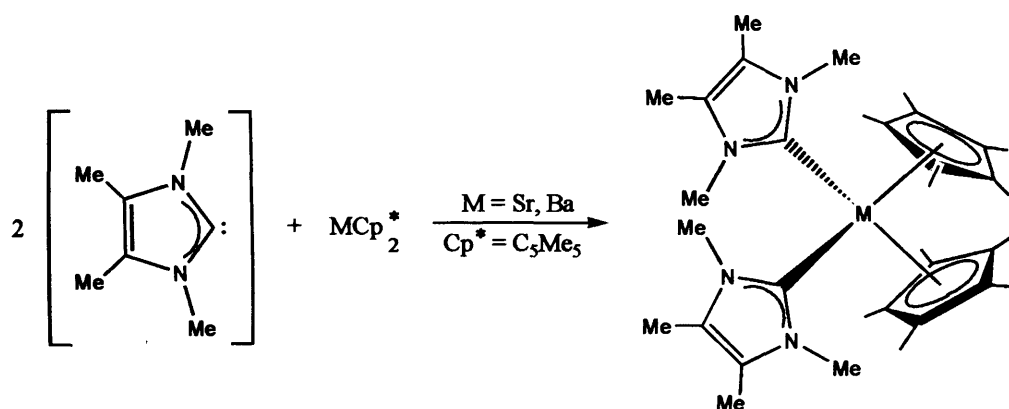


Figure 1.11 – Bis-carbene metallocene complex,  $M(Cp^*)_2(ITetMe)_2$ <sup>42</sup>

### 1.1.3.3 Group 13 Metal Carbene Complexes

In 1992 Arduengo reported the formation of the first group 13 metal adduct of a carbene, 1,3-bis(2,4,6-trimethylphenyl)imidazol-2-ylidene – aluminium trihydride<sup>43</sup>. This complex was afforded from the reaction of the free carbene with trihydro (trimethylamine) aluminium in toluene and displays a remarkable thermal robustness, melting only at temperatures greater than 246 °C, which is attributed to the nucleophilicity of the carbene ligand. The coordinated carbene ligand has a disrupted  $\pi$  delocalisation in the five membered hetero-atomic ring. This is evidenced by the upfield shift of the  $^{13}C$  NMR signal for the carbenoid carbon centre to 175.3 ppm from 219.7 ppm in the free carbene. This suggests that in the alane-carbene adduct the heterocycle bonding is intermediate between that observed in the free carbene and in the imidazolium salt (136 ppm). The work by Arduengo was then followed up with the formation of borane and fluoro-boron carbene adducts from the reactions of  $[BH_3(SMe_2)]$  and  $[BF_3(OEt_2)]$  respectively with carbenes.

Work from within our group<sup>44, 45, 46, 47</sup> and others<sup>48</sup> has led to the formation of some novel aluminium, gallium and indium trihalide, trihydride and trialkyl complexes. This work has yielded the first bis carbene-group 13 complexes ( $[\text{InCl}_3\{\text{CN}(\text{Pr}^i)\text{C}_2\text{Me}_2\text{N}(\text{Pr}^i)\}_2]$ ,  $[\text{InBr}_3\{\text{CN}(\text{Pr}^i)\text{C}_2\text{Me}_2\text{N}(\text{Pr}^i)\}_2]$ ) formed in the presence of excess carbene<sup>44, 46</sup>. Prior to this, only 1:1 group 13 carbene complexes had been reported, which is rather surprising considering the 1:2 and 1:3 group 2 carbene adducts already mentioned<sup>41, 42</sup>.

#### 1.1.3.4 Group 14 Metalloid Carbene Complexes

The reaction of *N*-heterocyclic carbenes with group 14 elements has yielded a broad assembly of silicon and tin halide/alkyl carbene complexes. A typical example of this is demonstrated with the reaction of 1,3-diethyl-4,5-dimethylimidazol-2-ylidene with trimethylsilyl iodide which affords a salt<sup>49</sup>. Interestingly, Kuhn was unable to reproduce these results in the analogous reaction with trimethylsilyl chloride (Figure 1.12).

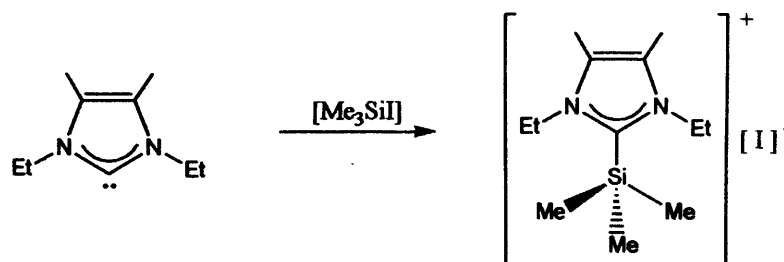


Figure 1.12 – Trimethylsilyl-1,3-diethyl-4,5-dimethylimidazol-2-ylidene<sup>49</sup>

The valence around the silicon and tin centres can be extended by the addition of a carbene to tetrachlorosilane or dialkyl dichloro silicon/tin complexes. This afforded the pentavalent group 14 carbene adduct species below, where  $\text{M} = \text{Si}$  or  $\text{Sn}$ . The formation of these complexes indicates the strong Lewis basicity of the imidazol-2-ylidenes (Figure 1.13)<sup>50</sup>.

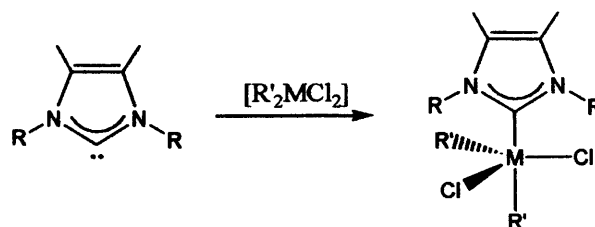


Figure 1.13 – Pentavalent group 14 carbene complexes<sup>50</sup>

Similarly, a low valent germanium(II) complex was formed in the reaction of germanium diiodide with a mesityl substituted carbene (Figure 1.14)<sup>51</sup>.

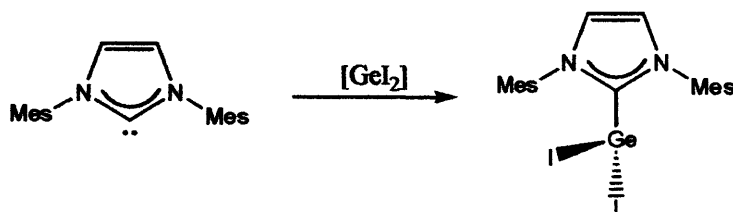


Figure 1.14 – Low valent germanium(II) iodide mesityl carbene<sup>51</sup>

### 1.1.3.5 Group 15 Metalloid Carbene Complexes

Group 15 element carbene adducts have been synthesised in the reactions of mesityl carbene with cyclopolyphosphines ( $[\text{PPh}]_5$ ,  $[\text{PCF}_3]_4$ ) and cyclopolyarsines ( $[\text{AsPh}]_6$ ,  $[\text{AsC}_6\text{F}_5]_4$ ). The degree of nucleophilicity of carbenes is again confirmed in these reactions with the carbene's ability to deoligomerise the phosphine and arsine species (Figure 1.15)<sup>52</sup>.

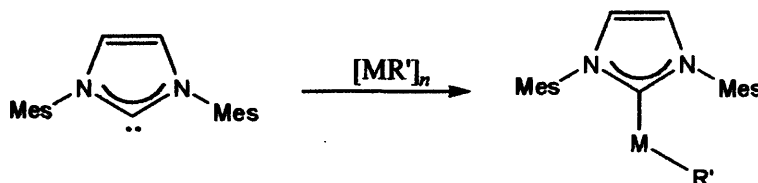


Figure 1.15 – Phosphine and arsine carbene complexes<sup>52</sup>

The reaction of 1,3-diisopropyl-4,5-dimethylimidazol-2-ylidene with chlorodiphenylphosphine afforded the analogous phosphinoimidazolium chloride salt. This complex was structurally characterised after the further addition of aluminium trichloride (Figure 1.16)<sup>53</sup>.

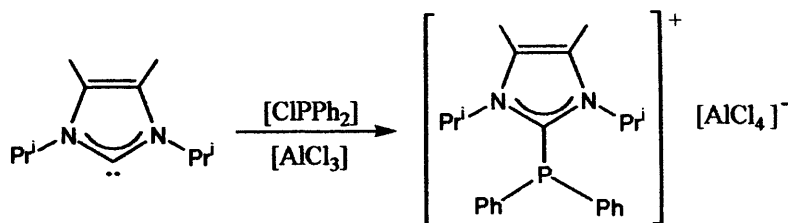


Figure 1.16 – Diphenyl-phosphinoimidazolium salt<sup>53</sup>

A report by the Nixon group illustrated the successful reaction of a triphospha benzene with tetramethyl carbene<sup>54</sup>. This reaction proceeds with extrusion of a C<sup>t</sup>Bu<sup>t</sup> fragment from the six membered aromatic ring to afford a five membered 1,2,4-triphosphole carbene complex. This contraction from a six membered ring to a five membered ring is dramatic in organic terms and is previously unheard of (Figure 1.17)<sup>54</sup>.

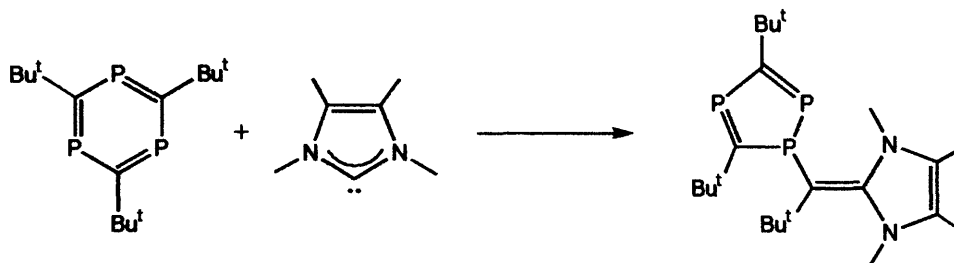


Figure 1.17 – Formation of a 1,2,4-triphosphole tetramethyl-carbene complex<sup>54</sup>

This structure was confirmed by addition of cycloheptatriene molybdenum tricarbonyl to afford the  $\eta^5$ -triphosphole-carbene ligated molybdenum tricarbonyl complex. Of special interest is the reversible nature of the triphospha benzene-(triphosphole-carbene) inter-conversion in treatment with  $[\text{PtCl}_2(\text{PMe}_3)_2]$  or  $[\text{PtCl}_2(\text{PMe}_2\text{Ph})_2]$  to regenerate the triphospha benzene ring and respective carbene-platinum complexes<sup>54</sup>. This work was followed up in an independent report by Hahn *et al* who described the reaction of phosphalkynes with *N*-heterocyclic carbenes to afford the identical and analogous compounds (Figure 1.18)<sup>55</sup>.

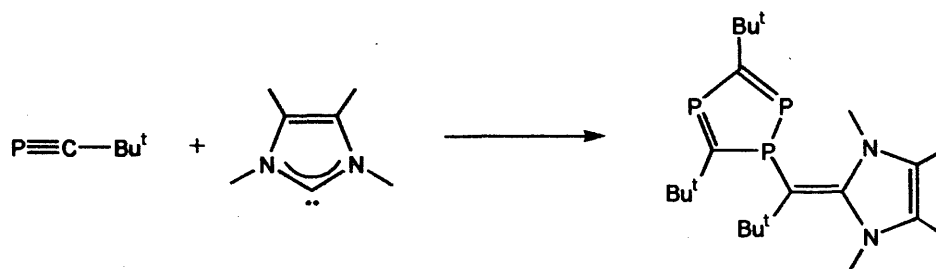


Figure 1.18 – Formation of a 2,4-triphosphole tetramethyl-carbene compound<sup>55</sup>

### 1.1.3.6 Group 16 Metalloid Carbene Complexes

Imidazol-2-ylidenes freely react with elemental sulphur, selenium and tellurium to afford stable chalcogenide adducts (Figure 1.19)<sup>56, 57, 58</sup>.

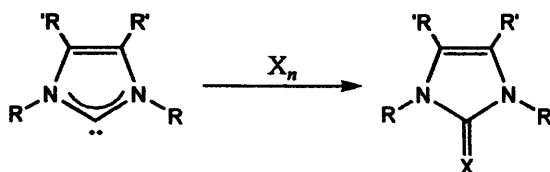


Figure 1.19 – Synthesis of chalcogenide-carbene complexes where  $X = S^{56}, Se^{57}, Te^{58}$

The crystallographic data for the tellurium complex, however, indicates a rather long  $C_{(ylide)}-Te$  double bond distance near to that of a single bond (2.0879(4) Å). This is due to the resonance structure formed whereby the  $\pi$ -electrons are localised on the tellurium atom to form an ionic (zwitter ion)  $C^+-Te^-$  single bond, which gives the complex its stability. A further illustration of the nucleophilic nature of the carbene was demonstrated by Kuhn *et al.* in the formation of sulphur dichloride and thionyl dichloride carbene adducts (Figure 1.20)<sup>59</sup>.

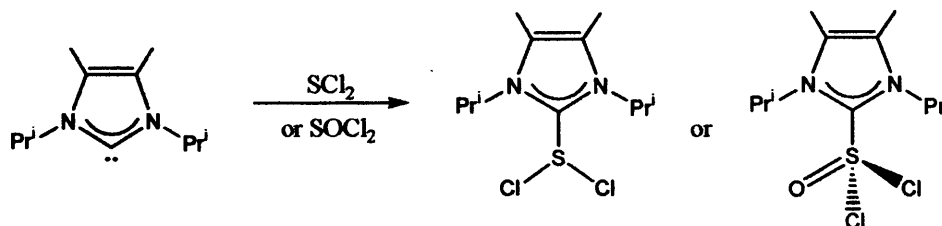


Figure 1.20 – Synthesis of Sulphur dichloride and thionyl dichloride carbene compounds respectively<sup>59</sup>

### 1.1.3.7 Group 17 Carbene Complexes

The first isolated diaminocarbene adduct of a halogen was afforded from the reaction of 1,3-diadamantylimidazol-2-ylidene with iodopentafluorobenzene existing in equilibrium with these starting reagents (Figure 1.21)<sup>60</sup>.

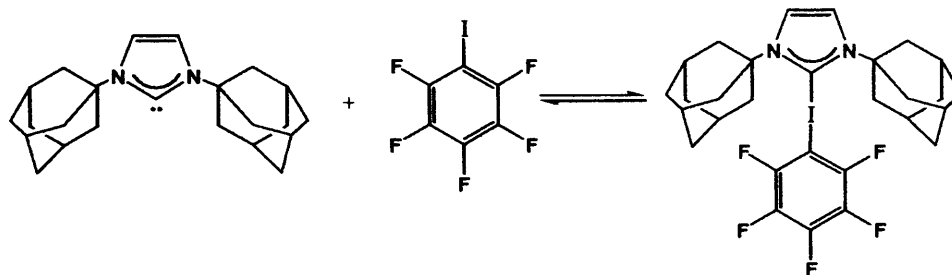


Figure 1.21 – Formation of the iodopentafluorobenzene-1,3-diadamantylimidazol-2-ylidene compound<sup>60</sup>

This complex features a near linear C–I–C angle ( $178.9(2)^\circ$ ) consistent with reverse ylide bonding<sup>61</sup>. NMR studies have also indicated that the  $\pi$ -delocalisation of the adducted carbene heterocycle is also enhanced by this reverse ylide bonding nature compared to the free carbene ligand<sup>60</sup>. In reaction with elemental iodide, however, the carbene acts as a basic  $\sigma$ -donor<sup>62</sup>. This was exemplified with the reaction of 1,3-diethyl-4,5-dimethylimidazol-2-ylidene and diiodine. The extended valence of the iodine molecule in this complex led to an increase in the I–I bond to 3.34 Å compared to 2.67 Å observed in the  $I_2$  molecule, with a I–I–C bond angle of  $176^\circ$  (Figure 1.22)<sup>62</sup>.

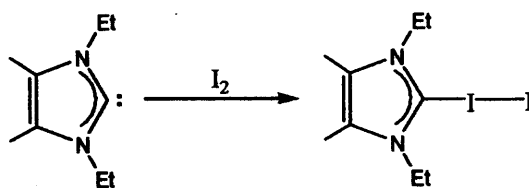
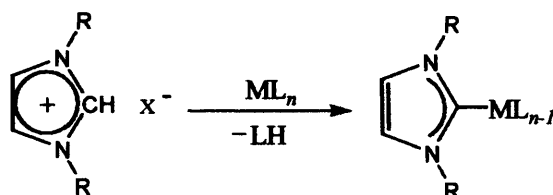


Figure 1.22 – Formation of a diiodo-diethyl-4,5-dimethylimidazolium compound<sup>62</sup>

### 1.1.3.8 Transition Metal Carbene Complexes

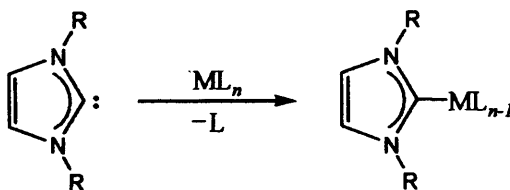
*N*-Heterocyclic carbene-transition metal complexes can be prepared via three main synthetic pathways.

1. The first route involves the *in situ* formation of the carbene by deprotonation of an imidazolium salt with a basic transition metal salt, as demonstrated by Ölefe<sup>32</sup> and Wanzlick<sup>33</sup>.



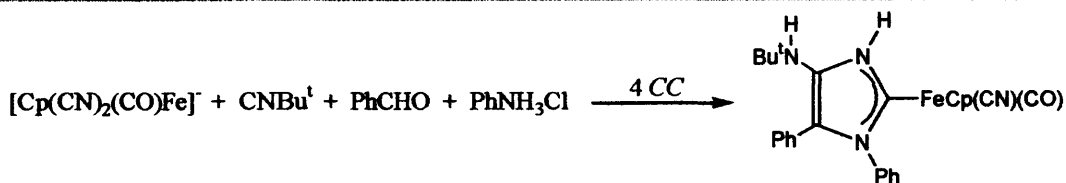
Scheme 1.5.1 – Deprotonation of an imidazolium salt with a basic transition metal salt to afford the transition metal carbene complex<sup>32, 33</sup>

2. The second method and possibly the most recent pathway to these transition metal-carbene complexes use the stable “Arduengo” type free carbenes. These nucleophilic ligands are reacted with a transition metal complex via nucleophilic substitution, replacing labile ligands coordinated to the transition metal centre<sup>3, 10</sup>.



Scheme 1.5.2 – Reaction of “Arduengo” type carbenes with transition metal complexes<sup>3, 10</sup>

3. The final synthetic pathway involves the transformation of existing ligands into the *N*-heterocyclic carbene at the metal centre. This can be done by successive treatment of hydrogen cyanide (generated from anionic metal-cyano precursors) with an aldehyde, isocyanide and an amine. This method was established by Fehlhhammer *et al.* and is referred to as the four-component condensation (4CC)<sup>63</sup>.



Scheme 1.5.3 – Fehlhhammer four-component condensation (4CC)<sup>63</sup>

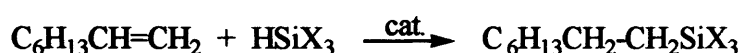


### 1.1.4 Reactivity and Applications

*N*-heterocyclic carbene complexes have the potential for implementation as catalysts in a number of organic reactions. This is due to the carbene's properties,  $\sigma$ -donating and poor  $\pi$ -accepting. This  $\sigma$ -donating character, which increases electron density at the metal centre, provides an alternative to the basic phosphine ligands. The cheap synthesis of the imidazolium salts and steric protection imposed in carbene complexes has increased their appeal for industrial applications.

#### 1.1.4.1 Hydrosilylation of Alkenes, Alkynes and Ketones

Rhodium-carbene complexes have been used in the selective anti-Markovnikov silane addition to unsaturated substrates in yields of up to 98%, which are considerably higher than those achieved by the analogous rhodium phosphine complex catalysed hydrosilations<sup>64</sup>.



#### 1.1.4.2 Hydrogenation of Olefins

Studies have revealed that mixed carbene-phosphine complexes with rhodium and ruthenium are the most active carbene catalysts in the hydrogenation of unsaturated compounds<sup>65</sup>. These complexes include  $[\text{RhCl}(\text{NHCarb})(\text{PPh}_3)_2]$  and  $[\text{RuCl}(\text{NHCarb})(\text{PPh}_3)_2]$ , which display notable stability under catalytic conditions. This is interesting as "hemi-labile co-ordination" is believed to be required in these processes (Figure 1.23)<sup>66</sup>.

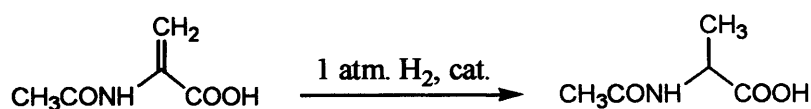


Figure 1.23 – A hydrogenation reaction catalysed by rhodium and ruthenium carbene complexes<sup>66</sup>

### 1.1.4.3 Heck Olefination

The application of palladium complexes in the catalysis of Heck type olefination is well-established<sup>37</sup>. New palladium carbene complexes such as  $[\text{PdCl}_2\{\text{CN}(\text{Me})\text{C}_2\text{H}_2\text{N}(\text{Me})\}_2]$  display potential with their oxygen, moisture, heat stability, and catalytic activity in reduction to  $\text{Pd}^0$  species (Figure 1.24). These attributes are important in the Heck process.

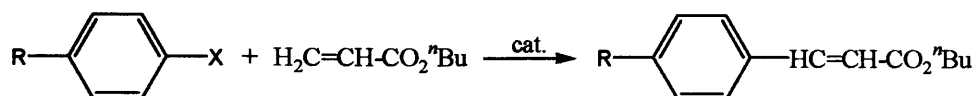


Figure 1.24 – A Palladium carbene catalysed Heck reaction<sup>37</sup>

### 1.1.4.4 Hydroformylation

The catalytic hydroformylation of unsaturated molecules is another example of a process benefiting from carbene complex chemistry. Rhodium and ruthenium complexes are well established in this area. Rhodium phosphine complexes are particularly well utilised in catalytic hydroformylation<sup>67</sup>, however these species commonly require the addition of excess phosphine ligand to the reaction mixture to avoid the decomposition of the complex under catalytic conditions<sup>6</sup>. Rhodium carbene complexes, however, can be used without excess ligand. This is an obvious advantage to implementing these catalysts over their phosphine analogues. Unfortunately, the higher electron density imposed on the metal centre by the carbene ligand, which is responsible for the greater complex stability, is also culpable for a reduced catalytic activity. Studies have revealed that mixed rhodium carbene-phosphine complexes are more effective in affording high yields and greater stability<sup>6</sup>.

#### 1.1.4.5 Ring Opening and Closing Metathesis

An increase in the ancillary phosphine ligand donor ability leads to increased catalytic activity in the Grubb's system. It is well established that carbene ligands can mimic these phosphine ligands and possess a stronger  $\sigma$ -donating character. Therefore the replacement of one tricyclohexyl phosphine (PCy<sub>3</sub>) group in this square pyramidal ruthenium catalysts with a carbene ligand leads to improved activity (Figure 1.25)<sup>5</sup>.

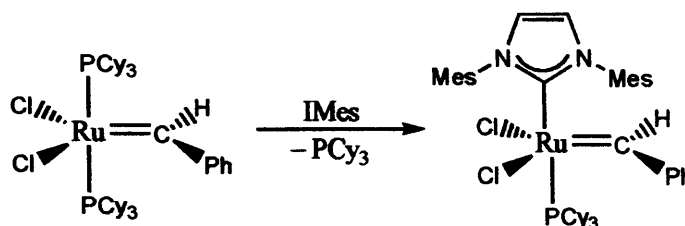
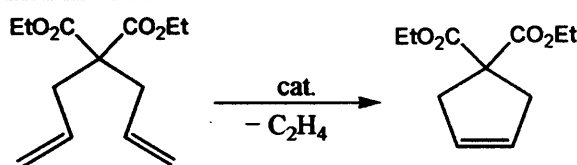


Figure 1.25 – A Ruthenium carbene phosphine complex<sup>5</sup>

The ring closing metathesis (RCM) catalytic activity of both catalysts was investigated with diethyldiallylmalonate (*Scheme 1.6*)<sup>5</sup>.



*Scheme 1.6 – Ring closing metathesis in diethyldiallylmalonate<sup>5</sup>*

Under identical conditions, the carbene containing catalyst afforded a 92% yield of the ring closed product after 25 mins. The original phosphine complex could only afford an 82% conversion yield in the same time. Furthermore, during this testing the remarkable stability of the carbene containing catalyst was observed, prompting a study into the robustness of the competing catalysts. This was done by recording the complexes thermal stability under inert atmosphere, monitored by <sup>1</sup>H and <sup>31</sup>P NMR. The phosphine complex decomposed after one hour. In comparison the carbene complex displayed no signs of decomposition after fourteen days<sup>5</sup>.

### 1.1.5 Research Proposal

The strong nucleophilicity of *N*-heterocyclic carbenes mean these ligands are capable of co-ordinating to electron poor main group metals, such as  $\text{Be}^{2+}$ , as they are to electron rich transition metals, such as  $\text{Pd}^0$ ,  $\text{Rh}^1$ . This has led to their co-ordination to elements in most groups of the periodic table. We were keen to extend this list of elements by coordination to heavy group 13 elements. Our initial interest in main group metal carbene chemistry, particularly group 13, was encouraged by the formation of a stable indium trihydride carbene complex<sup>47</sup>. It is even considered that these carbenes may stabilise the first thallium hydride species, although the possibility of preparing such a complex remains to be seen. However, there are as yet no thallium carbene complexes, an issue we were keen to address. In addition, we believe that there is potential for chiral carbene complexes in catalysis and we are eager to investigate this potential with the formation of an alane ( $\text{AlH}_3$ ), indane ( $\text{InH}_3$ ) or gallane ( $\text{GaH}_3$ ) chiral carbene reducing agents and an investigation of their utilization in organic synthesis. Moreover, we were interested in the reactions of carbenes with phosphalkynes in light of the reports of Nixon<sup>54</sup> and Hahn<sup>55</sup> on similar systems.

## 1.2 Results and Discussions

In light of the stable early group 13-carbene complexes formed from within our group, we were keen to extend the carbene ligation further down the group to include thallium, with the synthesis of the first thallium carbene complex. Thallium has a preference for the +1 oxidation state in its complexes, this means thallium(III) has a strong oxidising nature towards other molecules, actively scavenging their electrons to reduce the thallium to the preferred thallium(I) state. This has contributed to the paucity of thallium(III) complexes in the literature. Furthermore, there are no reported thallium trihalide phosphine complexes, which is important considering the analogies often drawn between “Arduengo” type carbenes and tertiary phosphines. The reason for the absence of any such thallium(III) halide phosphines complexes is due to the oxidation of the phosphine ligands by the thallium species when the two reagents are reacted<sup>68</sup>. Reactions with dialkylsulfides have echoed these findings. In spite of this, a handful of stable O- and N-donor thallium trihalide complexes have been synthesised<sup>69, 70</sup>. These successes and previous efforts from within our group are testament to the stabilising influence carbenes have within their respective complexes<sup>47</sup> and convinced us of the possibility of synthesising a stable thallium(III) halide-carbene adduct.

### 1.2.1 Group 13 Carbene Complexes

The treatment of a tetrahydrofuran solution of thallium trichloride with one equivalent of mesityl carbene IMes,  $\text{CN}(\text{Mes})\text{C}_2\text{H}_2\text{N}(\text{Mes})$ , afforded the first thallium halide-carbene complex in high yields after crystallisation from THF<sup>71</sup>. The crystal analysis of  $[\text{TlCl}_3(\text{IMes})]$  (1.1) confirms it as a monomer in the solid state with no significant intermolecular associations (Figure 1.26). The thallium centre occupies a distorted tetrahedral geometry (C(1)-Tl-Cl 112.7° average, Cl-Tl-Cl 106.1° average) with three near equivalent Tl-Cl bond distances of 2.419 Å average. In addition the Tl-C bond length is in the normal region for such interactions<sup>72</sup> at 2.179(9) Å. Furthermore, the geometry of the heterocycle is similar to that seen in the analogous complex  $[\text{InCl}_3(\text{IMes})]$ <sup>47</sup>, formed within our group and suggests a degree of delocalisation within the ring. Finally, a high degree of thermal stability was observed for this complex with decomposition, possibly to thallium(I) chloride, recorded at 208 °C.

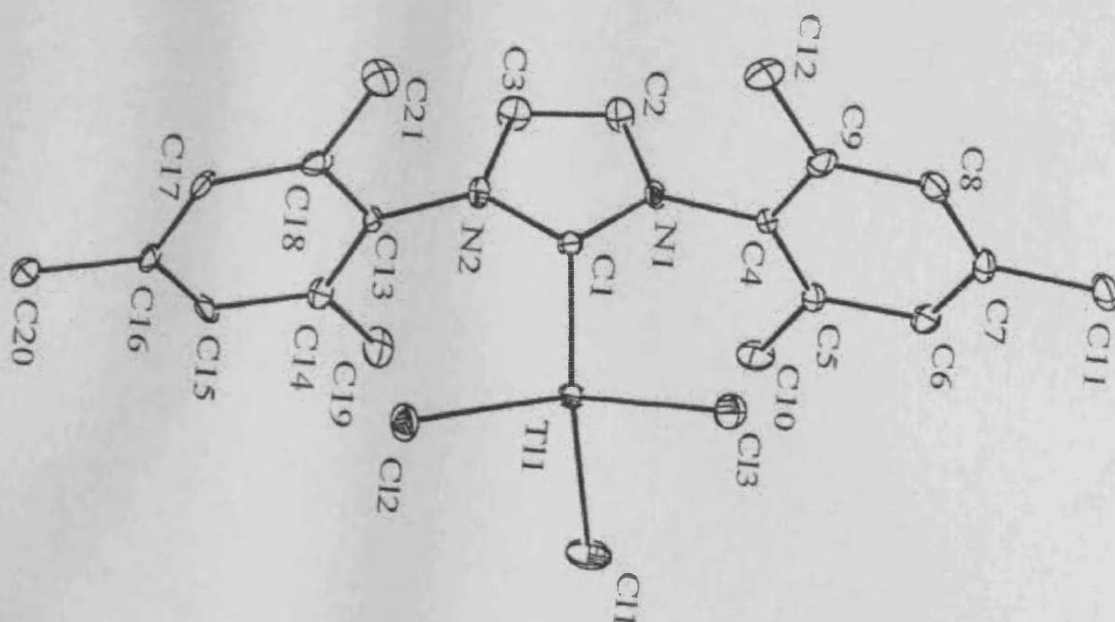


Figure 1.26 – Molecular Structure of  $[\text{TlCl}_3(\text{IMes})]$  (1.1)

Atoms	Distance	Atoms	Distance	Atoms	Distance
Tl(1)-C(1)	2.179(9)	Tl(1)-Cl(1)	2.423(3)	N(2)-C(1)	1.345(10)
Tl(1)-Cl(3)	2.416(2)	N(1)-C(1)	1.347(11)	N(2)-C(3)	1.400(10)
Tl(1)-Cl(2)	2.417(2)	N(1)-C(2)	1.359(13)	C(2)-C(3)	1.315(13)

Atoms	Angle	Atoms	Angle
C(1)-Tl(1)-Cl(3)	113.8(2)	Cl(2)-Tl(1)-Cl(1)	107.77(10)
C(1)-Tl(1)-Cl(2)	113.4(2)	N(2)-C(1)-N(1)	107.2(8)
C(1)-Tl(1)-Cl(1)	110.8(2)	N(2)-C(1)-Tl(1)	125.5(6)
Cl(3)-Tl(1)-Cl(2)	105.87(9)	N(1)-C(1)-Tl(1)	126.7(5)
Cl(3)-Tl(1)-Cl(1)	104.53(9)	C(3)-C(2)-N(1)	108.8(8)

Table 1.1 – Selected bond lengths (Å) and angles (°) for  $[\text{TlCl}_3(\text{IMes})]$  (1.1)

Previous endeavours within the group to successfully yield bis(carbene) adducts of  $\text{InCl}_3$  and  $\text{InBr}_3$  coupled with the existence of other 2:1 and even 3:1 donor adducts of thallium trihalide species encouraged us to attempt the synthesis of  $[\text{TlCl}_3(\text{IMes})_2]$  via the treatment of  $[\text{TlCl}_3(\text{IMes})]$  (1.1) with one equivalent of IMes in THF. Unfortunately this reaction did not proceed, presumably due to steric constraints associated with the proposed structure. With these restrictions in mind we set out to synthesise a less sterically demanding thallium trichloride adduct. Addition of  $:\text{CN}(\text{Me})\text{C}_2\text{Me}_2\text{N}(\text{Me})$ , (ITetMe), tetramethyl carbene, to thallium trichloride in THF resulted in the spectroscopically characterised thallium trichloride tetramethyl carbene adduct (1a) in moderate yields. Unfortunately, X-ray quality crystals of (1a) could not be grown but we propose a tetrahedral thallium geometry (Figure 1.26), as in (1.1).

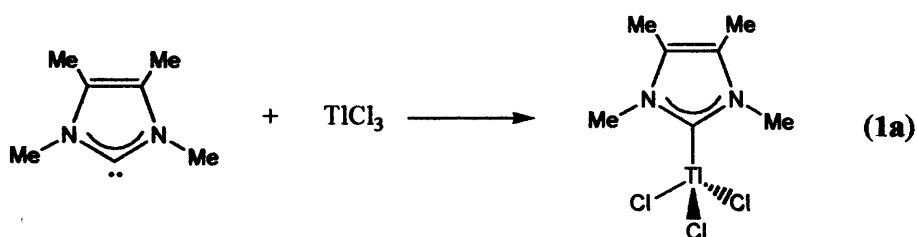


Figure 1.27 – Proposed Molecular Structure of  $\text{TlCl}_3(\text{ITetMe})$  (1a)

In an effort to generate a five-co-ordinate thallium complex, the reaction of two equivalents of ITetMe with thallium trichloride was attempted. Previous attempts within our group to yield such a species had proved fruitful; however no such complex has been crystallographically confirmed<sup>71</sup>. Spectroscopic analysis of the reaction product suggested that a five co-ordinate thallium centre was formed, but not the complex we were expecting. The mass spectroscopic and NMR data, and the CHN analysis did not coincide with the proposed biscarbene complex but the bis(thione) complex (Figure 1.28) (1b).

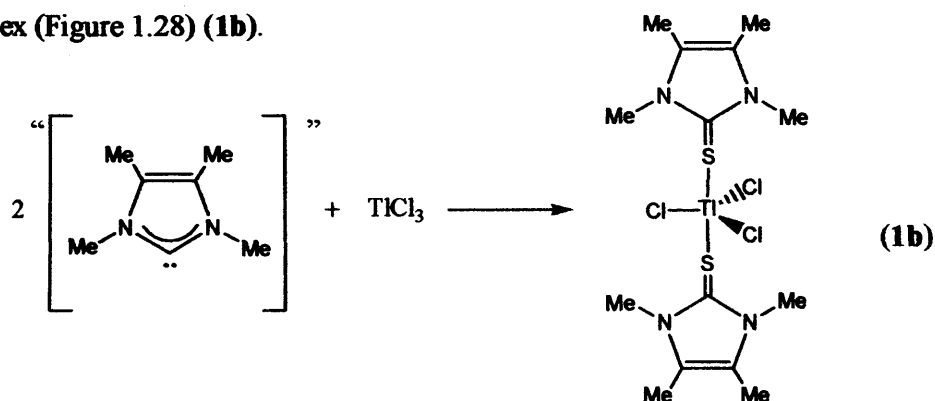


Figure 1.28 – Proposed Molecular Structure of  $\text{TlCl}_3(\text{TetMeThione})$  (1b)

The reasoning for the formation of this complex became apparent in closer inspection of the carbene reagent. NMR analysis of this starting material confirmed a 25% contamination of the free carbene with the thione precursor reagent. This thione precursor is used to form the carbene by reduction with potassium. Again we were unable to afford crystals of X-ray quality even with attempted layering experiments, however we assume the thallium to occupy the centre of a trigonal bipyramidal geometry with equatorial chloride atoms and axial thiones.

We were, however, able to successfully synthesise a thallium trichloride complex with a greater stability than that recorded for the  $[\text{TlCl}_3(\text{IMes})]$  (1.1) complex with the reaction of bis(2,6-diisopropylphenyl)imidazol-2-ylidene with thallium trichloride in THF (Figure 1.29) (1c).

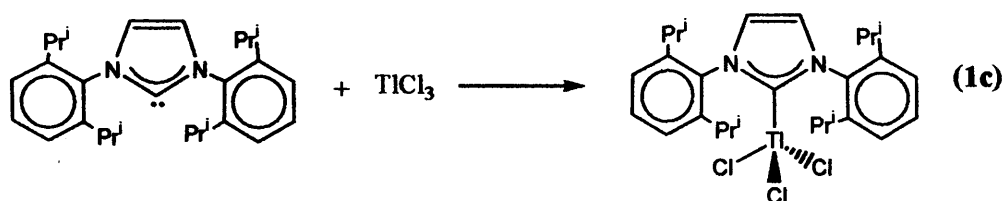


Figure 1.29 – Formation of  $\text{TlCl}_3(\text{IDipp})$  (1c)

This complex (1c) displays a remarkable thermal robustness decomposing at 226 °C compared to the decomposition temperature of  $[\text{TlCl}_3(\text{IMes})]$  (1.1) at 208 °C, which is unsurprising considering the extra steric bulk imposed on the complex by the carbene ligand. Again no crystals of X-ray quality were isolated, however we can confidently assume a tetrahedral geometry for the thallium centre.

It was expected that this bulky 2,6-diisopropylphenyl substituted carbene (IDipp) should stabilise the  $\text{InH}_3$  fragment to an even greater extent than IMes. However, the product  $[\text{InH}_3(\text{IDipp})]$  from the reaction of  $\text{LiInH}_4$  with IDipp was of disappointing thermal stability, slowly decomposing below -30 °C in solution and was thus impossible to fully characterise. We believe this decomposition is due to the close proximity of the isopropyl groups to the hydride ligands which effects metallation of the isopropyl substituents by the  $\text{InH}_3$  unit. This mechanism has been previously postulated for the decomposition of  $[\text{InH}_3\{\text{CN}(\text{Pr}^i)\text{C}_2\text{H}_2\text{N}(\text{Pr}^i)\}]$ <sup>46</sup>. In contrast, the 1:1 reaction of this carbene ligand with both  $\text{LiAlH}_4$  and  $\text{Me}_3\text{NAlH}_3$  in THF, afforded the



thermally stable carbene-alane complex  $[\text{AlH}_3(\text{IDipp})]$  (**1.2**) in high yields (Figure 1.30 and 1.31)<sup>73</sup>.

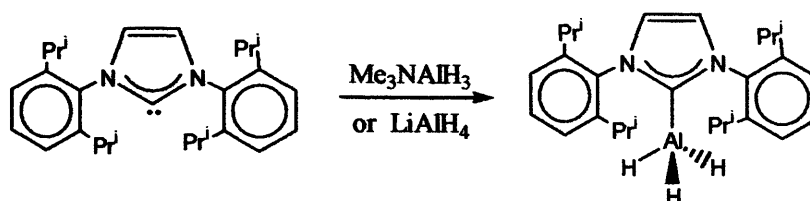


Figure 1.30 – Formation of  $[\text{AlH}_3(\text{IDipp})]$  (**1.2**)

The formation of this complex was indicated in the IR spectrum of crystals isolated from the reaction which displays a typically strong, broad Al-H stretch at  $1734.6\text{ cm}^{-1}$ . This is in the same region as other carbene adducts of alane, e.g.  $[\text{AlH}_3\{\text{CN}(\text{Pr}^i)\text{C}_2\text{H}_2\text{N}(\text{Pr}^i)\}]$   $\nu(\text{Al-H})\ 1730\text{ cm}^{-1}$ <sup>46</sup>. Crystals of X-ray quality were grown from THF. A crystal structure analysis of  $[\text{AlH}_3(\text{IDipp})]$  (**1.2**) confirms the formation of the complex with aluminium sitting at the centre of a distorted tetrahedral geometry (C(1)-Al-H  $105.4^\circ$  average, H-Al-H  $113.2^\circ$  average) with three near equivalent Al-H bond distances of  $1.53\text{ \AA}$  average. In addition the Al-C bond length of  $2.0566(13)\text{ \AA}$ , is in the normal region for such interactions. Furthermore, the geometry around the heterocycle is similar to that seen in the analogous  $[\text{InCl}_3(\text{IMes})]$ <sup>47</sup> and  $[\text{TlCl}_3(\text{IMes})]$  (**1.1**) complexes, indicative of a degree of delocalisation within the ring. The robustness of this complex is demonstrated by its thermal stability with the melting point recorded at  $229\text{--}239\text{ }^\circ\text{C}$  and the onset of decomposition observed at  $300\text{ }^\circ\text{C}$ .

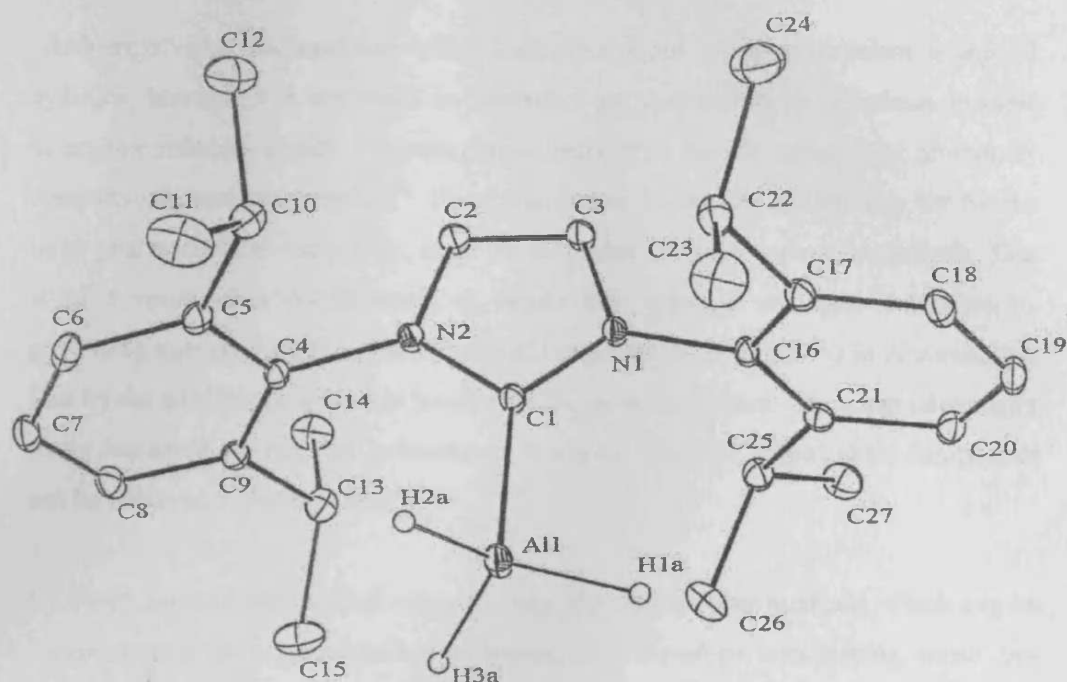


Figure 1.31 – Molecular Structure  $[\text{AlH}_3(\text{IDipp})]$  (1.2)

Atoms	Distance	Atoms	Distance	Atoms	Distance
Al(1)-H(1)	1.527(15)	Al(1)-C(1)	2.0556(13)	N(1)-C(16)	1.4488(14)
Al(1)-H(2)	1.546(17)	N(1)-C(1)	1.3562(15)	N(2)-C(4)	1.4474(15)
Al(1)-H(3)	1.510(17)	N(1)-C(2)	1.3567(15)	C(2)-C(3)	1.3417(18)

Atoms	Angle	Atoms	Angle
C(1)-Al(1)-H(1)	106.1(6)	H(2)-Al(1)-H(3)	114.3(9)
C(1)-Al(1)-H(2)	106.0(6)	N(2)-C(1)-N(1)	103.86(10)
C(1)-Al(1)-H(3)	104.6(6)	N(1)-C(1)-Al(1)	130.19(8)
H(1)-Al(1)-H(2)	111.1(9)	N(2)-C(1)-Al(1)	125.95(8)
H(1)-Al(1)-H(3)	113.9(9)	C(2)-C(3)-N(1)	106.88(10)

Table 1.2 – Selected bond lengths (Å) and angles (°) for  $[\text{AlH}_3(\text{IDipp})]$  (1.2)

### 1.2.2 A Chiral Aluminium Trihydride Carbene Complex

“Arduengo” type carbenes are often used within our group to stabilise group 13 hydrides, however it is important to remember the potential these complexes possess as organic reducing agents. The reducing selectivity of such complexes has previously been investigated successfully<sup>74</sup>. Recent emphasis in organic reductions, led by the large pharmaceutical companies, is on the formation of enantio-pure compounds. This is as a result of a combination of regulations enforced on these industries by governing agencies, such as the Food and Drugs Association (FDA) in America, but also by the advantages gained in producing the pure enantiomer. The main advantages being increased activity and reduction in waste by-products. Enantiopure compounds can be achieved via two methods:

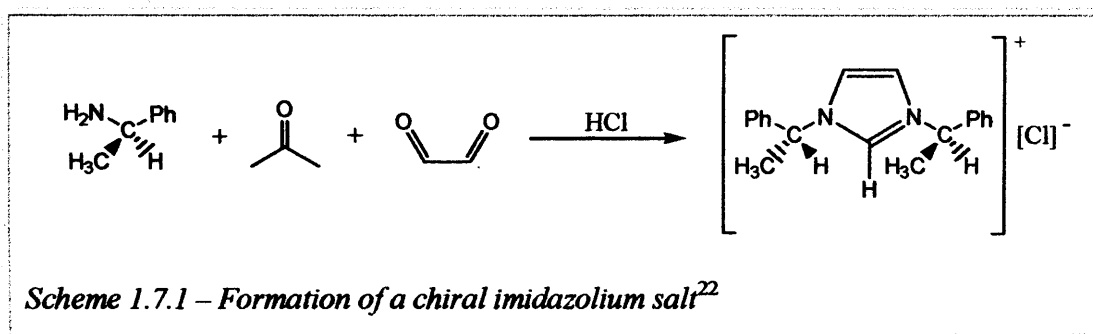
1. Purification of the racemic mixture using chromatographic methods, which can be considered as a post-reaction treatment, and therefore contributing waste by-products.
2. Introducing a stereo-selective reagent or catalyst at the critical pro-chiral stage of the process considered a pre-reaction treatment, reducing and in some cases even excluding waste by-products.

Obviously, both options have their own advantages with the most cost-effective route being chosen, which will depend on the expense of the stereo-selective reagent or catalysts and starting material. Extensive studies on chiral phosphines have led to their application in asymmetric homogeneous catalysis<sup>75</sup>, however these ligands have the failings of P-C bond degradation at elevated temperatures<sup>76, 77</sup>. Phosphine ligands also suffer from ligand dissociation from the metal centre in many catalytic operations, a problem previously discussed (see section 1.1.4.4 and 5). Nucleophilic carbenes have drawn comparisons with phosphine ligands to the extent that they are considered phosphine mimics in some instances. With this in mind we were intent on forming an asymmetric carbene-alane reducing agent. The formation of such a chiral carbene reducing reagent opens up a wide variety of exciting chemistry for us, which can be extended further by the introduction of more selective gallane and indane adducts. These would allow us not only enantio-selectivity but regio-selectivity and

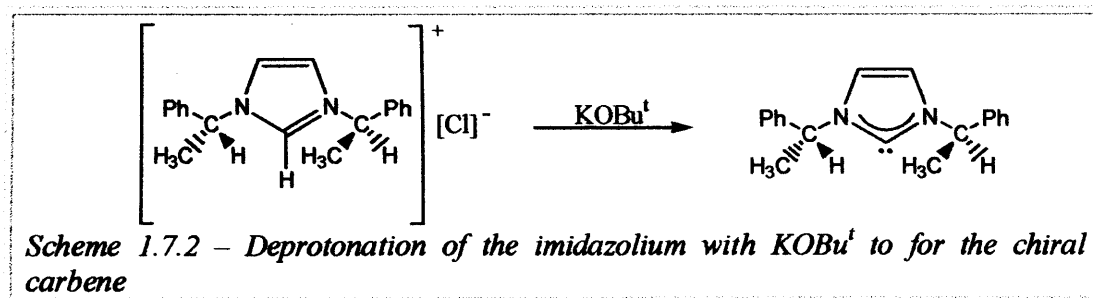
chemo-selectivity in the reduction of organic functionalities. The stability carbene-metal trihydride complexes have at higher temperatures and the fact that they experience no ligand-metal dissociation in their reactions offer advantages over their phosphine counterparts.

### 1.2.2.1 Synthesis of a Chiral Carbene

*N*-heterocyclic carbenes have been synthesised with chiral alkyl groups co-ordinated to the nitrogens<sup>22, 78</sup> and chiral backbone carbons<sup>23</sup>. However, we felt that to have any influence on the final product, it was necessary to have the chiral centre in close proximity to the alane group. This necessitated using a chiral alkyl group on the heterocycle carbene's nitrogen atoms. This was achieved by a slight modification to the literature method reported by Herrmann *et al.* This involved the formation of the chiral imidazolium salt precursor through a ring closure synthesis, which proceeds without racemization (Scheme 1.7.1)<sup>22</sup>.



We were then able to form the chiral carbene (IPhe) by deprotonation of the imidazolium salt with potassium *tert*-butoxide (Scheme 1.7.2).



### 1.2.2.2 Synthesis of a Chiral Carbene Alane Complex

A chiral carbene-alane adduct was afforded by reaction of the chiral carbene with lithium aluminium hydride or trimethyl amine alane (Figure 1.32).

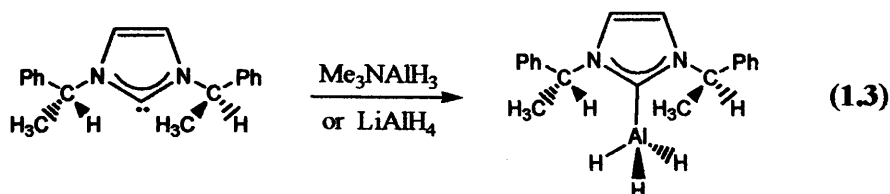


Figure 1.32 – Formation of a chiral carbene alane complex,  $[\text{AlH}_3(\text{IPhe})]$  (1.3)

Unfortunately due to the oily nature of the product (1.3) it was difficult to obtain any crystals for analysis. The analytical pure reagent was obtained by drying the filtered reaction mixture *in vacuo*. Computer modelling gave us an indication of the complex's structure and the possible influence on the complex by the chiral substituents, therefore possible restriction to rotation of the  $\text{AlH}_3$  caused by the phenyl groups of the chiral substituents. This was achieved by running a series of semi-empirical computer simulations and calculations. The first calculation involved rotating the  $\text{AlH}_3$  group on  $[\text{AlH}_3(\text{IPhe})]$  (1.3) to find the barrier to rotation of the  $\text{AlH}_3$  group. By plotting a graph of energies against angle of rotation Miss Rajinder Mann and Dr. David Willock of the computational section at Cardiff University were then able to deduce a transition state structure. This approximation of the transition state structure was good enough to place it into a more accurate and specific calculation to predict the actual transition state structure. The results from this calculation enabled the production of a profile of relative energy against rotation coordinate which helps to identify that a small barrier exists in trying to rotate the  $\text{AlH}_3$  group. Figure 1.33 displays this profile as the hydrogen atoms eclipse.

**Plot of the transition state region of the potential energy surface for  $\text{AlH}_3$  structure.**

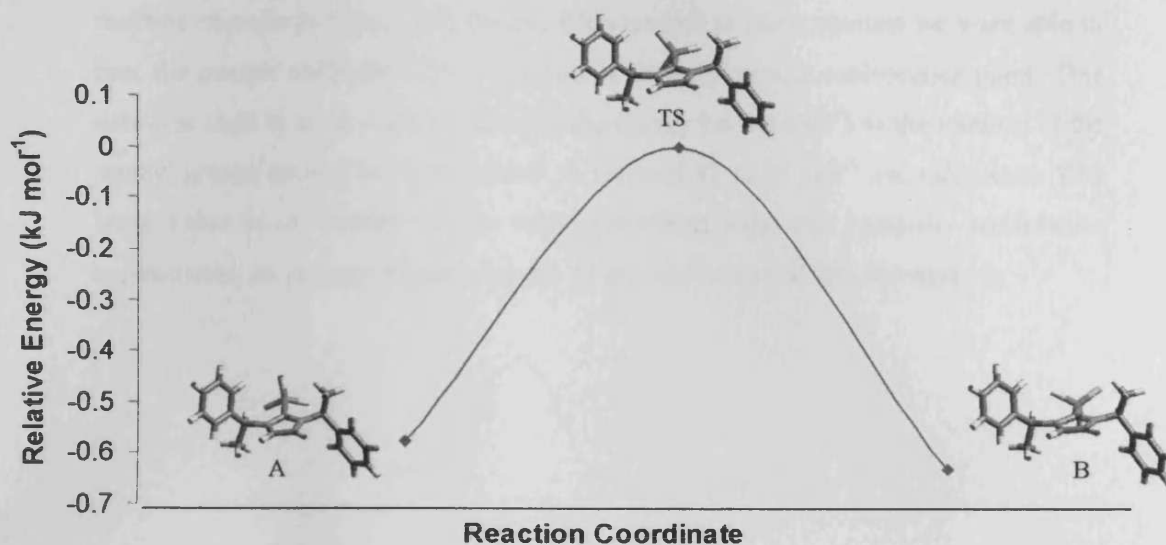


Figure 1.33 – Computer molecular modelling of  $[\text{AlH}_3(\text{IPhe})]$  (**1.3**) displaying a profile of relative energy versus rotation coordinate<sup>79</sup>

Such a profile illustrates that a small barrier, i.e. approximately  $0.6 \text{ kJ mol}^{-1}$ , to the rotation of the  $\text{AlH}_3$  group exists. To validate this transition state a frequency calculation was performed on the structure<sup>80</sup>. Thermochemical analysis of the transition state was also calculated by the frequency calculation and this was carried out at 298.15 K and 1 atmosphere of pressure, using the principal isotope for each element type.

This predicted barrier to rotation (although small) is generated by torsional strain of the type observed to a greater extent in ethane. There is a  $12 \text{ kJ mol}^{-1}$  barrier to internal rotation in this simple organic molecule from the staggered conformation (most stable) to the eclipsed conformation (least stable). This torsional strain is attributed to the slight repulsion between electron clouds in the carbon hydrogen bonds as they pass by each other in close proximity<sup>81</sup>.

From this computer model we were aware of an inequivalence between the two chiral substituents on the carbene due to the presence of the  $\text{AlH}_3$  unit with local 3-fold geometry. This was confirmed in the NMR data, which displayed two overlapping methine quartets at room temperature. With respect to these quartets we were able to heat the sample sufficiently in a solution of D8-toluene to a coalescence point. This data was used in an attempt to calculate the energy barrier ( $\Delta G^\ddagger$ ) to the rotation of the methyl groups around the chiral centre. A value of  $82.43 \text{ kJ mol}^{-1}$  was calculated. This large value is in contrast to the value calculated from the computer modulation experiments. At present we are unaware of the reason behind this discrepancy.

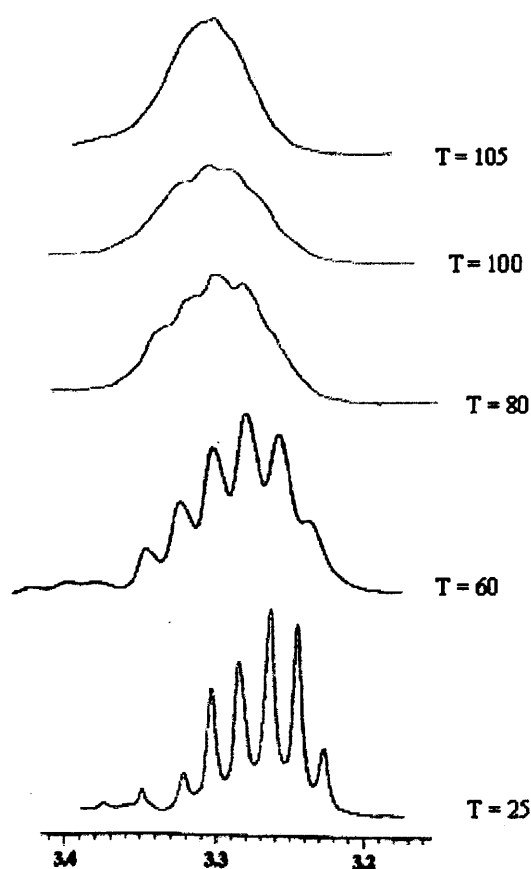


Figure 1.34 –  $^1\text{H}$  NMR of the two overlapping methine quartets in (1.3) at increasing temperatures to a coalescence at  $105^\circ\text{C}$

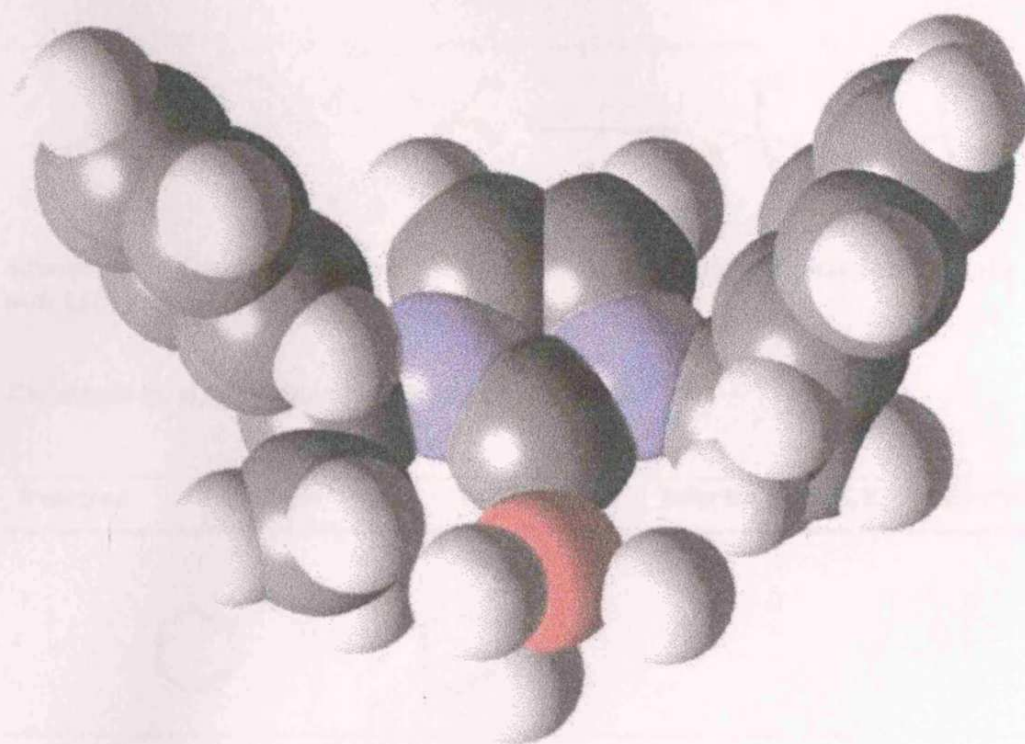
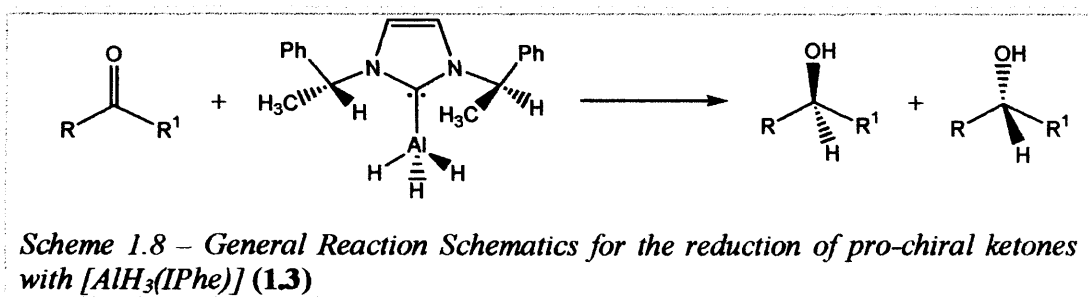


Figure 1.35 – Van der Waals space filling diagram for  $[\text{AlH}_3(\text{IPhe})]$  (**1.3**), generated by computer molecular modelling calculations. These van der Waals interactions predict an  $\text{Al-H}\cdots\text{H-CH}_2$  distance of 1.727 Å.



### 1.2.2.3 Asymmetric Reductions

Complex (1.3) was reacted with a range of pro-chiral reagents in order to see if any enantioselectivity would be induced in the reduction process (*Scheme 1.8*).



The results from this study are summarised in the table 1.3:

Reaction	Substrate	Products	Selectivity (%E.E)	Yield%
1			0	6
2			3	33
3			8	6
4			5	100

Table 1.3 – Reduction of organic compounds with [AlH<sub>3</sub>(IPhe)] (1.3)

As the results in table 1.3 indicate, there was very little enantio-selectivity in reactions involving the chiral carbene alane reducing agent. This reflects the small barrier to rotation hypothesised in the computer modulation ( $0.6 \text{ kJ mol}^{-1}$ ) affording relatively free rotation of the  $\text{AlH}_3$  and N-substituents and the fact that the latter are too distant from the reduction site to have a significant effect on selectivity. Furthermore, with the exception of the aliphatic ketone, the actual conversion rates (yields) were also very low. We believe this reflects the restrictions imposed on the reducing site of the complex by the bulky chiral alkyl groups. This factor in combination with the bulky alkyl groups on the ketones contributed to the poor yields.

### 1.2.3 Reaction of *N*-Heterocyclic Carbenes with a Phosphaalkyne

In a recent publication, Hahn *et al.* reported the results of the reaction of *N*-heterocyclic carbenes with phosphaalkynes to afford triphosphole compounds. For instance, treatment of *N,N'*-bis(2,2-dimethylpropyl)benzimidazolin-2-ylidene with *tert*-butylphosphaacetylene yielded the triphosphole derivative (Figure 1.36)<sup>82</sup>.

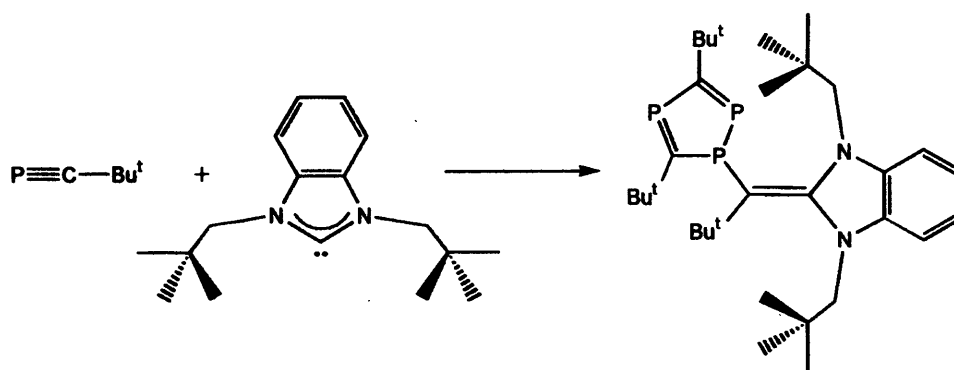


Figure 1.36 – Triphosphole-bis(2,2-dimethylpropyl)benzimidazolium adduct<sup>82</sup>

Similarly, Hahn *et al.* found the reaction of 1,3,4,5-tetramethylimidazol-2-ylidene with *tert*-butylphosphaacetylene afforded the analogous triphosphole derivative (Figure 1.37)<sup>55</sup>.

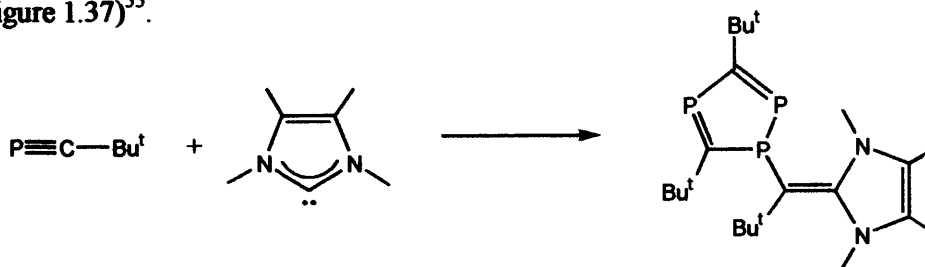


Figure 1.37 – Triphosphole-1,3,4,5-tetramethylimidazolium adduct<sup>55</sup>

This work complemented research by the Nixon group who reported the formation of the same 1,2,4-triphosphole carbene compound in the treatment of 2,4,6-tri-*tert*-butyl-1,3,5-triphospha benzene with 1,3,4,5-tetramethylimidazol-2-ylidene (Figure 1.38)<sup>54</sup>.

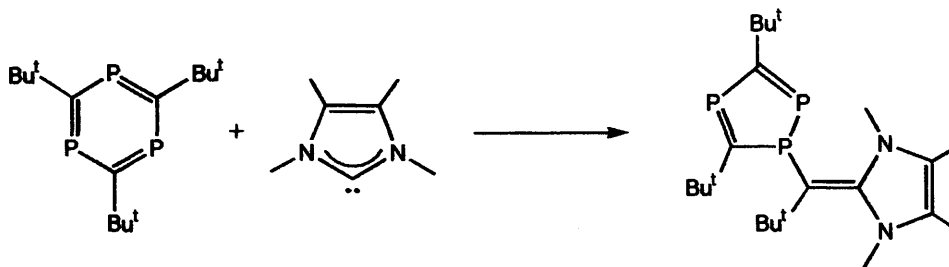


Figure 1.38 – Triphosphole-1,3,4,5-tetramethylimidazolium adduct<sup>54</sup>

This reaction is reversible when the product is treated with  $[\text{PtCl}_2(\text{PMe}_3)_2]$  or  $[\text{PtCl}_2(\text{PMe}_2\text{Ph})_2]$  to regenerate the triphospha benzene. The reversible nature of this reaction is of interest to us since it potentially provides a synthetic pathway to a range of 1,3,5-triphospha benzenes<sup>54</sup>.

We attempted an analogous reaction to that of Hahn *et al.*<sup>55</sup> with the 1:1 reaction of 1,3-bis(2,4,6-trimethylphenyl)imidazol-2-ylidene (IMes) with the phosphaaalkyne, *tert*-butylphosphaacetylene, in toluene (Figure 1.39).

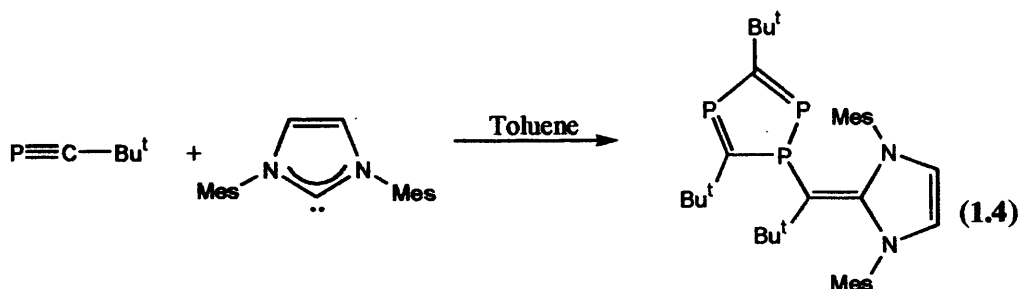


Figure 1.39 – Formation of  $[\text{P}_3\text{C}_2\text{Bu}_2\text{C}(\text{IMes})]$  (1.4)

This reaction afforded the expected  $[\text{P}_3\text{C}_2\text{Bu}_2\text{C}(\text{IMes})]$  (1.4) complex (Figure 1.39 and 1.40) in poor yields.

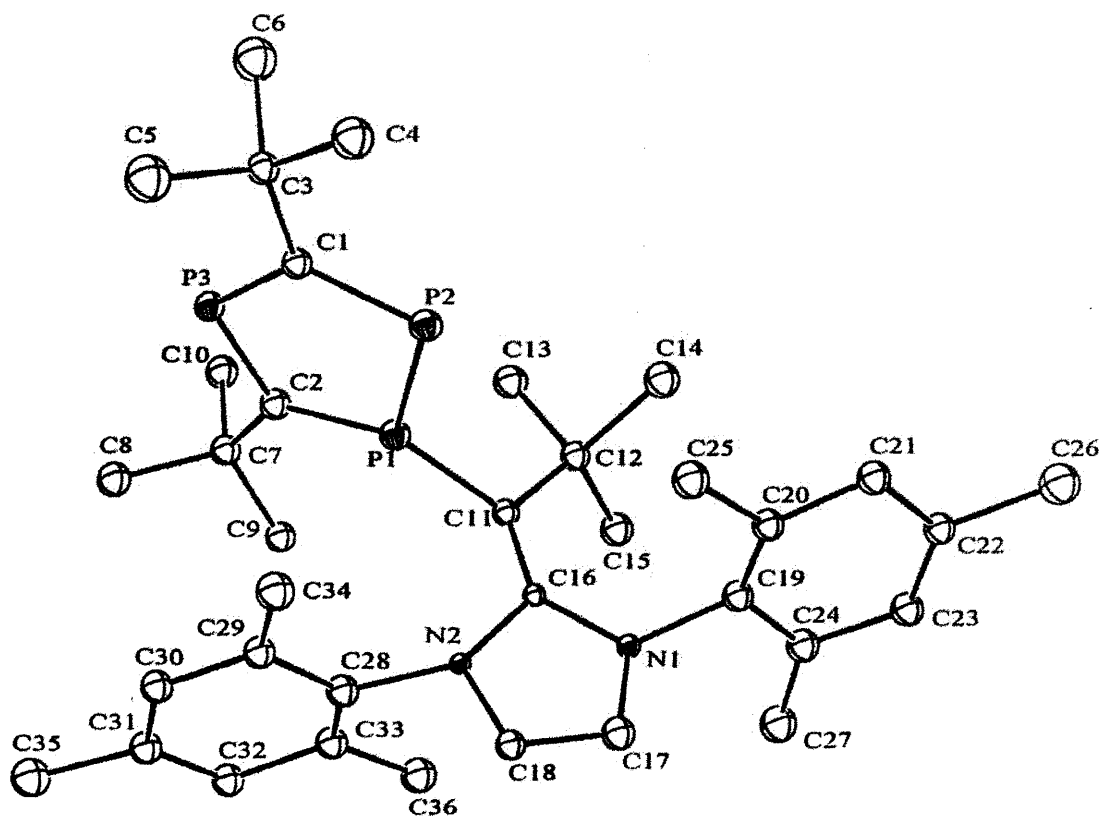


Figure 1.40 – Molecular Structure  $[P_3C_2Bu^tCBu^t(IMes)]$  (1.4) Unfortunately, the low precision of this structure means the bond lengths and angles are not accurate enough to comment on.

A repeat of this reaction using the correct stoichiometry (three phosphalkyne equivalents to one carbene) afforded the same product in high yields. The product is analogous to those complexes reported by both the Nixon<sup>54</sup> and Hahn groups<sup>55</sup> and probably forms by a mechanism identical to that proposed by Hahn for his complex. Following this work we were keen to investigate the reversibility of this reaction by the addition of  $[PtCl_2(PEt_3)_2]$  to (1.4), a reaction that was monitored by  $^{31}P$  NMR spectroscopy. Unfortunately, the Nixon<sup>54</sup> results could not be repeated as we were unable to form the 1,3,5-triphosphabenzene. We believe that the steric hindrance imposed by the mesityl groups on the carbene is responsible for the complex's lack of reactivity with  $[PtCl_2(PEt_3)_2]$ .

We were eager to follow the success of this reaction with the synthesis of analogous triphosphole-carbene complexes, by the treatment of stable Arduengo type carbenes with phosphalkyne. However reactions of phosphalkyne with IDipp and IPhe failed to yield any isolable crystals, although  $^{31}\text{P}$  NMR spectra of the reaction products were indicative of products analogous to (1.4). In an effort to confirm the nature of the products, they were treated with  $[\text{W}(\text{CO})_5(\text{THF})]$  with a view to form crystalline tungsten complexes, but again only intractable product mixtures resulted.

A further phosphalkyne reaction with biscarbene ( $\text{Et}\{\text{IBu}^t\}_2$ ) did yield crystals of X-ray quality (Figure 1.41). In contrary to the expected bistrifosphole product the crystal structure showed that the carbene rings have opened to give an unusual bicyclic product incorporating one molecule of *tert*-butylphosphaacetylene (Figure 1.2.15). This product was formed in a low and irreproducible yield and we were only able to obtain  $^{31}\text{P}$  NMR and crystallographic characterisation from the crystals formed (Figure 1.41). At present we have no evidence for the mechanism of formation of (1.5).

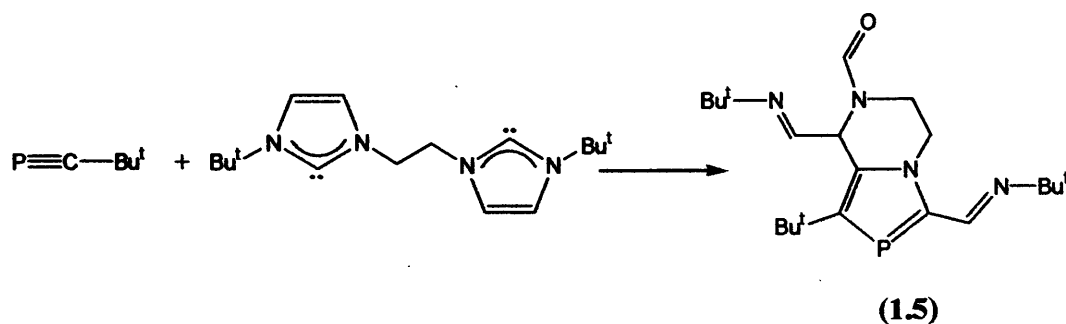


Figure 1.41 – Synthesis of  $[\text{PCBu}^t(\text{EtIBu}^t)\text{O}]$  (1.5)

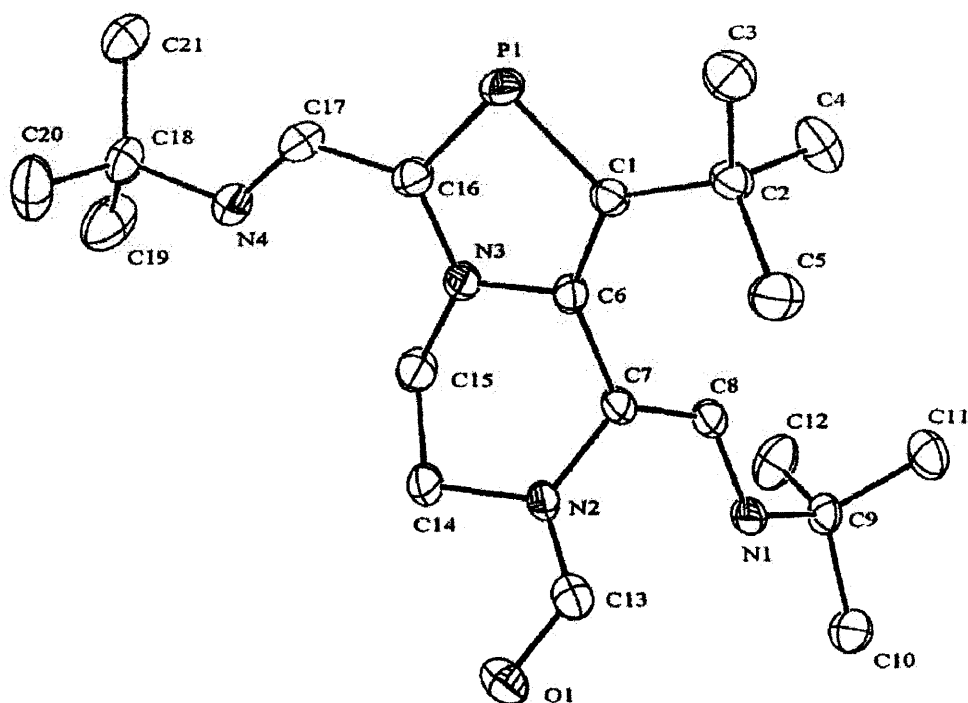


Figure 1.42 – Molecular Structure of [PCBu<sup>t</sup>(EtIBu<sup>t</sup>)O] (1.5)

Atoms	Distance	Atoms	Distance	Atoms	Distance
P(1)-C(1)	1.7690(17)	C(15)-C(14)	1.510(3)	C(7)-C(8)	1.345(2)
P(1)-C(16)	1.7290(18)	C(14)-N(2)	1.469(2)	C(8)-N(1)	1.366(2)
C(1)-C(6)	1.383(2)	N(2)-C(7)	1.442(2)	N(1)-C(9)	1.477(2)
C(6)-N(3)	1.386(2)	C(7)-C(6)	1.475(2)	C(16)-C(17)	1.459(2)
N(3)-C(16)	1.366(2)	N(2)-C(13)	1.339(2)	C(17)-N(4)	1.266(2)
N(3)-C(15)	1.470(2)	C(13)-O(1)	1.229(2)	N(4)-C(18)	1.481(2)

Atoms	Angle	Atoms	Angle
C(16)-P(1)-C(1)	90.94(8)	N(3)-C(15)-C(14)	109.78(15)
P(1)-C(1)-C(6)	109.94(12)	C(15)-C(14)-N(2)	109.11(14)
C(1)-C(6)-N(3)	113.43(14)	C(14)-N(2)-C(7)	117.04(14)
C(6)-N(3)-C(16)	114.08(14)	N(2)-C(7)-C(6)	112.58(13)
N(3)-C(16)-P(1)	111.58(12)	N(2)-C(13)-O(1)	124.33(16)

Table 1.4 – Selected bond lengths (Å) and angles (°) for [PCBu<sup>t</sup>(EtIBu<sup>t</sup>)O] (1.5)

### 1.3 Conclusions

We have synthesised the first crystallographically characterised thallium trihalide complex, which displays a remarkable thermal stability given that thallium trihalide complexes are generally thought to be very oxidising. We hope the synthesis of this complex will lead to the formation of the first thallium trihydride species. We were also able to prepare a chiral carbene alane complex, and test the enantioselectivity of this complex as a reducing agent towards pro-chiral ketones. Unfortunately the enantioselectivity of this complex left much to be desired as did its activity. Finally, we have extended research by both the Hahn and Nixon groups in reactions of a phosphalkyne with carbenes with the synthesis of a carbene-triphosphole complex and an unusual hetero-bicyclic compound.

## 1.4 Experimental

All manipulations requiring inert atmospheres were carried out using standard Schlenk and glove box techniques under an atmosphere of high purity argon or dinitrogen. The solvents diethyl ether, hexane, toluene and THF were distilled over either potassium or Na/K alloy then freeze/thaw degassed prior to use.  $\text{CH}_2\text{Cl}_2$  was purified by distillation from  $\text{CaH}_2$  under a dinitrogen atmosphere.  $^1\text{H}$ ,  $^{13}\text{C}$  and  $^{31}\text{P}$  NMR spectra were recorded on Bruker DPX400 or Jeol Eclipse 300 spectrometers in deuterated solvents and referenced to the residual  $^1\text{H}$  resonances of the solvent used ( $^1\text{H}$  NMR) or to external 85%  $\text{H}_3\text{PO}_4$ , 0.0 ppm ( $^{31}\text{P}$  NMR). Mass spectra were recorded using a VG Fisons Platform II instrument under APCI conditions. Melting points were determined in sealed glass capillaries under argon, and are uncorrected. Elemental analysis was carried out at the Warwick Analytical Service. Glyoxal was obtained as a 37% Wt aqueous solution from Aldrich. 2,4,6-trimethylphenylaniline, *N,N'*-dimethylthiourea, 1-hexanol, 3-hydroxy-2-butanone, 2,6-diisopropylaniline, (*R*)-1-phenylethyl-amine, paraformaldehyde, absolute ethanol and concentrated HCl were also obtained from Aldrich.  $[\text{LiAlH}_4]$  was purified by extraction into dry diethyl ether after being purchased from Aldrich.  $\text{TiCl}_3$ <sup>83</sup> was prepared via modified literature procedures, using  $\text{TiCl}_3 \cdot 4\text{H}_2\text{O}$ , which was purchased from Aldrich. The starting materials  $[\text{AlH}_3(\text{NMe}_3)]$ <sup>84</sup> and  $\text{EtIBu}$ <sup>19</sup> were prepared by literature methods, while the starting materials  $\text{IMes}$ <sup>85</sup>,  $\text{ITetMe}$ <sup>30</sup>,  $\text{IPr}$ <sup>31</sup> and  $\text{IPhe}$ <sup>22</sup> were all synthesised with a slight modification of their published procedures. All other reagents were used as received.

### 1.4.1 Group 13 Carbene Complexes

**$[\text{TiCl}_3(\text{IMes})]$  (1.1).** A THF solution (20 ml) of  $\text{IMes}$  (0.41g, 1.35 mmol) was added to a cooled ( $-30\text{ }^\circ\text{C}$ ) solution of  $\text{TiCl}_3$  (0.42g, 1.35 mmol) in THF (30 ml) over 20 mins. The resulting suspension was stirred overnight and warmed to room temperature. Volatiles were removed *in vacuo* and the residue re-crystallised from the minimum volume of THF to yield the product as colourless prisms after placement at  $-10\text{ }^\circ\text{C}$ . Yield 0.68g (83%), mp =  $208\text{ }^\circ\text{C}$  (decomp.).  $^1\text{H}$  NMR (300 MHz,  $\text{CD}_2\text{Cl}_2$ , 300K),  $\delta/\text{ppm}$  2.11 (s, 12H, *o*- $\text{CH}_3$ ), 2.36 (s, 6H, *p*- $\text{CH}_3$ ), 7.10 (s, 4H, *m*-H), 7.53 (d, 2H,  $^4J_{\text{TH}}$  89 Hz,  $\text{C}_2\text{H}_2$ ).  $^{13}\text{C}$  NMR (75.5 MHz,  $\text{CD}_2\text{Cl}_2$ , 300 K),  $\delta/\text{ppm}$  18.1 (s, *o*- $\text{CH}_3$ ), 21.8 (s, *p*- $\text{CH}_3$ ), 126.8 (d,  $^3J_{\text{TC}}$  221 Hz,  $\text{C}_2\text{H}_2$ ), 130.6 (s, *m*-C), 135.8 (s, *o*-C), 135.9 (s,



*p*-C), 142.5 (s, *ipso*-C). MS APCI *m/z* (%) 305 ( $\{M-TiCl_3\}H^+$ , 32), 339 ( $\{M-TiCl_2\}^+$ , 84), 580 ( $\{M-Cl\}^+$ , 100). IR (Nujol, NaCl plates) 1684(w,shp), 1661(w,shp), 1617(w), 1280(s,shp), 1094(s,br), 1022(s,br), 851(m,shp), 606(s)  $cm^{-1}$ .

**[TiCl<sub>3</sub>(ITetMe)] (1a).** A THF solution (20 ml) of ITetMe (0.55g, 4.4 mmol) was added to a cooled (−30 °C) solution of TiCl<sub>3</sub> (1.37g, 4.4 mmol) in THF (30 ml) over 20 mins. The resulting yellow suspension was stirred overnight and warmed to room temperature. Volatiles were removed *in vacuo* and the residue re-crystallised from the minimum volume of THF to yield the product as colourless crystals after placement at −10 °C. Yield 1.12g (60%), mp = 172 °C (decomp.). <sup>1</sup>H NMR (300 MHz, CD<sub>2</sub>Cl<sub>2</sub>, 300 K), δ/ppm 2.01 (s, 6H, backbone CH<sub>3</sub>), 2.92 (s, 6H, N-CH<sub>3</sub>). IR (Nujol, NaCl plates) 1624(m,shp), 1495(m,shp), 1458(s,br), 1401(m,shp), 1373(s,shp), 1258(m,shp), 1230(m,shp), 1187(w,shp), 1101(m,shp), 1029(m,shp), 850(s,shp)  $cm^{-1}$ . CHN analysis (%), calculated C 19.33, H 2.78, N 6.44, found C 19.78, H 2.78, N 6.07.

**[TiCl<sub>3</sub>(TetMeThione)<sub>2</sub>] (1b).** A THF solution (20 ml) of ITetMe (0.64g, 5.11 mmol) was added to a cooled (−30 °C) solution of TiCl<sub>3</sub> (0.79g, 2.56 mmol) in THF (30 ml) over 20 mins. The resulting suspension was stirred overnight and warmed to room temperature. The precipitate was isolated by cannular filtration, and re-crystallised from the minimum volume of CH<sub>2</sub>Cl<sub>2</sub> (2 ml) with diethyl ether (15 ml) to yield the product as colourless crystals after diffusion at room temperature. Yield 0.29g (18%), mp = 162 °C (decomp.). <sup>1</sup>H NMR (300 MHz, CD<sub>2</sub>Cl<sub>2</sub>, 300 K), δ/ppm 2.12 (s, 6H, backbone CH<sub>3</sub>), 3.62 (s, 6H, N-CH<sub>3</sub>). <sup>13</sup>C NMR (75.5 MHz, CD<sub>2</sub>Cl<sub>2</sub>, 300 K), δ/ppm 9.9 (s, backbone CH<sub>3</sub>), 33.9 (s, N-CH<sub>3</sub>), 126.1 (s, backbone CH), 156.4 (s, carbenic C). MS APCI *m/z* (%) 157( $\{M-Thione-TiCl_3\}H^+$ , 100), 313 ( $\{M-Thione_2\}H^+$ , 100), 589 ( $\{M-Cl\}^+$ , 24), 623 ( $\{M\}^+$ , 20). IR (Nujol, NaCl plates) 2347(w,shp), 1631(s,shp), 1573(w,shp), 1480(s,shp), 1452(s,shp), 1394(m,shp), 1373(m,shp), 1344(w,shp), 1266(w,shp), 1230(m,shp), 1187(m,shp), 1108(w,shp), 1029(w,shp), 972(w,shp), 858(s,shp), 779(w,shp), 729(w,shp)  $cm^{-1}$ . CHN analysis (%), calculated C 26.98, H 3.88, N 8.99, found C 26.71, H 3.77, N 8.60.

**[TiCl<sub>3</sub>(IDipp)] (1c).** A THF solution (10 ml) of IPr (0.25g, 0.64 mmol) was added to a cooled (−30 °C) solution of TiCl<sub>3</sub> (0.2g, 0.64 mmol) in THF (6 ml). The resulting suspension was stirred overnight and warmed to room temperature giving a red/purple solution. Volatiles were removed *in vacuo* and the residue re-crystallised from the minimum volume of THF to yield the product as colourless prisms after placement at −10 °C. Yield 0.35g (78%), mp = 226 °C (decomp.). <sup>1</sup>H NMR (300 MHz, CD<sub>2</sub>Cl<sub>2</sub>, 300 K), δ/ppm 1.11 (d, 12H, <sup>3</sup>J<sub>H,H</sub> 6.72 Hz, Pr<sup>i</sup>-CH<sub>3</sub>), 1.32 (d, 12H, <sup>3</sup>J<sub>H,H</sub> 6.78 Hz Pr<sup>i</sup>-CH<sub>3</sub>), 2.41 (sept, 4H, <sup>3</sup>J<sub>H,H</sub> 6.75 Hz, Pr<sup>i</sup>-CH), 7.33 (d, 4H, <sup>3</sup>J<sub>H,H</sub> 7.87 Hz, *m*-H), 7.37 (s, 2H, backbone C<sub>2</sub>H<sub>2</sub>), 7.55 (t, 2H, <sup>3</sup>J<sub>H,H</sub> 7.65 Hz, *p*-H). <sup>13</sup>C NMR (75.5 MHz, CD<sub>2</sub>Cl<sub>2</sub>, 300 K), δ/ppm 22.6 (s, Pr<sup>i</sup>-CH<sub>3</sub>), 25.5 (s, Pr<sup>i</sup>-CH<sub>3</sub>), 29.2 (s, Pr<sup>i</sup>-CH), 124.9 (s, *m*-C), 125.3 (s, *p*-C), 125.8 (s, *o*-C), 142.5 (d, <sup>3</sup>J<sub>TiC</sub> 12.7 Hz, backbone C<sub>2</sub>H<sub>2</sub>). MS APCI *m/z* (%) 237 ({M-IPrCl<sub>2</sub>}<sup>+</sup>, 10), 389 ({M-TiCl<sub>3</sub>}<sup>+</sup>, 100), 663 ({M-Cl}<sup>+</sup>, 15). IR (Nujol, NaCl plates) 2353(m,shp), 1589(w,shp), 1549(w,shp), 1262(m,shp), 1212(m,shp), 1102(m,br), 1017(m), 946(m,shp), 926(m,shp), 876(w,shp) cm<sup>−1</sup>. CHN analysis (%), calculated C 46.37, H 5.19, N 4.01, found C 46.30, H 5.30, N 3.70.

**[AlH<sub>3</sub>(IPr)] (1.2).** Method A. A diethyl ether solution (40 ml) of IPr (0.51g, 1.31 mmol) was added to a cooled (−30 °C) solution of LiAlH<sub>4</sub> (0.05g, 1.31 mmol) in diethyl ether (20 ml). The resulting suspension was stirred overnight and warmed to room temperature. Volatiles were removed *in vacuo* and the residue re-crystallised from the minimum volume of toluene to yield the product as colourless prisms after placement at −10 °C. Yield 0.43g (78%), mp = 229–239 °C (decomp. observed at 300 °C). <sup>1</sup>H NMR (300 MHz, CD<sub>2</sub>Cl<sub>2</sub>, 300 K), δ/ppm 1.16 (d, 12H, <sup>3</sup>J<sub>H,H</sub> 6.25 Hz, Pr<sup>i</sup>-CH<sub>3</sub>), 1.54 (d, 12H, Pr<sup>i</sup>-CH<sub>3</sub>), 2.79 (sept, 4H, Pr<sup>i</sup>-CH), 6.54 (s, 2H, backbone C<sub>2</sub>H<sub>2</sub>), 7.22 (d, 4H, <sup>3</sup>J<sub>H,H</sub> 7.72 Hz, *m*-H), 7.24 (t, 2H, <sup>3</sup>J<sub>H,H</sub> 7.84 Hz, *p*-H). <sup>13</sup>C NMR (75.5 MHz, CD<sub>2</sub>Cl<sub>2</sub>, 300 K), δ/ppm 23.40 (s, Pr<sup>i</sup>-CH<sub>3</sub>), 24.50 (s, Pr<sup>i</sup>-CH<sub>3</sub>), 28.75 (s, Pr<sup>i</sup>-CH), 123.26 (d, backbone C<sub>2</sub>H<sub>2</sub>), 123.86 (s, *m*-C), 130.15 (s, *p*-C), 135.25 (s, *o*-C), 145.49 (s, carbenic carbon). IR (Nujol, NaCl plates) 1774.8(m), 1744.7(m), 1724.6(s), 1599.0(w), 1553.8(m,sh), 1327.9(m,sh), 1257.6(m,sh), 1212.4(s,sh), 1101.9(s), 1061.8(m,sh), 936.2(w,sh) cm<sup>−1</sup>. CHN analysis (%), calculated C 77.47, H 9.39, N 6.69, found C 79.72, H 9.49, N 6.78.

**Method B.** A toluene solution (20 ml) of IPr (0.41g, 1.06 mmol) was added to a cooled (−30 °C) solution of (Me<sub>3</sub>N:AlH<sub>3</sub>) (0.09g, 1.06 mmol) in toluene (30 ml). The resulting suspension was stirred overnight and warmed to room temperature. Volatiles

were removed *in vacuo* and the residue re-crystallised from the minimum volume of toluene to yield the product as colourless prisms after placement at  $-10\text{ }^{\circ}\text{C}$ . Yield 0.37g (84%).

**[AlH<sub>3</sub>{IPhe}] (1.3).** Method A. A THF solution (40 ml) of IPhe (0.36g, 1.31 mmol) was added to a cooled ( $-30\text{ }^{\circ}\text{C}$ ) solution of LiAlH<sub>4</sub> (0.05g, 1.31 mmol) in THF (20 ml). The resulting suspension was stirred overnight and warmed to room temperature. Volatiles were removed *in vacuo* and the residue extracted into toluene, filtered and the filtrate dried *in vacuo* to yield the product as an orange powder. Yield 0.3g (76%), mp =  $170\text{ }^{\circ}\text{C}$  decomp. (onset  $\sim 139\text{ }^{\circ}\text{C}$ ). <sup>1</sup>H NMR (300 MHz, C<sub>6</sub>D<sub>6</sub>, 300 K),  $\delta$ /ppm 1.11 (d, 3H, <sup>3</sup>J<sub>H,H</sub> 6.6 Hz, CH<sub>3</sub>), 1.20 (d, 3H, <sup>3</sup>J<sub>H,H</sub> 6.6 Hz, CH<sub>3</sub>), 3.29 (quart, 1H, <sup>3</sup>J<sub>H,H</sub> 6.6 Hz, \*CH), 3.35 (quart, 1H, <sup>3</sup>J<sub>H,H</sub> 6.6 Hz, \*CH), 5.45 (s, 1H, backbone C<sub>2</sub>H<sub>2</sub>), 5.50 (s, 1H, backbone C<sub>2</sub>H<sub>2</sub>), 7.01-7.25 (m, 10H, H). <sup>13</sup>C NMR (75.5 MHz, C<sub>6</sub>D<sub>6</sub>, 300K),  $\delta$ /ppm 21.2 (s, CH<sub>3</sub>), 22.2 (s, CH<sub>3</sub>), 63.1 (s, \*CH), 63.4 (s, \*CH), 119.2 (s, backbone C<sub>2</sub>H<sub>2</sub>), 119.4 (s, backbone C<sub>2</sub>H<sub>2</sub>), 125.4 (s, *m*-C), 126.8 (s, *m*-C), 127.2 (s, *p*-C), 128.3 (s, *p*-C), 128.5 (s, *o*-C), 129.1 (s, *o*-C), 144.4 (s, *ipso*-C), 144.7 (s, *ipso*-C). IR (Nujol, NaCl plates) 1951(m), 1880(w), 1760(s,br) Al-H stretch, 1679(m), 1599(m,shp), 1303(w,shp), 1258(m,shp), 1207(w,shp), 1177(w,shp), 1092(m,br), 1027(m) cm<sup>-1</sup>. Method B. A THF solution (30 ml) of IPhe (0.37g, 1.34 mmol) was added to a cooled ( $-30\text{ }^{\circ}\text{C}$ ) solution of (Me<sub>3</sub>N:AlH<sub>3</sub>) (0.14g, 1.61 mmol) in THF (20 ml). The resulting suspension was stirred overnight and warmed to room temperature. Volatiles were removed *in vacuo* and the residue washed with cold hexane (20 ml) to yield the product as orange powder. Yield 0.29g (66%).

### Calculation of $\Delta G^\ddagger$ from $^1\text{H}$ NMR Coalescence<sup>86</sup>

These calculations form the basis of our first attempt to identify a barrier to rotation in (1.3) and are unreliable.

Temperature of Coalescence = 105 °C, 378 K

Position of quartets at room temperature = 3.3013 and 3.2533 ppm

$$\begin{aligned}\text{Hence, } \Delta\nu &= (3.3013 - 3.2533) \times 300.53 \text{ Hz} \\ &= 14.42544 \text{ Hz}\end{aligned}$$

Rate Constant  $k = \frac{\pi \Delta\nu}{\sqrt{2}}$  at  $T_\infty$

$$\begin{aligned}&\sqrt{2} \\ k &= 32.045 \text{ s}^{-1}\end{aligned}$$

$$k = \frac{KT}{h} e^{-\Delta G^\ddagger/RT}$$

$$\Delta G^\ddagger = -(\ln k - \ln KT/h) RT$$

$$\Delta G^\ddagger = \frac{-(\ln 32.045 - \ln 7.8763 \times 10^{12}) \times 8.31451 \times 378}{1000}$$

$$\Delta G^\ddagger = \frac{-(3.46714 - 29.694878) \times 8.31451 \times 378}{1000}$$

$$\Delta G^\ddagger = \frac{-(-26.22774) \times 8.31451 \times 378}{1000}$$

$$\Delta G^\ddagger = 82.43 \text{ kJ mol}^{-1}$$

$\Delta\nu$  =  $^1\text{H}$  NMR separation of the two resonances of the quartets

$K$  = Boltzmann Constant,  $1.38066 \times 10^{-23}$

$T$  = Absolute Temperature, 378 K (105 °C)

$h$  = Planck Constant,  $6.62608 \times 10^{-34}$  Js

$R$  = Gas Constant,  $8.31451 \text{ J K}^{-1} \text{ mol}^{-1}$

## 1.4.2 Asymmetric Reductions

### General Reduction Procedure

A substrate (*ca.* 1.4 mmol) was added as an ethereal solution to a suspension of  $[\text{AlH}_3\{\text{IPhe}\}]$  (**1.3**) (*ca.* 1.4 mmol) in diethyl ether at  $-78^\circ\text{C}$ . The resulting solution was stirred for 15-18 hrs whilst warming to room temperature. The reaction mixture was quenched with 0.1 M HCl at  $-10^\circ\text{C}$  and allowed to warm to room temperature. Extraction with diethyl ether (*ca.* 30 ml) followed by NaCl(aq.)/Et<sub>2</sub>O work-up, drying over MgSO<sub>4</sub>, filtration and drying *in vacuo* to afford the reduced alcohol products. All samples/reduced products were analysed by GCMS using a chiral column which enabled us to decipher enantiomeric excesses.

### 1.4.3 Phosphaalkyne – Carbene Complexes

$[\text{P}_3\text{C}_2\text{Bu}^t_2\text{CBu}^t(\text{IMes})]$  (**1.4**). A toluene solution (6 ml) of IMes (0.31g, 1.02 mmol) was added dropwise to a cooled ( $-30^\circ\text{C}$ ) solution of *tert*-butyl phosphaalkyne (0.5 ml, 3.07 mmol) in toluene (6 ml). The resulting golden solution was stirred for 2 days and warmed to room temperature. Volatiles were removed *in vacuo* and the residue recrystallised from the minimum volume of hexane to yield the product as red prisms after placement at  $-10^\circ\text{C}$ . Yield 0.53g (86%), mp =  $217-224^\circ\text{C}$ .  $^1\text{H}$  NMR (300 MHz, C<sub>6</sub>D<sub>6</sub>, 300 K),  $\delta$ /ppm 1.05 (s, 9H, Bu<sup>t</sup>), 1.63 (s, 9H, Bu<sup>t</sup>), 1.82 (s, 9H, Bu<sup>t</sup>), 2.08 (s, 12H, *o*-CH<sub>3</sub>), 2.21 (s, 6H, *p*-CH<sub>3</sub>), 5.44 (s, 2H, backbone C<sub>2</sub>H<sub>2</sub>), 6.64 (s, 4H, *m*-H).  $^{13}\text{C}$  NMR (75.5 MHz, C<sub>6</sub>D<sub>6</sub>, 300 K),  $\delta$ /ppm 18.49 (s, *p*-CH<sub>3</sub>), 22.69 (s, *o*-CH<sub>3</sub>), 33.05 (s, Bu<sup>t</sup>), 35.10 (s, Bu<sup>t</sup>), 35.87 (s, Bu<sup>t</sup>), 36.49 (s, Bu<sup>t</sup>), 39.96 (s, Bu<sup>t</sup>), 40.15 (s, Bu<sup>t</sup>), 118.90 (s, backbone C<sub>2</sub>H<sub>2</sub>), 129.63 (s, *m*-C), 137.60 (s, *o*-C), 138.88 (s, *p*-C), 149.22 (s, *ipso*-C), 155.25 (s, *carbenic*-C).  $^{31}\text{P}$  NMR (121 MHz, C<sub>6</sub>D<sub>6</sub>, 300 K,  $\delta$ /ppm) 116.35, 168.29, 231.27 ( $^1J_{\text{PP}}$  505.94 Hz,  $^2J_{\text{PP}}$  38.67 Hz and  $^2J_{\text{PP}}$  17.26 Hz). MS APCI *m/z* (%) 305 ( $\{\text{M}-\text{P}_3\text{C}_2\text{Bu}^t_2\text{CBu}^t\}^+\text{H}^+$ , 100), 605 ( $\{\text{M}\}^+$ , 38). IR (Nujol, NaCl plates) 3098(m,shp), 2725(w,shp), 1917(m,shp), 1888(w,shp), 1674(m,shp), 1638(w,shp), 1609(m,shp), 1545(w,shp), 1449(s), 1384(s,shp), 1355(w,shp), 1318(m,shp), 1283(w,shp), 1254(s,shp), 1225(w,shp), 1181(w,shp), 1160(m,shp), 1095(s,shp), 1022(s,shp), 972(m,shp), 936(w,shp), 908(m,shp), 872(w,shp), 850(m,shp), 800(s,shp), 707(m,shp), 685(m,shp) cm<sup>-1</sup>.

**[PCBu<sup>t</sup>(EtIBu<sup>t</sup>)O] (1.5).** A toluene solution (25 ml) of EtIBu<sup>t</sup> (0.065g, 0.24 mmol) was added dropwise to a cooled (−30 °C) solution of *tert*-butyl phosphalkyne (0.23 ml, 1.42 mmol) in toluene (6 ml). The resulting pale yellow solution was stirred for 2 days and warmed to room temperature. Volatiles were removed *in vacuo* and the residue re-crystallised from the minimum volume of hexane to yield the product as yellow prisms after placement at −10 °C. Yield 0.04g (43%). <sup>31</sup>P NMR (121 MHz, C<sub>6</sub>D<sub>6</sub>, 300 K, δ/ppm) 141.79.

## 1.5 References

- <sup>1</sup> P.S. Skell, S.R. Sandler, *J. Am. Chem. Soc.*, **1958**, 80, 2024.
- <sup>2</sup> E.O. Fischer, A. Maasböl, *Angew. Chem., Int. Ed. Engl.*, **1964**, 3, 580.
- <sup>3</sup> A.J. Arduengo III, R.L. Harlow, M. Kline, *J. Am. Chem. Soc.*, **1991**, 113, 361.
- <sup>4</sup> H.-W. Wanzlick, *Angew. Chem., Int. Ed. Engl.*, **1962**, 1, 75.
- <sup>5</sup> D. Bourissou, O. Guerret, F.P. Gabbi, G. Bertrand, *Chem. Rev.*, **2000**, 100, 39.
- <sup>6</sup> W.A. Herrmann, C. Köcher, *Angew. Chem., Int. Ed. Engl.*, **1997**, 36, 2162.
- <sup>7</sup> M. Regitz, *Angew. Chem., Int. Ed. Engl.*, **1996**, 35, 7.
- <sup>8</sup> M. Brookhart, W.B. Studabaker, *Chem. Rev.*, **1987**, 87, 411.
- <sup>9</sup> R.H. Grubbs, "Comprehensive Organometallic Chemistry", Vol. 8, G. Wilkinson, F.G.A. Stone, E.W. Abel Eds., Pergamon, Oxford, **1982**.
- <sup>10</sup> D. A. Dixon, K.D. Hobbs, A.J. Arduengo III, G. Bertrand, M. Kline, *J. Am. Chem. Soc.*, **1991**, 113, 8782.
- <sup>11</sup> A.J. Arduengo III, J.R. Goerlich, W.J. Marshall, *J. Am. Chem. Soc.*, **1995**, 117, 11027.
- <sup>12</sup> D. Enders, K. Breuer, G. Raabe, J. Runsink, J.H. Teles, J.P. Melder, K. Ebel, S. Brode, *Angew. Chem., Int. Ed. Engl.*, **1995**, 34, 1021.
- <sup>13</sup> Typical N-C bond length = 1.470 Å from *Revised book of Data*, Nuffield Advanced Science, Revised 1<sup>st</sup> Edition, Longman, UK, **1984**.
- <sup>14</sup> A.J. Arduengo III, J.R. Goerlich, W.J. Marshall, *Liebigs Ann.*, **1997**, 365.
- <sup>15</sup> W.A. Herrmann, C. Köcher, *J. Organomet. Chem.*, **1997**, 532, 261.
- <sup>16</sup> W.A. Herrmann, M. Elison, J. Fischer, C. Köcher, *Chem. Eur. J.*, **1996**, 2, 772.
- <sup>17</sup> R.J. Baker, M.L. Cole, C. Jones, M.F. Mahon, *J. Chem. Soc., Dalton Trans.*, **2002**, 1992.
- <sup>18</sup> R.E. Douthwaite, M.L.H. Green, P.J. Silcock, P.T. Gomes, *Organomet.*, **2001**, 20, 2611.
- <sup>19</sup> R.E. Douthwaite, D. Hausinger, M.L.H. Green, P.J. Silcock, P.T. Gomes, A.M. Martins, *Organomet.*, **1999**, 18, 4584.
- <sup>20</sup> H.V.R. Dias, W. Jin, *Tetrahedron Lett.*, **1994**, 35, 1365.
- <sup>21</sup> W.A. Herrmann, C. Köcher, G.R.J. Artus, *Chem. Eur. J.*, **1996**, 2, 1627.
- <sup>22</sup> W.A. Herrmann, L.J. Goossen, C. Köcher, G.R.J. Artus, *Angew. Chem., Int. Ed. Engl.*, **1996**, 35, 2805.
- <sup>23</sup> J. Pytkowicz, S. Roland, P. Mangeney, *J. Organomet. Chem.*, **2001**, 631, 157.

- 
- <sup>24</sup> H.M.J. Wang, I.J.B. Lin, *Organomet.*, **1998**, 17, 972.
- <sup>25</sup> D.S. McGuinness, K.J. Cavell, *Organomet.*, **2000**, 19, 741.
- <sup>26</sup> (a) S. Gründermann, A. Kovacevic, M. Albrecht, J.W. Faller, R.H. Crabtree, *Chem. Commun.*, **2001**, 2274. (b) S. Gründermann, A. Kovacevic, M. Albrecht, J.W. Faller, R.H. Crabtree, *J. Am. Chem. Soc.*, **2002**, 124, 10473.
- <sup>27</sup> R.W. Alder, P.R. Allen, M. Murray, A.G. Orpen, *Angew. Chem., Int. Ed. Engl.*, **1996**, 35, 1121.
- <sup>28</sup> J.V. Nef, *Justus Liebigs Ann. Chem.*, **1895**, 287, 359.
- <sup>29</sup> A.J. Arduengo III, *Organomet.*, **1999**, 18, 529.
- <sup>30</sup> N. Kuhn, T. Kratz, *Synthesis*, **1993**, 561.
- <sup>31</sup> L. Jafarpour, E.D. Stevens, S.P. Nolan, *J. Organomet. Chem.*, **2000**, 606, 49.
- <sup>32</sup> K. Öfele, *J. Organomet. Chem.*, **1968**, 12, 42.
- <sup>33</sup> H.-W. Wanzlick, H.-J. Schönherr, *Angew. Chem., Int. Ed. Engl.*, **1968**, 7, 141.
- <sup>34</sup> W.A. Herrmann, M. Denk, J. Behm, W. Scherer, F.R. Klingan, H. Bock, B. Solouki, M. Wagner, *Angew. Chem., Int. Ed. Engl.*, **1992**, 31, 485.
- <sup>35</sup> M. Denk, R. Lennon, R. Hayashi, R. West, A.V. Belyakov, H.P. Verne, A. Haaland, M. Wagner, N. Metzler, *J. Am. Chem. Soc.*, **1994**, 116, 2691.
- <sup>36</sup> R.J. Baker, M. Kloth, C. Jones, *Unpublished results*, **2003**.
- <sup>37</sup> W.A. Herrmann, M. Elison, J. Fischer, C. Köcher, G.R.J. Artus, *Angew. Chem., Int. Ed. Engl.*, **1995**, 34, 2371.
- <sup>38</sup> W.vE. Doering, A.K. Hoffmann, *J. Am. Chem. Soc.*, **1954**, 76, 6162.
- <sup>39</sup> G. Boche, C. Hilf, K. Harms, M. Marsch, J.C.W. Lohrenz, *Angew. Chem., Int. Ed. Engl.*, **1995**, 34, 4.
- <sup>40</sup> C. Hilf, F. Bosold, K. Harms, J.C.W. Lohrenz, M. Marsch, M. Schimeczek, G. Boche, *Chem. Ber.*, **1997**, 130, 1201.
- <sup>41</sup> W.A. Herrmann, O. Runte, G.R.J. Artus, *J. Organomet. Chem.*, **1995**, 501, C1.
- <sup>42</sup> A.J. Arduengo III, F. Davidson, R. Krafczyk, W.J. Marshall, M. Tamm, *Organomet.*, **1998**, 17, 3375.
- <sup>43</sup> A.J. Arduengo III, H.V. R. Dias, J.C. Calabrese, F. Davidson, *J. Am. Chem. Soc.*, **1992**, 114, 9724.
- <sup>44</sup> S.J. Black, D.E. Hibbs, M.B. Hursthouse, C. Jones, K.M.A. Malik, N.A. Smithies, *J. Chem. Soc., Dalton Trans.*, **1997**, 4313.



- 
- <sup>45</sup> D.E. Hibbs, M.B. Hursthouse, C. Jones, N.A. Smithies, *Chem. Commun.*, **1998**, 869.
- <sup>46</sup> M.D. Francis, D.E. Hibbs, M.B. Hursthouse, C. Jones, N.A. Smithies, *J. Chem. Soc., Dalton Trans.*, **1998**, 3249.
- <sup>47</sup> C.D. Abernethy, M.L. Cole, C. Jones, *Organomet.*, **2000**, 19, 4852.
- <sup>48</sup> N. Kuhn, G. Henkel, T. Kratz, J. Kreutzberg, R. Boese, A.H. Maulitz, *Chem. Ber.*, **1993**, 126, 2041.
- <sup>49</sup> N. Kuhn, T. Kratz, D. Bläser, R. Boese, *Chem. Ber.*, **1995**, 128, 245.
- <sup>50</sup> A. Schaefer, M. Weidenbruch, W. Saak, S. Pohl, *J. Chem. Soc., Chem. Commun.*, **1995**, 1157.
- <sup>51</sup> A.J. Arduengo III, H.V. R. Dias, J.C. Calabrese, F. Davidson, *Inorg. Chem.*, **1993**, 32, 1541.
- <sup>52</sup> A.J. Arduengo III, C.J. Carmalt, J.A.C. Clyburne, A.H. Cowley, R. Pyati, *Chem. Commun.*, **1997**, 981.
- <sup>53</sup> N. Kuhn, J. Fahl, D. Bläser, R. Boese, *Z. Anorg. Allg. Chem.*, **1999**, 625, 729.
- <sup>54</sup> S.B. Clendenning, P.B. Hitchcock, J.F. Nixon, L. Nyulászi, *Chem. Commun.*, **2000**, 1305.
- <sup>55</sup> F.E. Hahn, D.L. Van, M.C. Moyes, T. von Fehren, R. Fröhlich, E-U. Würthwein, *Angew. Chem., Int. Ed. Engl.*, **2001**, 40, 3144.
- <sup>56</sup> N. Kuhn, G. Henkel, T. Kratz, *Z. Naturforsch. B.*, **1993**, 48, 973.
- <sup>57</sup> D.J. Williams, M.R. Fawcett-Brown, R.R. Ray, D. van Derveer, Y.T. Pang, R.L. Jones, K.L. Bergbauer, *Heteroatom Chem.*, **1993**, 4, 409.
- <sup>58</sup> N. Kuhn, G. Henkel, T. Kratz, *Chem. Ber.*, **1993**, 126, 2047.
- <sup>59</sup> N. Kuhn, H. Bohnen, J. Fahl, D. Bläser, R. Boese, *Chem. Ber.*, **1996**, 129, 1579.
- <sup>60</sup> A.J. Arduengo III, M. Kline, J.C. Calabrese, F. Davidson, *J. Am. Chem. Soc.*, **1991**, 113, 9704.
- <sup>61</sup> A.J. Arduengo III, E.P. Janulis, *J. Am. Chem. Soc.*, **1983**, 105, 3563.
- <sup>62</sup> N. Kuhn, G. Henkel, T. Kratz, *J. Chem. Soc., Chem. Commun.*, **1993**, 1778.
- <sup>63</sup> W.P. Fehlhammer, K. Bartel, A. Völkl, D. Achatz, *Z. Naturforsch. B.*, **1982**, 37, 1044.
- <sup>64</sup> J.E. Hill, T.A. Nile, *J. Organomet. Chem.*, **1977**, 137, 293.
- <sup>65</sup> M.F. Lappert in *Transition Metal Chemistry*, Ed. A. Müller, E. Diemann, Verlag Chemie, Weinheim, **1981**.

- 
- <sup>66</sup> A.M. Trzeciak, J.J. Ziolkowski, *Abstr. Pap. XX. Colloquy on Organomet. Chem., Germany-Poland (Halle-Wittenberg), 1996*, 11.
- <sup>67</sup> F.A. Cotton, G. Wilkinson, *Advanced Inorganic Chemistry*, 5<sup>th</sup> Edition, Wiley Interscience, New York, 1988
- <sup>68</sup> A.J. Downs (Ed.), *Chemistry of Aluminium, Gallium, Indium and Thallium*, Blackie Academic, Glasgow, 1993.
- <sup>69</sup> S.E. Jeffs, R.W.H. Small, I.J. Worrall, *Acta. Crystallogr. C.*, **1984**, 40, 65.
- <sup>70</sup> C.J. Carmalt, L.J. Farrugia, N.C. Norman, *Acta. Crystallogr. C.*, **1996**, 1, 339.
- <sup>71</sup> M.L. Cole, A.J. Davies, C. Jones, *J. Chem. Soc., Dalton Trans.*, **2001**, 2451.
- <sup>72</sup> Value reported with reference to a survey of the Cambridge Crystallographic Database.
- <sup>73</sup> R.J. Baker, A.J. Davies, C. Jones, M. Kloth, *J. Organomet. Chem.*, **2002**, 203.
- <sup>74</sup> C.D. Abernethy, M.L. Cole, A.J. Davies, C. Jones, *J. Chem. Soc., Dalton Trans.*, **2000**, 7567.
- <sup>75</sup> R. Noyori, *Asymmetric Catalysis in Organic Synthesis*, Wiley-Interscience, New York, 1994.
- <sup>76</sup> L.H. Pignolet, Ed., *Homogeneous Catalysis with Metal Phosphine Complexes*, Plenum, New York, 1983.
- <sup>77</sup> G.W. Parshall, S.D. Ittel, *Homogeneous Catalysis*, Wiley-Interscience, New York, 1992.
- <sup>78</sup> J. Huang, L. Jafarpour, A.C. Hillier, E.D. Stevens, S.P. Nolan, *Organomet.*, **2001**, 20, 2878.
- <sup>79</sup> Gaussian 98 (Revision A.11), M. J. Frisch, G. W. Trucks, H. B. Schlegel, G. E. Scuseria, M. A. Robb, J. R. Cheeseman, V. G. Zakrzewski, J. A. Montgomery, Jr., R. E. Stratmann, J. C. Burant, S. Dapprich, J. M. Millam, A. D. Daniels, K. N. Kudin, M. C. Strain, O. Farkas, J. Tomasi, V. Barone, M. Cossi, R. Cammi, B. Mennucci, C. Pomelli, C. Adamo, S. Clifford, J. Ochterski, G. A. Petersson, P. Y. Ayala, Q. Cui, K. Morokuma, P. Salvador, J. J. Dannenberg, D. K. Malick, A. D. Rabuck, K. Raghavachari, J. B. Foresman, J. Cioslowski, J. V. Ortiz, A. G. Baboul, B. B. Stefanov, G. Liu, A. Liashenko, P. Piskorz, I. Komaromi, R. Gomperts, R. L. Martin, D. J. Fox, T. Keith, M. A. Al-Laham, C. Y. Peng, A. Nanayakkara, M. Challacombe, P. M. W. Gill, B. Johnson, W. Chen, M. W. Wong, J. L. Andres, C. Gonzalez, M. Head-Gordon, E. S. Replogle, and J. A. Pople, Gaussian, Inc., Pittsburgh PA, 2001.

---

All calculations were performed using the Linux-based Beowulf cluster within the Helix machine, which is a 3D semi-immersive visualisation facility located in the Main Building of Cardiff University by Miss R. Mann, and Dr. D. Willock.

<sup>80</sup> As suggested in James B. Foresman and Æleen Frisch, *Exploring Chemistry with Electronic Structure Methods*, 2<sup>nd</sup> Ed. New York, 1998.

<sup>81</sup> McMurray, *Organic Chemistry*, 4<sup>th</sup> Ed., Brooks/Cole, New York, 1996.

<sup>82</sup> F.E. Hahn, L. Wittenbecher, D.L. Van, R. Fröhlich, B. Wibbeling, *Angew. Chem., Int. Ed. Engl.*, 2000, 39, 2307.

<sup>83</sup> Herrmann-Brauer, *Synthetic Methods of Organometallic and Inorganic Chemistry*, 3<sup>rd</sup> Ed., G. Thieme, Verlag, 1996.

<sup>84</sup> J.K. Ruff, M.F. Hawthorne, *J. Am. Chem. Soc.*, 1960, 82, 2141.

<sup>85</sup> A.J. Arduengo III, H.V.R. Dias, R.L. Harlow, M. Kline, *J. Am. Chem. Soc.*, 1992, 114, 5530.

<sup>86</sup> K.S. Laidler, Harper and Row, *Using Transition State Theory – Chemical Kinetics*, London, 1987.

## CHAPTER 2

### The Use of Gallium(I) Iodide in C–C Bond Forming Reactions

#### 2.1 Introduction

Aluminium aside, the use of group 13 metal compounds in organic synthesis is limited. Interest in indium however has expanded on the back of the success by Butsugan and co-workers, describing the effectiveness of metallic indium in Barbier type allylations and Reformatsky type reactions<sup>1</sup>, which encouraged the warranted reviews<sup>2, 3, 4</sup> in this field. Indium, as highlighted by Cintas<sup>2</sup>, with chemistry similar to that observed with zinc and tin, provides a useful alternative to these and some transition metals in organic synthesis with the added advantage of its thermal, water and air stability. This is an attractive prospect for organic and industrial chemists alike. It is reasonable to suggest that the scarcity of indium in the earth's crust has discouraged its use (its rarity is comparable to silver). However, this has not hindered the research of osmium and ruthenium for example. The synthetic applicability of indium is demonstrated by its first ionisation potential of 5.79 eV, which is lower than that observed for zinc (9.4 eV) and tin (7.3 eV), being more comparable to lithium and sodium (~5 eV). This affords indium as a prime candidate in single electron transfer processes (SET) as a reducing agent<sup>2</sup>. Indium also has a low nucleophilicity allowing a degree of chemo-selectivity in its reactions. Gallium shares many similarities with indium, however, the use of gallium has been somewhat overlooked.

##### 2.1.1 Indium Metal in C–C Bond Forming Reactions

Metallic indium has proved effective in Barbier allylations and Reformatsky reactions involving a wide variety of aldehydes and ketones to quantitatively afford homoallylic alcohols and  $\beta$ -hydroxy esters<sup>5, 6</sup> respectively, in water at room temperature under aerobic conditions. These reactions are reported to take place via indium sesquihalide ( $R_3In_2X_3$ ) intermediates<sup>1</sup>.

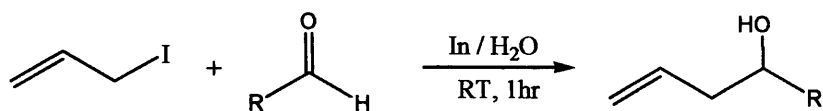


Figure 2.1 – Barbier allylation of aldehydes mediated by metallic indium

Allyl iodide is preferred in these Barbier reactions with high activities affording greater yields (Figure 2.1). In comparison allyl chlorides require longer reaction times and give lower yields. This methodology has since been employed to allylate aldimines in similar Barbier type reactions (Figure 2.2), with aldimines prepared from aromatic amines such as aniline ( $R' = \text{Ph}$ ), give the best results with high yields in short reaction times (1 hr).

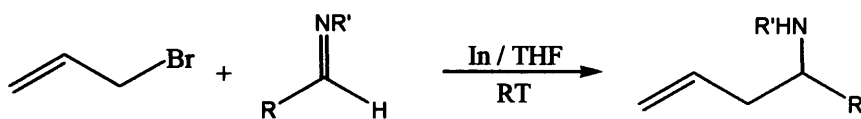


Figure 2.2 – Barbier-type allylation of aldimines mediated by metallic indium

Indium metal successfully promotes Reformatsky-type reactions of  $\alpha$ -haloesters with carbonyl compounds to afford  $\beta$ -hydroxy esters (Figure 2.3).

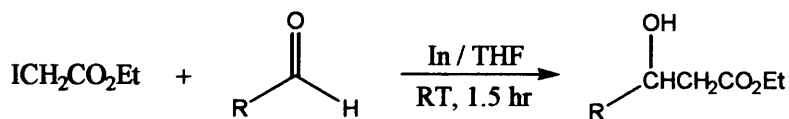


Figure 2.3 – Reformatsky reactions of aldehydes mediated by metallic indium

Ethyl  $\alpha$ -bromoacetate can just as productively be employed, whereas ethyl  $\alpha$ -chloroacetate afforded lower yields<sup>2</sup>. Investigations into these reactions revealed a variety of aldehydes and ketones that react to afford the corresponding  $\beta$ -hydroxy esters in high yields. These reactions do, however, require longer reaction times than comparable Barbier allylations. Chemo-selectivity was observed with allylation taking place exclusively at the carbonyl group in multi-functional organic molecules containing hydroxyl groups. These Barbier type reactions were extended to the discovery of regio- and diastereo-selective allenylation of aldehydes<sup>7</sup>. The reaction of propargyl bromide with an aldehyde can produce either the propargylated or

allenylated products in both a *syn* and *anti* fashion (Figure 2.4). Interestingly, in trials of this reaction, indium displayed the highest selectivity in aqueous methanol towards the homopropargyl alcohol product. Further investigations revealed this selectivity, which is controlled by steric and electronic factors, was as a result of the equilibrium existing between the propargylindium and allenylindium species, both possessing the ability to attack the carbonyl.

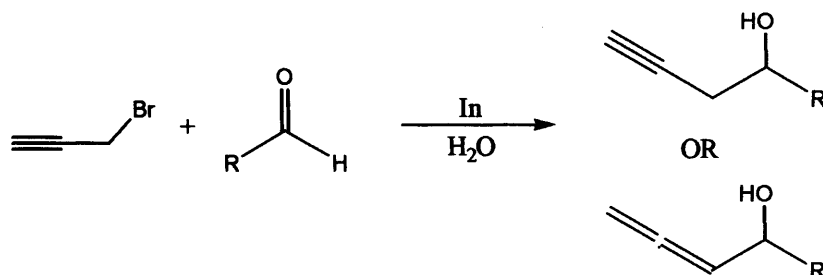


Figure 2.4 – Propargylated and allenylated products for the Barbier-type reaction with propargyl bromide and aldehydes

Indium metal can also be employed to mediate a host of other C-C bond forming reactions where the presence of aldehydes or ketones is not a prerequisite. Such a reaction is that with unactivated terminal alkynes. These investigations found the reaction to proceed with slightly elevated temperatures in THF<sup>8</sup>. The regio-selective Markovnikov addition occurs via an indium sesquibromide intermediate. This reaction worked well on all the alkynes investigated, affording the 1,4-diene product in high yields (Figure 2.5)<sup>8</sup>.

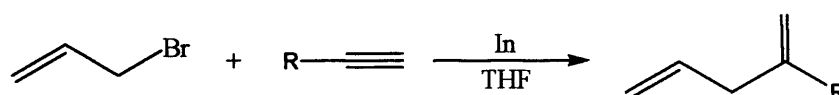


Figure 2.5 – Markovnikov Barbier-type allylation of unactivated terminal alkynes<sup>8</sup>

Another aspect of investigation was the ability of metallic indium to mediate C-C coupling. This was initially observed with the coupling of aromatic aldehydes in aqueous media to afford the corresponding pinacols. Further investigations revealed the limitations of this process with the failure of ketones, aliphatic and solid aromatic aldehydes to react under the reaction conditions<sup>9</sup>. Substituents on the aromatic ring

affect the *dl/meso* ratio in the coupled product, although the reason behind this is not fully understood (Figure 2.6)<sup>9</sup>.

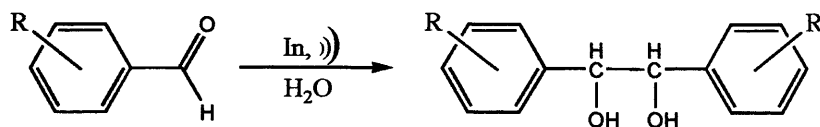


Figure 2.6 – C-C coupling reaction mediated by metallic indium<sup>9</sup>

Similarly 1,2-diketones were synthesised from a variety of acyl cyanides (Figure 2.7)<sup>10</sup>. These are the first examples of indium mediated reductive couplings. The introduction of indium to this area of chemistry provides a useful alternative to air and moisture sensitive  $\text{SmI}_2$  which to date is the standard one electron reducing agent. Other advantages of indium include its chemo-selectivity in coupling reactions, hence other functional groups on the aromatic ring remain unaffected during this procedure<sup>10</sup>.

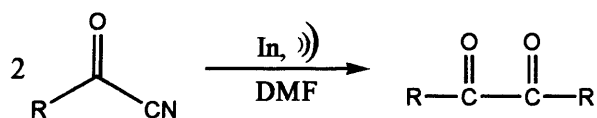


Figure 2.7 – Synthesis 1,2-diketones from acyl cyanides<sup>10</sup>

This reaction was found to proceed in DMF media only, and not in other solvents typically used in indium mediated reactions<sup>10</sup>. The suggested reason for this was that the reaction occurs via a SET process, with indium being slightly more reactive in DMF<sup>10</sup>. A proposed reaction mechanism is via the formation of an acyl cyanide radical intermediate, which is cleaved to form a reactive  $\text{RCO}^\bullet$  species, which couples to afford the product<sup>10</sup>.

Aldimines have also been reported to undergo indium mediated reductive couplings in aqueous ethanol to afford diamines (Figure 2.8)<sup>11</sup>. The presence of ammonium chloride, although not essential to the reaction process, was found to accelerate product synthesis. Furthermore, due to the formation of amines and not imines, coupling products were found to be a mixture of *d,l* and *meso* isomers. Reaction requirements included an aqueous ethanol medium, since reaction in acetonitrile and

DMF failed, even in “wet” solutions. The process was only successful with aromatic alkyl groups, hence aldimines formed from aromatic aldehydes and aromatic amines<sup>11</sup>.

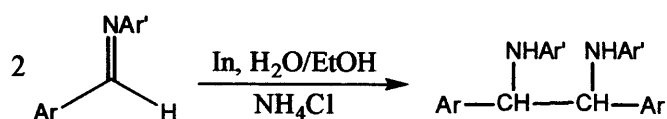


Figure 2.8 – Synthesis of 1,2-diamines from aryl aldimines<sup>11</sup>

More recently metallic indium has been reported to promote intramolecular cyclisation<sup>12, 13</sup> and cyclic ring expansions<sup>14</sup>. The indium mediated intramolecular cyclisation of tethered phenyl ketones proved useful in synthesising *syn* adducts irrespective of the original double bond geometry (Figure 2.9). The reaction of both (*E*) and (*Z*) isomers of 7-bromo-5-heptenophenones with metallic indium in a mixed THF / water medium yielded exclusively the *syn*-vinylcyclopentanol product. The proposed mechanism of this reaction involves the oxidative addition of indium to the C-Br bond, while co-ordinating to the oxygen centre to form an indium(III) species.

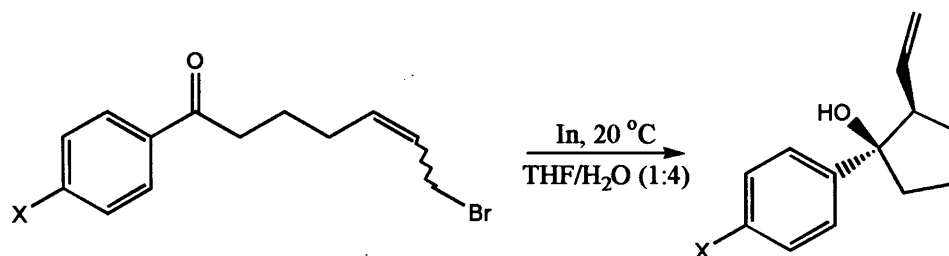


Figure 2.9 – Indium mediated intramolecular cyclisation

The ring expansion of the six membered ring in ethyl-4-oxo-thiotetrahydropyran-3-carboxylate to form the corresponding eight membered thiocyclo ether is a recent development (Figure 2.10)<sup>14</sup>. The product has found an application as a stomach secretion inhibitor.

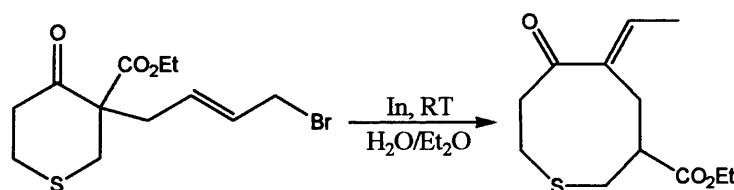


Figure 2.10 - Indium mediated ring expansion<sup>14</sup>



Indium metal has also been found to catalyse Barbier type allylation of aldehydes and ketones (Figure 2.11). Although different reaction conditions are required compared to the stoichiometric indium mediated allylations<sup>15</sup>. The reaction proceeds via the formation of an indium alkoxide from the metal, and TMSCl transmetallating this species to afford an indium(III) species. This in turn is reduced to metallic indium by manganese. This reaction is more efficient than the stoichiometric indium mediated process, suggesting that the regeneration of the indium metal by reduction of manganese is viable<sup>15</sup>.

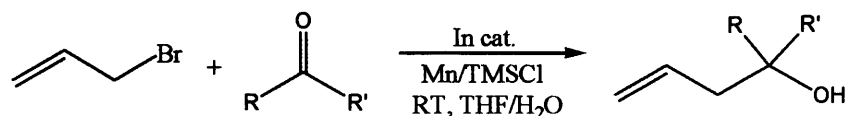


Figure 2.11 – Barbier Allylations catalysed by metallic indium

The association of group 13 metal complexes with Friedel-Craft alkylations is synonymous since it was reported by Charles Friedel and James Craft in 1877 that phenyl rings could be alkylated by alkyl chlorides in the presence of an aluminium trichloride catalyst. Metallic indium however, has only recently been introduced to this chemistry and is reported to successfully catalyse the Friedel-Crafts type allylation of aromatic compounds with allylic chloride (Figure 2.12)<sup>16</sup>. This is a groundbreaking revelation against the existing understanding of the reaction where vinylic halides were thought to be unreactive in this mechanism<sup>17</sup>. Again the introduction of indium eliminated the necessity of inert conditions, to afford homoallylated products with varying *ortho/para* ratios in moderate to high yields. A number of by-products from this reaction were also observed with mixed chlorinated products and trace amounts of diaryl-substituted alkanes. Interestingly, no reaction took place with aniline. It is thought that the indium metal in this reaction acts solely as a Lewis acid catalyst, as the aluminium trichloride reagent in the original Friedel-Craft reaction<sup>16</sup>.

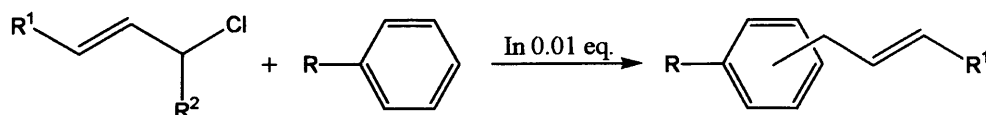


Figure 2.12 – Friedel-Craft allylation of aromatic rings<sup>16</sup>

### 2.1.2 Indium(III) Halides in C–C Bond Forming Reactions

Indium trichloride is affiliated with reactions incorporating the use of indium powder, since the reduction of this precursor affords a highly reactive indium powder. This was confirmed in the indium trichloride catalysed allylation of aldehydes with allyl bromide mediated by aluminium or zinc in water<sup>18</sup>. This reaction, however, proved to be less effective than the metallic indium catalysed reaction. Recent work has indicated the potential of indium trichloride in regio-selective catalysis of tin mediated allylation of aldehydes in water<sup>19</sup> (Figure 2.13). This allylation favoured the formation of the *anti* isomer, with an *anti:syn* ratio of 99:1<sup>19</sup>.

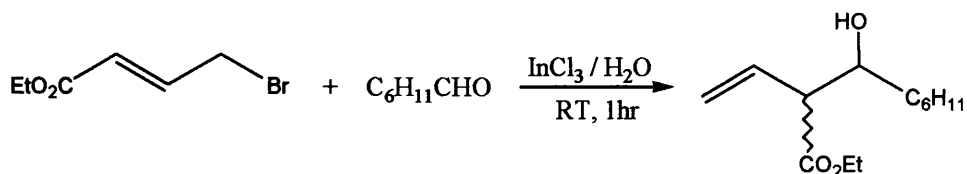


Figure 2.13 – Allylation of aldehydes catalysed by indium trichloride

Indium trichloride was also found to successfully catalyse Diels-Alder reactions with a variety of dienes and dienophiles in water. Endo and exo selectivity plays a vital role in these reactions and is substrate dependent; however selectivity and yield are found to be high with the use of this catalyst. This compares favourably with the reaction where the catalyst is absent, which affords a product with reduced selectivity and yield (Figure 2.14)<sup>20</sup>.

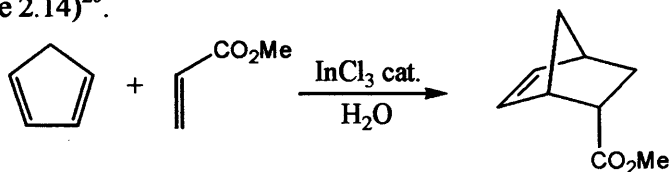


Figure 2.14 – Indium trichloride catalysed Diels-Alder reactions

Here, the reaction proceeds with a 20% equivalent of the catalyst to afford a product in high yield and high selectivity, *endo:exo* = 90:10<sup>20</sup>. This catalyst was effective for all substrates investigated<sup>20</sup>. Unfortunately these successes could not be replicated in the synthesis of enantio-pure products affording only moderate diastereoselectivity<sup>20</sup>,

Indium trihalides have also been employed, in stoichiometric quantities, as mediating reagents in C-C bond formation cyclisation reactions. Cyclisations have been observed in the reaction of aldehydes with chloro homoallyl alcohol to afford the dichloro tetrahydropyran (Figure 2.15)<sup>22</sup>.

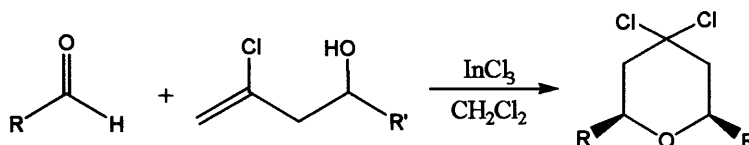


Figure 2.15 – Cyclisation reactions mediated by indium trichloride<sup>22</sup>

### 2.1.3 Indium(I) Halides in C–C Bond Forming Reactions

It is the nature of group 13 elements to form compounds with the element in the stable +3 oxidation state, however as the group is descended, the affinity these lower group 13 metals have for the +1 state increases. This can be observed in the formation of thallium (I) complexes, which are preferred to the analogous thallium (III) species. It is therefore not unusual to find indium(I) species, although the existence of gallium(I) complexes is rare while aluminium(I) complexes are rarer still. The implementation of indium(I) halides into organic synthesis (C–C bond formation) is limited to their use as mediators in Barbier allylations and Reformatsky reactions. However, the employment of indium(I) iodide in this case has dramatic consequences with increased efficiency. Indium(I) iodide encourages quantitative yields of the allylic alcohol in these reactions. In comparison, the metallic indium mediated formation of the sesquihalide ( $\text{R}_3\text{In}_2\text{X}_3$ ) intermediate allows for only two of the three alkyl groups to be transferred to the carbonyl group hence diminishing yields<sup>1</sup>. Indium(I) iodide is synthesised from the reaction of indium metal with iodine, and mediates the Barbier allylation (Figure 2.16) in THF, the preferred solvent, via allylindium(III) diiodide intermediates which have successfully been isolated<sup>23</sup> and spectroscopically characterised<sup>1</sup>.

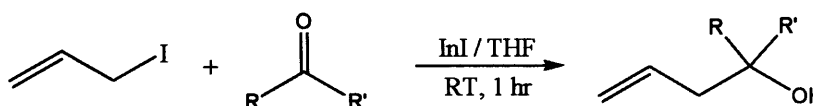


Figure 2.16 – Barbier allylation mediated by indium(I) iodide<sup>1</sup>

The yields for these reactions are high, and can be increased further with a slight excess of indium(I) iodide. This investigation revealed the similar properties indium(I) iodide shares with the metallic element, however indium(I) iodide proved significantly less regio-selective in the coupling of allylic halides than indium metal<sup>1</sup>. The Barbier allylation procedure has been improved with the introduction of a palladium catalyst to the reaction mechanism<sup>24</sup>. This alteration overcomes the substrate and solvent specificity of the oxidative addition of indium(I) iodide to allyl iodide to form the allylindium(III) diiodide intermediate. The Barbier allylation of allyl acetate to benzaldehyde mediated by indium(I) iodide and catalysed by palladium tetrakis(triphenylphosphine) afforded excellent yields of the corresponding homoallylic alcohol (Figure 2.17)<sup>24</sup>.

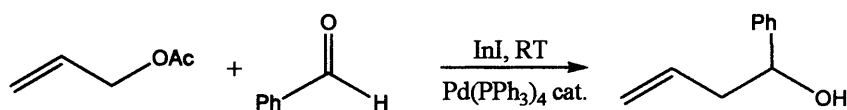


Figure 2.17 – Barbier allylation mediated by indium(I) iodide using a Pd catalysis<sup>24</sup>

The reaction readily proceeded in many solvents though displayed a preference for water. This affinity was reflected in the lower yields observed when the reaction was carried out in non-polar solvents. In addition, it was found that indium(I) chloride and bromide were equally capable of mediating this reaction with a variety of leaving groups employed on the allylic molecule<sup>24</sup>. Indium(I) iodide was also discovered to be effective in the mediation of Reformatsky type reactions with a variety of aldehydes and ketones to afford the corresponding  $\beta$ -hydroxy esters. The reaction times for the Reformatsky reactions are significantly longer than that of the Barbier allylations, however the yields reported appear to be similar (Figure 2.18)<sup>1</sup>.

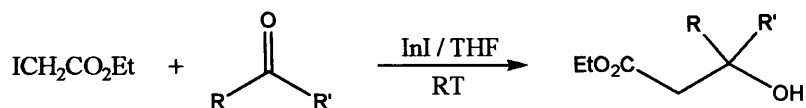


Figure 2.18 – Reformatsky reactions mediated by indium(I) iodide in THF<sup>1</sup>

The typical Reformatsky characteristics are abided in this reaction as 1,2-additions of  $\alpha,\beta$ -unsaturated carbonyl compounds are only observed. Furthermore, no protection of

hydroxyl substituent groups is required. These features ensure that the reaction is similar to the indium metal mediated Reformatsky reaction. It is assumed that these reactions occur via the formation of an organoindium(III) diiodide intermediate from the oxidative addition of indium(I) iodide with ethyl iodoacetate<sup>1</sup>.

#### 2.1.4 Gallium in C–C Bond Forming Reactions

The favourable comparisons between gallium and indium, including most importantly the first ionisation potentials (Ga 5.99 eV, In 5.79 eV) has attracted the employment of gallium metal in Barbier type allylations. These properties were exploited by Wang *et al.* with the investigation into gallium mediated Barbier type allylation of carbonyl compounds in water, using benzaldehyde (Figure 2.19)<sup>25</sup>.

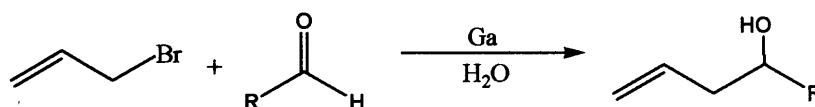


Figure 2.19 – Barbier allylation mediated by metallic gallium<sup>25</sup>

Most aromatic and aliphatic aldehydes and ketones investigated afforded moderate to high yields, with exclusive formation of the corresponding homoallylic alcohol product. This research was extended with investigations to the diastereo-selectivity of the reaction using the allylation of 2,3-dihydroxypropanal with allyl bromide (Figure 2.20)<sup>25</sup>.

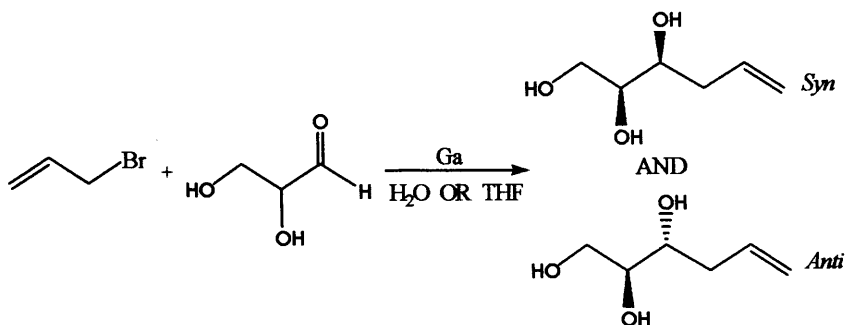


Figure 2.20 – Diastereo-selective Barbier Allylation mediated by gallium metal<sup>25</sup>

The diastereo-selectivity was found to be solvent dependent. When the reagents were reacted in water the *syn* isomer was the dominant product in an 8.3:1 ratio. However,

the identical reaction in a THF media afforded the *anti*-isomer as the major product in a 4.2:1 ratio. The formation of the *syn*-isomer is believed to be chelation controlled, with the two hydroxyl groups hydrogen bonding to each other in the aqueous environment to favour chelation of the  $\alpha$ -hydroxyl. This type of chelating hydrogen bonding was discouraged in organic solvents and favoured the formation of the *anti*-isomer<sup>25</sup>. These gallium-mediated allylations display significant advantages over indium mediated allylations. Gallium mediated allylation of aldehydes and ketones successfully in the absence of acidic co-reagents or mixed solvent systems, although an amount of heating is required. In fact, addition of acidic co-reagents had a negative effect, generating complicated product mixtures. This is an important consideration in the advancement towards Green Chemistry<sup>25</sup>. Environmentally benign gallium mediated allylations include the reaction of aldonitrones and hydrazones, which were derived from the parent aldehydes. These investigations revealed that allyl gallium, generated *in situ* from allyl bromide and gallium metal converted the substrates to their corresponding allylated alcohols. Microwaves are employed to increase reaction rates, although the reaction proceeds in their absence. Trace amounts of ammonium chloride, however, are crucial to the reaction taking place. It is assumed that this additive affects the generation of an active gallium reagent. The use of water is preferred to organic solvents and is environmentally sound<sup>26</sup>.

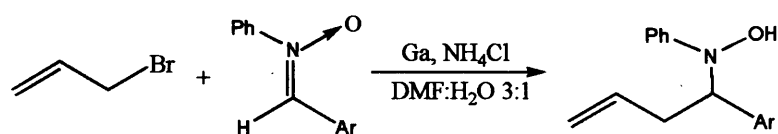


Figure 2.21 – Allylation of aldonitrones mediated by metallic gallium<sup>26</sup>

Homoallylic hydroxylamines and hydrazides were exclusively afforded from these reactions respectively. This is not the case however when indium is used as 1,2-diamines are formed as by-products. The nucleophilic attack of C=N groups by organometallics is problematic since the carbon is a poor electrophile and the preference is for deprotonation from the enol forms of the functional groups. Nitrones have an adequate electrophilic carbon and a reactive oxygen atom, making them more susceptible to homoallylation. This is a very useful synthetic pathway for the

preparation of homoallyl hydroxylamines and hydrazides in excellent yields and with minimum by-product formation (Figure 2.22)<sup>26</sup>.

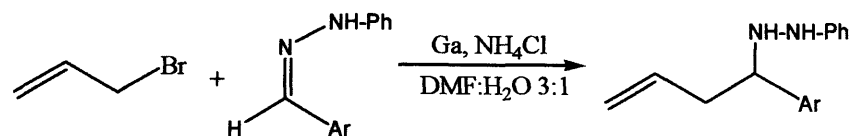


Figure 2.22 – Allylation of mediated by metallic gallium<sup>26</sup>

An independent investigation reported the allylation of carbonyl groups with an allylic gallium reagent. This reagent was prepared in the reaction of allyl magnesium chloride with gallium trichloride. Different allylic gallium reagents were prepared by the use of various Grignard reagents, including allyl, crotyl, prenyl and methallyl magnesium chloride<sup>27</sup>. These reagents are displayed in Figure 2.23:

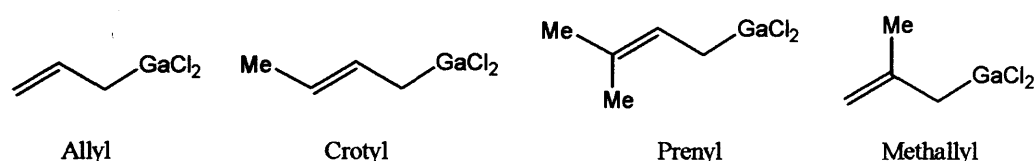


Figure 2.23 – Allylic gallium reagents prepared from allyl magnesium chloride<sup>27</sup>

These reagents were then used to treat benzaldehyde and acetophenone to afford the corresponding homoallylic alcohols. The  $\alpha$ -adduct is the only adduct observed with the allyl gallium dichloride reagent, however with the crotyl, prenyl and methallyl gallium dichloride reagents the alcohol is produced with the  $\gamma$ -adduct as the major product and the  $\alpha$ -adduct as the minor product (Figure 2.24)<sup>27</sup>.

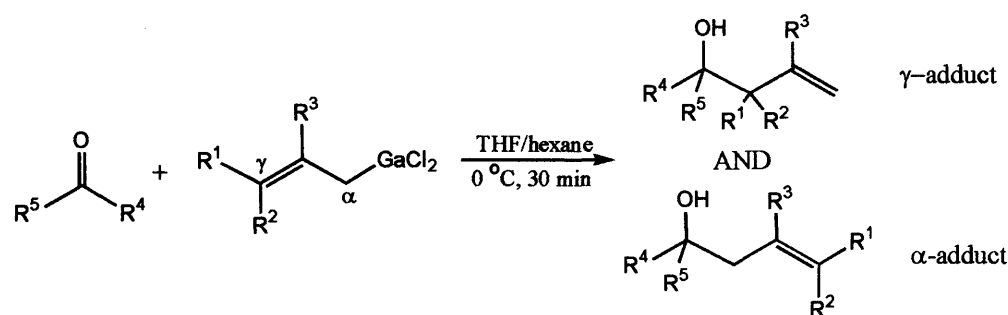


Figure 2.24 – Formation of homoallylic alcohols from the reaction of the allyl gallium dichloride reagent with benzaldehyde and acetophenone<sup>27</sup>

This “backwards” allylation ( $\gamma$ -adduct) is only observed when there are R group substituents present on the  $\gamma$ -carbon providing stabilisation of the nucleophilic  $\gamma$ -carbon. This “backwards” allylation was again witnessed in aqueous solutions with increased reactivity and selectivity in the allylation of aldehydes<sup>27</sup>. The results of these investigations mirrored similar results from a previous related independent investigation<sup>28</sup>. Huang was one of the first synthetic chemists to appreciate the potential for gallium in organic chemistry<sup>28</sup>. With the objective of increasing regioselectivity in allyl and allenylations Huang *et al.* successfully introduced metallic gallium to the reaction<sup>28</sup>. An *in situ* trimethylsilyl propargyl gallium intermediate thus reacted with a range of aldehydes and ketones in refluxing THF in the presence of KI and LiCl or Lewis acids ( $\text{MgBr}_2$ ,  $\text{BF}_3\text{OEt}_2$ ) and hydrolysing with dilute acid to exclusively afford in high yields the corresponding homopropargylic alcohols<sup>28</sup>.

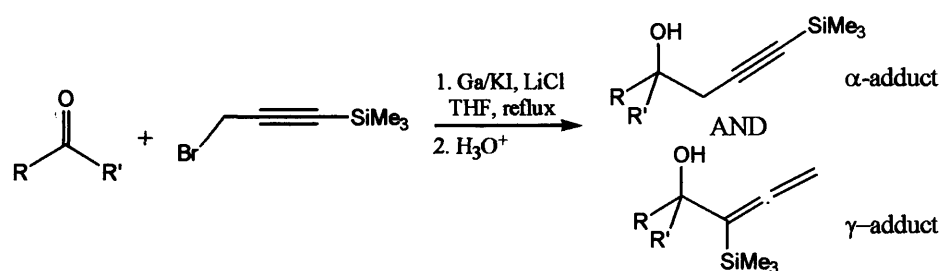


Figure 2.25 – Allylation of aldehydes and ketones via a propargyl gallium intermediate<sup>28</sup>

The  $\alpha$ -adduct is the major product observed in these reactions which we can confidently predict is due to lack of substituents on the  $\gamma$ -carbon. The use of gallium further increases this acetylinic selectivity. Using the same reaction conditions, gallium was able to promote the Barbier type allylation reaction of trimethylsilylallyl bromide with aldehydes and ketones to exclusively afford the  $\alpha$ -adducted homoallyl alcohol<sup>28</sup>. This reaction proved to be stereo-selective towards the *E*-isomer irrespective of the isomer proportion in the trimethylsilyl bromide starting material (Figure 2.26)<sup>28</sup>.



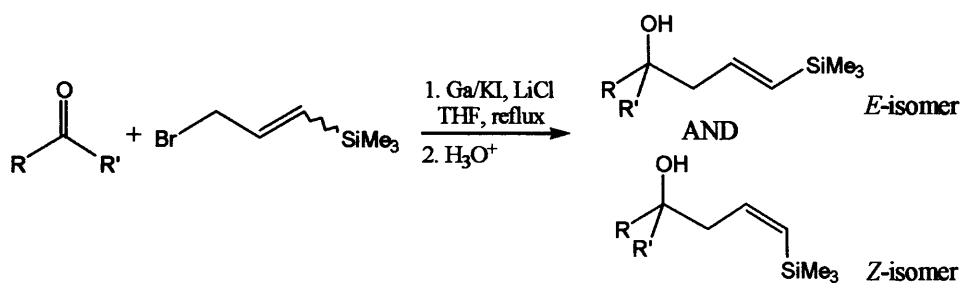


Figure 2.26 – Barbier Allylation of carbonyls with trimethylsilylallyl<sup>28</sup>

All the discussed reactions involve gallium in its elemental metal state or gallium(III) complexes. There have also been investigations carried out on low valent gallium dichloride, a divalent compound (double salt) consisting of a univalent and trivalent gallium,  $\text{Ga(I)[Ga(III)Cl}_4\text{]}^{29}$ . It was hoped this compound would mediate reductive dimerisation of benzaldehyde in a similar manner to that previously discussed with indium<sup>10, 11</sup>. The desired diol expected from this reaction was not afforded. Further investigation revealed the product attained in low yields was as a result of a reductive Friedel-Crafts reaction between benzaldehyde and the solvent benzene<sup>30</sup>. This finding warranted the further attention the Saigo group invested in the reaction, with the introduction of anisole to the reaction. Anisole, being more nucleophilic than benzene was expected to encourage this reaction and hence improve yields. The desired *ortho*- and *para*-benzylanisoles were achieved in 25% and 19% yields; however the unwanted diphenylmethane was also produced in 30% as a hazard of using the benzene solvent system. Removal of benzene from the system afforded more impressive yields (73%), with the slight affinity for the *ortho* substituted product remaining (Figure 2.27)<sup>30</sup>. *Para* substituted products were encouraged by introduction of electron-donating substituents at the *para* position of the aromatic group on the carbonyl. Furthermore, this procedure was successfully repeated with a variety of aromatic, cyclic and aliphatic carbonyls<sup>30</sup>.

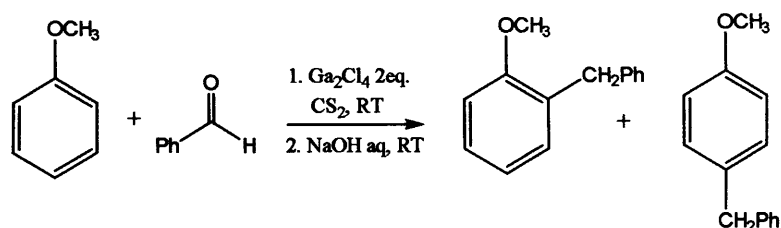


Figure 2.27 – Friedel-Crafts reaction of anisole with benzaldehyde<sup>30</sup>

More recently, the C-C bond coupling reactivity of “GaI” towards a 1,3-diyne has been investigated<sup>31</sup> since this substrate is known to undergo C-C coupling reactions (Figure 2.28)<sup>32</sup>.

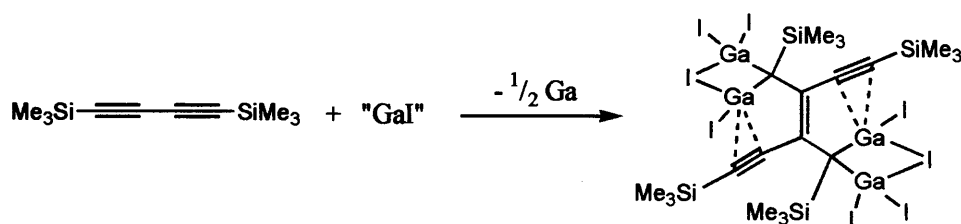


Figure 2.28 – Reaction of 1,3-diyne with gallium(I) iodide<sup>31</sup>

### 2.1.5 Research Proposal

A simple synthesis of gallium(I) iodide was established by Green *et al.* in 1990<sup>34</sup>. The resultant pale green “GaI” powder is prepared from the reaction of metallic gallium with iodine in toluene under ultrasonic conditions at slightly elevated temperatures<sup>34</sup>. It was reported that this compound is insoluble in toluene, however separation from the protecting solvent leads to decomposition<sup>34</sup>. Further investigation has revealed the true nature of the gallium(I) iodide complex as a double salt  $2\text{Ga}^+ [\text{Ga}_2\text{I}_6]^{2-}$ <sup>33</sup>. We were eager to introduce this gallium(I) halide, “GaI”<sup>34</sup> to organic synthesis where the introduction of indium iodide has proved successful. This initially involved Barbier allylations and Reformatsky reactions, however we were keen to extend this investigation further. This eagerness is based on the use of gallium metal proving successful in organic synthesis, promoting and mediating reactions where indium metal is well established. We believe a “GaI” species would behave similarly to indium(I) iodide in the Barbier and Reformatsky reactions<sup>1</sup> though we propose that it will possess a stronger reducing character.

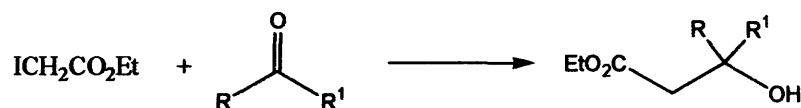
Barbier allylations in particular are simple reactions offering enormous potential with the advent of regio- and stereo-selective reagents. This selectivity is reportedly solvent dependent and hence we were interested in the influence toluene has over these reactions since this medium appears imperative to the stability of “GaI”.

## 2.2 Results and Discussions

Indium metal and its halides have a proven track record as catalysts and mediating reagents in Reformatsky and Barbier type reactions. We were keen to investigate the effectiveness of the reported gallium(I) iodide in these reactions.

### 2.2.1 Reformatsky Reactions with Gallium(I) Iodide

Gallium(I) iodide successfully mediates Reformatsky type reactions of carbonyl compounds to afford the corresponding  $\beta$ -hydroxyesters. These results are best summarised in table 2.1, in the Reformatsky reaction with various carbonyl compounds (*Scheme 2.1*):



*Scheme 2.1 – Reformatsky Reaction of aldehydes and ketones<sup>1</sup>*

Reaction	Substrate	Solvent	Product	Yield (%)
1.		Toluene		21
2.		Toluene		89
3.		Toluene		47
4.		Toluene		99

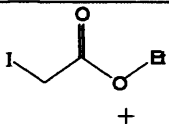
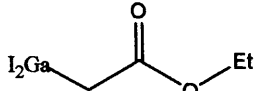
5.	 + "GaI"	Toluene		N/A
----	--	---------	--	-----

Table 2.1 – Reformatsky type reactions as mediated by gallium(I) iodide<sup>1</sup>.

As indicated by table 2.1, gallium(I) iodide successfully mediated the Reformatsky type reactions with a variety of aldehydes and ketones in low to moderate and high yields. Furthermore we are convinced that by allowing these Reformatsky reactions (particularly reactions 1 and 3) to proceed for longer periods we would observe a positive effect on the final yield. This is based on a comparison with Butsugan's results<sup>1</sup> where greater yields were achieved with extended reaction times. All results have been quantified assuming the ionisation potential of the Reformatsky products formed is equal to that of the mesitylene internal standard employed. We believe these reactions proceed via the formation of a gallium(III) intermediate. We investigated the existence of this intermediate with the treatment of gallium(I) iodide with ethyl iodoacetate in toluene in experiment 5. The reaction mixture was left stirring for an extended period of time and analysed by GCMS. The results of the GCMS analysis showed iodine as the only identifiable product. Unfortunately we were unable to isolate the gallium(III) complex:

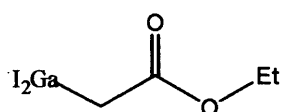


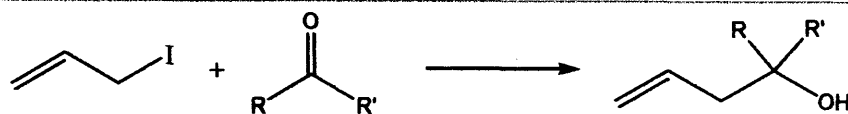
Figure 2.29 – Gallium(III) intermediate

We are confident to hypothesise however that these reactions proceed via this intermediate based on the report by Butsugan<sup>1</sup> who suggested a similar indium intermediate form in the Barbier type allylation as mediated by indium(I) iodide.

<sup>i</sup> The carbonyl compound (0.8mmol) was added to a slurry of "GaI" (1mmol) and ethyliodoacetate (1mmol) in toluene (10 ml). Reaction mixture stirred for 12 hours at room temperature. After acidic work-up the product was extracted with ether and examined with GCMS.

### 2.2.2 Barbier-Type Allylation

Barbier reactions involve the allylation of aldehydes and ketones to form the analogous homoallylic alcohols (*Scheme 2.1*):



*Scheme 2.1 – Barbier Reaction of aldehydes and ketones<sup>1</sup>*

After formation of the “GaI” compound via the reported synthetic pathway, the reagent was then used to mediate the Barbier type allylation of benzaldehyde with allyl iodide<sup>34</sup>. <sup>1</sup>H NMR data of the product proved inconclusive in the determination of a Barbier type homoallyl alcohol product, however GCMS convinced us of the absence of this product. This analytical method, however, did bring to our attention the formation of a product with a relative molecular mass equal to 224. Further investigation revealed by-product formation with a relative molecular mass of 160. Extensive NMR studies undertaken in collaboration with Dr. Guy-Lloyd Jones at Bristol University enabled us to identify the products as isomers of methylphenyl allylated compounds after extensive NMR investigations. Interestingly, these products have previously been reported as by-products in an indium catalysed Friedel-Craft allylation<sup>16</sup>. Furthermore the by-products from our reaction were identified as the Friedel-Craft product Kim *et al.* were attempting to form<sup>16</sup>. A full summary of these reactions is illustrated in table 2.2.

Reaction	Substrate	Solvent	Product	Yield (%)
1.		Toluene	 T1	35
1b.		Toluene		15

2.		Toluene	99	
3.		Toluene	36	
4.		Toluene	37	
5*.		Toluene	No Reaction	0
5b.		Toluene	No Reaction	0
6.		Toluene	19	
6b.		Toluene	6	
6c.		Toluene	8	
7**.		Hexane	84	
8.		Benzene	8	

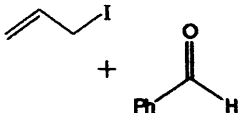
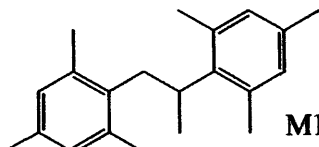
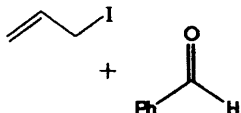
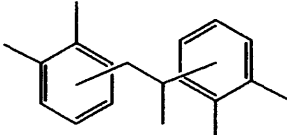
9.		Mesitylene		25
10.		<i>o</i> -xylene		14

Table 2.2 – Gallium(I) iodide mediated coupling and Barbier type reactions. All yields have been calculated with respect to allyl iodide added.<sup>ii</sup>

\* Denotes reaction mediated by metallic gallium.

\*\* Denotes product formed is Barbier-type homoallylic alcohol.

From these results we can conclude that reactions in the toluene solvent yield a bis toluene allylated product. There are however three main isomers of this compound including the isomer recorded in the table as the Barbier product, all of which were observed in equal amounts (Figure 2.30):

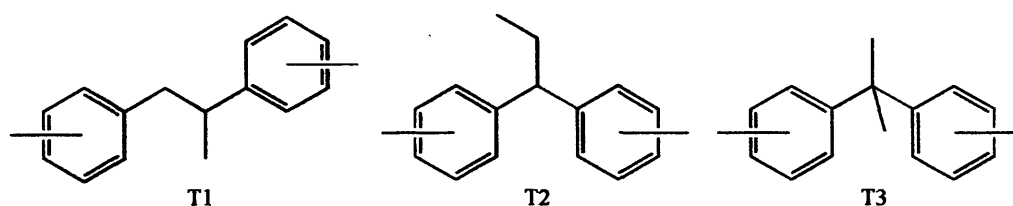


Figure 2.30 – Allylated bis-toluene product isomers, T1 (toluene isomer 1), T2 (Toluene isomer 2) and T3 (toluene isomer 3)

There are six possible isomers each, depending on the position of the methyl group on the aromatic rings. This is excluding the enantiomers generated by the chiral carbon in the T1 and T2 products (Figure 2.30).

<sup>ii</sup> The carbonyl compound (1.1 mmol) was added to a slurry of “GaI” (1.3 mmol) and allyl iodide (1.3 mmol) in toluene (10 ml). Reaction mixture stirred for 12 hours at room temperature. After acidic work-up the product was extracted with ether and examined with GCMS.

Similarly the analogous three main isomers were observed for the benzene allylated product (Figure 2.31).

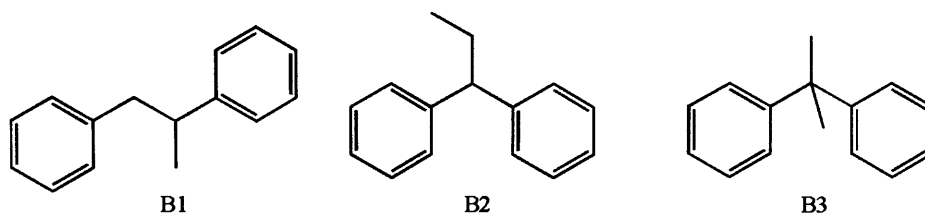


Figure 2.31 – Allylated bis-benzene product isomers, B1 (benzene isomer 1), B2 (benzene isomer 2) and B3 (benzene isomer 3)

In this scenario there are no positional isomers possible due to the absence of methyl groups on the benzene, however enantiomers exist for products B1 and B2 affording five isomers in total. Furthermore this reaction afforded only trace amounts of the B3 product while both the B1 and B2 products were recorded in approximately equal yields.

The mesitylene products formed in reaction 9 enforce similar restraints on the number of positional isomers formed and of the three main isomers we have come to expect, only the M1 product was observed (Figure 2.32). This isomer (M1) affords two enantiomers. The absence of positional isomers from this reaction has led to mesitylene being the focus of our investigations since the NMR spectra it affords are less complicated.

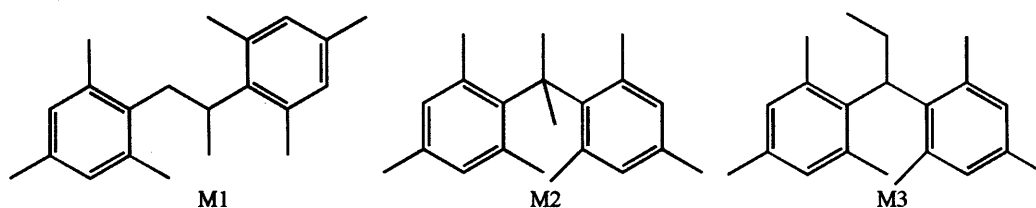


Figure 2.32 – Possible bis-mesitylene allylated product isomers, M1 (mesitylene isomer 1), M2 (mesitylene isomer 2) and M3 (mesitylene isomer 3)

Repetition of this experiment confirmed M1 as the only isomer observed, hence possibly due to steric restraint products M2 and M3 were not witnessed.



Reactions 1 – 4 were run with the aim of forming the Barbier type homo-allyl alcohol and hence the variations in the carbonyl group used. These reactions involved the treatment of the aldehyde or ketone with allyl iodide and “GaI” in toluene. It soon became apparent that the homo-allyl alcohol product was not afforded; this was deduced from the  $^1\text{H}$  NMR and GCMS analysis. It was also clear that the product formed contained two coupled aromatic rings and a propyl group from the allylic reagent. These findings were consistent with the coupling of two-toluene rings, though the exact nature of this coupling was confirmed by endeavours outside of our group<sup>35</sup>. Closer inspection of the GCMS results from these four experiments, however, revealed the consistent synthesis of a by-product being the same in all reactions. Previous work by Kim *et al.* indicated the possible products and by-products similar reactions can afford<sup>16</sup>. Using this reference we were able to identify the by-product from these reactions as the allylated toluene Kim-type compound (Figure 2.33)<sup>16</sup>. The formation of this by-product however is complicated by the three isomers possible.

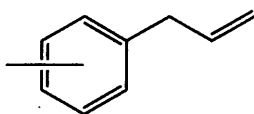


Figure 2.33 – Mono allylated toluene by-product (Kim-type product)<sup>16</sup>

Gallium metal was employed in reaction 5 in an attempt to mediate the reaction with gallium in its elemental form. This was to confirm that the reactions witnessed in experiments 1 – 4 were a true reflection on the reactivity of “GaI” or whether these results were affected by the presence of excess metallic gallium. The fact that no reaction occurred was a very positive result for us, confirming the mediating abilities of “GaI”. In an effort to understand this reaction further we were keen to examine the role of the carbonyl group in the reaction. From existing results it was apparent that there was little difference between the presence of an aldehyde or ketone in the reaction. For these reasons an experiment (reaction 6) was carried out in the absence of a carbonyl group. The results indicate that the reaction is able to proceed successfully without the presence of a carbonyl group. Furthermore it was observed

from this reaction that the ratio of the product to the Kim-type product by-product was doubled.

The original reaction was then repeated in a non-aromatic solvent, hexane (reaction 7). We realised that the Friedel-Crafts type allylation of this saturated compound was impossible and hence hopeful that we would be able to encourage the Barbier type reaction mediated by “Gal”. Analysis of the product found that this was indeed the case and hence gallium(I) iodide behaves similarly to metallic indium and indium(I) iodide and is capable of Barbier type allylation of carbonyl groups to homo allylic alcohols in high yields in non-aromatic solvents. This reaction however does have the restriction of requiring a hexane medium, and hence will only be applicable to hexane soluble carbonyls.

The coupling of unsaturated, unsubstituted rings with a propyl linker is to our knowledge nearly unprecedented. It is worth mentioning that Kim *et al.* makes the only reference to the formation of this type of product which was synthesised in trace amounts as a by-product<sup>16</sup>. We were hopeful of addressing this issue and to investigate the capabilities of gallium iodide as a mediating reagent for aromatic coupling reactions. For these reasons we used the original reaction conditions as in experiment 1 but using benzene as opposed to toluene in experiment 8. Gallium(I) iodide proved its versatility by affording the allylated benzene product with its respective isomers, although the number of regio-isomers was restricted by the absence of methyl groups on the ring. The Kim-type mono allylated by-product was also observed but perhaps more importantly a further by-product was also identified as the iodide equivalent of the chlorinated Kim by-product (Figure 2.34)<sup>16</sup>.

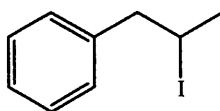


Figure 2.34 – Mono iodoallylated benzene (Kim-type by-product)<sup>16</sup>

The adaptability of this reaction was further investigated by the implementation of another aromatic compound, mesitylene (experiment 9). Again the reaction proceeded

successfully with the moderate yield of the bis(mesitylene)propyl coupled product, the identification of which was made easier by the absence of M2 and M3 isomers and with M1 existing as two enantiomers, compared to the twelve observed with toluene. Furthermore a mono-annulated mesitylene by-product (**2a**) was also observed with a Kim-type iodide by-product (**2b**) analogous to that previously observed in the benzene reaction (experiment 8, Figure 2.35)<sup>16</sup>. Initial attempts within our group to form the mono-annulated mesitylene product in isolation were successful which has enabled us to provide a <sup>1</sup>H NMR analysis of this product.

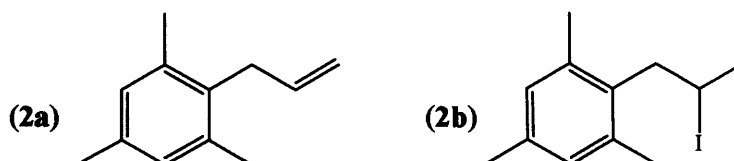


Figure 2.35 – Mono allylated mesitylene by-product (**2a**) (Kim-type product) and the mono iodoallylated mesitylene by-product (**2b**) (Kim-type by-product)<sup>16</sup>

The final reaction (experiment 10) involved the coupling of *ortho*-xylene with allyl iodide. The only identifiable by-product synthesised again was the Kim-type homoallylated *ortho*-xylene product. <sup>1</sup>H NMR spectroscopy of the main product mixture is complicated by the number of isomers possible, eight in total including the enantiomers (Figure 2.36).

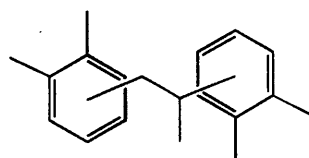


Figure 2.36 – Proposed bis- *ortho*-xylene allylated product

We believe all these reactions proceed via the formation of an allylgallium(III) diiodide intermediate formed by the oxidative addition of gallium(I) iodide to allyl iodide. This intermediate is analogous to the allylindium(III) diiodide as proposed by Butsugan *et al.* in the Barbier reactions involving indium(I) iodide (Figure 2.37)<sup>1</sup>.

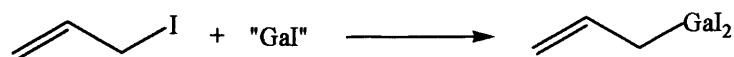


Figure 2.37 – Allylgallium(III) diiodide intermediate<sup>1</sup>

## 2.3 Conclusions

We have extended the chemistry of gallium(I) iodide while providing a useful synthetic reagent for organic chemistry with the coupling of a variety of aromatic substrates with allyl fragments. We have also revealed the ability of the gallium(I) iodide reagent to mediate Barbier type allylations. Furthermore we have proved the versatility of this “Gal” reagent with its implementation into the Reformatsky type reaction with aldehydes and ketones. The Reformatsky reaction appears to proceed with no addition to the aromatic ring of the aromatic solvent.

## 2.4 Future Work

We believe an investigation into the diastereo-selectivity of Reformatsky and Barbier type reactions mediated by “Gal” is warranted. We would also wish to extend these investigations with the determination of the diastereo-selectivity of Kim type allyl aryl-coupling reactions with gallium(I) iodide in a variety of aromatic solvents. Furthermore, although we have proved that metallic gallium is incapable of mediating Barbier and Reformatsky type reactions in toluene we have not repeated these studies in alternative media such as water and THF. Such studies could also induce Barbier type products in the Barbier reactions and extend the research initiated by Wang *et al*<sup>25</sup>. In relation to this we would relish the opportunity to examine the use of the gallium(I) iodide reagent in Barbier and Reformatsky type reactions with aldimine substrates.

## 2.5 Experimental

All manipulations requiring inert atmospheres were carried out using standard Schlenk techniques under an atmosphere of high purity argon. The solvents/substrates hexane, toluene, benzene, mesitylene and *ortho*-xylene were distilled over sodium prior to use.  $^1\text{H}$  and  $^{13}\text{C}$  NMR spectra were recorded on Bruker DPX 400 or Jeol Eclipse 300 spectrometers in deuterated solvents and referenced to the residual  $^1\text{H}$  NMR resonances of the solvent used. GCMS analysis was undertaken on a Hewlett Packard 5890 spectrometer under inert conditions. Gallium metal, iodine and concentrated HCl were purchased from Aldrich. Gallium(I) iodide was prepared via literature method<sup>34</sup>. All other reagents were used as received.

### 2.5.1 General Synthesis of Gallium(I) Iodide<sup>34</sup>

To an ingot of gallium (0.094 g,  $1.35 \times 10^{-3}$  moles) in toluene (10 mls) was added iodine (0.1711 g,  $6.75 \times 10^{-4}$  moles). This was then sonicated in a sonic bath with warm water for 2 hrs, after which a white/pale-green precipitate had formed<sup>34</sup>. This was then used as the gallium(I) iodide reagent to which the relevant substrates were added. In reactions where toluene was not the reaction media or substrate it was removed via filtration and the “GaI” precipitate washed with hexane and then the hexane was removed by combination of filtering and drying *in vacuo*. Fresh hexane, benzene, mesitylene or *ortho*-xylene was then added as the reaction medium.

#### 2.5.2.1 General Reformatsky Type Reaction

Reactions followed a slight modification of a published procedure<sup>1</sup>, whereby ethyl iodoacetate (0.19 mls,  $1 \times 10^{-3}$  moles) and the carbonyl compound ( $8.4 \times 10^{-4}$  moles) were added to a stirred suspension of “GaI” ( $1 \times 10^{-3}$  moles) in toluene (10 mls). This was allowed to react overnight, before being quenched with dilute HCl and extracted into ether. The ether extracts were combined and washed with water and brine, dried over  $\text{MgSO}_4$  before filtering and removal of volatiles *in vacuo*. Product yield was then recorded prior to a 0.1 g of product mixture being removed for GCMS analysis.

**2.5.2.2  $\beta$ -phenyl hydroxyester (Reformatsky Product as observed in table 2.1 reaction 1).** Yield 0.293g, 20.68%.  $^1\text{H}$  NMR (400 MHz,  $\text{C}_6\text{D}_6$ , 300 K,  $\delta/\text{ppm}$ ) 1.19 (t, 3H,  $\text{CH}_3$ , J 7.1 Hz), 2.64 (dd, 2H,  $\text{CH}_2$ , J 12.3 Hz, 4.1 Hz), 2.7 (dd, 2H,  $\text{CH}_2$ , J 7.6 Hz, 8.9 Hz), 3.37 (br, 1H, OH), 4.12 (q, 2H,  $\text{CH}_2$ , J 7.1 Hz), 5.1 (dd, 1H, CH, J 4.1 Hz, 4.8 Hz), 7.17 – 7.55 (m, 5H, *ar*-H). GCMS Retention time mins, Toluene 6.15 min; Mesitylene 12.68 min; ethyl iodoacetate 13.18 min, Product 23.32 mins, APCI  $m/z$  (%), 43 ( $\{\text{MI-C}_6\text{H}_5\text{CHOHCH}_2\text{OC}\}^+$ , 73%), 77 ( $\{\text{MI-CHOHCH}_2\text{OCOCH}_2\text{CH}_3\}^+$ , 100%), 88 ( $\{\text{MI-OHCH}_2\text{OCOCH}_2\text{CH}_3\}^+$ , 10%), 107 ( $\{\text{MI-CH}_2\text{OCOCH}_2\text{CH}_3\}^+$ , 82%), 120 ( $\{\text{MI-OCOCH}_2\text{CH}_3\}^+$ , 10%), 131 ( $\{\text{MI-OOCH}_2\text{CH}_3\}^+$ , 18%), 147 ( $\{\text{MI-OCH}_2\text{CH}_3\}^+$ , 8%), 194 ( $\{\text{Molecular Ion}\}^+$ , 10%).

**2.5.2.3  $\beta$ -phenyl methyl hydroxyester (Reformatsky Product as observed in table 2.1 reaction 2).** Yield 0.138g, 88.67%.  $^1\text{H}$  NMR (400 MHz,  $\text{C}_6\text{D}_6$ , 300 K,  $\delta/\text{ppm}$ ) 1.02 (t, 3H,  $\text{CH}_3$ , J 7.1 Hz), 1.14 (dd, 2H,  $\text{CH}_2$ , J 7 Hz, 5.8 Hz), 1.183 (dd, 2H,  $\text{CH}_2$ , J 2.4 Hz, 2.6 Hz), 3.37 (br, 1H, OH), 3.95 (q, 2H,  $\text{CH}_2$ , J 7.12 Hz), 4.08 (dd, 1H, CH, J 1.86 Hz, 5.23 Hz), 7.04 – 7.38 (m, 5H, *ar*-H). GCMS Retention time mins, Toluene 11.85 min; Mesitylene 17.48 min; Acetophenone 19.70 min, Product 27.20 mins, APCI  $m/z$  (%), 45 ( $\{\text{MI-C}_6\text{H}_5\text{CCH}_3\text{OHCH}_2\text{CO}\}^+$ , 1.8%), 57 ( $\{\text{MI-C}_6\text{H}_5\text{CCH}_3\text{OHCH}_2\text{O}\}^+$ , 1.4%), 73 ( $\{\text{MI-C}_6\text{H}_5\text{CCH}_3\text{OHCH}_2\}^+$ , 1.4%), 77 ( $\{\text{MI-CH}_3\text{OHCCH}_2\text{OCOCH}_2\text{CH}_3\}^+$ , 26%), 85 ( $\{\text{MI-HHCOHCH}_3\text{CH}_2\text{CH}_3\}^+$ , 3%), 87 ( $\{\text{MI-COHCH}_3\text{CH}_2\text{CH}_3\}^+$ , 1.4%), 105 ( $\{\text{MI-OHCH}_2\text{OCOCH}_2\text{CH}_3\}^+$ , 55%), 121 ( $\{\text{MI-CH}_2\text{OCOCH}_2\text{CH}_3\}^+$ , 69%), 147 ( $\{\text{MI-OOCH}_2\text{CH}_3\}^+$ , 5%), 192 ( $\{\text{MI-OH}\}^+$ , 11%).

**2.5.2.4  $\beta$ -methylphenyl methyl hydroxyester (Reformatsky Product as observed in table 2.1 reaction 3).** Yield 0.259g, 46.72%.  $^1\text{H}$  NMR (400 MHz,  $\text{C}_6\text{D}_6$ , 300 K,  $\delta/\text{ppm}$ ) 1.05 (t, 3H,  $\text{CH}_3$ , J 7.1 Hz), 1.44 (s, 1H,  $\text{CH}_3$ ), 2.23, 2.32, 2.48 (s, 1H,  $\text{CH}_3$ ), 2.78 (dd, 2H,  $\text{CH}_2$ , J 15.89 Hz, 59.72 Hz), 3.946 (q, 2H,  $\text{CH}_2$ , 3.6 Hz), 7.04 – 7.29 (m, 3H, *ar*-H), 7.77 (m, 1H, *ar*-H). GCMS Retention time mins, Toluene 6.13 min; Mesitylene 12.67 min; 4-methylacetophenone 17.60 min, Product 24.30 mins, APCI  $m/z$  (%), 45 ( $\{\text{MI-CH}_3\text{C}_6\text{H}_4\text{CCH}_3\text{OHCH}_2\text{CO}\}^+$ , 8.6%), 77 ( $\{\text{C}_6\text{H}_4\text{H}\}^+$ , 8.2%), 91 ( $\{\text{MI-C}_6\text{H}_4\text{CH}_3\}^+$ , 75.5%), 115 ( $\{\text{MI-OCC}_6\text{H}_3\text{C}\}^+$ , 16.8%), 119 ( $\{\text{MI-OCC}_6\text{H}_4\text{CH}_3\}^+$ ,

100%), 135 ( $\{\text{MI-C}_2\text{H}_5\text{CO}_2\text{CH}_2\}^+$ , 30.9%), 159 ( $\{\text{MI-C}_2\text{H}_5\text{O}_2\}^+$ , 10.91%), 175 ( $\{\text{MI-(CH}_3)_2\text{OH}\}^+$ , 2.73%), 207 ( $\{\text{MI-CH}_2\}^+$ , 6.4%).

**2.5.2.5  $\beta$ -isobutylmethylalcohol hydroxyester (Reformatsky Product as observed in table 2.1 reaction 4).** Yield 0.216g, 122.62%.  $^1\text{H}$  NMR (400 MHz,  $\text{C}_6\text{D}_6$ , 300 K,  $\delta/\text{ppm}$ ) 1.05 (t, 3H,  $\text{CH}_3$ , J 7.1 Hz), 1.44 (s, 1H,  $\text{CH}_3$ ), 2.23, 2.32, 2.48 (s, 1H,  $\text{CH}_3$ ), 2.78 (dd, 2H,  $\text{CH}_2$ , J 15.89 Hz, 59.72 Hz), 3.946 (q, 2H,  $\text{CH}_2$ , 3.6 Hz), 7.04 – 7.29 (m, 3H, *ar*-H), 7.77 (m, 1H, *ar*-H). GCMS Retention time mins, Toluene 11.87 min; Mesitylene 17.50 min; Iodoethylacetate 17.82 min, Product 22.22 mins, APCI  $m/z$  (%), 43 ( $\{\text{CH}(\text{CH}_3)_2\}^+$ ,  $\{\text{OCCH}_3\}^+$  100%), 57 ( $\{\text{MI-H}_3\text{CCH}_2\text{OOCOCH}_2\text{COHCH}_3\}^+$ , 29%), 69 ( $\{\text{MI-CH}_3\text{CH}_2\text{OCOCH}_2\text{COHCH}_3\}^+$ , 3.2%), 85 ( $\{\text{MI-2HHOCCH}_3\text{CH}_2\text{CH}(\text{CH}_3)_2\}^+$ , 33%), 87 ( $\{\text{MI-HOCCH}_3\text{CH}_2\text{CH}(\text{CH}_3)_2\}^+$ , 1.8%), 101 ( $\{\text{MI-CH}_3\text{CH}_2\text{OCOCH}_2\}^+$ , 12%), 125 ( $\{\text{MI-2HOHCH}(\text{CH}_3)_2\}^+$ , 2.7%), 131 ( $\{\text{MI-CH}_2\text{CH}(\text{CH}_3)_2\}^+$ , 36%), 173 ( $\{\text{MI-OH}\}^+$ , 3.6%).

### 2.5.3.1 General Aryl Ring Allyl Coupling Reaction<sup>1, 16</sup>

These syntheses followed a slight modification of a published method<sup>1</sup>. To a stirred slurry of “Gal” ( $1.35 \times 10^{-3}$  moles) was added allyl iodide (0.1233 mls,  $1.35 \times 10^{-3}$  moles). This was followed by the addition of the aldehyde or ketone ( $1.125 \times 10^{-3}$  moles) and left stirring overnight. After which the reaction was quenched with dilute HCl (1M, 5 mls). The product was then extracted into ether (3 x 30 mls), washed with thiosulphate (30 mls), water (30 mls) and brine (30 mls). Drying of the product was completed by  $\text{MgSO}_4$  before filtering and removal of volatiles *in vacuo*. Product yield was then recorded prior to a 0.1 g of product being removed for GCMS analysis.

**2.5.3.2 Toluene Product (as observed in table 2.2 reactions 1, 1b, 2, 3, 4, 6, 6b and 6c).** Yield 0.407g, 0.341g, 0.490g, 0.446g, 0.226g, 0.363g, 0.199g, 0.290g (Product yields as shown in table 2.2).  $^1\text{H}$  NMR (400 MHz,  $\text{C}_6\text{D}_6$ , 300 K,  $\delta/\text{ppm}$ ) 2.055 (d, 3H,  $\text{CH}_3$  linker), 2.150 – 2.232 (s, 18H, *ar*- $\text{CH}_3$ ), 2.659 – 2.844 (dd, 1H, diastereotopic  $\text{CH}_2$ ), 3.152 (m, 1H, chiral CH), 6.881-7.245 (m, 4H, *ar*-H). GCMS Retention time mins, Toluene 6.15 min; Mesitylene 12.70 min; By-products 13.98 – 15.07 min, APCI

*m/z* (%): 41 ( $\text{CH}_2\text{CHCH}_2$ , 15.5%), 77 ( $\text{C}_6\text{H}_5$ , 12.7%), 91 ( $\text{C}_6\text{H}_5\text{CH}_3$ , 36.4%), 103 ( $\text{C}_6\text{H}_5\text{CH}_3\text{C}$ , 4.1%), 115 ( $\text{C}_6\text{H}_5\text{CH}_3\text{CC}$ , 11.4%), 117 ( $\text{C}_6\text{H}_5\text{CH}_3\text{CH}_2\text{C}$ , 19.5%), 119 ( $\text{C}_6\text{H}_5\text{CH}_3\text{CH}_2\text{CH}+\text{H}^+$ , 100%), 134 ( $\{\text{Molecular Ion}\}+2\text{H}^+$ ); Product 26.78 – 27.62 mins, APCI *m/z* (%): 41 ( $\text{CH}_2\text{CHCH}_2$ , 3.6%), 77 ( $\text{C}_6\text{H}_4+\text{H}^+$ , 20%), 78 ( $\text{C}_6\text{H}_4+2\text{H}^+$ , 6.4%), 91 ( $\text{C}_6\text{H}_4\text{CH}_3$ , 26.4%), 105 ( $\text{C}_6\text{H}_4\text{CH}_3\text{CH}_2$ , 25.9%), 119 ( $\text{C}_6\text{H}_4\text{CH}_3\text{CHCH}_3$ , 100%), 120 ( $\text{C}_6\text{H}_4\text{CH}_3\text{CHCH}_3+\text{H}^+$ , 8.6%), 195 ( $\text{MI}-2\text{CH}_3+\text{H}^+$ , 29.1%), 196 ( $\text{MI}-2\text{CH}_3$ , 4.1%), 224 ( $\{\text{MI}\}$ , 7.3%).

#### 2.5.3.3 Barbier Product from Hexane 7

Yield 0.154 g (84%).  $^1\text{H}$  NMR (400 MHz,  $\text{C}_6\text{D}_6$ , 300 K,  $\delta/\text{ppm}$ ) 9.929 (s, 1H, OH). GCMS Retention time mins; Mesitylene 17.27 min; Product 22.87 min, APCI *m/z* (%): 41 ( $\text{CH}_2\text{CHCH}_2$ , 5.5%), 51 ( $\text{CH}_2\text{CHCH}_2\text{C}-2\text{H}$ , 13.2%), 52 ( $\text{CH}_2\text{CHCH}_2\text{C}-\text{H}$ , 2.3%), 77 ( $\text{C}_6\text{H}_5$ , 50.9%), 91 ( $\text{C}_6\text{H}_5\text{CH}+\text{H}^+$ , 2.7%), 105 ( $\text{C}_6\text{H}_5\text{CHO}$ , 8.2%), 107 ( $\text{C}_6\text{H}_5\text{CHOH}+\text{H}^+$ , 100%), 127 ( $\text{MI}-\text{OH}+4\text{H}^+$ , 1%), 128 ( $\text{MI}-\text{OH}+3\text{H}^+$ , 1.4%), 129 ( $\{\text{MI}-\text{OH}+2\text{H}\}^+$ , 1%).

#### 2.5.3.4 Benzene Product 8

Yield 0.206g (8%).  $^1\text{H}$  NMR (400 MHz,  $\text{C}_6\text{D}_6$ , 300 K,  $\delta/\text{ppm}$ ) 1.133 (d, 3H,  $^1J_{\text{HH}}$  6.76 Hz,  $\text{CH}_3$  linker), 2.656 (dd, 1H,  $^1J_{\text{HH}}$  7.96 and 7.96 Hz,  $^2J_{\text{HH}}$  4.88 Hz, diastereotopic  $\text{CH}_2$ ), 2.813 – 2.920 (dd, 1H, diastereotopic  $\text{CH}_2$  and m, 1H, chiral CH), 7.045 – 7.192 (m, 10H, *ar*-H). GCMS Retention time mins; Mesitylene 13.08 min; Product 24.97 mins, APCI *m/z* (%): 41 ( $\text{CH}_2\text{CHCH}_2-\text{H}$ , 3.2%), 77 ( $\text{C}_6\text{H}_5$ , 11.8%), 91 ( $\text{C}_6\text{H}_5\text{CH}_2$ , 12.3%), 105 ( $\text{C}_6\text{H}_5\text{CHCH}_3$ , 100%), 115 ( $\text{C}_6\text{H}_5\text{CHCH}_3\text{C}-2\text{H}$ , 5%), 178 ( $\text{MI}-\text{CH}_3$ , 1%), 196 ( $\{\text{Molecular Ion}\}^+$ ).

#### 2.5.3.5 Mesitylene Product (as observed in table 2 reaction 9)

Yield 0.303g (25%).  $^1\text{H}$  NMR (400 MHz,  $\text{C}_6\text{D}_6$ , 300 K,  $\delta/\text{ppm}$ ) 1.25 (d, 3H,  $\text{CH}_3$  linker), 1.939 (s), 2.11 (s, 6H, *ar*- $\text{CH}_3$ ), 2.15 (s, 6H, *ar*- $\text{CH}_3$ ), 2.19 (s, 6H, *ar*- $\text{CH}_3$ ), 2.476 (s), 2.88 (dd, 1H,  $^1J_{\text{HH}}$  6.35 and 6.36 Hz,  $^2J_{\text{HH}}$  7.29 Hz, diastereotopic  $\text{CH}_2$ ), 3.01 (dd, 1H,  $^1J_{\text{HH}}$  7.66 and 7.62 Hz,  $^2J_{\text{HH}}$  5.95 Hz, diastereotopic  $\text{CH}_2$ ), 3.30 (m, 1H, chiral CH), 6.658-6.74 (m, 4H, *ar*-H). GCMS Retention time mins; Mesitylene 12.97 min; Mono-annulated product 19.20 – 19.47 mins, APCI *m/z* (%): 41 ( $\text{CH}_2\text{CHCH}_2$ ,



9.5%), 77 ( $C_6H_2+3H$ , 17.3%), 91 ( $C_6H_2CH_3+2H$ , 37.3%), 105 ( $C_6H_2(CH_3)_2+H$ , 24.5%), 119 ( $C_6H_2(CH_3)_3$ , 23.6%), 131 ( $C_6H_2(CH_3)_3C$ , 8.2%), 145 ( $C_6H_2(CH_3)_3CH_2C$ , 11.4%), 147 ( $C_6H_2(CH_3)_3CH_2CH+H$ , 100%), 148 ( $C_6H_2(CH_3)_3CH_2CH+2H$ , 14.1%), 162 ( $MI+2H^+$ , 33%); By-product 29.72 min, APCI  $m/z$  (%): 41 ( $CH_2CHCH_2$ , 14.5%), 77 ( $C_6H_2+3H$ , 5%), 91 ( $C_6H_2CH_3+2H$ , 8.6%), 105 ( $C_6H_2(CH_3)_2+H$ , 10%), 133 ( $C_6H_2(CH_3)_3CH_2$ , 10.9%), 147 ( $C_6H_2(CH_3)_3CH_2CH+H$ , 100%), 166 ( $CH_2CHICH_3-H^+$ , 1.4%), 286 ( $\{MI - 2H^+\}$ , 1.8%). Product 32.22 – 32.57 min, APCI  $m/z$  (%): 41 ( $CH_2CHCH_2$ , 10.5%), 77 ( $C_6H_2+3H$ , 6.4%), 91 ( $C_6H_2CH_3+2H$ , 19.5%), 105 ( $C_6H_2(CH_3)_2+H$ , 14.5%), 117 ( $C_6H_2(CH_3)_3-2H^+$ , 17.3%), 133 ( $C_6H_2(CH_3)_3CH_2$ , 23.6%), 147 ( $C_6H_2(CH_3)_3CHCH_3$ , 100%), 148 ( $C_6H_2(CH_3)_3CHCH_3+H^+$ , 11.4%), 280 ( $\{Molecular\ Ion\}$ , 3.2%).

#### 2.5.3.6 Mono annulated Mesitylene By-Product 9a

$^1H$  NMR (400 MHz,  $C_6D_6$ , 300 K,  $\delta/ppm$ ) 1.809 (d, 3H,  $CH_3$  linker), 2.131 (s, 3H,  $p-CH_3$ ), 2.196 (s, 6H,  $o-CH_3$ ), 3.159 (dd, 1H,  $^1J_{HH}$  9.82 and 9.83 Hz,  $^2J_{HH}$  4.35 Hz, diastereotopic  $CH_2$ ), 3.351 (dd, 1H,  $^1J_{HH}$  5.59 and 5.66 Hz,  $^2J_{HH}$  8.64 Hz, diastereotopic  $CH_2$ ), 4.307 (m, 1H, chiral CH), 6.679-6.731 (m, 4H,  $^2J_{HH}$  6.405 OR 3.242 Hz,  $m-H$ ).

#### 2.5.3.7 *ortho*-Xylene Product 10

Yield 0.307g (14%).  $^1H$  NMR (400 MHz,  $C_6D_6$ , 300 K,  $\delta/ppm$ ) 1.07 (d, 3H,  $CH_3$  bridging), 1.95 (d), 2.10 (s, 6H,  $ar-CH_3$ ), 2.11 (s, 6H,  $ar-CH_3$ ), 2.39 – 2.67 (2 dd, 2H, diastereotopic  $CH_2$  gps), 2.80 (m, 1H, chiral CH gp), 3.19 (m, 1H, chiral CH gp), 6.74 – 7.19 (m, 8H,  $ar-H$ ). GCMS Retention time mins; *o*-Xylene 12.93 min; Mesitylene 17.27 min; By-Product 17.52 – 17.95 min, APCI  $m/z$  (%): 41 ( $CH_2CHCH_2$ , 7.3%), 77 ( $C_6H_3 + 2H^+$ , 21%), 89 ( $C_6H_3CH_3 - H^+$ , 4.1%), 91 ( $C_6H_3CH_3 + H^+$ , 41%), 102 ( $C_6H_3(CH_3)_2 - 3H^+$ , 3.2%), 103 ( $C_6H_3(CH_3)_2 - 2H^+$ , 9.1%), 105 ( $C_6H_3(CH_3)_2$ , 36%), 107 ( $C_6H_3(CH_3)_2 + 2H^+$ , 3.6%), 115 ( $C_6H_3(CH_3)_2C - 2H^+$ , 21.4%), 119 ( $C_6H_3(CH_3)_2CH_2$ , 20%), 120 ( $C_6H_3(CH_3)_2CH_2 + H^+$ , 2.3%), 128 ( $C_6H_3(CH_3)_2CH_2C - 3H^+$ , 3.6%), 131 ( $C_6H_3(CH_3)_2CH_2C$ , 12%), 133 ( $C_6H_3(CH_3)_2CHCH_3$ , 100%), 134 ( $C_6H_3(CH_3)_2CHCH_3 + H^+$ , 12%), 148 ( $MI + H^+$ , 36%); Product 30.85 – 31.49 min, APCI  $m/z$  (%): 41 ( $CH_2CHCH_2$ , 4.5%), 77 ( $C_6H_3 + 2H^+$ , 11%), 91 ( $C_6H_3CH_3 + H^+$ ,

23%), 105 ( $\text{C}_6\text{H}_3(\text{CH}_3)_2$ , 6.4%), 119 ( $\text{C}_6\text{H}_3(\text{CH}_3)_2\text{CH}_2$ , 21%), 131 ( $\text{C}_6\text{H}_3(\text{CH}_3)_2\text{CH}_2\text{C}$ , 5.9%), 133 ( $\text{C}_6\text{H}_3(\text{CH}_3)_2\text{CHCH}_3$ , 100%), 134 ( $\text{C}_6\text{H}_3(\text{CH}_3)_2\text{CHCH}_3 + \text{H}^+$ , 13%), 252 ( $\{\text{MI}\}$ , 5.5%).

## 2.6 References

- <sup>1</sup> S. Araki, H. Ito, N. Katsumura, Y. Butsugan, *J. Organomet. Chem.*, **1989**, 369, 291.
- <sup>2</sup> P. Cintas, *Synlett.*, **1995**, 1087.
- <sup>3</sup> K.K. Chauhan, C.G. Frost, *J. Chem. Soc., Perkin Trans. 1*, **2000**, 3015.
- <sup>4</sup> B.C. Ranu, *Eur. J. Org. Chem.*, **2000**, 2347.
- <sup>5</sup> S. Araki, H. Ito, Y. Butsugan, *J. Org. Chem.*, **1988**, 53, 1831.
- <sup>6</sup> S. Araki, H. Ito, Y. Butsugan, *Synth. Commun.*, **1988**, 18, 453.
- <sup>7</sup> X.-H. Yi, Y. Meng, X.-G. Hua, C.-J. Li, *J. Org. Chem.*, **1998**, 63, 7472.
- <sup>8</sup> B.C. Ranu, A. Majee, *Chem. Commun.*, **1997**, 1225.
- <sup>9</sup> H.J. Lim, G. Keum, S.B. Kang, B.Y. Chung, Y. Kim, *Tet. Lett.*, **1998**, 39, 4367.
- <sup>10</sup> H.S. Baek, S.J. Lee, B.W. Hoo, J.J. Ko, S.H. Kim, J.H. Kim, *Tet. Lett.*, **2000**, 41, 8097.
- <sup>11</sup> N. Kalyanam, G.V. Rao, *Tet. Lett.*, **1993**, 34, 1647.
- <sup>12</sup> V.J. Bryan, T.H. Chan, *Tet. Lett.*, **1996**, 37, 5341.
- <sup>13</sup> L.A. Paquette, J.L. Mendez-Andino, *J. Org. Chem.*, **1998**, 63, 1831.
- <sup>14</sup> C.-J. Li, D.-I. Chen, *Synlett.*, **1999**, 735.
- <sup>15</sup> J. Augé, N. Lubin-Germain, A. Thiaw-Woaye, *Tet. Lett.*, **1999**, 40, 9245.
- <sup>16</sup> H.J. Lim, G. Kjeum, S.B. Kang, Y. Kim, B.Y. Chung, *Tet. Lett.*, **1999**, 40, 1547.
- <sup>17</sup> McMurray, *Organic Chemistry*, 4<sup>th</sup> Ed., **1996**, Chpt 16, pg 579.
- <sup>18</sup> S. Araki, S.J. Jin, Y. Idol, Y. Butsugan, *Bull. Chem. Soc. Jpn.*, **1992**, 65, 1736.
- <sup>19</sup> X.R. Li, T.P. Loh, *Tetrahedron Asym.*, **1996**, 7, 1535.
- <sup>20</sup> T.-P. Loh, J. Pei, M. Lin, *Chem. Commun.*, **1996**, 2315.
- <sup>21</sup> G. Babu, T. Perumal, *Tetrahedron*, **1998**, 54, 1627.
- <sup>22</sup> J. Yang, C.-J. Li, *Synlett.*, **1999**, 717.
- <sup>23</sup> M.J.S. Gynane, L.G. Waterworth, I.J. Worrall, *Inorg. Nucl. Chem. Lett.*, **1973**, 9, 543.
- <sup>24</sup> S. Araki, T. Kamei, T. Hirashita, H. Yamamamura, *Org. Lett.*, **2000**, 2, 847.
- <sup>25</sup> Z. Wang, S. Yuan, C.-J. Li, *Tet. Lett.*, **2002**, 43, 5097.
- <sup>26</sup> D.D. Laskar, M. Gohain, D. Prajapati, J.S. Sandhu, *New J. Chem.*, **2002**, 26, 193.
- <sup>27</sup> T. Tsuji, S.-i. Usuga, H. Yorimitsu, H. Shinnokubo, S. Matsubara, K. Oshima, *Chem. Lett. Chem. Soc. Jpn.*, **2002**, 2.
- <sup>28</sup> Y. Han, Y.-Z. Huang, *Tet. Lett.*, **1994**, 35, 9433.

- 
- <sup>29</sup> L.A Woodward, G. Garton, H.L. Roberts, *J. Chem. Soc.*, **1956**, 3723.
- <sup>30</sup> Y. Hashimoto, K. Hirata, N. Kihara, M. Hasegawa, K. Saigo, *Tet. Lett.*, **1992**, 33, 6351.
- <sup>31</sup> R.J. Baker, C. Jones, *Chem. Commun.*, **2003**, 390.
- <sup>32</sup> U. Rosenthal, P.M. Pellney, F.G. Kirchbauer, V.V. Burkalov, *Acc. Chem. Res.*, **2000**, 33, 119.
- <sup>33</sup> A. Schnepf, C.U. Doriat, E. Möllhausen, H. Schnöckel, *Chem. Commun.*, **1997**, 2111.
- <sup>34</sup> M.L.H. Green, P. Mountford, G.J. Smout, S.R. Speel, *Polyhedron*, **1990**, 9, 2763.
- <sup>35</sup> G. Lloyd-Jones, Bristol University, **2003**.

## CHAPTER 3

### Synthesis of s- and p-Block Formamidinate Complexes

#### 3.1 Introduction

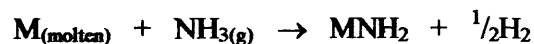
##### 3.1.1 Group 1 Amides

Alkali metal amides are complexes containing a group 1 metal bonded to an amide ligand,  $\text{NR}_2$ , where the R groups are not necessarily equivalent, varying from hydrogen to the alkyls, aryls and silyls.

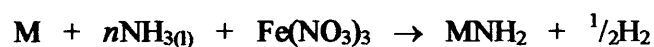
The nature of the M-N bond has been the topic of investigation in previous years, with numerous textbooks describing it as having an appreciable covalent character. However, it is now generally accepted that it is predominately ionic. The misinterpretation of this bond is encouraged by the physical properties of complexes containing it, such as low melting points and solubility's in hydrocarbon/non polar solvents. These characteristics, however, are very misleading since they are attributed to the overall size and shape of the units making up these complexes.

##### 3.1.1.1 Preparation

Synthesis of the group 1 amides, where both R groups are hydrogen, involves reaction of the metal with ammonia. Passing gaseous ammonia over the molten metal with heating to  $350\text{ }^\circ\text{C}^1$  can achieve this:

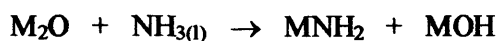


Alternatively, the metal can be dissolved in liquid ammonia, in the presence of a catalyst that accelerates the formation of the metal amide:



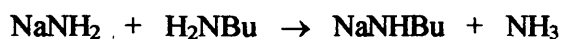
The catalyst's role is as an H<sub>2</sub> acceptor, allowing the reaction to proceed at room temperature<sup>2</sup>.

Other preparatory routes include the reaction of a metal oxide with liquid ammonia<sup>3</sup>:

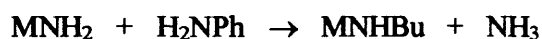


On heating, these amides decompose to form the M<sub>2</sub>NH imide, which is followed by decomposition to the M<sub>3</sub>N nitride after further heating<sup>2</sup>.

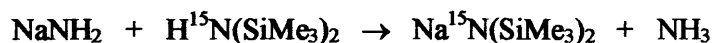
Synthesis of alkali metal amides can be achieved by reacting NaNH<sub>2</sub> with certain primary and secondary amines in toluene<sup>4</sup>:



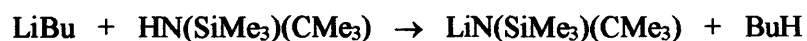
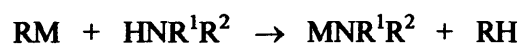
Aromatic amines are more readily metallated by alkali metals in benzene<sup>5</sup>:



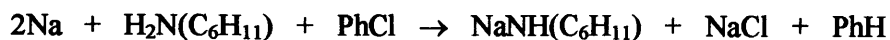
Sodium bis(trimethylsilyl)amide, a common commercial reagent is made via a similar route, using a <sup>15</sup>N-label to monitor the process<sup>6</sup>:



However, a more convenient way of forming these alkyl, aryl and silyl alkali metal amides is in the reaction of metal alkyls with primary and secondary amines at low temperatures<sup>7, 8</sup>:

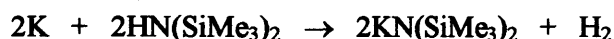
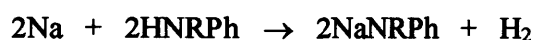


Alternatively, the metal can be reacted with primary or secondary amines in the presence of an unsaturated organic compound.

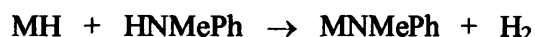


As shown, the unsaturated organic compounds benzylethene<sup>9</sup> and chlorobenzene<sup>10</sup> respectively act as hydrogen acceptors.

It has also been reported that secondary amines can be metallated by alkali metals in liquid ammonia<sup>11, 12</sup>:



Furthermore, sodium and potassium hydrides in toluene can metallate primary and secondary amines<sup>13</sup>:



### 3.1.1.2 Structure and Bonding

The structure of metal amides cannot be fully appreciated or comprehended until we are familiar with and have a basic understanding of the structures formed with the metal imides. Lithium metal imides  $[\text{RR}^1\text{C}=\text{NLi}]_n$  have a planar ( $\text{sp}^2$ ) nitrogen centre as dictated by the  $\text{C}=\text{N}$  double bond. This favours the formation of  $(\text{LiN})_6$  hexamers. These hexamers comprise a  $\text{Li}_6\text{N}_6$  cluster skeleton formed by the stacking of two slightly puckered heterocyclic eclipsing  $\text{Li}_3\text{N}_3$  rings<sup>14</sup>, where the Li atoms of the first ring are directly above the N atoms of the second eclipsing ring. The formation of these hexamers is a stepwise process, with the association of three  $\text{Li}^+ [\text{N}=\text{CR}^1\text{R}^2]^-$  monomers in the first stage, to form the cyclic trimer. The second stage involves the vertical stacking of these two trimer rings to form the hexamer. This face to face

fusion increases the co-ordination around the lithium centre to three while initiating the loss of the planarity in the original monomer species and hence prevents any further ring stacking (Figure 3.1).

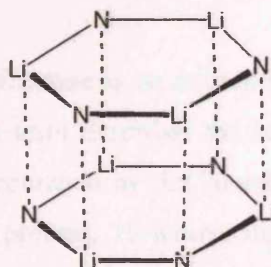


Figure 3.1 – Vertical stacking of two imide trimer rings to form the  $(\text{Li}_3\text{N}_3)_2$  hexamer

Contrary to these imines, the  $[\text{RR}^1\text{NLi}]_n$  lithium amides possess a tetrahedral ( $\text{sp}^3$ ) nitrogen due to the absence of a double bond. This gives exocyclic/tetrahedral R groups pointing above and below the  $[\text{LiN}]_n$  ( $n = 2, 3$  or  $4$ ) plane.

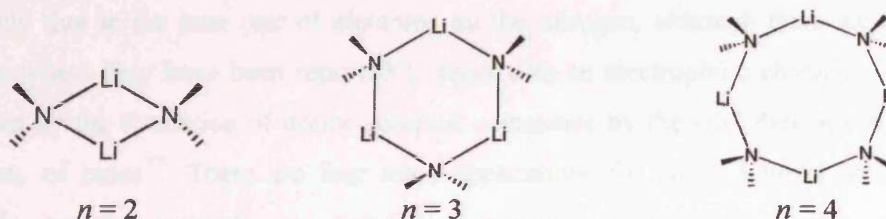


Figure 3.2 – Lithium amide dimers ( $n = 2$ ), trimers ( $n = 3$ ) and tetramers ( $n = 4$ )

These protruding alkyl groups, although not harming ring formation, prevent any vertical stacking. A development can be observed with the 4-membered heterocycles  $[\text{LiN}]_2$  (hence,  $n = 2$ ). These dimeric rings are able to associate further by a lateral edge to edge fusion termed ring laddering (Figure 3.3)<sup>15</sup>.

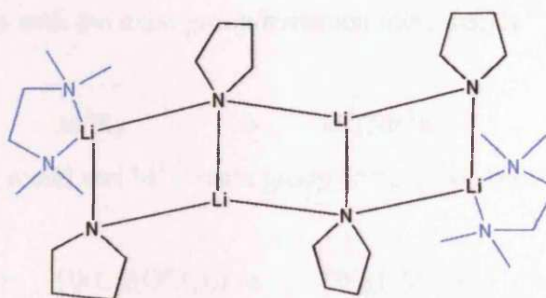


Figure 3.3 – Ring Laddering<sup>15</sup>



More recently a di-octameric ring structure [ $\{\text{Bu}^t\text{N}(\text{H})\text{Li}\}_8$ ] was reported<sup>16</sup>:



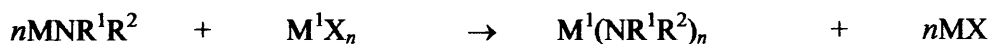
This octamer double crown structure is an extension to ring laddering association, yielding a cyclic ladder. This term describes the self-assembly of the ring via the laddering process. This is encouraged by the lateral fusion of four identical (NLi)<sub>2</sub> dimeric rings, the laddering process. However, due to van der Waals repulsion, curving is incorporated in the ladder; hence the ring is formed not via stacking, but by laddering.

### 3.1.1.3 Reactivity and Applications

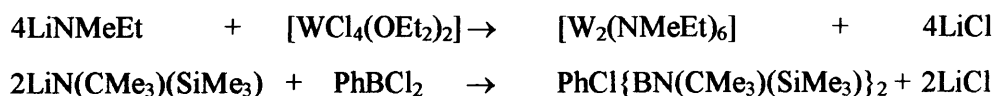
In the majority of their reactions alkali metal amides react as strong nucleophiles, mainly due to the lone pair of electrons on the nitrogen, although there are several cases where they have been reported to react with an electrophilic character. This is shown by the formation of donor-acceptor complexes by the silyl derivatives with a variety of bases<sup>17</sup>. There are four main applications for group I metal amides: as amide transfer reagents, as metallation species, as insertion agents, and as polymerisation initiators.

#### 3.1.1.3.1 Amide Transfer Reagents

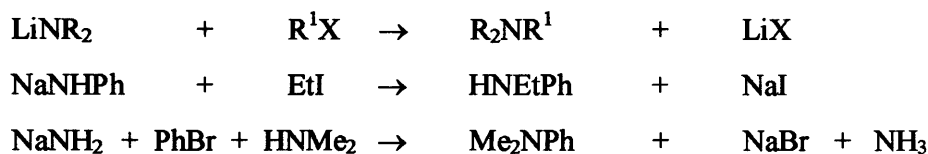
A large bulk of alkali metal amide chemistry is concerned with transferring the amide group to a main group or transition metal. This is usually done with the reaction of the alkali metal amide with the main group/transition metal halide<sup>18, 19</sup>:



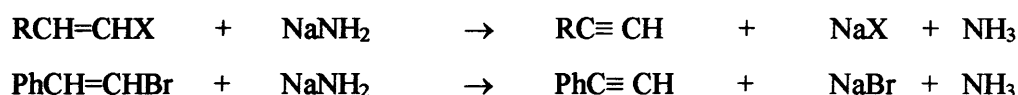
Where M = alkali metal and M<sup>1</sup> = main group or transition metal e.g.



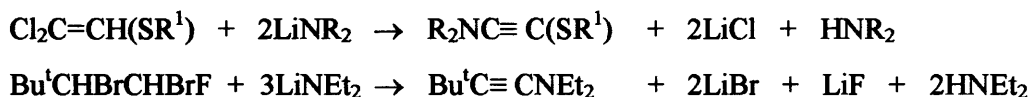
This principle can be employed to transfer amides to non-metal/metalloid substrates such as the alkyl and aryl groups to form the corresponding alkyl or aryl amines<sup>20, 21</sup>:



Vinyl halides undergo de-hydrohalogenation to produce an alkyne in the presence of alkali metal amides<sup>22</sup>:

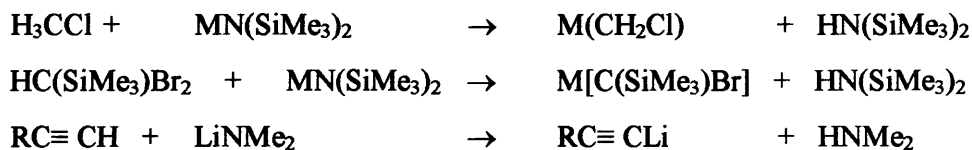


However if more than one halogen group is present in the saturated or unsaturated carbon chain in reaction with group I metal amides, then we see the production of an alkynylamine<sup>23, 24</sup>:



### 3.1.1.3.2 Metallation

Although the metal amide is considered as a strong nucleophile it can occasionally be hindered sterically. In these cases it can be thought of as a proton scavenger<sup>25, 26, 27</sup>:





#### 3.1.1.3.4 Polymerisation Initiation

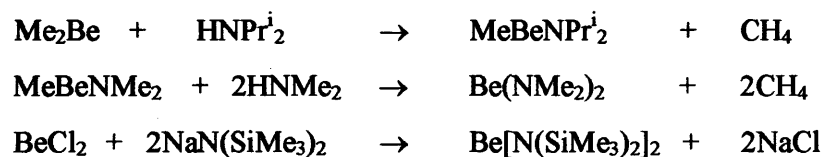
Alkali metal amides are able to initiate the polymerisation of some vinyl monomers. The mechanism is one of anionic polymerisation, or similarly it involves the opening of the C=C bond by the amide ion to form a 2-aminoalkyl carbanion which propagates the chain. The vinyl monomer, therefore, needs to be one that is electron deficient. Acrylonitrile or methacrylonitrile are such monomers that in the presence of NaNH<sub>2</sub> in liquid ammonia or LiNPh<sub>2</sub> in ether can be polymerised at -85 °C to give high molecular weight polymers<sup>35</sup>.

#### 3.1.2 Group 2 Amides

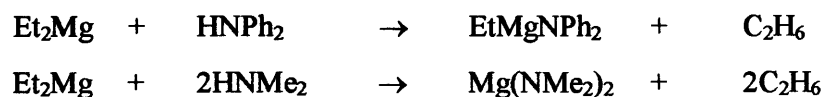
The interest in research of group 2 amides lies mainly with magnesium. Some beryllium and calcium amide complexes have been investigated but not to the same extent. The magnesium amides [Mg(NH<sub>2</sub>)<sub>2</sub>]<sub>n</sub> (and also their beryllium and calcium counterparts) can be prepared from the reaction of the metal with ammonia at high pressures at 130-370 °C<sup>36</sup>.

##### 3.1.2.1 Preparation

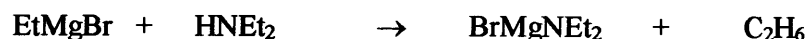
Beryllium amides are prepared by the elimination of alkanes and salts<sup>37, 38, 39</sup>:



Magnesium amides have a diversity of preparative routes. They can be prepared by alkane elimination, in a similar manner to their beryllium cousins<sup>40</sup>:



Likewise primary or secondary amines can also react with Grignard reagents to afford the halogeno(amido)magnesium compound<sup>41</sup>:



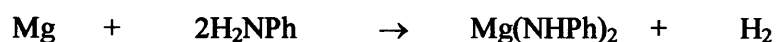
Insertion reactions are an alternative route to these compounds, particularly those of a more complex nature<sup>42</sup>:



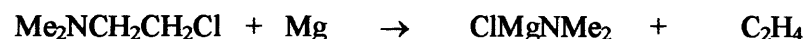
A less complex product yields from the insertion of an imine into a Mg–C bond<sup>43</sup>:



A high yield of bis(anilido)magnesium can be prepared by the reaction of aniline with hot magnesium<sup>44</sup>:



A further route is with the reaction of magnesium with 2-(dimethylamino)chloroethane, which eliminates the ethyl group from the amine<sup>45</sup>:



### 3.1.2.2 Structure and Bonding

Beryllium normally has four co-ordination sites for saturation, however in its amides we often see two and three co-ordinate beryllium centres. This is possible because of the presence of bulky R groups. High co-ordination numbers are achieved with intra<sup>46</sup> and inter-molecular<sup>47</sup> dative bonding, chelation and dimerisation respectively. It is this intermolecular donating (from the N group) and accepting (from the Be metal) of electrons that give rise to dimerisation<sup>48</sup> and higher oligomers<sup>49</sup>.



The formation of these monomers, dimers and trimers is largely dependent on steric effects and the absence of polymers is also due to these effects. This becomes apparent when we consider the crystal structure of beryllium bis(dimethylamide),  $[\text{Be}(\text{NMe}_2)_2]_3$ .<sup>50</sup>

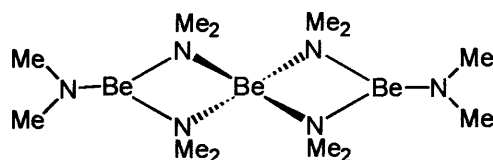


Figure 3.4 - Beryllium bis(dimethylamide)<sup>50</sup>

This trimer is completed with two 3-coordinate beryllium atoms and one 4-coordinate centre and is sterically preferable to an infinite polymer due to the small ionic radius of beryllium.

Magnesium amides however tend to be polymeric, unless bulky ligands are employed on the magnesium or nitrogen centres. Complexation with a co-ordinating solvent can reduce this degree of polymerisation. Dimeric  $[\text{Mg}(\text{NPr}^i)_2\text{Pr}^i]_2$  is formed via bridging  $\text{NPr}^i_2$  groups<sup>39</sup>, which is a common structural motif for bulky amido-group 2 complexes<sup>51</sup>.

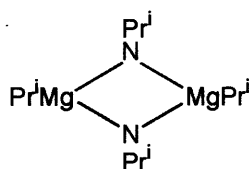
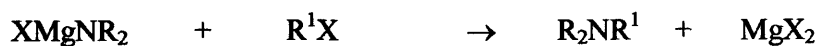


Figure 3.5 -  $[\text{Mg}(\text{NPr}^i)_2\text{Pr}^i]_2$ <sup>39</sup>

### 3.1.2.3 Reactivity and Applications

The halogeno(dialkylamido)magnesium reagent is termed “magnesyamine” and reacts with alkyl halides to give further alkylation of the amino group<sup>52</sup>:

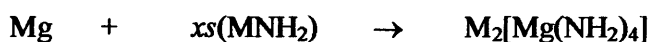


Similarly, this magnesium reagent can be used to produce an amidine/guanidine by reacting it with a nitrile<sup>52, 53</sup>:

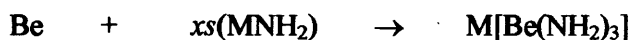


Magnesium and beryllium amides also play a role in polymerisation. Both can catalyse the polymerisation of aldehydes, with magnesium also able to catalyse methacrylonitrile<sup>54</sup> polymerisation.

Double amides of magnesium with the group 1 metals have been obtained from the reaction of Mg and liquid ammonia solutions of the alkali metal<sup>35</sup>:



Beryllium reacts in a similar way forming an ionic tris amide with the alkali metal<sup>55</sup>:



### 3.1.3 Group 13 Amides

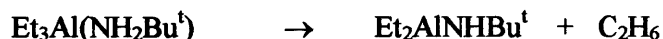
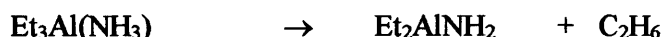
Boron-nitrogen chemistry has received a great deal of attention in previous years<sup>56</sup>, to the extent that the subject is well understood. Reasons for this interest include the isoelectronic relationship of BN and CC atomic pairs and the potential of these compounds to form polymers, due to the N electron donor and B electron acceptor sites<sup>57</sup>.

The chemistry of compounds containing Al-N bonds is another area of chemistry that has blossomed<sup>58</sup> despite the difficulties associated with these compounds due to their moisture and oxygen sensitivity. The majority of aminoalanes are polymeric, giving dimers, trimers or longer polymers, which are formed by intermolecular covalent bonding between the monomers, encouraged by the electron donating nitrogen and the electron accepting aluminium centres. Excluding the thallium I oxidation state the

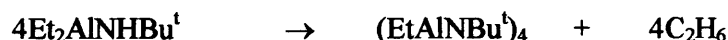
gallium, indium and thallium III derivatives resemble the aluminium analogues. Likewise, the main synthetic routes to them involve alkyl/alkane or in some cases hydrogen elimination.

### 3.1.3.1 Preparation

Aminoalanes can be synthesised by elimination of an alkane from an amine-alane adduct<sup>59, 60, 61, 62</sup>:

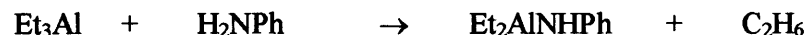


A second alkyl group can be eliminated at elevated temperatures giving polymeric imido derivatives<sup>61</sup> e.g:



Only mild conditions are required for the loss of the first alkyl group, with the reactions proceeding at room temp, although further heating to ~100 °C is preferred for the second elimination.

Use of aryl amines makes the elimination of the alkyl group even more amicable, probably due to the more labile protons on the aryl-amino group. This allows the following reaction to proceed at -78 °C<sup>63</sup>:



Elimination of hydrogen is the most affable preparatory method of amino alanes<sup>64, 65</sup>:

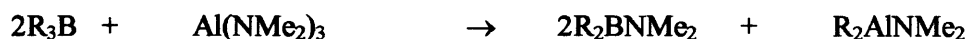




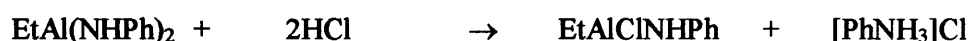
Other methods for preparing aminoalanes include, salt elimination<sup>66</sup>:



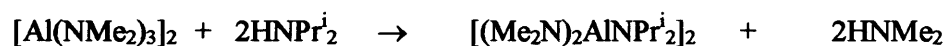
Metathetical exchange<sup>65</sup>:



Cleavage of one Al-N bond in compounds containing more than one Al-N bond has been used to give mixed halogeno(amino)alanes<sup>637</sup>:



Transamination can be used to prepare both aluminium and gallium complexes<sup>61</sup>:



Another more “direct” procedure, is with the metal in its elemental form reacting with a secondary amine under an atmosphere of hydrogen<sup>67</sup>:



### 3.1.3.2 Structure and Bonding

Most tris(amino)boranes are monomeric, however some alane analogues are reported to be dimeric, with  $\text{Al}(\text{NMe}_2)_3$  being an example of these dimers. There are also instances where this compound has also been reported as a monomer<sup>68</sup>. The dimethylaminoalane trimer  $[\text{H}_2\text{AlNMe}_2]_3$  is comparable to the chair conform adopted by cyclohexane (hydrogen atoms have been omitted for clarity)<sup>69</sup>:

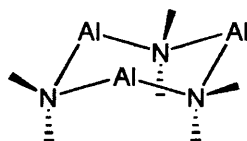


Figure 3.6 - Dimethylaminoalane trimer adopting the chair conform<sup>59</sup>

The six-membered  $(\text{AlN})_3$  ring is formed from alternate Al and amido groups, giving four co-ordinate distorted tetrahedral aluminium centres. A related structure has been reported for ethylene imino(dimethyl)alane<sup>70</sup>. This chair conformation, is also observed for the aziridinylgallane trimer  $[\{(\text{C}_2\text{H}_4)\text{NGaH}_2\}_3]$ , with a  $[\text{GaN}]_3$  ring. This similarity is replicated with the average bond lengths of 1.93 Å (Al-N) for the amido-alane being very close to the 1.97 Å (Ga-N) bond lengths for the amido-gallane complex. The near identical covalent radii of the two group 13 metal atoms can explain this<sup>71</sup>.

The tetrameric iminoalane below displays one of the most interesting Al-N structures with the formation of a cube. The faces of these  $\text{Al}_4\text{N}_4$  cubes are significantly planar, with Al-N bond distances of 1.914 Å<sup>72</sup>.

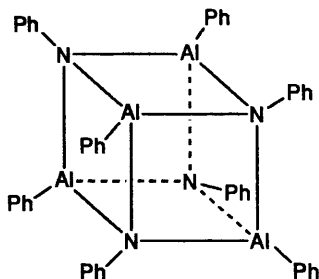


Figure 3.7 - Tetrameric iminoalane cube<sup>72</sup>

A four membered  $\text{In}_2\text{N}_2$  ring can be synthesised by elimination of alkanes to form, for example,  $[\text{Me}_2\text{InNMe}_2]_2$  which unsurprisingly bears a resemblance to its alane analogue  $[\text{Me}_2\text{AlNMe}_2]_2$ .<sup>73</sup>

Iminoalanes also exhibit interesting hexamer cage structures, of the like already seen with the alkali metal amides, e.g.  $\text{Al}_6\text{N}_6$ , with  $(\text{HAlNPr}^i)_6$ ,<sup>74</sup>  $(\text{HAlNPr})_6$ <sup>75</sup> and  $(\text{ClAlNPr}^i)_6$ .<sup>76</sup>

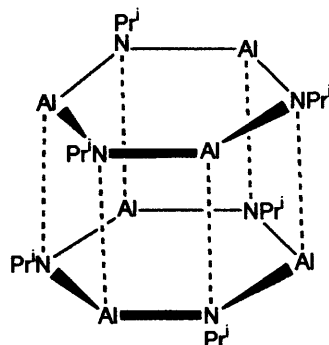
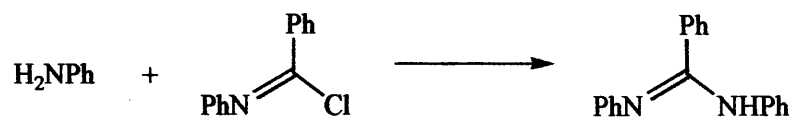


Figure 3.8 – Iminoalane hexamer, the hydride/chloride ligands have been removed for clarity.

### 3.1.4 Amidines

Gerhardt prepared the first amidine ligand in 1858 by reacting aniline with *N*-phenylbenzimidyl chloride (*Scheme 3.1*)<sup>80</sup>.



*Scheme 3.1 – Synthesis of N,N'-diphenylbenzamidine*

The amidine name is therefore given to a group of ligands with a similar skeleton:

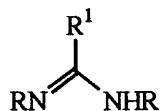


Figure 3.9 – Amidine skeleton

Variations of the different R groups give the compound its name and unique identity. The name is derived from the acid or amide formed in the hydrolysis of the ligand. The simplest case is where  $R^1 = H$ , the ligand is then termed a formamidine. Alkylamidine is the general name given to the ligands where  $R^1 = \text{alkyl group}$ . More specifically where  $R^1 = CH_3$  the ligand is known as acetamidine and likewise where  $R^1 = C_4H_9$  the ligand is termed butyramidine. The aryl/benzylamidines are the general names given to those ligands with a phenyl backbone R group, an example of which is benzamidine where  $R^1 = C_6H_5$ . This bulky aryl group on the backbone carbon increases the steric bulk to such an extent that the bidentate *N,N'*-bis(trimethylsilyl)benzamidine ligand,  $[PhC(NSiMe_3)_2]$  is comparable with  $C_5Me_5$ <sup>77</sup> and can be considered as a useful alternative to cyclopentadienyl ligands<sup>78</sup>. New attributes can be gained in the amidine group when  $R^1 = NR_2$ . These amidines are called guanidines. Alternatively the systematic names derived from the corresponding acid of these ligands are often used in literature. This name is derived by replacing the carboxyl group with  $C(:NH)NH_2$ . Hence, formamidine becomes methanimidamine and acetamidine becomes ethanimidamine.

Fundamentally, these amidines act as two electron donors via the more basic and less sterically crowded imino lone pair. They are also capable of donating the lone pair on the amino group (four-electron donor), and co-ordinating as neutral  $RNCR^1N(H)R$  amidine, or more usually as the amidinate  $[RNCR^1NR]^-$ , giving a variety of interesting bonding modes, such as:

### 1. Monodentate Complexes

This bonding interaction is through one nitrogen  $\sigma$ -bonded to the metal. The imino nitrogen is double bonded to the central carbon atom.

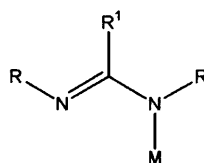


Figure 3.10 – Monodentate amidinate coordination

## 2. Chelating Complexes

These complexes present distortion and steric strain of the valence angles by the formation of the four membered ring, MNCN. This type of bonding can be divided by the nature of the attachment:

- $\sigma, \sigma$ -symmetrical bonding where the NCN bonding is delocalised.
- $\sigma, \sigma$ -unsymmetrical bonding where both nitrogen atoms bond to the metal, but the imino nitrogen bonds by donating its lone pair to the metal.
- $\sigma, \pi$  bonding where the amino nitrogen  $\sigma$  bonds to the metal, while the localised imino double bond associates as in an alkene-type manner. However, there are no reported cases of this bonding mode in main group chemistry.

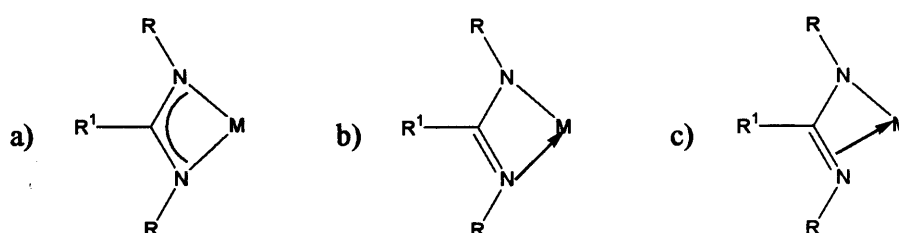


Figure 3.11 – Examples of alternative amidinate chelation

## 3. Bridging Complexes

This involves the formation of a five membered  $M_2NCN$  ring and can encourage metal-metal bonding by bringing two metal centres into close proximity, a fact exploited by Cotton<sup>79</sup>. Interestingly the metal atoms can be different. This bridging takes place via:

- monodentate  $\mu\text{-}\eta^1\eta^1$  amidinate ligand
- chelating  $\mu\text{-}\eta^2\eta^2$  amidinate ligand
- Via a more unusual mixed  $\mu\text{-}\eta^1\eta^2$  bridging-chelating ligand

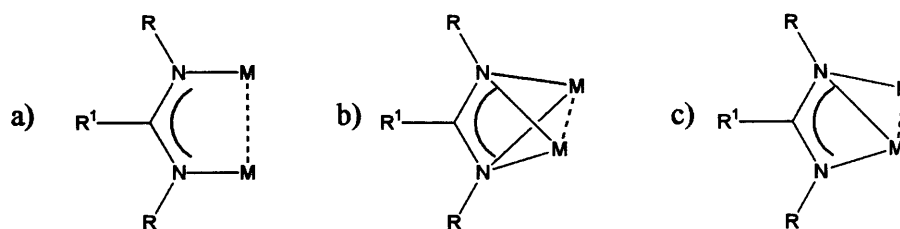


Figure 3.12 – Complexes with amidinate bridging

#### 4. Carbene Complexes

This is where the R group has been removed from the backbone carbon, which is stabilised by feeding its electron density into the delocalisation on the three atom centre, NCN. Any bonding is via the carbon atom, and reminds us that the amidinate group of ligands can be regarded as carbenes in some complexes.

The majority of these bonding modes were discovered by scanning the chemistry of transition metal amidinates. This is a vast field<sup>80</sup> but will not be discussed here. By contrast, the known chemistry of s- and p-block amidine complexes is not substantial and forms the basis of the current work.

### 3.1.5 Group 1 Amidinates

#### 3.1.5.1 Preparation

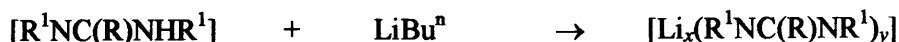
There are three general methods used in the preparation of these group 1 amidinate complexes. The first is the treatment of the amidine ligand with the group 1 metal hydride:



Alternatively these complexes are formed by transamination using the metal bis(trimethylsilyl)amide reagent:



In the case of lithium complexes, they are usually formed by the reaction of *n*-butyl lithium with an amidine:



### 3.1.5.2 Structure and Bonding

Very few group 1 amidinate complexes have been structurally characterised. Those that have display a variety of structural motifs depending on the N-substituents, alkali metal and co-ordinating solvent employed. A summary of the known complexes follows with the first structurally characterised group 1 metal amidinate reported in 1993<sup>81</sup>. This complex was prepared by the reaction of *n*-butyl lithium with *N,N'*-diphenylbenzamidine and pentamethyldiethylenetriamine (PMDETA) in a toluene-THF solution to afford the lithium diphenylbenzamidinate PMDETA complex:



The crystal structure of the complex reveals a five co-ordinate trigonal bipyramidal lithium cation chelated by the bidentate amidinate anion and a tridentate PMDETA donor ligand.

The low co-ordinate monodentate terphenylamidinate lithium complex (Figure 3.13) was formed by reacting *N,N'*-diisopropyl(2,6-dimesityl)benzamidinate (dimb) ligand with *n*-butyl lithium in hexanes with the addition of tetramethylethylenediamine (TMEDA)<sup>82</sup>, giving a three co-ordinate lithium amidinate complex:

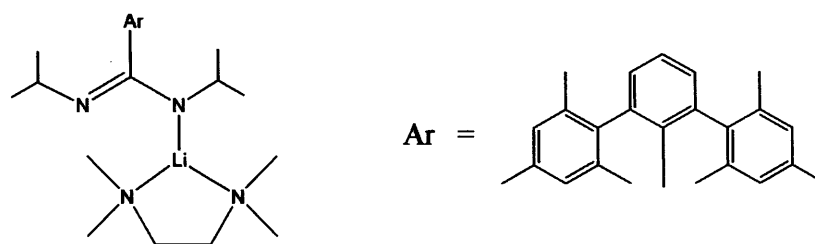
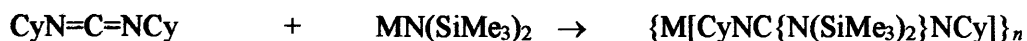


Figure 3.13 - Terphenylamidinate lithium TMEDA complex<sup>82</sup>

The terphenyl substituent (Ar) was introduced to the amidine backbone to induce a “bowl” shaped environment providing a steric hindrance in the plane of the ligand and also above and below this plane. Related guanidinate complexes of alkali metals have also been reported for lithium, sodium and potassium. These complexes were

prepared from the reaction of 1,3-dicyclohexylcarbodiimide with the corresponding alkali metal amide in a hexane or toluene medium<sup>83</sup>:



The lithium complex crystallises with two guanidinate ligands perpendicular to each other, hence  $n = 2$ . The first guanidinate ligand is monodentate and bridges across the two lithium centres, while the second ligand chelates to both lithium centres while bridging between them to complete a low three co-ordinate lithium centre, giving the complex an unusual  $\text{N}_4\text{Li}_2$  atom core (Figure 3.14)<sup>83</sup>.

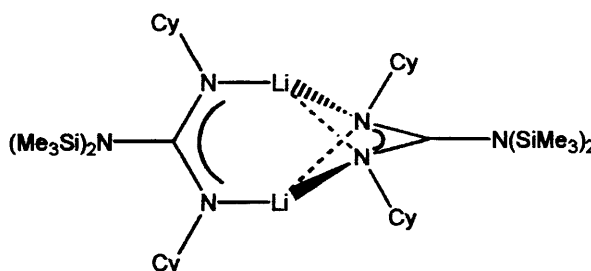


Figure 3.14 – Dinuclear lithium complex containing both monodentate bridging ( $\mu\text{-}\eta^1\eta^1$ ) amidinate and chelating  $\mu\text{-}\eta^2\eta^2$  amidinate ligands<sup>83</sup>

The sodium derivative crystallises as a cyclic trimer aggregate, hence  $n = 3$ . This is achieved by chelate bridging guanidinate ligands giving the complex a novel  $\text{N}_6\text{Na}_3$  atom core<sup>83</sup>.  $\text{N}(\text{SiMe}_3)_2$  and Cy groups have been omitted for clarity.

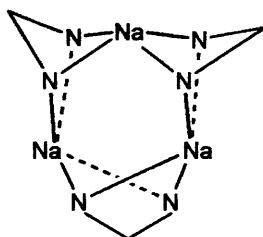


Figure 3.15 – Cyclic sodium amidinate trimer<sup>83</sup>



The potassium salt is a dimer complex, with  $n = 2$ , resembling the lithium complex to an extent. This complex, however, has two equivalent chelate bridging guanidinate ligands parallel to each other with a  $N_4K_2$  atom core (Figure 3.16)<sup>83</sup>.

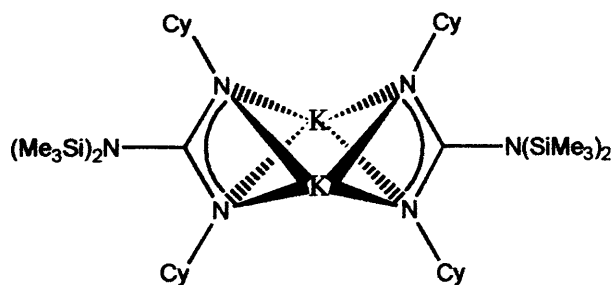


Figure 3.16 – Bis-chelating  $\mu\text{-}\eta^2\eta^2$  amidinate ligands<sup>83</sup>

This area of chemistry has been extended by the Junk group to the development of novel group 1 formamidinate complexes. The underlying theme throughout this chemistry is the different bonding modes and structures enforced by simply changing the solvent medium used in the preparation of formamidinate complexes. For example, the reaction of butyl lithium with  $N,N'$ -di(*p*-tolyl)formamidine (*p*-tolylform) in the co-ordinating solvent THF afforded a dinuclear lithium bis-*p*-tolylformamidinate species (Figure 3.17)<sup>84</sup>. This complex has a THF molecule bridging between the two lithium centres

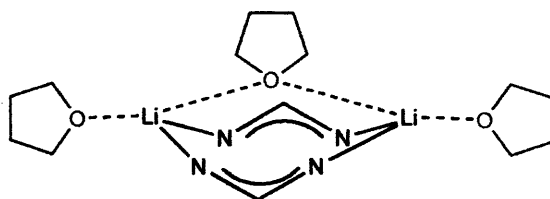


Figure 3.17 - Dinuclear lithium bis-*p*-tolylformamidinate complex (the *p*-tolyl groups have been omitted for clarity).

A similar reaction of butyl lithium with *N,N'*-di(*p*-tolyl)formamidine in the co-ordinating solvent DME afforded a dinuclear lithium tris-*p*-tolylformamidinate anion species which is counterbalanced by a lithium cation<sup>84</sup>:

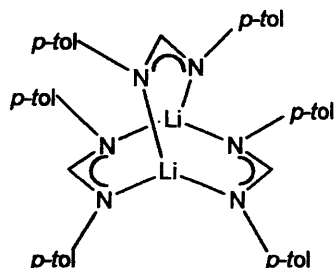


Figure 3.18 – Unusual dinuclear lithium tris-*p*-tolylformamidinate complex<sup>84</sup>

This reaction was repeated using a non-co-ordinating solvent in the presence of TMEDA to form a polymeric structure<sup>84</sup>. This dinuclear complex crystallises with lithium centres bridged by two *p*-tolylformamidine ligands. The  $[\text{Li}_2(p\text{-tolylform})_2]$  dimer units are unusually bridged to each other by TMEDA, forming a polymer (Figure 3.19).

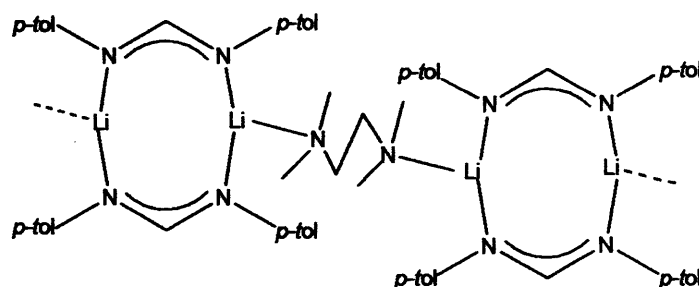


Figure 3.19 – Dinuclear lithium bis-amidinate TMEDA bridged polymer<sup>84</sup>

Sodium hydride was also reacted with *N,N'*-di(*p*-tolyl)formamidinate in DME to yield a dinuclear complex with sodium centres bridged by two *p*-tolylformamidinate

ligands, which also chelate, and chelating DME giving a five co-ordinate sodium centre in a distorted trigonal bipyramidal geometry<sup>84</sup>.

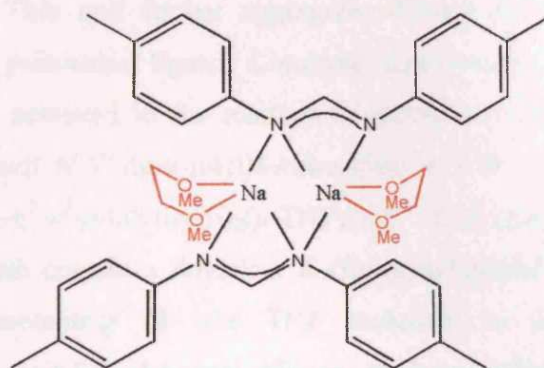


Figure 3.20 – Dinuclear sodium complex with mixed  $\mu\text{-}\eta^1\eta^2$  bridging-chelating formamidinate ligands<sup>84</sup>

The Junk group also reported the first structurally characterised potassium formamidinate complex which displays the affinity of potassium for  $\pi$ -arene interactions, with the synthesis of bis-di(mesityl)formamidinate potassium, formed in the reaction of *N,N'*-di(mesityl)formamidine (FMes) with potassium hydride and also with bis(trimethyl)silyl potassium<sup>85</sup>:

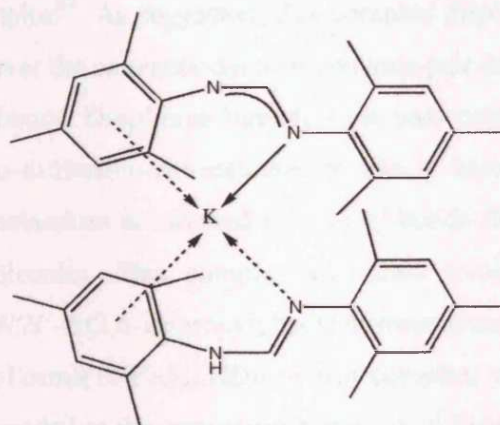
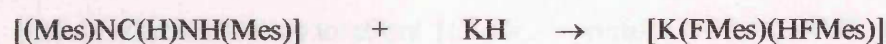


Figure 3.21 – Potassium di(mesityl)formamidine-formamidinate complex<sup>85</sup>

This complex incorporates a monodentate deprotonated FMes ligand with  $\eta^6$  arene – potassium interactions, and a protonated HFmes ligand with dative bonding from the imino nitrogen in addition to a potassium-arene  $\pi$ -interaction. The imine, amide and mesitylene centroid donors generate a cumbersome tetrahedron geometry around the potassium centre. This unit further aggregates through intermolecular hydrogen bonding from the protonated ligand. Complete deprotonation of the formamidine amino groups was achieved in the reaction of potassium hydride with *N,N'*-di(*p*-tolyl)formamidine and *N,N'*-di(*m*-tolyl)formamidine in THF yielding the respective polymers,  $[\{K_2(\mu-\eta^2:\eta^2\text{-}p\text{-tolylform})_2(\mu\text{-THF})_3\}_\infty]$ ,  $[\{K_2(\mu-\eta^2:\eta^2\text{-}m\text{-tolylform})_2(\mu\text{-THF})_3\}_\infty]$ . Both contain a dinuclear  $K_2(\text{formamidinate})_2(\text{THF})_3$  fragment with the latter also containing of one THF molecule of solvation to give a  $K_2(\text{formamidinate})_2$  unit linked to two adjacent  $K_2(\text{formamidinate})_2$  units by six ( $\mu$ ) bridging THF molecules. These complexes were formed with the absence of  $\eta^6\pi$ -arene interactions. This reaction was repeated with potassium hydride and *N,N'*-di(*p*-tolyl)formamidine in DME to afford the related  $[\{K(\mu-\eta^2:\eta^2\text{-}p\text{-tolylform})(\mu-\eta^2:\eta^1\text{-DME})\}_\infty]$  polymer containing a  $[\{K_2(\mu-\eta^2:\eta^2\text{-}p\text{-tolylform})_2(\mu-\eta^2:\eta^1\text{-DME})_2\}]$  fragment to give a  $K_2(p\text{-tolylform})_2$  unit linked to two adjacent  $K_2(p\text{-tolylform})_2$  units by four ( $\mu-\eta^2:\eta^1$ ) bridging DME molecules<sup>86</sup>. Again no  $\eta^6\pi$ -arene interactions are observed in this complex, probably due to the presence of the bidentate DME donor. These  $\eta^6\pi$ -arene interactions, however, are reported in the complex formed in the reaction of *N,N'*-di(2,6-isopropylphenyl)formamidine, (HDippForm) with potassium bis(trimethylsilyl)amide to afford  $[\{K(\text{DippForm})_2K(\text{THF})_2\}_n].n\text{THF}$ , a deprotonated formamidinate complex<sup>87</sup>. As suggested, this complex displays a preference for  $\eta^6\pi$ -arene interactions over the conventional nitrogen lone pair donation, to yield unevenly shared two  $\eta^6:\eta^1$  bound DippForm ligands over two potassium centres. The first potassium has its co-ordination site saturated by two  $\eta^6$  interactions and two  $\eta^1$  bonds while the second potassium is satisfied by two  $\eta^1$  bonds from the DippForm ligand and two THF molecules. This complex was then reacted further with another equivalent of the *N,N'*-di(2,6-isopropylphenyl)formamidine (HDippForm) ligand to yield the  $[\{K(\text{DippForm})(\text{THF})_3\}_n].\text{HDippForm}$  complex, which has a deprotonated DippForm ligand bonded to the potassium metal via  $\eta^1$  bond from the nitrogen and a  $\eta^6$  interaction from the aryl group on the ligand. Three THF molecules then saturate

the potassium co-ordination site. The free ligand associates to the co-ordinated ligand with hydrogen-bonding through its remaining proton.

### 3.1.6 Group 2 Amidinates

Cotton and co-workers take the credit for the first structurally characterised group 2 metal formamidinate, with the formation in 1997 of  $[(\mu\text{-Cl})_2(\mu\text{-THF})\{\text{Mg}(\eta^2\text{-diphenylform})(\text{THF})_2\}_2]^{88}$  synthesised from the reaction of *N,N'*-di(phenyl)formamidine, (DiphenylForm) with methylmagnesium chloride.

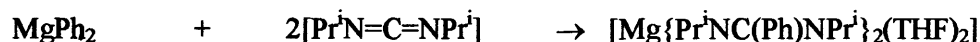
Group 2 formamidinate chemistry has been extended with the research of the Junk group; providing some novel six co-ordinate octahedral magnesium complexes. These complexes,  $[\text{Mg}(p\text{-tolylform})_2(\text{THF})_2]_n$ ,  $[\text{Mg}(o\text{-tolylform})_2(\text{THF})_2]_n$ , are formed from the reaction of dibutyl magnesium with *N,N'*-di(*p*-tolyl)formamidine and *N,N'*-di(*o*-tolyl)formamidine respectively<sup>89</sup>. These reactions were also extended to that of the *N,N'*-di(*p*-tolyl)formamidine ligand with dibutyl magnesium in DME and TMEDA, to afford the octahedral magnesium complexes,  $[\text{Mg}(p\text{-tolylform})_2(\text{DME})_2]_n$ .DME and  $[\text{Mg}(p\text{-tolylform})_2(\text{TMEDA})]_n$ .

#### 3.1.6.1 Preparation

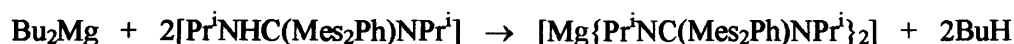
Magnesium amidinate complexes have been prepared from the reaction of magnesium bromide with the appropriate lithium amidinate reagent<sup>90</sup>:



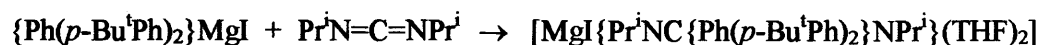
They have also been prepared by reaction of the alkyl magnesium reagents with carbodiimides<sup>91</sup>:



Sterically hindered magnesium amidinates have been synthesised directly by reaction of the bulky amidine ligand with dibutylmagnesium<sup>92</sup>:



An alternative method for the formation of magnesium amidinates with terphenyl substituents is shown below<sup>92</sup>:



### 3.1.6.2 Structure and Bonding

An indication of the variety of structures and bonding observed with the amidinate complexes is demonstrated in the recent Winter *et al*<sup>90</sup> publication. This publication demonstrated the two main structural forms in which group 2 amidinate complexes exist.

1. A bis chelating  $[\text{Mg}\{\text{Bu}^t\text{NC}(\text{Ph})\text{NBu}^t\}_2]^{90}$  tetrahedral complex which forms as a consequence of the bulky tertiary butyl groups on the nitrogen, and phenyl group on the backbone carbon. The phenyl backbone narrows the NCN angle encouraging chelation (Figure 3.22).

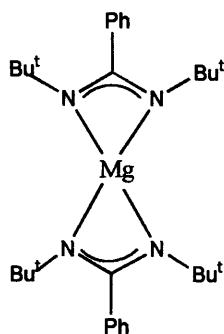


Figure 3.22 - Bis di(*tert*-butyl)benzamidinate chelating magnesium complex

2. The bridging  $[\{\mu\text{-Pr}^i\text{NC}(\text{CH}_3)\text{NPr}^i\}_2\text{Mg}_2\{\eta^2\text{-Pr}^i\text{NC}(\text{CH}_3)\text{NPr}^i\}_2]^{90}$  complex is formed by substitution of the bulky substituents observed in the above complex,

for the less sterically hindering groups. This includes isopropyl groups on the nitrogen atoms. Furthermore, the methyl backbone is not as bulky as the phenyl group in the previous complex, which results with a slightly more open NCN angle. The complex does however, contain two chelating amidinate ligands to satisfy the magnesium distorted tetrahedral co-ordination sites (Figure 3.23).

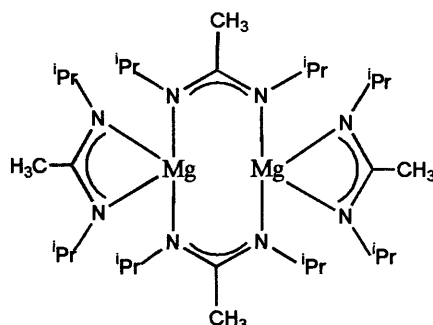


Figure 3.23 – Magnesium amidine complex with two monodentate bridging and two chelating amidine ligands

An interesting cross over between these two main bonding modes is observed in the reaction of a mixed substituent amidinate reagent,  $[\text{Li}\{\text{Bu}^t\text{NC}(\text{CH}_3)\text{NEt}\}]$ , with magnesium bromide. This yields a high valent five co-ordinate magnesium complex, with a distorted square pyramidal geometry at the magnesium atoms. The afforded product contains two chelate bridging ligands ( $\mu, \eta^2:\eta^1$  as opposed to  $\mu, \eta^1:\eta^1$ ) and two chelating bidentate ligands,  $[\{\mu, \eta^2:\eta^1\text{-Bu}^t\text{NC}(\text{CH}_3)\text{NEt}\}_2\text{Mg}\{\eta^2\text{-Bu}^t\text{NC}(\text{CH}_3)\text{NEt}\}_2]^{90}$ . This unusual bonding interaction arises because of the reduced steric demand of the ethyl substituent on the nitrogen atom (Figure 3.24).

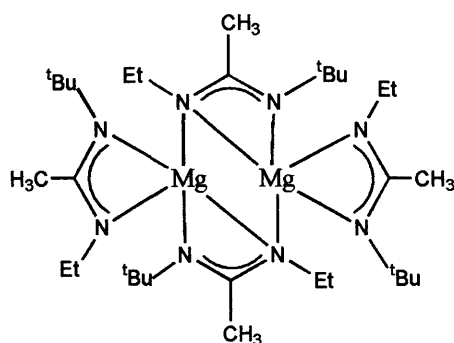


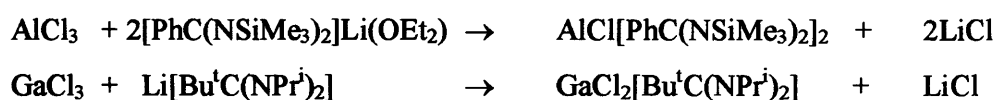
Figure 3.24 – Magnesium amidine complex with two  $\mu, \eta^2:\eta^1$ -bridging amidine ligands and two  $\eta^2$ -chelating amidine ligands

### 3.1.7 Group 13 Amidinates

Several groups<sup>93, 94, 95</sup> have chosen to exploit the adaptability that amidinate ligands provide in the preparation of a range of group 13 complexes, many of which are finding applications in catalysis.

#### 3.1.7.1 Preparation

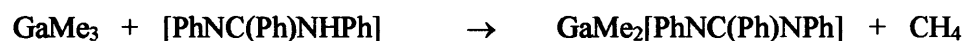
Salt elimination is a useful preparatory route to group 13 amidinate complexes<sup>96, 97</sup>:



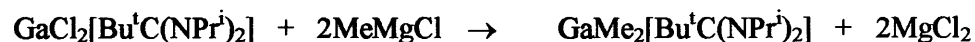
Subsequent treatment of the aluminium chloride amidinate with potassium triethylborohydride affords the hydride<sup>98</sup>:



Gallium amidinate complexes have been prepared in the reaction of trimethylgallium with amidine ligands in hexane, to liberate methane<sup>98</sup>:



They have also been prepared in the reaction of a gallium dichloride amidinate complex with a Grignard reagent<sup>97</sup>:



Preparation of the related bis(amidinato) complex can precede with addition of trimethylgallium to two equivalents of the amidine ligand at elevated temperatures (145 °C) liberating two equivalents of methane. The bis(amidinato) complex can also



be synthesised by reacting the initial dimethyl gallium amidine complex with a second equivalent of the amidine ligand at 100 °C liberating methane<sup>98</sup>:



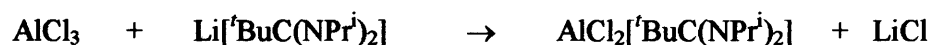
Continued heating at 200 °C in the presence of a third amidine equivalent yields the tris(amidinato) gallium complex<sup>98</sup>:



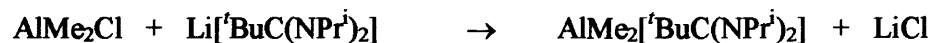
The Jordan group was able to form several mono(amidinato) aluminium alkyl species by addition of aluminium alkyls with carbodiimides in hexane e.g.<sup>99</sup>:



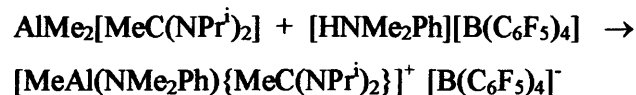
However, to form the tertiary butyl substituted amidinate aluminium halide and alkyl complexes, aluminium trichloride was reacted with the required lithium amidinate reagent<sup>99</sup>:



An alternative to this route is to replace the aluminium trichloride with dimethylaluminium chloride<sup>99</sup>:



These dimethyl aluminium amidinate complexes, e.g.  $\text{AlMe}_2[\text{MeC(NPr}^i)_2]$ , can be activated for use in catalysis by reaction with  $[\text{HNMe}_2\text{Ph}][\text{B(C}_6\text{F}_5)_4]$ <sup>100</sup>:



### 3.1.7.2 Structure and Bonding

There are a number of group 13 amidinate complexes reported, however they tend to form similar structures, with the smaller amidinates favouring multinuclear complexes while the use of sterically bulky amidinates encourages mononuclear complexes. Hence, mono(amidinato) group 13 complexes tend to form chelated complexes with four co-ordinate distorted tetrahedral metal geometries as in  $\text{GaMe}_2[\text{PhNC}(\text{Ph})\text{NPh}]$ .<sup>98</sup>

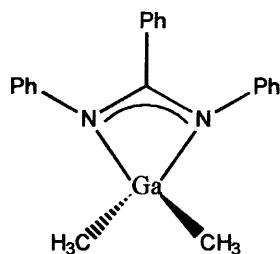


Figure 3.25 – Dimethylgallium diphenylbenzamidinate complex<sup>98</sup>

Bis(amidinato) group 13 metal complexes tend to form bis-chelated 5-coordinate structures as in  $\text{AlCl}[\text{PhC}(\text{NSiMe}_3)_2]_2$  (Figure 3.26)<sup>97</sup>. Whereas, further amidinate substitution affords the tri(amidinato) complexes, generating six co-ordinate octahedral geometries, as seen with the gallium tri(benzamidinate) species,  $\text{Ga}[\text{PhNC}(\text{Ph})\text{NPh}]_3$ .<sup>98</sup>

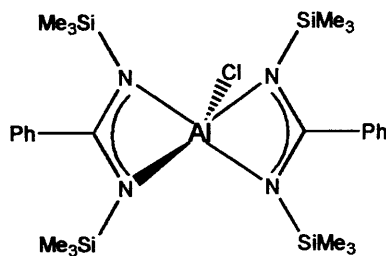


Figure 3.26 – Bis chelated aluminium amidinato complex<sup>97</sup>

There are also dinuclear group 13 amidinate complexes, where the ligand bridges between two metal centres to afford an unusual puckered eight membered ring. An example of this includes the 4-coordinate gallium amidinate species<sup>101</sup>:

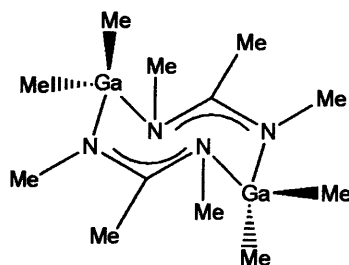


Figure 3.27 – Dinuclear gallium bis(amidinato) eight membered ring<sup>101</sup>

A related methyl indium formamidinate complex has also been reported, (below). This dinuclear indium complex also contains two bridging formamidine ligands<sup>102</sup>.

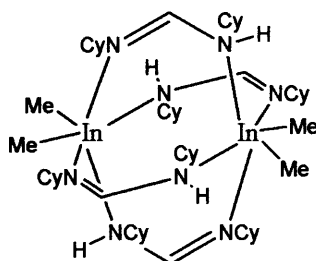


Figure 3.28 – Dinuclear indium formamidinate “paddle-wheel” complex<sup>102</sup>

Group 13 guanidinate complexes typically exhibit bidentate chelating bonding modes. The bicyclic guanidinate ligand, 1,3,4,6,7,8-hexahydro-2*H*-pyrimido[1,2-*a*]pyrimidinato anion (hpp<sup>-</sup>), however, is restricted from this chelation by a rigid backbone and hence is compelled to form monodentate bridging complexes<sup>103</sup>.

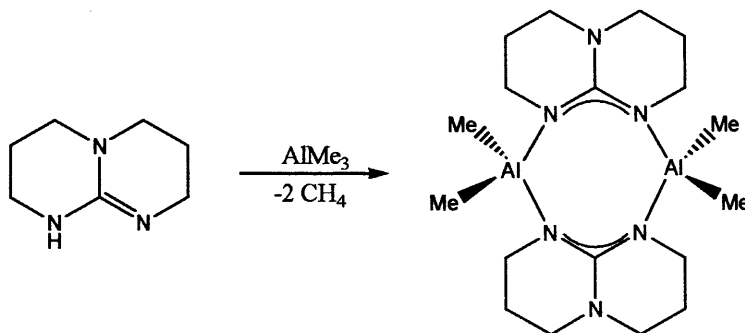


Figure 3.29 – Dinuclear aluminium bis(hpp) complex<sup>103</sup>

### 3.1.8 Research Proposal

The attributes of amidinate ligands and hence the advantages/influences they impart in complexation can be tailored by the modification and substitution of the substituent R groups.

The co-ordination chemistry of amidinate ligands involves metallic elements spanning the periodic table<sup>14, 104</sup>. In particular transition metal amidinate complexes have been widely studied and often form the dinuclear “paddle-wheel” complexes.

The use of group 1 metal amidinates in the preparation of these “paddle-wheel” dinuclear transition metal complexes has encouraged the perception of these complexes as mere precursor species. As such, the study of s-block amidinate chemistry, in particular the formamidinate class has been neglected.

Our initial interest in main group metal amidinate chemistry, particularly complexes of group 1, stemmed from our desire to prepare unprecedented f-block metal complexes of the formamidinates via metathetical exchange.

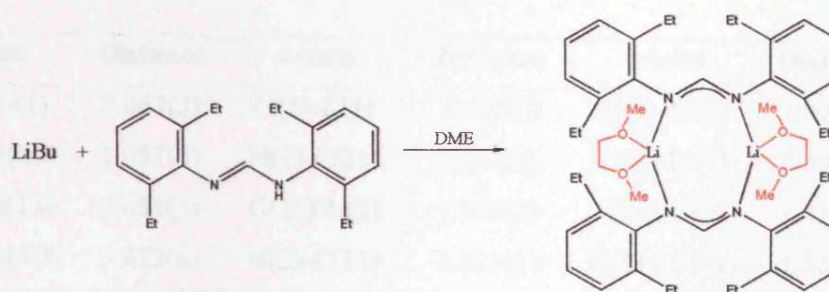
It was considered that sodium and potassium reagents offer an advantage over the lithium reagents in these lanthanide halide metathesis reactions due to the greater solubility's of lithium halides in organic reaction solvents. As a result, we believe that the potential structural diversity exhibited by the p-block and alkaline earth metals amidinate species warranted research. Such an investigation forms the basis of this chapter.

### 3.2 Results and Discussion

Due to the interesting bonding modes shown by the formamidinate ligands in complexation with lithium, potassium and magnesium<sup>84, 85, 89</sup> we were keen to investigate further whether the metal centre-formamidinate association could be sterically frustrated by increasing the size of the formamidinate ligand. We were also aware of the effect that the introduction of co-ordinating solvents at the group 1 metal centre could achieve.

#### 3.2.1 Lithium Formamidinate Complexes with Oxygen Donor Solvents

Lithium amidinate complexes are often used as precursors or transamination reagents in the formation of transition metal amidinate complexes. They are generally synthesised in the reaction of  $\text{Bu}^n\text{Li}$  with the amidine ligand and reacted with a transition metal halide *in situ*<sup>105</sup>. Alternatively, these complexes can be formed from alkylcarbodiimides in reaction with the bis(trimethylsilyl)amide lithium complex<sup>82</sup>. We opted for the former, with the addition of *N,N'*-di(2,6-dimethylphenyl)formamidine (HFXyl) to a solution of  $\text{Bu}^n\text{Li}$  in hexane and DME failed to yield an isolable product. Undeterred by this we repeated the reaction using the analogous *N,N'*-di(2,6-diethylphenyl)formamidine, (HFPheEt) with  $\text{Bu}^n\text{Li}$  in hexane and DME to afford high yields of the exceptionally stable  $[\{\text{Li}(\text{FPhEt})(\text{DME})\}_2]$  dimer (**3.1**), which displays no noticeable decomposition at temperatures reaching 350 °C (Figure 3.30).



Scheme 3.2 - Synthesis of a dinuclear bis-formamidinate complex (**3.1**)

This complex adopts a dimeric eight membered-puckered ring with an  $\text{Li}_2\text{N}_4\text{C}_2$  ring-core formed from two bridging formamidinate ligands and two lithium metal centres. This puckered ring-core resembles the chair conformation embraced by cyclohexane.

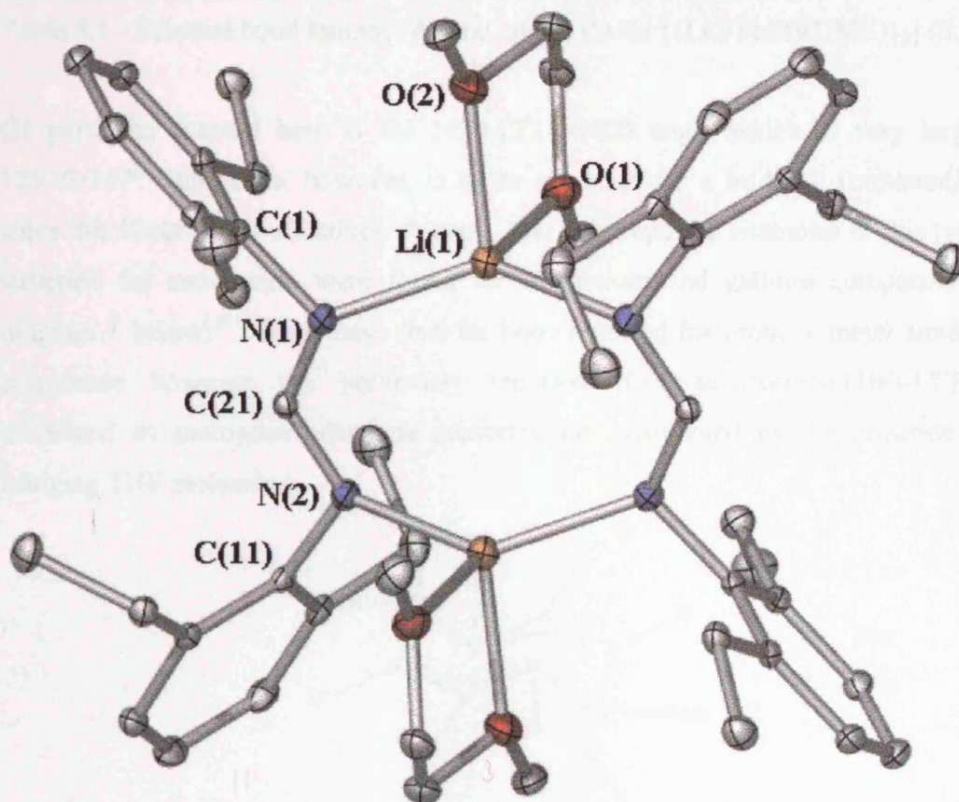


Figure 3.30 - Molecular Structure of  $[\{\text{Li}(\text{FPhEt})(\text{DME})\}_2]$  (3.1)

Atoms	Distance	Atoms	Distance	Atoms	Distance
Li(1)-N(1)	2.047(3)	N(1)-C(1)	1.432(2)	O(1)-Li(1)	2.074(3)
Li(1)-N(2)#	2.051(3)	N(1)-C(21)	1.316(2)	O(2)-Li(1)	2.097(3)
N(2)-Li(1)#	2.051(3)	C(21)-N(2)	1.324(2)	C(1)-C(2)	1.410(3)
Li(1)-Li(1)#	3.422(6)	N(2)-C(11)	1.421(2)	C(11)-C(12)	1.419(3)



Atoms	Angle	Atoms	Angle
N(1)-C(21)-N(2)	125.93(16)	N(1)-Li(1)-N(2)#	132.75(16)
C(21)-N(1)-Li(1)	128.02(14)	C(1)-N(1)-C(21)	113.40(14)
C(21)-N(2)-Li(1)#	122.53(14)	C(11)-N(2)-C(21)	114.78(15)

Table 3.1 - Selected bond lengths (Å) and angles (°) for [ $\{\text{Li}(\text{FPhEt})(\text{DME})\}_2$ ] (**3.1**)

Of particular interest here is the N(1)-C(21)-N(2) angle which is very large at 125.93(16)°. This angle, however, is to be expected for a bridging formamidinate, since this backbone is effectively “open”. The only reported examples of this type of structure for amidinates, were found for aluminium and gallium complexes (see diagram 1 below)<sup>101</sup>. None have thus far been reported for group 1 metal amidinate complexes however the previously reported  $[\text{Li}_2(p\text{-tolylform})_2(\text{THF})_3] \cdot 2\text{THF}$ <sup>87</sup> embraced an analogous boat type conformation encouraged by the presence of a bridging THF molecule.

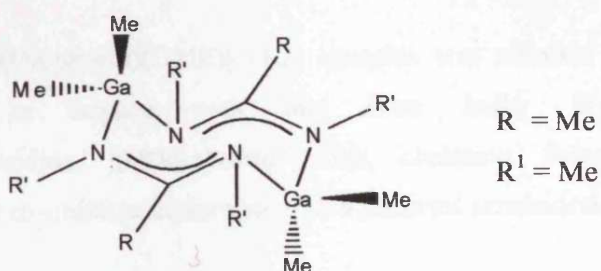
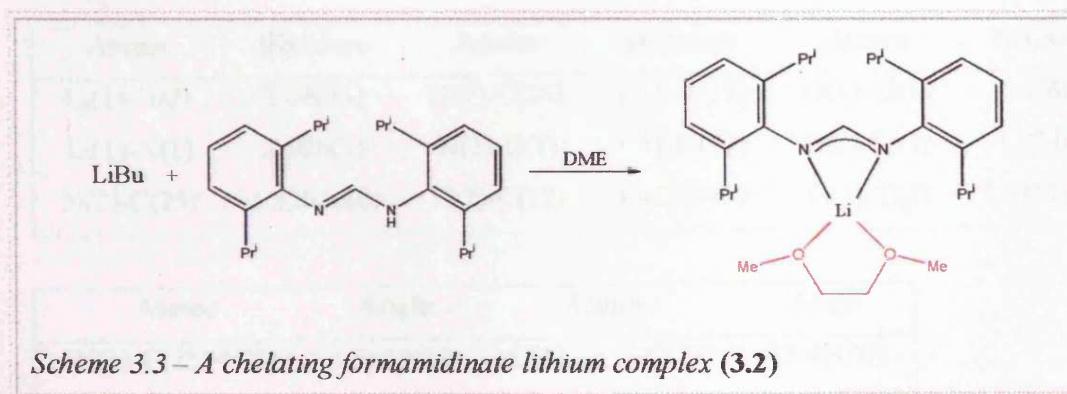


Figure 3.31 – Structure of a Gallium Amidinate “Chair” Complex  $[(\text{CH}_3)_2\text{Ga}(\text{NCH}_3)_2\text{CCH}_3]_2$ <sup>101</sup>

The previously reported gallium complex (diagram 1) displays an acute N-C-N angle at 117.4(4)° compared to the 125.93(16)° observed in our group 1 metal formamidinate complex. This can be attributed to the steric effect the methyl group imposes on the NCN backbone and the differences in size of the metals. This effect is also observed in the N-Ga-N bridging angle at 110.0(2)° compared to the more obtuse N(1)-Li(1)-N(2)# at 132.75(16)° in (**3.1**). The gallium metal is also closer to the bonding amidinate nitrogen atoms *ca.* 1.98 Å compared to the lithium centres at *ca.* 2.05 Å in our complex.

Comparisons of (3.1) with the “boat” shaped complex  $[\text{Li}_2(p\text{-tolylform})_2(\text{THF})_3] \cdot 2\text{THF}$ <sup>87</sup> are more favourable (see section 3.1.5.2). The most obvious difference between these complexes is the bidentate DME molecules in (3.1) giving a distorted tetrahedral geometry around the lithium centre and the fact that the THF co-ordinated complex has a boat conformation. This geometry is achieved by the inclusion of two terminal monodentate THF molecules co-ordinating to each lithium atom and an equal share in one bridging THF molecule between the two metal centres<sup>87</sup>. Also apparent is the  $[\{\text{Li}(\text{FPhEt})(\text{DME})\}_2]$  (3.1) complex having equal Li-N bond lengths 2.047(3) Å, compared to the less symmetric bonding exhibited by the  $[\text{Li}_2(p\text{-tolylform})_2(\text{THF})_3] \cdot 2\text{THF}$  complex with Li-N bond lengths of 2.015(7) Å and 2.041(8) Å. Due to the absence of a bridging THF molecule in  $[\{\text{Li}(\text{FPhEt})(\text{DME})\}_2]$  (3.1), the lithium centres are not forced into such close proximity and hence are further apart at 3.422(6) Å compared to the case in  $[\text{Li}_2(p\text{-tolylform})_2(\text{THF})_3] \cdot 2\text{THF}$ , 2.807(13) Å<sup>87</sup>.

A stable monomeric  $[\text{Li}(\text{DippForm})(\text{DME})]$  (3.2) complex was afforded from the reaction of  $\text{Bu}^n\text{Li}$  in hexane with the more bulky *N,N'*-di(2,6-diisopropylphenyl)formamidine, (HDippForm). This chelating formamidinate complex possesses a four co-ordinate lithium atom in a distorted tetrahedral geometry (Scheme 3.3).





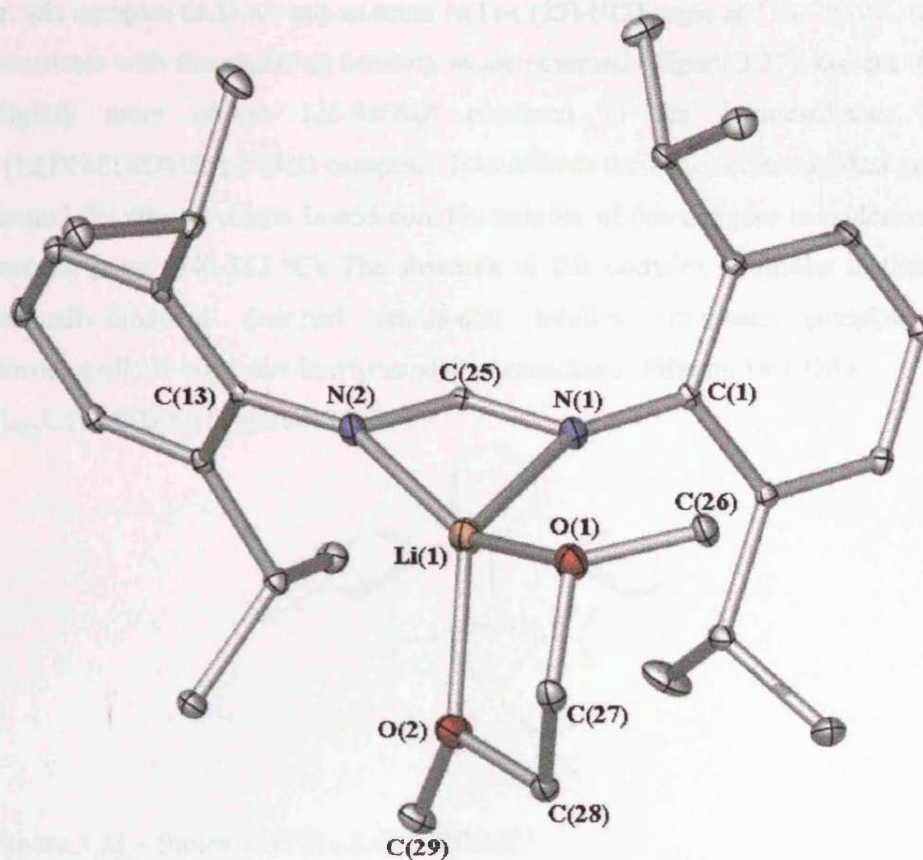


Figure 3.32 – Molecular Structure of [Li(DippForm)(DME)] (3.2)

Atoms	Distance	Atoms	Distance	Atoms	Distance
Li(1)-N(2)	2.046(3)	N(1)-C(25)	1.3184(17)	O(1)-Li(1)	2.028(3)
Li(1)-N(1)	2.026(3)	N(1)-C(1)	1.4106(17)	O(2)-Li(1)	1.974(3)
N(2)-C(25)	1.3204(16)	N(2)-C(13)	1.4213(17)	C(1)-C(2)	1.4152(19)

Atoms	Angle	Atoms	Angle
N(1)-C(25)-N(2)	120.43(12)	O(1)-Li(1)-O(2)	83.48(10)
C(25)-N(1)-Li(1)	85.73(10)	N(1)-Li(1)-O(1)	108.12(12)
C(25)-N(2)-Li(1)	84.87(10)	N(1)-Li(1)-O(2)	125.07(13)
C(25)-N(1)-C(1)	118.53(11)	N(2)-Li(1)-O(1)	153.69(14)
N(1)-Li(1)-N(2)	68.45(9)	N(2)-Li(1)-O(2)	120.54(13)

Table 3.2 – Selected bond lengths (Å) and angles (°) for [Li(DippForm)(DME)] (3.2)

In this complex (**3.2**) we see an acute N(1)-C(25)-N(2) angle at  $120.43(12)^\circ$ , which is consistent with the chelating bonding mode observed (Figure 3.32), compared to the slightly more obtuse  $125.93(16)^\circ$  observed in the formamidinate bridged  $[\{\text{Li}(\text{FPhEt})(\text{DME})\}_2]$  (**3.1**) complex. This affords the distorted tetrahedral geometry around the lithium centre. In addition, the stability of this complex is evidenced by its melting point ( $340\text{--}353^\circ\text{C}$ ). The structure of this complex is similar to that of the sterically-hindered distorted tetrahedral lithium amidinate complex, *N,N'*-diisopropyl[2,6-bis(4-*tert*-butylphenyl)]benzamidinato-lithium(TMEDA)  $[\text{L}_{\text{Bu}}\text{Li}(\text{TMEDA})]$  (Figure 3.33)<sup>92</sup>.

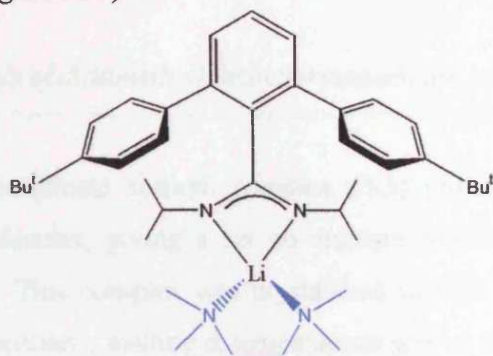


Figure 3.33 – Structure of  $[\text{L}_{\text{Bu}}\text{Li}(\text{TMEDA})]$ <sup>92</sup>

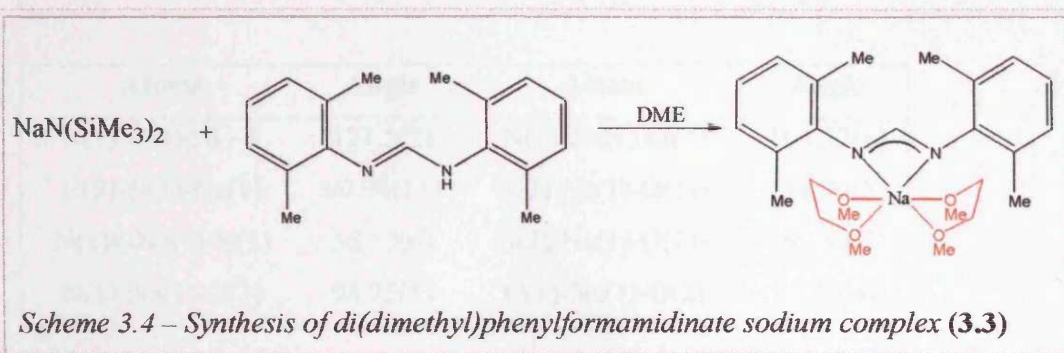
The  $[\text{L}_{\text{Bu}}\text{Li}(\text{TMEDA})]$  complex (Figure 3.33) has a more acute N(1)-C(1)-N(2) chelating angle of  $116.3(4)^\circ$  compared to  $120.43(12)^\circ$  in  $[\text{Li}(\text{DippForm})(\text{DME})]$  (**3.2**). This acuteness is caused by the steric hindrance imposed on the amidinate from the bulky phenyl substituent on the NCN backbone. This restriction coupled with the TMEDA N(3)-Li(1)-N(4) “bite angle” at  $86.5(4)^\circ$ , DME O(1)-Li(1)-O(2) “bite angle” at  $83.48(10)^\circ$  in  $[\text{Li}(\text{DippForm})(\text{DME})]$  (**3.2**), gives rise to the similarities and distortions imposed on the tetrahedral geometries.

### 3.2.2 Sodium Formamidinate Complexes with Oxygen Donor Solvents

Sodium amidinate precursors to salt elimination reactions offer an advantage over their lithium counterparts in the fact that sodium chloride is insoluble in organic solvents. Therefore in reactions with the f-block halides, traces of sodium chloride in the products are eliminated. The increased reactivity associated with sodium



amidinates is another advantage to using these complexes over their lithium counterparts. Using the sodium bis(trimethylsilyl)amide reagent, which had proved successful with previous work within the Junk group<sup>84</sup>, we attempted its reaction with *N,N'*-di(2,6-dimethylphenyl)formamidine, (HFXyl) (*Scheme 3.4*).



The chelating formamidinate sodium complex (**3.3**) obtained contained two co-ordinating DME molecules, giving a six co-ordinate sodium centre in a distorted octahedral geometry. This complex was crystallised in high yields and displayed a moderate thermal robustness, melting at temperatures greater than 62 °C.

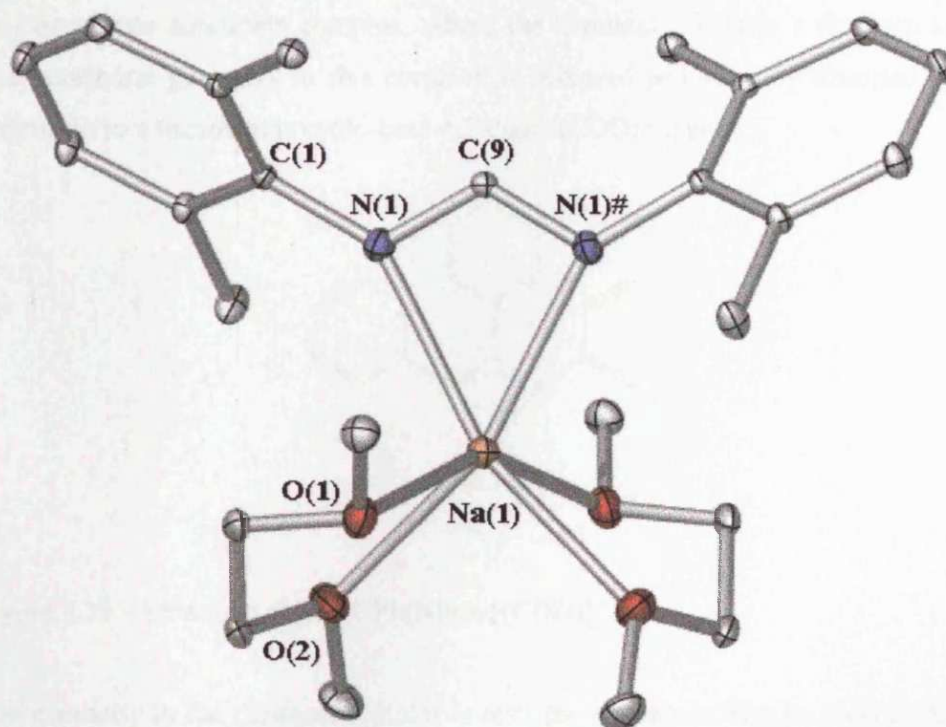


Figure 3.34 – Molecular Structure of [Na(FXyl)(DME)<sub>2</sub>] (**3.3**)

Atoms	Distance	Atoms	Distance	Atoms	Distance
Na(1)-N(1)	2.4270(15)	C(9)-N(1)#	1.3178(16)	Na(1)-O(2)#	2.3659(13)
Na(1)-N(1)#	2.4270(15)	N(1)-C(1)	1.3981(19)	Na(1)-O(1)	2.4362(17)
N(1)-C(9)	1.3178(16)	Na(1)-O(2)	2.3659(13)	Na(1)-O(1)#	2.4362(17)

Atoms	Angle	Atoms	Angle
N(1)-C(9)-N(1)#	121.5(2)	N(1)-Na(1)-O(2)	104.37(4)
C(9)-N(1)-Na(1)	90.94(11)	N(1)-Na(1)-O(1)#	111.93(5)
N(1)#-Na(1)-N(1)	56.57(6)	N(1)-Na(1)-O(2)#	160.50(5)
N(1)-Na(1)-O(1)	94.75(5)	O(1)-Na(1)-O(2)	70.70(4)

Table 3.3 – Selected bond lengths (Å) and angles (°) for [Na(FXyl)(DME)<sub>2</sub>] (**3.3**)

With this complex we observe a slightly more obtuse N(1)-C(9)-N(1)# angle of 121.5°, than observed in (**3.2**), which is anticipated for such a chelating ligand. This increase in bite angle (*ca.* 1°) to the lithium complex (**3.2**) is attributed to the ionic radius of sodium being greater than lithium. This complex is comparable with another six co-ordinate amidinate complex, where the amidinate chelates a rhodium centre. The octahedral geometry in this complex is achieved and severely distorted by co-ordination to a tetradentate cyclo-octa-1,5-diene (COD) ligand<sup>106</sup>.

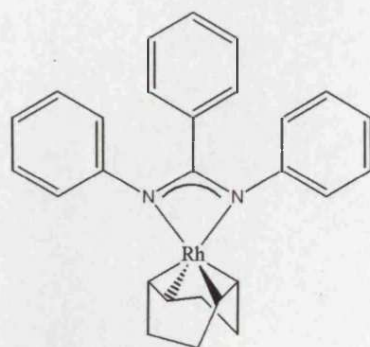


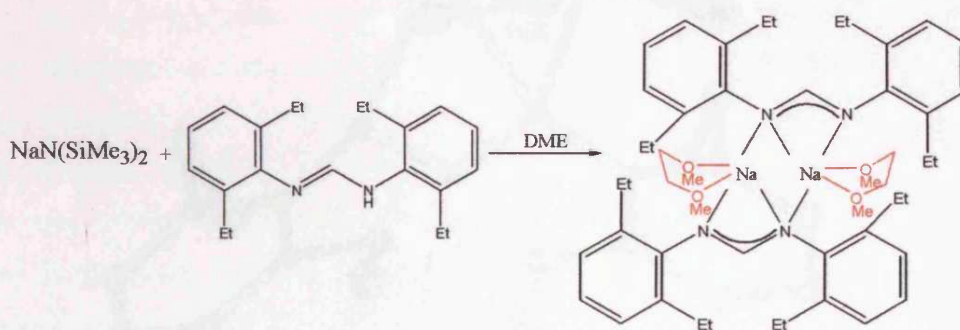
Figure 3.35 – Structure of [Rh{CPh(NPh)<sub>2</sub>}(COD)]<sup>106</sup>

The geometry in the rhodium complex is restricted from reaching its ideal octahedral geometry by both the chelating benzamidinate and the tetradentate COD ligands. This is highlighted by the amidinates N(1)-Rh-N(2) “bite angle” of 63.2(2)° compared to



the preferred  $90^\circ$ . The COD ligand forms an even more acute “bite angle” at rhodium of  $38.5(3)^\circ$ . Unsurprisingly, the benzamidinate backbone angle  $N(1)-C(1)-N(2)$  is more acute at  $110.0(6)^\circ$  when compared to *ca.*  $120^\circ$  in the formamidinate complexes. This is due to a phenyl group on the backbone carbon encouraging chelation due to its steric obligations, as opposed to the hydrogen substituent in formamidinates.

We proposed that the slightly more sterically demanding analogous diethyl phenyl substituted ligand (HFPhEt) would frustrate these two DME molecules from binding to one sodium centre which appears to be the case as highlighted in *Scheme 3.5* and *Figure 3.36*.



*Scheme 3.5 – Formation of the dinuclear chelating bridging di(diethyl)phenyl formamidinate complex (3.4)*

The dinuclear complex (**3.4**) places each sodium atom at the centre of a distorted trigonal bipyramidal geometry. The five co-ordinate sites demanded by this geometry are occupied by a unusual ( $\mu:\eta^2\eta^1$ ) chelate bridging formamidinate bonding mode and a chelating DME molecule. This is a primitive example of ring laddering<sup>16, 107</sup> with a  $\text{Na}_2\text{N}_2$  core. The bulky diethylphenyl groups on the amidinate nitrogen prohibit further laddering.

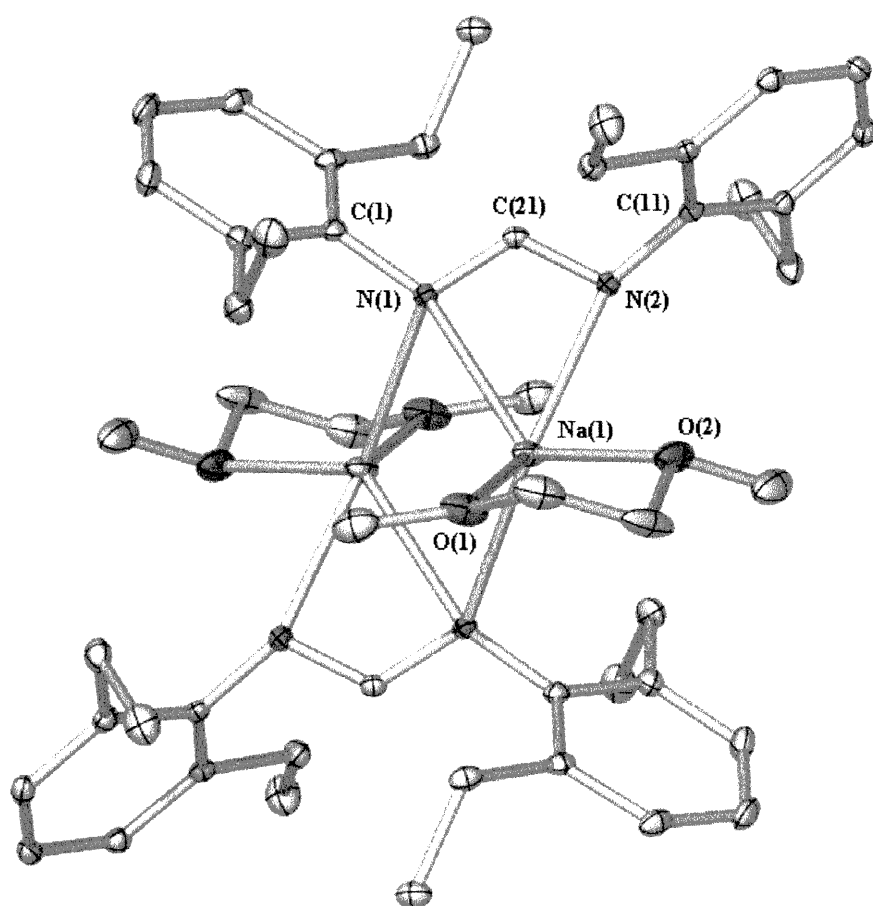


Figure 3.36 – Molecular Structure of [ {Na(FPhEt)(DME)}<sub>2</sub>] (3.4)

Atoms	Distance	Atoms	Distance	Atoms	Distance
Na(1)-Na(1)#	3.147(2)	N(1)-Na(1)#	2.4757(16)	N(2)-C(11)	1.416(2)
Na(1)-N(1)	2.6177(15)	N(1)-C(1)	1.417(2)	Na(1)-O(1)	2.3773(17)
Na(1)-N(2)	2.394(5)	N(1)-C(21)	1.332(2)	Na(1)-O(2)	2.3690(16)
Na(1)-N(1)#	2.4757(16)	C(21)-N(2)	1.309(2)	Na(1)#-C(1)	2.9738(19)

Atoms	Angle	Atoms	Angle
N(2)-C(21)-N(1)	123.63(15)	N(2)-Na(1)-O(1)	132.68(6)
C(21)-N(1)-Na(1)	83.23(10)	N(2)-Na(1)-O(2)	85.00(6)
C(21)-N(2)-Na(1)	93.27(10)	N(1)-Na(1)#-N(1)#	103.69(5)
C(21)-N(1)-Na(1)#	140.16(11)	Na(1)#-N(1)-Na(1)	76.31(5)
N(1)-Na(1)-N(2)	55.14(5)	O(1)-Na(1)-O(2)	70.65(6)
N(1)-Na(1)-O(1)	118.63(6)	N(2)-Na(1)-N(1)#	133.40(6)
N(1)-Na(1)-O(2)	134.43(5)	C(1)-N(1)-Na(1)#	95.77(10)

Table 3.4 – Selected bond lengths (Å) and angles (°) for [ $\{\text{Na}(\text{FPhEt})(\text{DME})\}_2$ ] (**3.4**)

The Na-N(bridging) distances of 2.4757 Å are, as expected, longer than the Na(1)-N(2)(chelating) distance of 2.395 Å but importantly shorter than the Na(1)-N(1)(chelating) extended distance of 2.618 Å. The N(2)-C(21)-N(1) angle of 123.63° is considered quite large for a chelating ligand even when the metal it chelates is sodium. However, the obtuseness of this angle is encouraged by the partial bridging/chelating bonding mode of the ligand. This complex bears a remarkable resemblance to a number of other previously reported alkali metal formamidinate and amidinate complexes. The first complexes of this type were synthesised by the Mulvey group<sup>108</sup> who reported the crystallographically analysed [ $\text{Me}(2\text{-Pyr})\text{NNa}(\text{TMEDA})$ ]<sub>2</sub> and [ $\text{Ph}(2\text{-Pyr})\text{NK}(\text{TMEDA})$ ]<sub>2</sub> complexes. These contained elongated amido N-M bond lengths at 2.446(4) Å, 2.454(4) Å and 2.805(2) Å, 2.805(3) Å respectively. These complexes differ from our complex in that both amido nitrogen atoms are bridging and chelating to yield a  $\mu_2\eta^2\eta^2$  bonding mode.

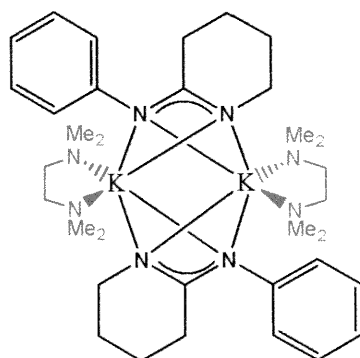


Figure 3.37 – Structure of [ $\text{Ph}(2\text{-Pyr})\text{NK}(\text{TMEDA})$ ]<sub>2</sub><sup>108</sup>

Also worth comparing with (3.4) is the first crystallography characterised formamidinate group 1 metal complex,  $[\text{Li}_2(\mu\text{-DTolF})_2(\text{Et}_2\text{O})_2]$ , which similarly contains the  $\mu:\eta^2\eta^1$  bond modes<sup>88</sup>. However, in this complex the lithium centre is closer to the bridging N-centre than the solely chelating N-centre observed in (3.4)<sup>88</sup>.

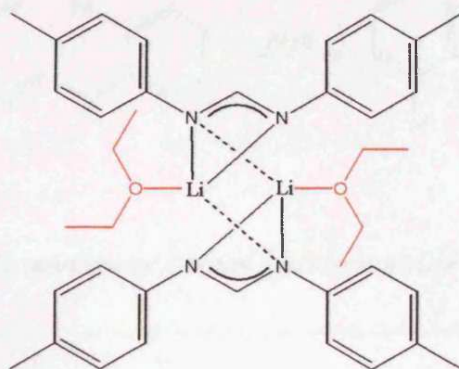


Figure 3.38 – Structure of  $[\text{Li}_2(\mu\text{-DTolF})_2(\text{Et}_2\text{O})_2]$ <sup>88</sup>

Another closely related complex is a sodium formamidinate complex reported by the Junk group<sup>84</sup>. This was formed in a reaction using the same *para*-tolylformamidine ligand, with sodium hydride in DME. This afforded the dinuclear  $[\text{Na}_2(p\text{-tolylform})_2(\text{DME})_2]$ <sup>84</sup> which displays a  $\mu:\eta^2\eta^1$  bonding mode.

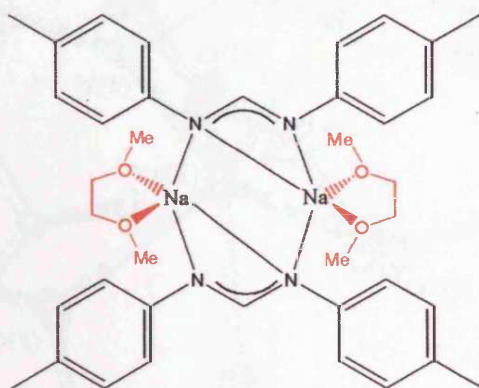
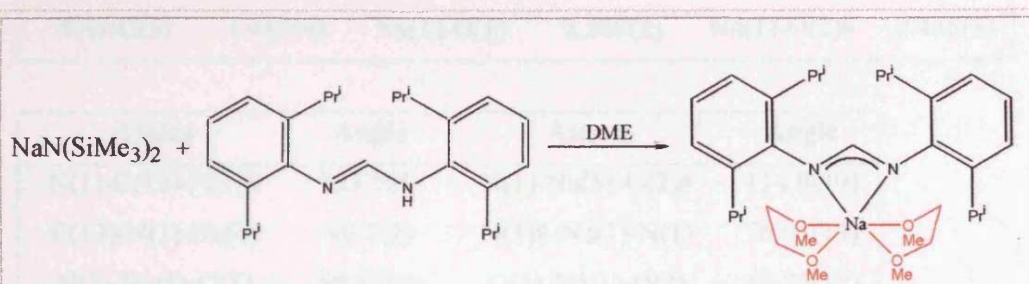


Figure 3.39 – Structure of  $[\text{Na}_2(p\text{-tolylform})_2(\text{DME})_2]$ <sup>84</sup>



We then progressed to the bulkier *N,N'*-di(2,6-diisopropylphenyl)formamidine ligand, which was reacted with the  $\text{NaN}(\text{SiMe}_3)_2$  reagent in DME to yield a chelate monomer  $[\text{Na}(\text{DippForm})(\text{DME})_2]$  complex. This complex is very similar to (3.3).



Scheme 3.6 – Synthesis of a monomeric sodium di(diisopropyl)phenyl formamidinate complex (3.5)

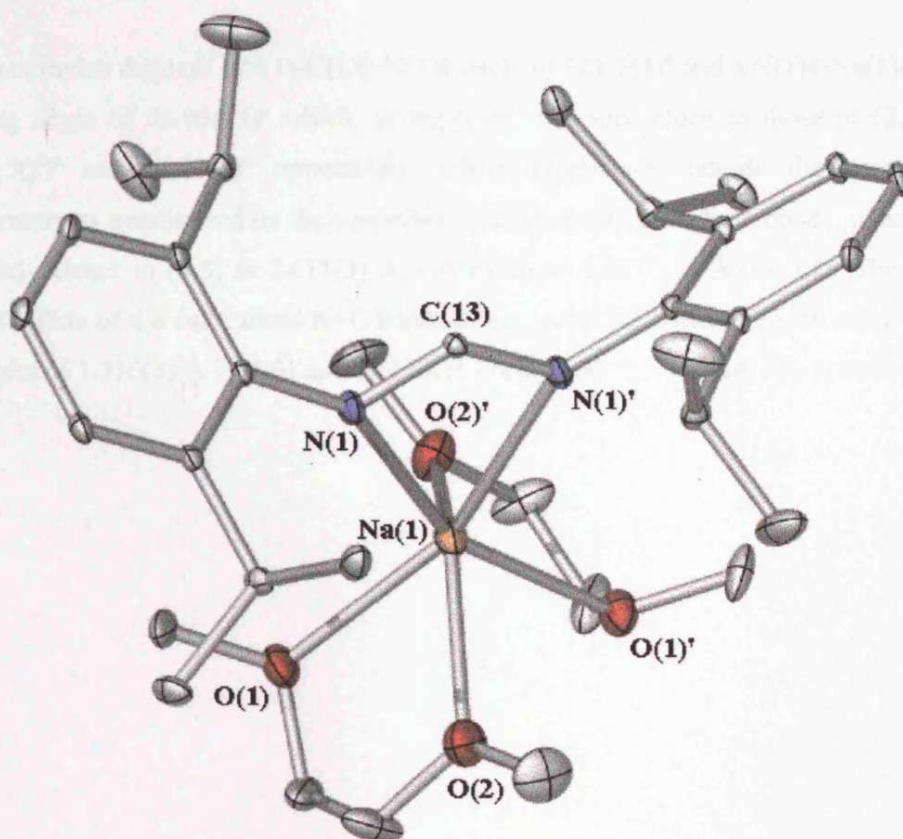


Figure 3.40 – Molecular Structure of  $[\text{Na}(\text{DippForm})(\text{DME})_2]$  (3.5)

Atoms	Distance	Atoms	Distance	Atoms	Distance
Na(1)-N(1)	2.411(3)	N(1)-C(13)	1.316(3)	Na(1)-O(2)	2.438(3)
Na(1)-N(1)#	2.411(3)	C(13)-N(1)#	1.316(3)	Na(1)-O(1)#	2.388(2)
N(1)-C(1)	1.412(4)	Na(1)-O(1)	2.388(2)	Na(1)-O(2)#	2.438(3)

Atoms	Angle	Atoms	Angle
N(1)-C(13)-N(1)#	121.7(4)	N(1)-Na(1)-O(2)#	114.04(9)
C(13)-N(1)-Na(1)	90.7(2)	N(1)#-Na(1)-N(1)	56.95(13)
N(1)-Na(1)-O(1)	99.87(9)	O(1)-Na(1)-O(2)	69.25(10)
N(1)-Na(1)-O(2)	103.56(9)	O(1)-Na(1)-O(1)#	103.32(13)
N(1)-Na(1)-O(1)#	156.80(9)	O(1)-Na(1)-O(2)#	84.33(10)

Table 3.5. Selected bond lengths (Å) and angles (°) for [Na(DippForm)(DME)<sub>2</sub>] (**3.5**)

This complex displays a N(1)-C(13)-N(1)# angle of 121.7(4)° and a N(1)#-Na(1)-N(1) biting angle of 56.95(13)° which, as expected, are very close to those in (**3.3**) at 121.5(2)° and 56.57(6)° respectively. Other similarities include the complex's symmetry as emphasised by the equivalence of the amido N-sodium bonds, which are slightly closer in (**3.5**) at 2.411(3) Å, compared to 2.427(15) Å in (**3.3**). The even distribution of the delocalised N=C bonds to give an NCN backbone with equal bond lengths of 1.316(3) Å in (**3.5**) and 1.3178(16) Å in (**3.3**) also stresses this symmetry.

### 3.2.3 Potassium Formamidinate Complexes with Oxygen Donor Solvents

There is a scarcity of potassium amidinate and guanidinate complexes in the literature, with initially only three such complexes reported<sup>83, 109, 110</sup>. Since then work by the Junk group has done much to address this imbalance with the publication of the first potassium formamidinate complex<sup>85</sup>. This work has been followed up with reports of other related potassium formamidinate complexes<sup>86, 87</sup>. Like their sodium counterparts, potassium amidinates have potential as useful transamination reagents, offering increased reactivity. They have the added bonus that potassium halides are insoluble in organic solvents. In addition, potassium has a larger ionic radius to co-ordinate ligands and as seen from the above references, has an affinity for  $\eta^6\pi$ -arene interactions. The first potassium formamidinate complex, reported by the Junk group<sup>85</sup>, consisted of a monomeric molecular structure which incorporates one protonated dimesitylene formamidine chelating through the both  $\eta^6$ -arene and N-imino functionalities, and a deprotonated dimesitylene formamidinate ligand co-ordinating through an unorthodox near symmetric NCN  $\eta^1$ -amide mode with an  $\eta^6$ -arene group ligation. The protonated ligand allows for further association in this complex by hydrogen bonding to the adjacent monomer's deprotonated ligand. This complex was prepared from both potassium hydride and the bis(trimethylsilyl) amide reagent in mixed solutions of toluene-TMEDA and THF. We utilised the related bis-xylene formamidine ligand (HFXyl) in a reaction with potassium bis(trimethylsilyl) amide in DME to successfully yield a complex with three different potassium environments  $[K_3(FXyl)_3(DME)_3]$  (3.6).

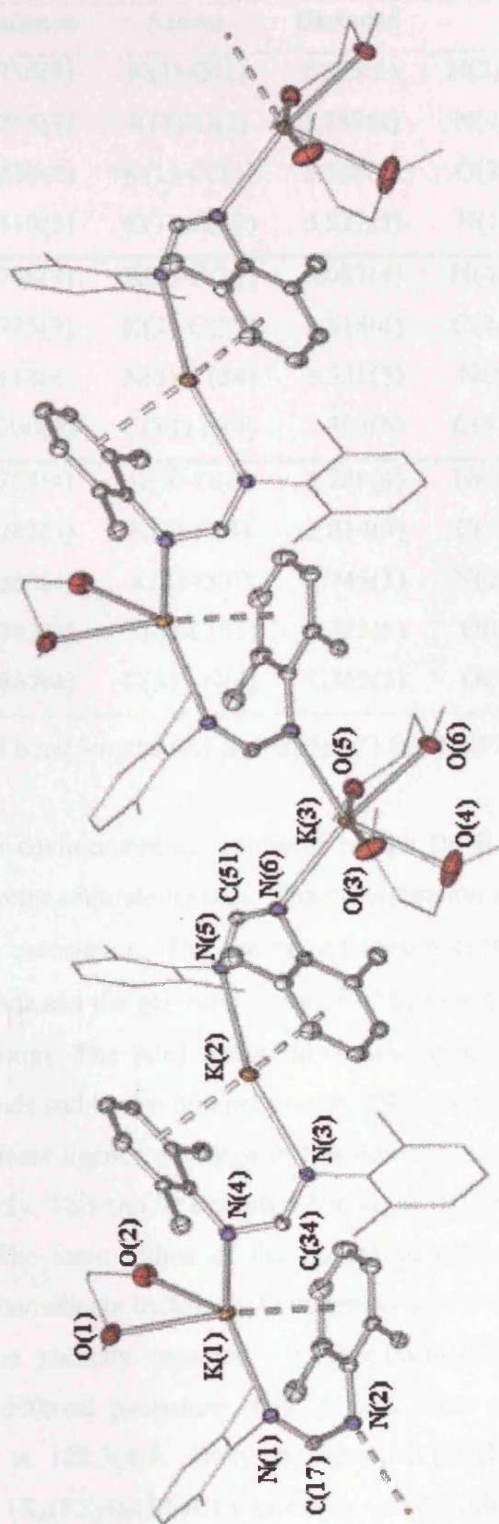


Figure 3.41 – Molecular Structure of  $[K_3(FXyl)_3(DME)_3]$  (3.6)

Atoms	Distance	Atoms	Distance	Atoms	Angle
K(1)-N(1)	2.736(3)	K(1)-O(1)	2.819(3)	N(2)-C(17)-N(1)	128.1(4)
K(1)-N(4)	2.715(3)	K(1)-O(2)	2.757(3)	N(4)-K(1)-N(1)	114.43(10)
N(1)-C(17)	1.324(5)	K(1)-C(14)	3.188(4)	O(2)-K(1)-O(1)	59.42(10)
N(2)-C(17)	1.310(5)	K(1)-C(12)	3.527(5)	N(1)-K(1)-O(1)	98.78(10)
K(2)-N(3)	2.766(3)	K(2)-C(31)	3.087(4)	N(4)-C(34)-N(3)	128.3(4)
K(2)-N(5)	2.775(3)	K(2)-C(27)	3.318(4)	C(34)-N(3)-K(2)	125.0(3)
K(2)-C(44)	3.148(4)	N(3)-C(34)	1.331(5)	N(3)-K(2)-N(5)	146.52(10)
K(2)-C(47)	3.300(4)	C(34)-N(4)	1.303(5)	C(51)-N(5)-K(2)	126.9(3)
K(3)-N(6)	2.758(4)	K(3)-O(4)	2.789(4)	N(6)-C(51)-N(5)	127.1(4)
K(3)-N(2)#	2.742(4)	K(3)-O(5)	2.814(3)	C(51)-N(6)-K(3)	138.2(3)
K(3)-C(17)#	3.380(4)	K(3)-O(6)	2.745(3)	N(2)#-K(3)-N(6)	117.44(11)
N(2)-K(3)#	2.742(4)	N(5)-C(51)	1.328(5)	O(6)-K(3)-O(5)	61.29(10)
K(3)-O(3)	2.867(4)	C(51)-N(6)	1.312(5)	O(4)-K(3)-O(3)	58.77(12)

Table 3.6 – Selected bond lengths (Å) and angles (°) for [K<sub>3</sub>(FXyl)<sub>3</sub>(DME)<sub>3</sub>] (3.6)

The first potassium environment is fabricated by the DME molecule co-ordination and two bridging formamidinate ligands. The co-ordination site is saturated with an  $\eta^6$ -arene-potassium association. The second potassium centre shares two bridging formamidinate ligands and the geometry is satisfied by two  $\eta^6$ -arene rings associating to the potassium atom. The third potassium centre again shares in two bridging formamidinate ligands and is also bonded to two DME molecules. The NCN angles of all three formamidinate ligands are large in this complex at 128.1(4)°, 128.3(4)° and 127.1(4)° respectively. This can be expected due to the bridging nature of the ligands in this complex. The ionic radius of the potassium centres also encourages this opening of the formamidinate backbone. Unsurprisingly this complex bears a striking resemblance to the recently reported [ $\{K(\text{DippForm})_2K(\text{THF})_2\}_n$ ]<sup>87</sup> complex, a species with two different potassium environments. That complex also displays a large NCN angle at 128.3(4)Å. Both the reported [ $\{K(\text{DippForm})_2K(\text{THF})_2\}_n$ ]<sup>87</sup> complex and our [K<sub>3</sub>(FXyl)<sub>3</sub>(DME)<sub>3</sub>] complex exhibit similar  $\eta^6$ -arene-potassium interactions to that displayed in the first potassium formamidine complex reported [K{( $\eta^6$ -Mes)NC(H)N(Mes)}{( $\eta^6$ -Mes)NHC(H)N(Mes)}]<sup>85</sup>. The difference between



these products is that the previously reported complex exists as monomeric units, which associate further through hydrogen bonding. However, both our  $[K_3(FXyl)_3(DME)_3]$  (3.6) and the reported  $[K(DippForm)_2K(THF)_2]_n$ <sup>87</sup> complex associate further through bridging formamidinate ligands.

The  $\eta^6$ arene-potassium association was further established in the complex obtained in a reaction of  $KN(SiMe_3)_2$  with the diethylphenyl formamidinate ligand (Figure 3.42 (3.7)).

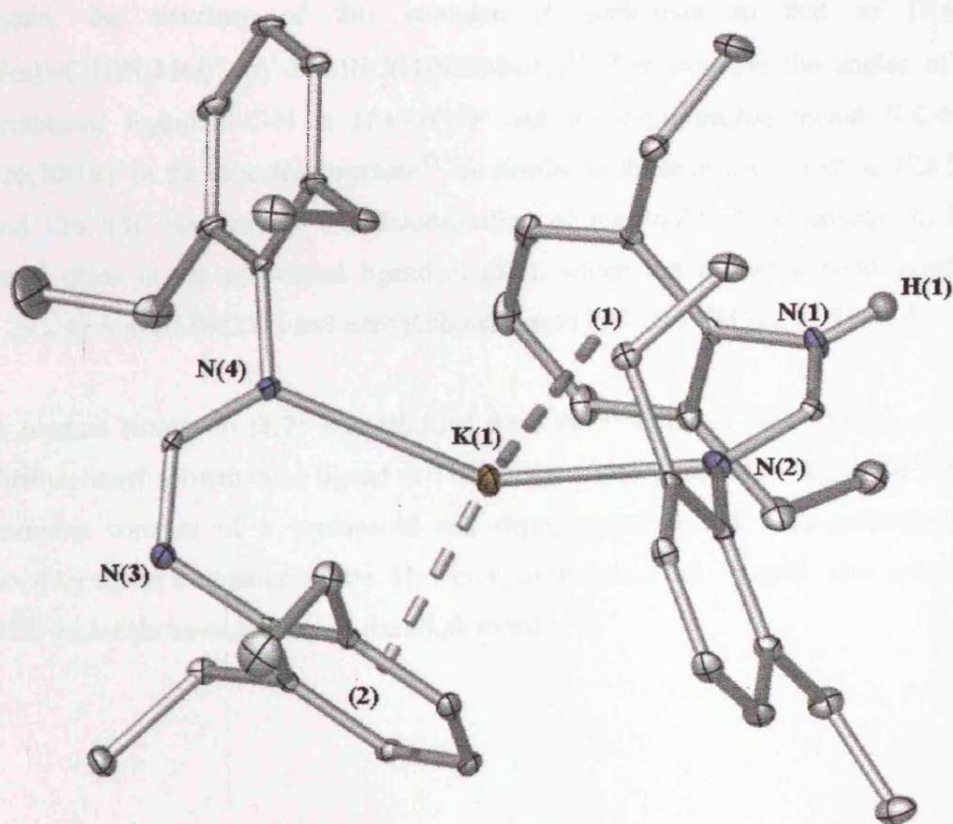


Figure 3.42 – Molecular Structure of  $[K(FPhEt)(HFPhEt)]$  (3.7)

Atoms	Distance	Atoms	Distance	Atoms	Distance
K(1)-N(2)	2.832(3)	C(21)-N(1)	1.341(4)	K(1)-C(2)	3.196(4)
K(1)-N(4)	2.754(3)	N(4)-C(42)	1.312(4)	K(1)-C(4)	3.268(4)
N(2)-C(21)	1.291(4)	C(42)-N(3)	1.327(4)	K(1)-C(27)	3.161(3)

Atoms	Angle	Atoms	Angle
N(2)-C(21)-N(1)	123.5(3)	N(1)-Na(1)-O(2)#	114.04(9)
C(21)-N(2)-K(1)	130.3(2)	N(1)#-Na(1)-N(1)	56.95(13)
N(4)-K(1)-N(2)	136.88(9)	O(1)-Na(1)-O(2)	69.25(10)
N(4)-C(42)-N(3)	126.7(3)	O(1)-Na(1)-O(1)#	103.32(13)
C(42)-N(4)-K(1)	128.6(2)	O(1)-Na(1)-O(2)#	84.33(10)

Table 3.7 – Selected bond lengths (Å) and angles (°) for [K(FPhEt)(HFPhEt)] (**3.7**)

Again, the structure of this complex is analogous to that of  $[K\{(\eta^6\text{-Mes})\text{NC(H)N(Mes)}\}\{(\eta^6\text{-Mes})\text{NC(H)NH(Mes)}\}]]^{85}$ . For example the angles of the protonated ligand N-C-N at  $124.78(17)^\circ$  and the deprotonated ligand N-C-N at  $126.30(18)^\circ$  in the reported structure<sup>85</sup> are similar to those in our complex,  $123.5(3)^\circ$  and  $126.7(3)^\circ$  respectively. No delocalisation of the double bond appears to have taken place in the protonated ligand of (**3.7**), which has a double bond length of  $1.291(4)$  Å in N(2)-C(21) and a single bond length in C(21)-N(1) of  $1.341(4)$  Å.

A product similar to (**3.7**) was afforded from the reaction of  $\text{KN}(\text{SiMe}_3)_2$  with the diethylphenyl formamidine ligand in THF, viz (**3.8**), (Figure 3.43). Again the formed complex consists of a protonated and deprotonated ligand both monodentately bonding to the potassium centre. However, in this case the complex also contains a THF molecule co-ordinating to the alkali metal.



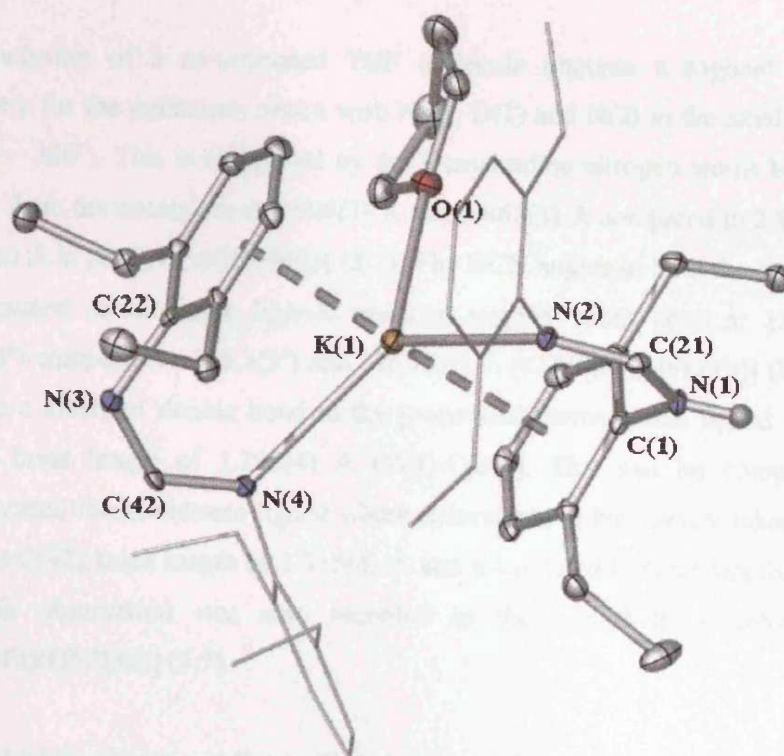


Figure 3.43 – Molecular Structure of [K(FPhEt)(HPhEt)(THF)] (3.8)

Atoms	Distance	Atoms	Distance	Atoms	Distance
K(1)-N(2)	2.908(3)	C(21)-N(1)	1.343(4)	C(42)-N(3)	1.325(4)
K(1)-N(4)	2.867(3)	N(1)-C(1)	1.427(4)	N(3)-C(22)	1.416(4)
K(1)-O(1)	2.841(3)	N(4)-C(32)	1.427(4)	K(1)-centroid(1)	3.103(10)
N(2)-C(11)	1.430(4)	N(4)-C(42)	1.315(4)	K(1)-centroid(2)	2.990(10)
N(2)-C(21)	1.295(4)				

Atoms	Angle	Atoms	Angle
N(2)-C(21)-N(1)	124.4(3)	N(4)-C(42)-N(3)	127.3(3)
C(21)-N(2)-K(1)	129.4(2)	C(42)-N(4)-K(1)	128.3(2)
N(2)-K(1)-O(1)	107.79(9)	N(4)-K(1)-O(1)	128.58(9)
N(4)-K(1)-N(2)	123.61(8)	cent.(1)-K(1)-cent.(2)	173.6(3)
centroid(1)-K(1)-N(2)	77.7(2)	centroid(2)-K(1)-N(4)	78.7(2)
centroid(1)-K(1)-O(1)	86.1(2)	centroid(2)-K(1)-N(2)	107.2(2)
centroid(1)-K(1)-N(4)	102.3(2)	centroid(2)-K(1)-O(1)	88.4(2)

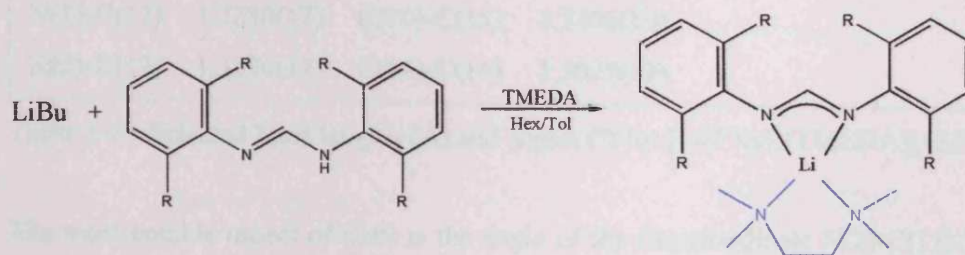
Table 3.8 – Selected bond lengths (Å) and angles (°) for [K(FPhEt)(HPhEt)(THF)] (3.8)



The inclusion of a co-ordinated THF molecule imposes a trigonal bipyramidal geometry for the potassium centre with N(4), O(1) and N(2) in the axial positions ( $\Sigma$  angles =  $360^\circ$ ). This is completed by the formamidine nitrogen atoms being slightly further from the potassium at 2.908(3) Å and 2.867(3) Å compared to 2.832(3) Å and 2.754(3) Å in [K(FPhEt)(HFPhEt)] (3.7). The NCN angles in both the protonated and deprotonated formamidine ligands are also slightly more open at  $124.4(3^\circ)$  and  $127.3(3^\circ)$  compared to  $123.5(3^\circ)$  and  $126.7(3^\circ)$  in [K(FPhEt)(HFPhEt)] (3.7). We can observe a localised double bond in the protonated formamidine ligand with a N=C double bond length of 1.295(4) Å (N(2)-C(21)). This can be compared to the deprotonated formamidinate ligand where delocalisation has clearly taken place with an N(4)-C(42) bond length of 1.315(4) Å and a C(42)-N(3) bond length of 1.325(4) Å. This observation was also recorded in the non THF solvated complex, [K(FPhEt)(HFPhEt)] (3.7).

### 3.2.4 Lithium Formamidinate Complexes with Nitrogen Donor Solvents

The bidentate ligand, tetramethylethylenediamine (TMEDA) was introduced to compare its effect on metal-amidinate bonding relative to O-donor solvents, e.g. DME. First, butyl lithium with *N,N'*-di(2,6-dimethylphenyl)formamidine (HFXyl) in a mixed hexane/TMEDA solution was reacted to afford the chelated monomer (3.9) containing one chelating TMEDA molecule. Identical bonding modes in complexes tetrahedral metal geometries have been seen in the products of the analogous reactions of *N,N'*-di(2,6-diethylphenyl)formamidine (HFPhEt) and *N,N'*-di(2,6-diisopropylphenyl)formamidine (HDippForm) with butyl lithium.



Scheme 3.7 – Reaction of butyl lithium with HFXyl ( $R = \text{Me}$  (3.9)), HFPhEt ( $R = \text{Et}$  (3.10)) and HDippForm ( $R = \text{Pr}^i$  (3.11))

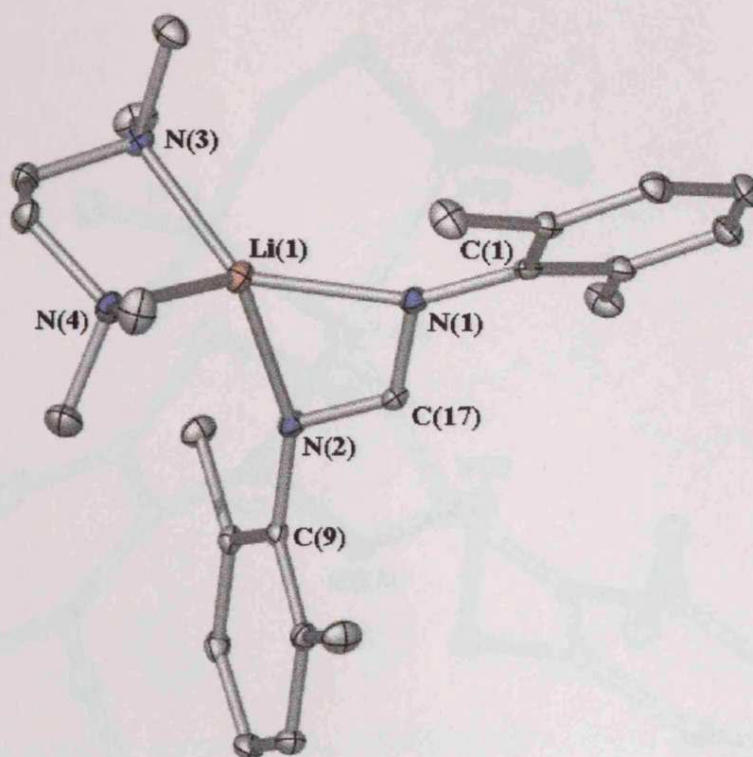


Figure 3.44 – Molecular Structure of [Li(FXyl)(TMEDA)] (**3.9**)

Atoms	Distance	Atoms	Distance	Atoms	Angle
Li(1)-N(2)	2.073(3)	C(21)-C(20)	1.516(2)	N(2)-C(17)-N(1)	120.41(12)
Li(1)-N(1)	2.035(3)	N(3)-C(20)	1.466(2)	N(1)-Li(1)-N(2)	67.86(9)
Li(1)-C(17)	2.357(3)	N(4)-C(21)	1.4717(19)	N(3)-Li(1)-N(4)	87.41(11)
Li(1)-N(3)	2.094(3)	C(2)-C(7)	1.497(2)	N(1)-Li(1)-N(3)	132.29(14)
Li(1)-N(4)	2.125(3)	C(6)-C(8)	1.507(2)	N(2)-Li(1)-N(4)	113.86(12)
N(1)-C(17)	1.3230(17)	C(10)-C(15)	1.5106(19)		
N(2)-C(17)	1.3196(17)	C(14)-C(16)	1.5023(19)		

Table 3.9 – Selected bond lengths (Å) and angles (°) for [Li(FXyl)(TMEDA)] (**3.9**)

The most notable aspect of (**3.9**) is the angle of the formamidinate N(2)-C(17)-N(1) backbone at 120.41(12)°. This compares well to the N(2)-C(21)-N(1) angle in (**3.10**) of 120.10(13)°, and the N(1)-C(25)-N(2) angle of 119.85(11)° in (**3.11**). All are close to the values seen in related O-donor lithium formamidinate complexes such as (**3.2**).



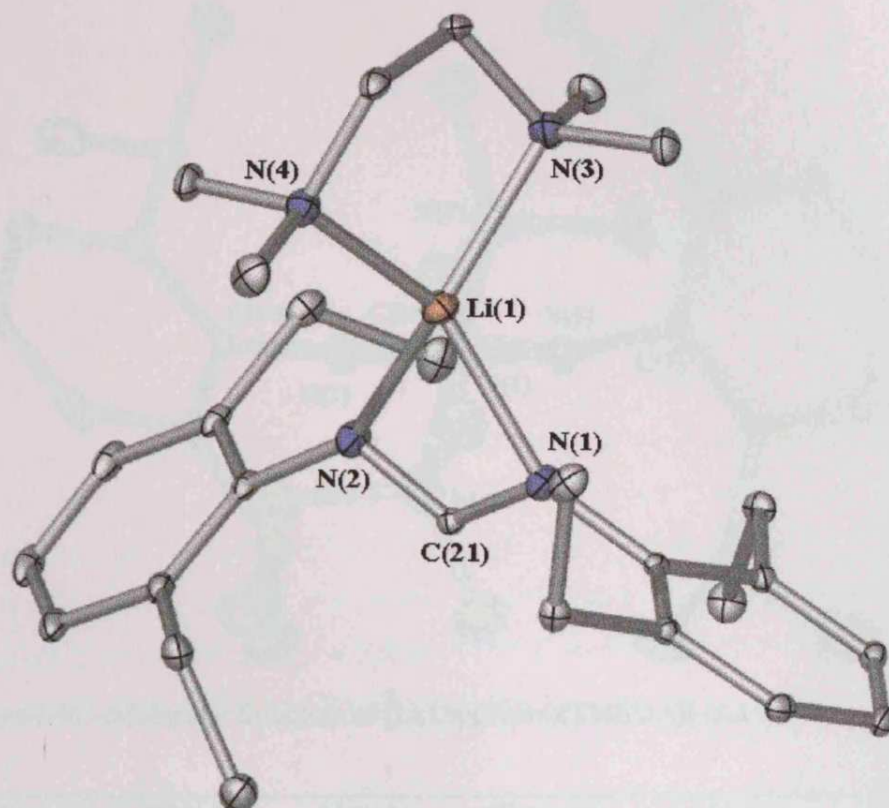


Figure 3.45 – Molecular Structure of [Li(FPhEt)(TMEDA)] (3.10)

Atoms	Distance	Atoms	Distance	Atoms	Angle
Li(1)-N(2)	2.015(3)	C(25)-C(24)	1.510(3)	N(2)-C(21)-N(1)	120.10(13)
Li(1)-N(1)	2.025(3)	N(3)-C(24)	1.480(2)	N(1)-Li(1)-N(2)	68.73(9)
Li(1)-C(21)	2.324(3)	N(4)-C(25)	1.464(2)	N(3)-Li(1)-N(4)	88.43(10)
Li(1)-N(3)	2.063(3)	C(2)-C(7)	1.516(2)	N(1)-Li(1)-N(3)	118.37(12)
Li(1)-N(4)	2.059(3)	C(6)-C(9)	1.510(2)	N(2)-Li(1)-N(4)	113.74(12)
N(1)-C(21)	1.3150(18)	C(12)-C(17)	1.510(3)		
N(2)-C(21)	1.3167(18)	C(16)-C(19)	1.511(2)		

Table 3.10 – Selected bond lengths (Å) and angles (°) for [Li(FPhEt)(TMEDA)] (3.10)

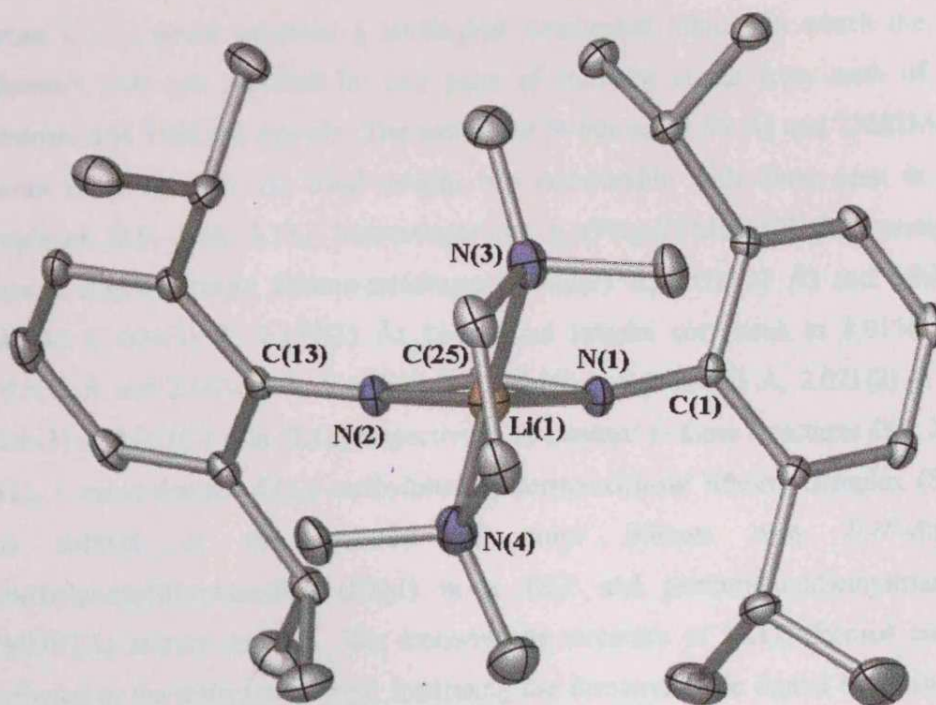


Figure 3.46 – Molecular Structure of [Li(DippForm)(TMEDA)] (3.11)

Atoms	Distance	Atoms	Distance	Atoms	Angle
Li(1)-N(2)	2.024(2)	C(28)-C(29)	1.513(2)	N(1)-C(25)-N(2)	119.85(11)
Li(1)-N(1)	2.021(2)	N(3)-C(28)	1.4747(17)	N(1)-Li(1)-N(2)	68.85(9)
Li(1)-C(25)	2.314(2)	N(4)-C(29)	1.4728(19)	N(3)-Li(1)-N(4)	86.88(9)
Li(1)-N(3)	2.096(3)	C(2)-C(7)	1.5209(17)	N(1)-Li(1)-N(3)	118.62(11)
Li(1)-N(4)	2.067(2)	C(6)-C(10)	1.5230(16)	N(2)-Li(1)-N(4)	121.60(12)
N(1)-C(25)	1.3211(16)	C(14)-C(19)	1.5222(19)		
N(2)-C(25)	1.3218(16)	C(18)-C(22)	1.5149(18)		

Table 3.11 – Selected bond lengths (Å) and angles (°) for [Li(DippForm)(TMEDA)] (3.11)

In (3.11), the C(25)-Li(1) bond length of 2.314(2) Å is considerably longer than the mean Li-C bond distance of 2.255 Å, of previously characterised complexes<sup>111</sup>. This confirms that the backbone carbon is not actually bonded to the lithium metal, but is participating solely as part of an anionic 1,3-diazaallyl chelating unit. These complexes are analogous to the previously described  $L_{Bu}Li(TMEDA)$ <sup>92</sup> complex (see



section 3.2.1), which contains a tetrahedral-coordinated lithium in which the coordination sites are satisfied by two pairs of nitrogen atoms from each of the amidinate and TMEDA ligands. The amidinato N-lithium (1.99 Å) and TMEDA N-lithium (2.09 Å, 2.11 Å) bond lengths are comparable with those seen in our complexes (3.9, 3.10, 3.11). Interestingly the [Li(FXyl)(TMEDA)] (3.9) complex contains slightly longer lithium-amidinate (2.073(3) Å, 2.035(3) Å) and lithium-TMEDA (2.094(3) Å, 2.125(3) Å) Li-N bond lengths compared to 2.015(3) Å, 2.025(3) Å and 2.063(3) Å, 2.059(3) Å in (3.10) and 2.024(2) Å, 2.021(2) Å and 2.096(3) Å, 2.067(2) Å in (3.11) respectively. In contrast to these structures (3.9, 3.10, 3.11), a mono-dentate di(2,6-methylphenyl) formamidinate lithium complex (3.12) was formed in the reaction of butyl lithium with *N,N'*-di(2,6-dimethylphenyl)formamidine (FXyl) in a THF and pentamethyldiethyltriamine (PMDETA) solvent mixture. The monodentate structure of (3.12) formed can be attributed to the tridentate solvent frustrating the formamidinate ligand by taking up more co-ordination sites around the lithium metal.

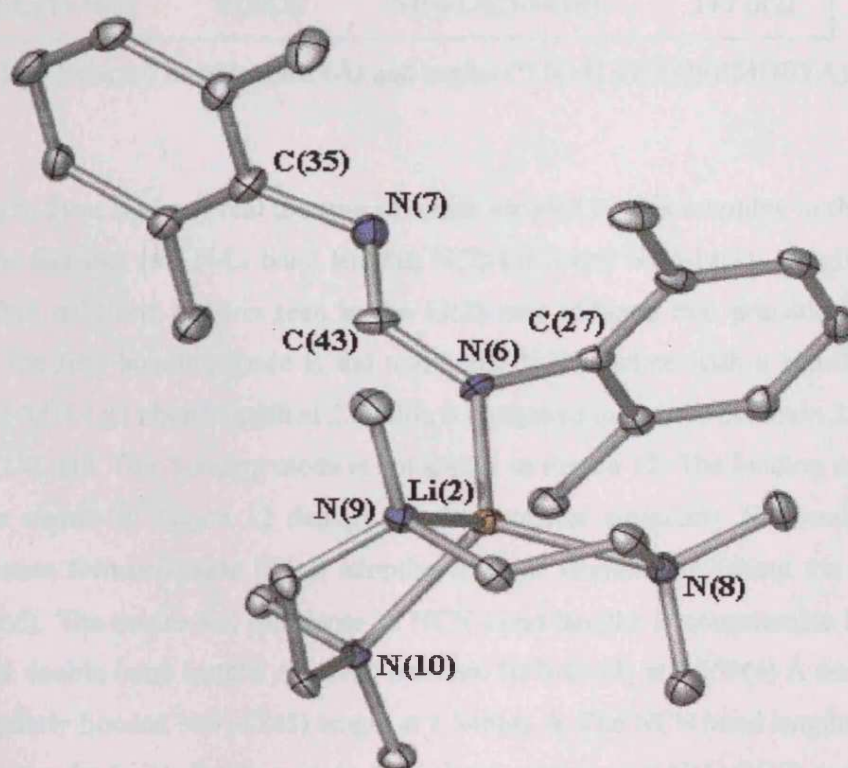


Figure 3.47 – Molecular Structure of [Li(FXyl)(PMDETA)] (3.12)

Atoms	Distance	Atoms	Distance	Atoms	Distance
Li(1)-N(1)	2.025(5)	Li(1)-N(4)	2.224(6)	N(1)-C(17)	1.337(4)
Li(1)-N(2)	2.544(6)	Li(1)-N(5)	2.177(6)	N(2)-C(17)	1.308(4)
Li(1)-N(3)	2.196(6)	N(3)-C(20)	1.421(6)	N(5)-C(24)	1.424(5)
Li(2)-N(6)	1.976(5)	Li(2)-N(10)	2.176(5)	N(8)-C(46)	1.474(4)
Li(2)-N(8)	2.152(5)	N(6)-C(43)	1.348(4)	N(9)-C(47)	1.471(4)
Li(2)-N(9)	2.073(5)	N(7)-C(43)	1.259(4)	N(10)-C(50)	1.488(4)

Atoms	Angle	Atoms	Angle
N(2)-C(17)-N(1)	122.9(3)	N(7)-C(43)-N(6)	129.3(3)
N(1)-Li(1)-N(2)	59.82(16)	C(43)-N(6)-Li(2)	127.7(3)
C(17)-N(1)-Li(1)	99.4(2)	N(9)-Li(2)-N(8)	88.2(2)
C(17)-N(2)-Li(1)	77.7(2)	N(9)-Li(2)-N(10)	87.3(2)
N(3)-Li(1)-N(4)	82.5(2)	N(6)-Li(2)-N(8)	120.7(3)
N(3)-Li(1)-N(5)	114.0(2)	N(6)-Li(2)-N(9)	117.4(3)
N(4)-Li(1)-N(5)	82.9(2)	N(6)-Li(2)-N(10)	117.0(2)

Table 3.12 – Selected bond lengths (Å) and angles (°) for [Li(FXyl)(PMDETA)] (3.12)

The data in these tables reveal the true structure adopted by this complex in the solid state. The fact that two N-Li bond lengths, N(2)-Li(1) and N(1)-Li(1), are given for Li(1) when only one N-Li is seen in the Li(2) case indicate two possible binding modes. The first bonding mode is the traditional N,N'-chelate with a significantly extended N(2)-Li(1) bond length at 2.544(6) Å compared to a more common 2.025(5) Å of N(1)-Li(1). This bonding mode is not shown in Figure 12. The binding mode of Li(2), as shown in Figure 12 depicts a rather unusual singularly N-co-ordinating monodentate formamidinate ligand adopting a *Z-syn* isomeration (about the C(43)-N(6) bond). The nature and difference in NCN bond lengths is considerable for this with near double bond lengths observed between N(7)-C(43) at 1.259(4) Å compared to a singularly bonded N(6)-C(43) length at 1.348(4) Å. The NCN bond lengths in the first instance for Li(1) display a more delocalised system with N(1)-C(17) and N(2)-C(17) bond lengths of 1.337(4) Å and 1.308(4) Å respectively. These differences are

reflected in the chelating N(2)-C(17)-N(1) angle observed at  $122.9(3)^\circ$  compared to the monodentate *Z-syn* formamidinate N(7)-C(43)-N(6) angle at a more “open”  $129.3(3)^\circ$ . This monodentate behaviour of a formamidinate ligand was also displayed in the product of the reaction of *N,N'*-di(2,6-diethylphenyl)formamidine (HFPhEt) with butyl lithium in THF/PMDETA, (3.13).

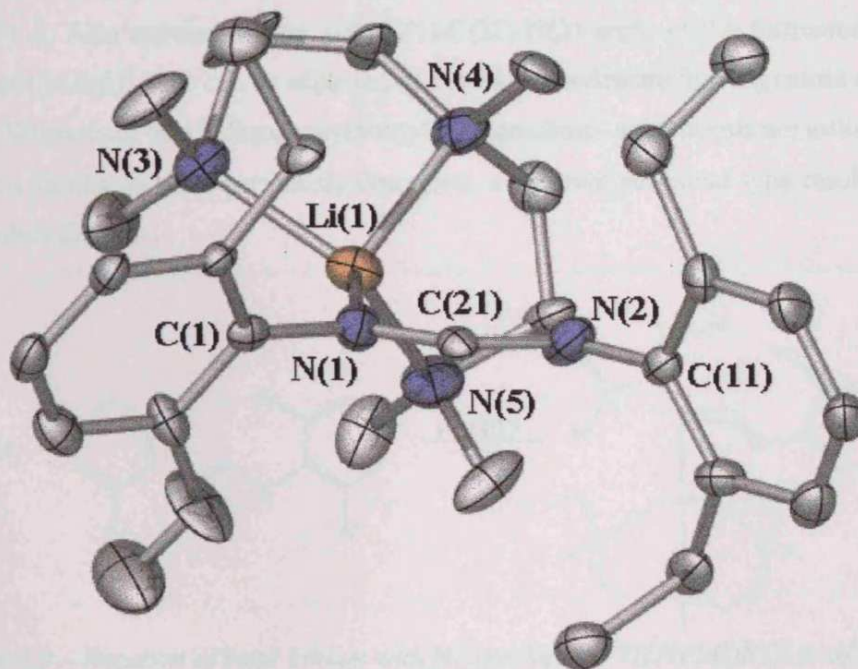
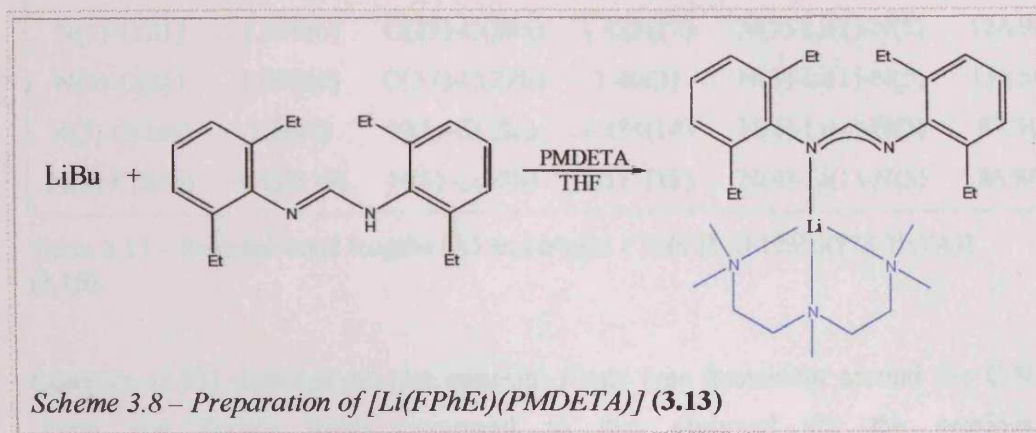


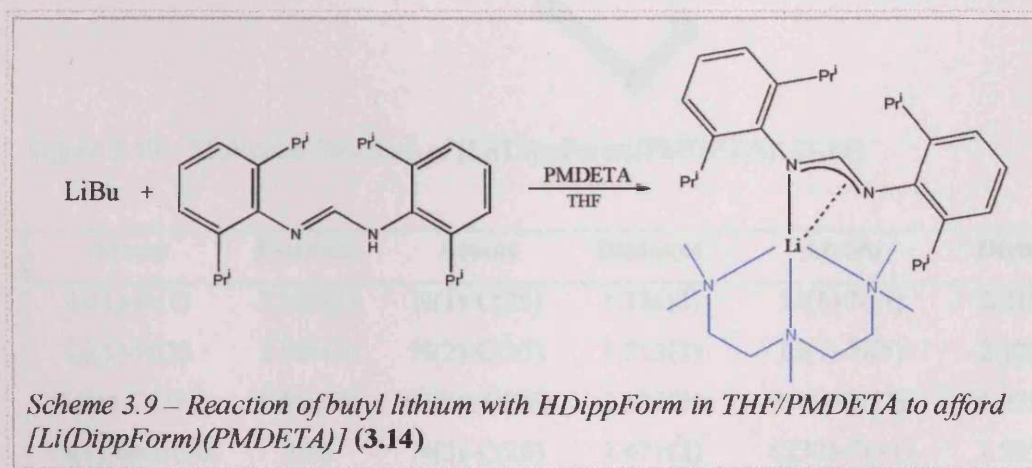
Figure 3.48 – Molecular Structure of  $[Li(FPhEt)(PMDETA)]$  (3.13)



Atoms	Distance	Atoms	Distance	Atoms	Angle
Li(1)-N(1)	1.960(10)	C(25)-C(24a)	1.44(4)	N(1)-C(21)-N(2)	126.6(6)
Li(1)-N(3)	2.130(11)	C(25)-C(24b)	1.333(17)	C(21)-N(1)-Li(1)	125.0(5)
Li(1)-N(4)	2.055(10)	N(4)-C(25)	1.479(8)	N(1)-Li(1)-N(3)	116.6(5)
Li(1)-N(5)	2.149(10)	N(4)-C(27)	1.419(8)	N(1)-Li(1)-N(4)	124.7(5)
N(1)-C(21)	1.319(6)	C(27)-C(28a)	1.427(17)	N(1)-Li(1)-N(5)	118.9(5)
N(2)-C(21)	1.291(6)	C(27)-C(28b)	1.40(3)	N(3)-Li(1)-N(5)	115.5(5)
N(3)-C(24a)	1.56(4)	N(5)-C(28a)	1.474(14)	N(4)-Li(1)-N(3)	87.3(4)
N(3)-C(24b)	1.432(19)	N(5)-C(28b)	1.571(18)	N(4)-Li(1)-N(5)	86.8(4)

Table 3.13 – Selected bond lengths (Å) and angles (°) for [Li(FPhEt)(PMDETA)] (3.13)

Complex (3.13) demonstrates the opposite *E-syn* type isomerism around the C-N single and double bonds compared to that observed for the previous [Li(FXyl)(PMDETA)] (3.12) *Z-syn* complex. As with (3.12) there appears to be a localisation of electrons between N(2)-C(21) which is recognised from the near double bond length of 1.291(6) Å, compared to a N(1)-C(21) single bond distance of 1.319(6) Å. Also apparent is the wide N(1)-C(21)-N(2) angle of the formamidinate ligand at 126.6(6)°. This can be expected due to the monodentate ligating nature of the ligand. When more bulky diisopropylphenyl formamidinate substituents are utilised in reactions similar to those previously described, a different structural type results for the product (3.14).





This complex (**3.14**) displays an unusual (not only in formamidinate-main group chemistry but also in transition metal-amidinate chemistry)  $\eta^2$ -association with the former C-N double bond. One nitrogen  $\sigma$  bonds to the lithium, whilst the partially delocalised double bond interacts in an alkene-type manner, as observed in Figure 3.48 and Table 3.14.

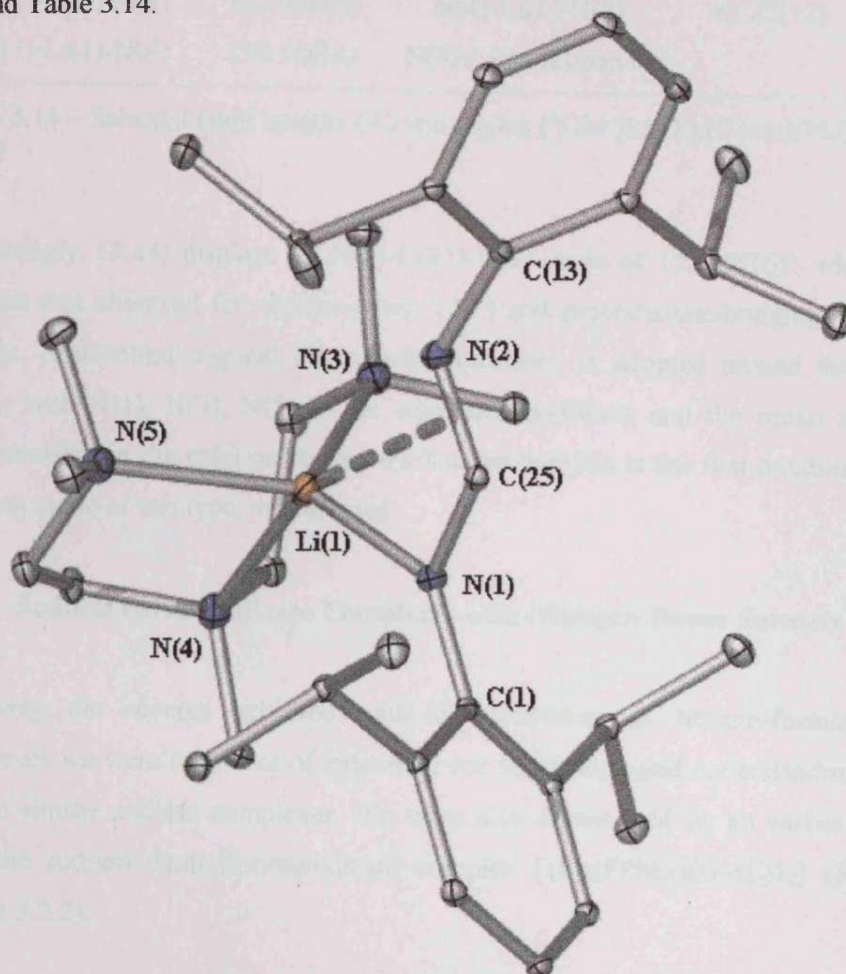


Figure 3.49 – Molecular Structure of [Li(DippForm)(PMDETA)] (**3.14**)

Atoms	Distance	Atoms	Distance	Atoms	Distance
Li(1)-N(1)	2.030(3)	N(1)-C(25)	1.326(2)	Li(1)-N(4)	2.210(3)
Li(1)-N(2)	2.626(3)	N(2)-C(25)	1.312(2)	Li(1)-N(5)	2.225(3)
Li(1)-C(25)	2.662(4)	C(29)-C(28)	1.524(3)	N(4)-C(31)	1.479(3)
Li(1)-centroid	2.56	N(3)-C(28)	1.471(2)	C(32)-C(31)	1.505(3)
Li(1)-N(3)	2.207(3)	N(4)-C(29)	1.474(2)	N(5)-C(32)	1.469(2)

Atoms	Angle	Atoms	Angle
N(2)-C(25)-N(1)	122.09(16)	N(1)-Li(1)-N(5)	118.51(15)
C(25)-N(1)-Li(1)	102.97(13)	N(3)-Li(1)-N(4)	81.79(12)
N(1)-Li(1)-N(2)	57.77(9)	N(3)-Li(1)-N(5)	117.64(14)
N(1)-Li(1)-N(3)	122.42(15)	N(4)-Li(1)-N(5)	81.32(12)
N(1)-Li(1)-N(4)	118.10(14)	N(4)-Li(1)-alkene(1)	

Table 3.14 – Selected bond lengths (Å) and angles (°) for [Li(DippForm)(PMDTA)] (3.14)

Interestingly, (3.14) displays an N(2)-C(25)-N(1) angle of 122.09(16)°, which is in between that observed for chelating (*ca.* 120°) and monodentate/bridging (*ca.* 126°) ligands. A distorted trigonal bipyramidal geometry is adopted around the lithium centre, with N(1), N(3), N(5) in the equatorial positions and the imino and N(4) functionalities in the axial positions. We believe that this is the first amidinate-metal bonding mode of this type, yet reported.

### 3.2.5 Sodium Formamidinate Complexes with Nitrogen Donor Solvents

Following the success achieved with the formation of lithium-formamidinate complexes we were confident of extending our knowledge and understanding in this area to similar sodium complexes. We were also encouraged by an earlier success with the sodium diethylformamidinate complex [ $\{\text{Na}(\text{FPhEt})(\text{DME})\}_2$ ] (3.4) (see section 3.2.2).

In the current study the reaction of sodium bis(trimethylsilyl) amide with *N,N'*-di(2,6-dimethylphenyl)formamidine in toluene/TMEDA yielded a sodium formamidinate complex solvated by TMEDA in a 1:1:1, Na:(FXyl):(TMEDA) ratio as characterised by NMR (3b). Unfortunately attempts to obtain any crystals of X-ray quality proved fruitless. We were also unable to obtain crystallised products from the reactions of the diethyl and diisopropyl formamidine ligands with  $\text{NaN}(\text{SiMe}_3)_2$  in toluene/TMEDA solutions.

Greater success was achieved when repeating these reactions in THF/PMDETA solutions. This success was initially reported in the reaction of sodium bis(trimethylsilyl) amide with *N,N'*-di(2,6-dimethylphenyl)formamidine in a THF/PMDETA solution to yield **(3.15)**, *Scheme 3.10* and Figure 3.50.

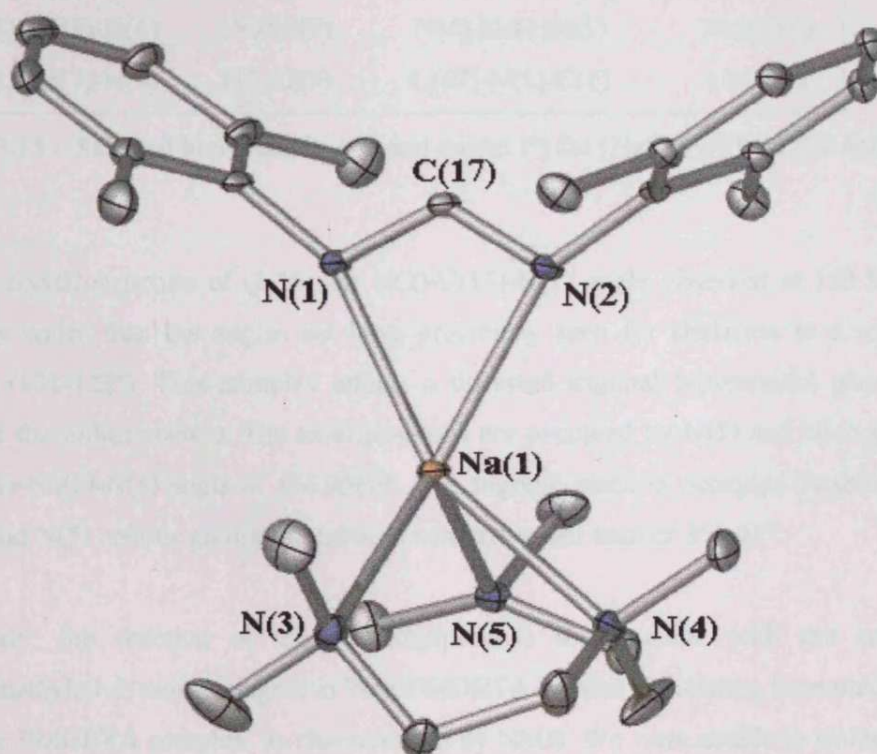
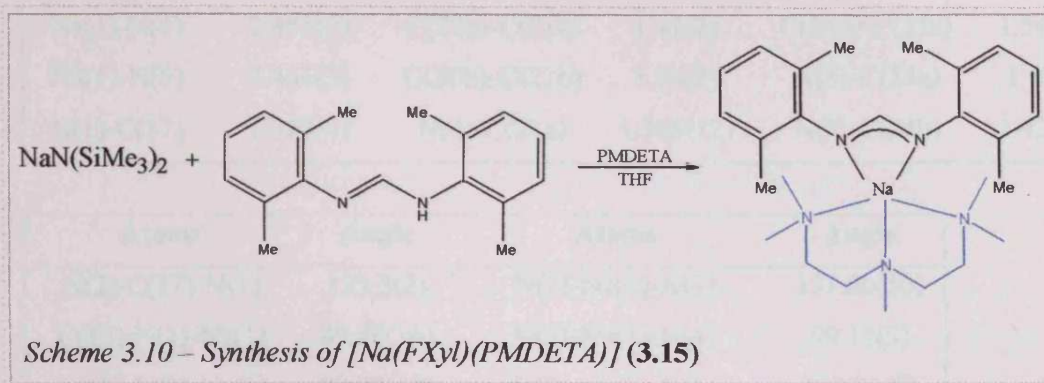


Figure 3.50 – Molecular Structure of [Na(FXyl)(PMDETA)] **(3.15)**

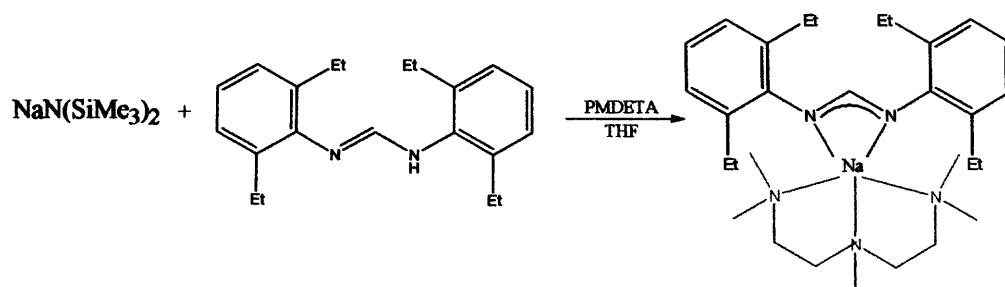
Atoms	Distance	Atoms	Distance	Atoms	Distance
Na(1)-N(1)	2.398(2)	C(17)-N(2)	1.313(4)	N(4)-C(21b)	1.407(15)
Na(1)-N(2)	2.407(2)	N(3)-C(20a)	1.452(9)	N(4)-C(23a)	1.453(6)
Na(1)-N(3)	2.523(3)	N(3)-C(20b)	1.507(16)	C(24a)-C(23a)	1.297(8)
Na(1)-N(4)	2.485(3)	C(20a)-C(21a)	1.47(2)	C(24b)-C(23a)	1.541(15)
Na(1)-N(5)	2.461(3)	C(20b)-C(21b)	1.58(3)	N(5)-C(24a)	1.494(8)
N(1)-C(17)	1.323(4)	N(4)-C(21a)	1.543(12)	N(5)-C(24b)	1.427(10)

Atoms	Angle	Atoms	Angle
N(2)-C(17)-N(1)	123.5(2)	N(2)-Na(1)-N(3)	131.60(10)
C(17)-N(1)-Na(1)	89.36(16)	N(2)-Na(1)-N(4)	99.13(9)
C(17)-N(2)-Na(1)	89.22(17)	N(2)-Na(1)-N(5)	117.30(9)
N(1)-Na(1)-N(2)	57.82(8)	N(3)-Na(1)-N(4)	72.46(9)
N(1)-Na(1)-N(3)	121.88(9)	N(3)-Na(1)-N(5)	106.51(9)
N(1)-Na(1)-N(4)	156.95(9)	N(4)-Na(1)-N(5)	74.99(10)
N(1)-Na(1)-N(5)	113.32(9)	C(17)-N(1)-C(1)	116.4(2)

Table 3.15 – Selected bond lengths (Å) and angles (°) for [Na(FXyl)(PMDETA)] (3.15)

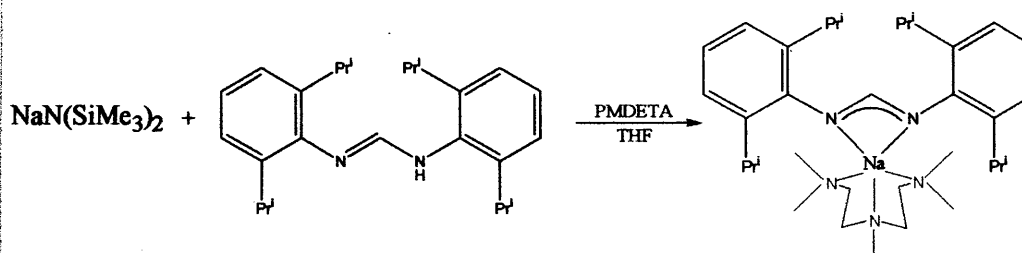
In the crystal structure of (3.15) the N(2)-C(17)-N(1) angle observed at 123.52°, is slightly wider than the angles we have previously seen for chelation to a sodium centre (121-122°). This complex adopts a distorted trigonal bipyramidal geometry around the sodium centre. The axial positions are occupied by N(1) and N(4) giving an N(1)-Na(1)-N(4) angle of 156.95(9)°. The trigonal plane is occupied by the N(2), N(3) and N(5) centres giving a combined near triangular sum of 355.41°.

Similarly, the reaction of the di(diethylphenyl) formamidine with the sodium bis(trimethylsilyl) amide reagent in THF/PMDETA yielded a chelating formamidinate sodium PMDETA complex, as characterised by NMR. We were unable to isolate any crystals of X-ray quality, however the product (3c) shown in Scheme 3.11 is in agreement with the spectroscopic data collected.



**Scheme 3.11 – Proposed sodium di(diethylphenyl) formamidinate complex (3c)**

In the reaction of  $N,N'$ -di(2,6-dimethylphenyl)formamidine with  $\text{NaN}(\text{SiMe}_3)_2$  in a THF/PMDETA solution, success was had and complex (3.16) was formed in high yield as a crystalline solid. The  $\text{N}(1)\text{-C}(25)\text{-N}(2)$  angle at  $122.56(18)^\circ$  is very close to the analogous angle in (3.15). In fact this structure is very similar to that of (3.15) in many aspects. This structure also embraces a trigonal bipyramidal geometry around the sodium centre with the  $\text{N}(2)$  and  $\text{N}(4)$  atoms displaying a near linear  $\text{N}(2)\text{-Na}(1)\text{-N}(4)$  angle of  $168.82(7)^\circ$ . The  $\text{N}(1)$ ,  $\text{N}(3)$  and  $\text{N}(5)$  atoms sit in the trigonal plane, at near right angles to the  $\text{N}(2)\text{-Na}(1)\text{-N}(4)$  axis, to yield a triangular sum of  $358.54^\circ$ . It is noteworthy that the structures of both  $[\text{Na}(\text{FXyl})(\text{PMDETA})]$  (3.15) and  $[\text{Na}(\text{DippForm})(\text{PMDETA})]$  (3.16) resemble that of the  $[\text{Li}\{\text{CPh}(\text{NPh})_2\}(\text{PMDETA})]^{81}$  species.



**Scheme 3.12 – Preparation of  $[\text{Na}(\text{DippForm})(\text{PMDETA})]$  (3.16)**



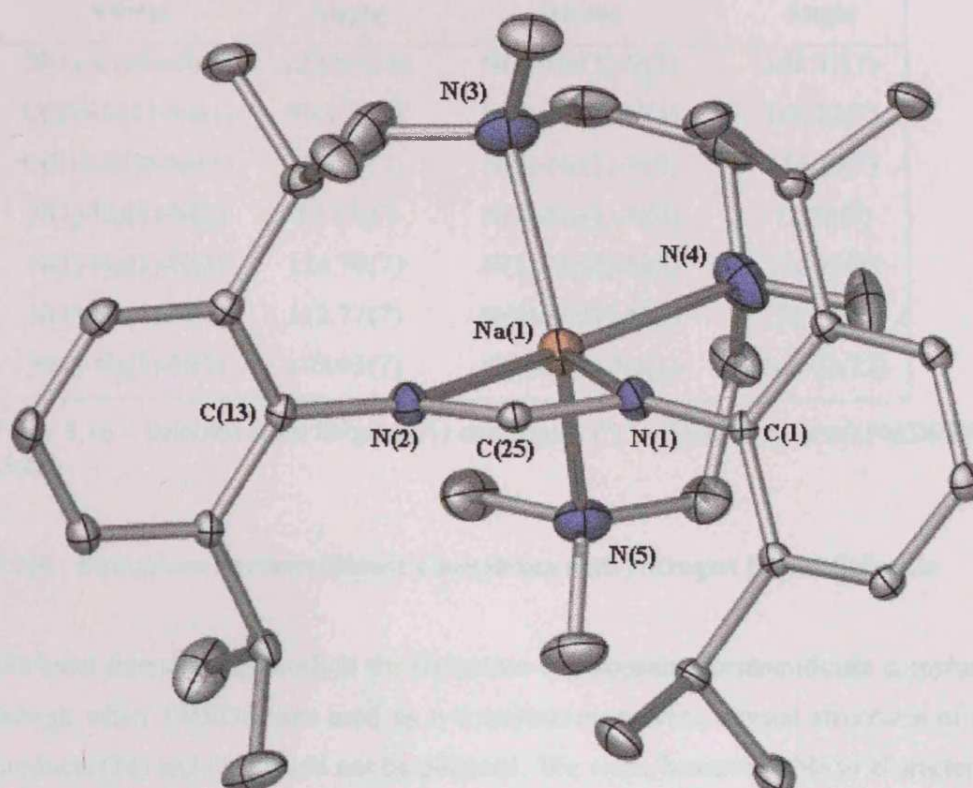


Figure 3.51 – Molecular Structure of [Na(DippForm)(PMDETA)] (3.16)

Atoms	Distance	Atoms	Distance	Atoms	Distance
Na(1)-N(1)	2.3363(17)	N(1)-C(1)	1.398(2)	C(29)-C(28)	1.517(5)
Na(1)-N(2)	2.4757(18)	N(1)-C(25)	1.315(2)	N(4)-C(29)	1.429(4)
Na(1)-N(3)	2.460(2)	C(25)-N(2)	1.313(2)	N(4)-C(31)	1.454(3)
Na(1)-N(4)	2.529(2)	N(2)-C(13)	1.412(2)	C(31)-C(32)	1.476(4)
Na(1)-N(5)	2.503(2)	N(3)-C(28)	1.461(4)	N(5)-C(32)	1.464(3)

Atoms	Angle	Atoms	Angle
N(1)-C(25)-N(2)	122.56(18)	N(2)-Na(1)-N(3)	108.37(7)
C(25)-N(1)-Na(1)	93.17(11)	N(2)-Na(1)-N(4)	168.82(7)
C(25)-N(2)-Na(1)	87.12(11)	N(2)-Na(1)-N(5)	116.20(7)
N(1)-Na(1)-N(2)	57.15(6)	N(3)-Na(1)-N(4)	72.58(9)
N(1)-Na(1)-N(3)	124.78(7)	N(3)-Na(1)-N(5)	114.73(7)
N(1)-Na(1)-N(4)	112.77(7)	N(4)-Na(1)-N(5)	72.07(7)
N(1)-Na(1)-N(5)	119.03(7)	C(1)-N(1)-Na(1)	146.02(12)

Table 3.16 – Selected bond lengths (Å) and angles (°) for [Na(DippForm)(PMDETA)] (3.16)

### 3.2.6 Potassium Formamidinate Complexes with Nitrogen Donor Solvents

We have extended this work to the formation of potassium formamidinate complexes though when TMEDA was used as a coordinating solvent, crystal structures of the products (3d) and (3e) could not be obtained. We were, however, able to characterise the products from a reaction of the potassium bis(trimethylsilyl) amide reagent with the dimethyl formamidine ligand in toluene/TMEDA by NMR spectroscopy. These spectroscopic studies, however, could not define the ligating mode of the formamidinate ligand in this complex.

As far as crystallisation was concerned, greater success was achieved in repeating this reaction in a THF/PMDETA mixture. The reaction of *N,N'*-di(2,6-dimethylphenyl)formamidine with  $\text{NaN}(\text{SiMe}_3)_2$  yielded product (3.17) which exhibits two different potassium coordination environments, one of which is formed by  $\eta^6$ arene interactions from the aryl groups of two bridging ligands. The other has a trigonal bipyramidal coordination environment incorporating the PMDETA ligand and N-coordination from bridging formamidinate ligands (Figure 3.52). The structure presented by this complex is nearly identical with the  $[\{\text{K}(\text{DippForm})_2\text{K}(\text{THF})_2\}_n] \cdot n\text{THF}$  species, with a tridentate PMDETA replacing the THF molecules.

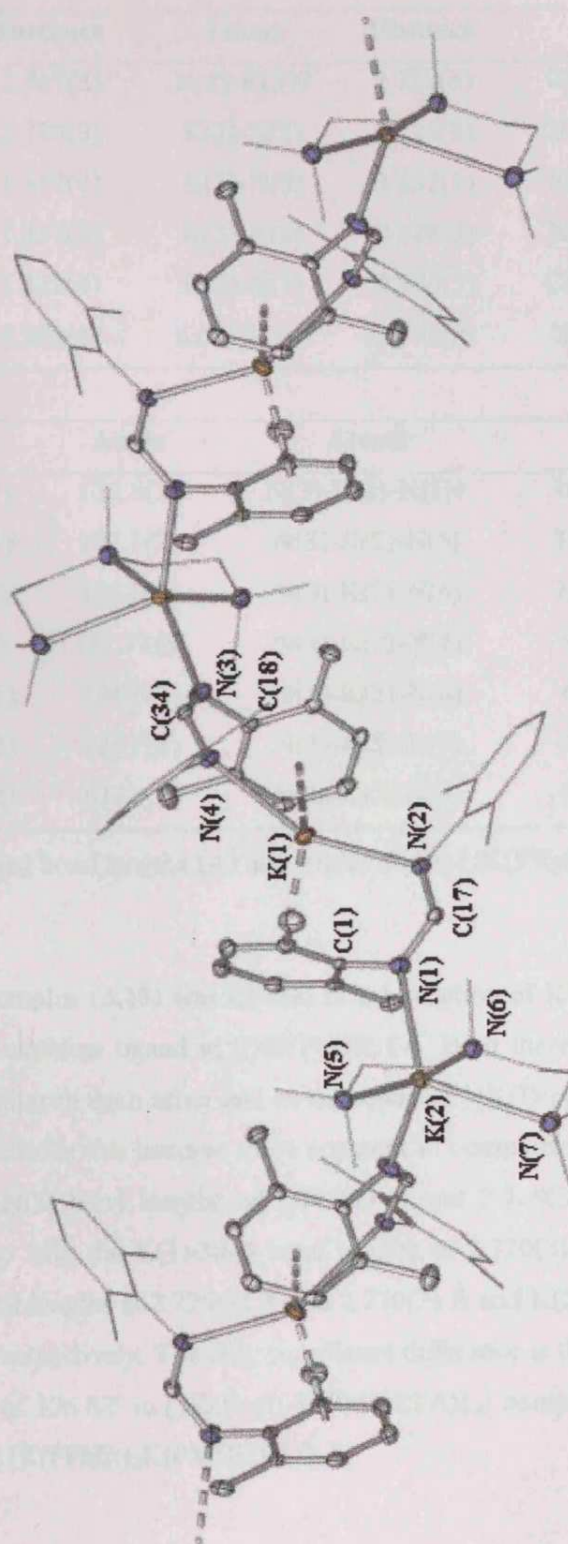


Figure 3.52 – Molecular Structure of  $[\{K(\text{FXyl})_2K(\text{PMDETA})\}_n]$  (3.17)



Atoms	Distance	Atoms	Distance	Atoms	Distance
K(1)-N(2)	2.747(2)	N(1)-K(2)#	2.732(3)	C(37)-N(5)	1.455(4)
K(1)-N(4)	2.770(3)	K(2)-N(3)	2.726(3)	C(37)-C(38)	1.510(4)
N(2)-C(17)	1.317(4)	K(2)-N(5)	2.852(3)	N(6)-C(38)	1.469(4)
N(1)-C(17)	1.317(4)	K(2)-N(6)	2.928(2)	N(6)-C(40)	1.463(4)
N(4)-C(34)	1.321(4)	K(2)-N(7)	2.930(3)	C(40)-C(41)	1.507(4)
N(3)-C(34)	1.298(4)	K(2)-N(1#)	2.732(3)	N(7)-C(41)	1.462(4)

Atoms	Angle	Atoms	Angle
N(2)-C(17)-N(1)	126.8(3)	N(3)-K(2)-N(1#)	107.47(9)
C(17)-N(2)-K(1)	127.1(2)	N(3)-K(2)-N(5)	107.30(8)
C(17)-N(1)-K(2)#	133.6(2)	N(3)-K(2)-N(6)	148.64(8)
N(2)-K(1)-N(4)	131.73(8)	N(3)-K(2)-N(7)	98.51(8)
C(34)-N(4)-K(1)	124.5(2)	N(5)-K(2)-N(6)	61.44(7)
N(4)-C(34)-N(3)	128.7(3)	N(5)-K(2)-N(7)	108.50(8)
C(34)-N(3)-K(2)	134.5(2)	N(6)-K(2)-N(7)	62.49(7)

Table 3.17 – Selected bond lengths (Å) and angles (°) for [ $\{K(FXyl)_2K(PMDETA)\}_n$ ] (**3.17**)

An isostructural complex (**3.18**) was formed in the reaction of  $KN(SiMe_3)_2$  with the diethylphenyl formamidine ligand in THF/PMDETA. Both these complexes, (**3.17**) and (**3.18**), are similar to each other and to the reported [ $\{K(DippForm)_2K(THF)_2\}_n$ ] complex<sup>87</sup>. These similarities become more apparent in comparisons with each other, such as the K(1)-N(2) bond lengths of 2.747(2) Å and 2.769(3) Å for (**3.17**) and (**3.18**) respectively. Also the K(1)-N(4) bond lengths of 2.770(3) Å and 2.778(3) Å, and K(2)-N(3) bond lengths at 2.726(3) Å and 2.730(3) Å and K(2)-N(1#) at 2.732(3) Å and 2.747(3) Å respectively. The only significant difference is the more acute N(2)-C(17)-N(1) angle of 126.83° in [ $\{K(Fxyl)_2K(PMDETA)\}_n$ ] compared to N(2)-C(21)-N(1) 128.3(4)° in [ $\{K(FPhEt)_2K(PMDETA)\}_n$ ].

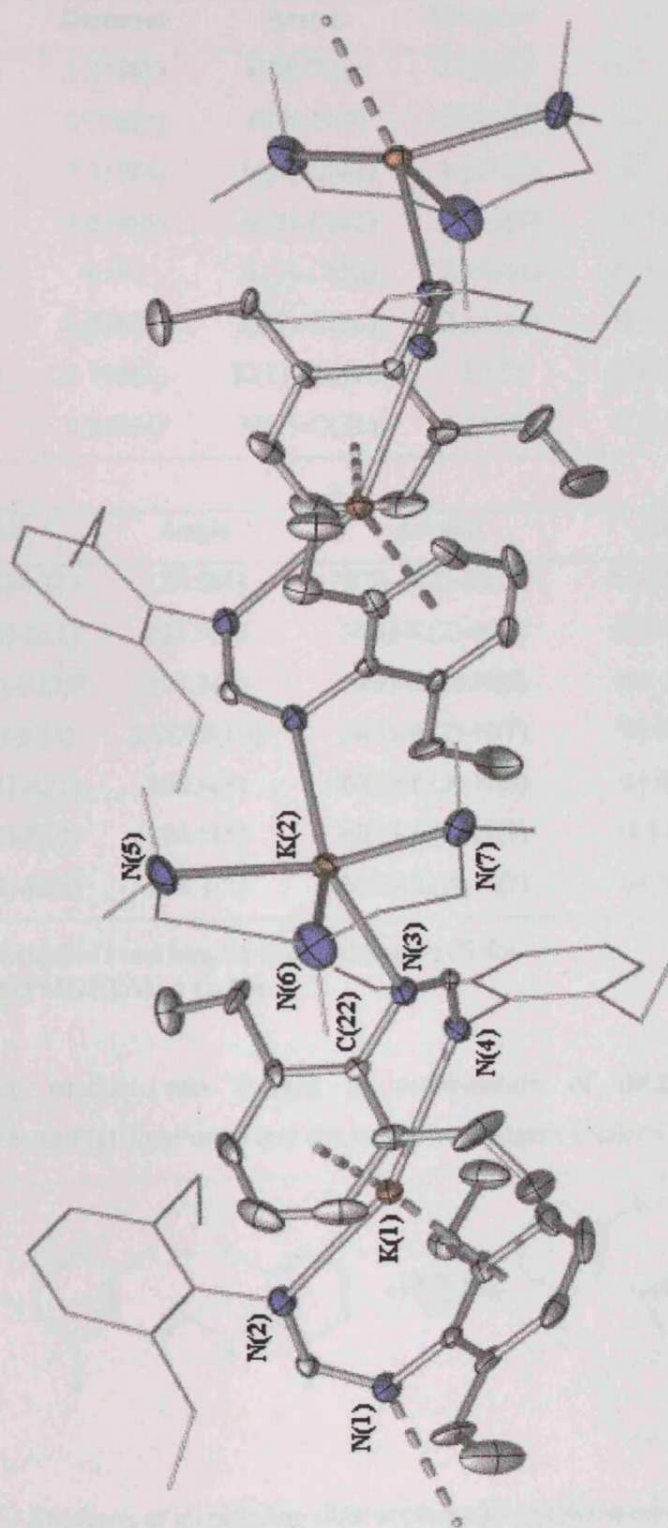


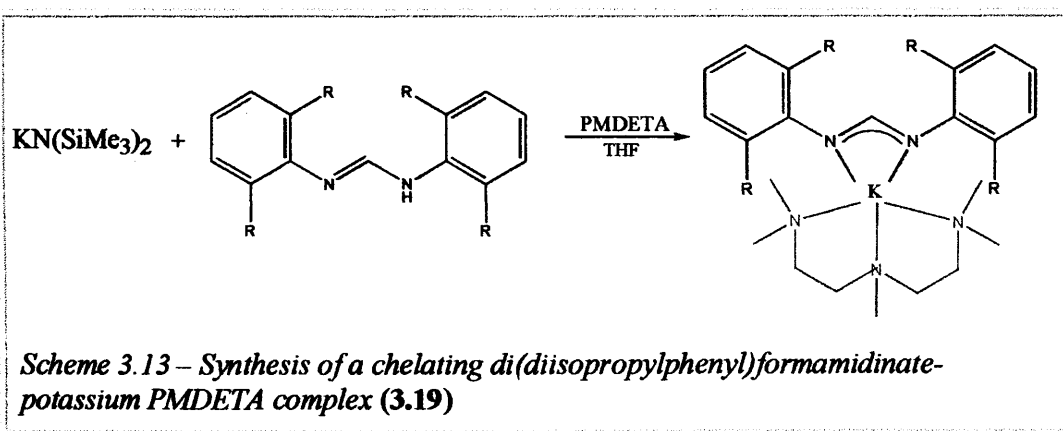
Figure 3.53 – Molecular Structure of  $[\{K(FPhEt)_2K(PMDETA)\}_n]$  (3.18)

Atoms	Distance	Atoms	Distance	Atoms	Distance
K(1)-N(2)	2.769(3)	K(2)-N(6)	2.909(5)	N(2)-C(21)	1.317(5)
K(1)-N(4)	2.778(3)	K(2)-N(7)	2.787(4)	N(1)-K(2)#	2.747(3)
K(1)-C(1)	3.119(4)	N(4)-C(42)	1.311(5)	N(5)-C(45)	1.374(10)
K(1)-C(3)	3.234(5)	N(3)-C(42)	1.314(5)	C(46)-C(45)	1.348(12)
K(1)-PhAve.	3.181	K(1)-C(22)	3.107(4)	N(6)-C(46)	1.502(9)
K(2)-N(3)	2.730(3)	K(1)-C(26)	3.241(6)	N(6)-C(48)	1.402(7)
K(2)-N(1)#	2.747(3)	K(1)-PhAve.	3.172	C(48)-C(49)	1.519(8)
K(2)-N(5)	2.842(4)	N(1)-C(21)	1.310(5)	N(7)-C(49)	1.470(7)

Atoms	Angle	Atoms	Angle
N(2)-C(21)-N(1)	128.3(4)	N(3)-K(2)-N(1)#	114.85(11)
C(21)-N(2)-K(1)	125.3(3)	N(3)-K(2)-N(5)	126.48(11)
C(21)-N(1)-K(2)#	134.1(3)	N(3)-K(2)-N(6)	101.12(13)
N(2)-K(1)-N(4)	147.49(10)	N(3)-K(2)-N(7)	99.63(11)
C(42)-N(4)-K(1)	124.8(3)	N(5)-K(2)-N(6)	61.92(15)
N(4)-C(42)-N(3)	128.5(4)	N(5)-K(2)-N(7)	113.49(14)
C(42)-N(3)-K(2)	125.1(2)	N(6)-K(2)-N(7)	64.55(15)

Table 3.18 – Selected bond lengths (Å) and angles (°) for  $[\{K(FPhEt)_2K(PMDETA)\}_n]$  (3.18)

A contrasting product was formed in combination of di(diisopropylphenyl)formamidine ligand (HDippForm) and the potassium reagent (Scheme 3.13).



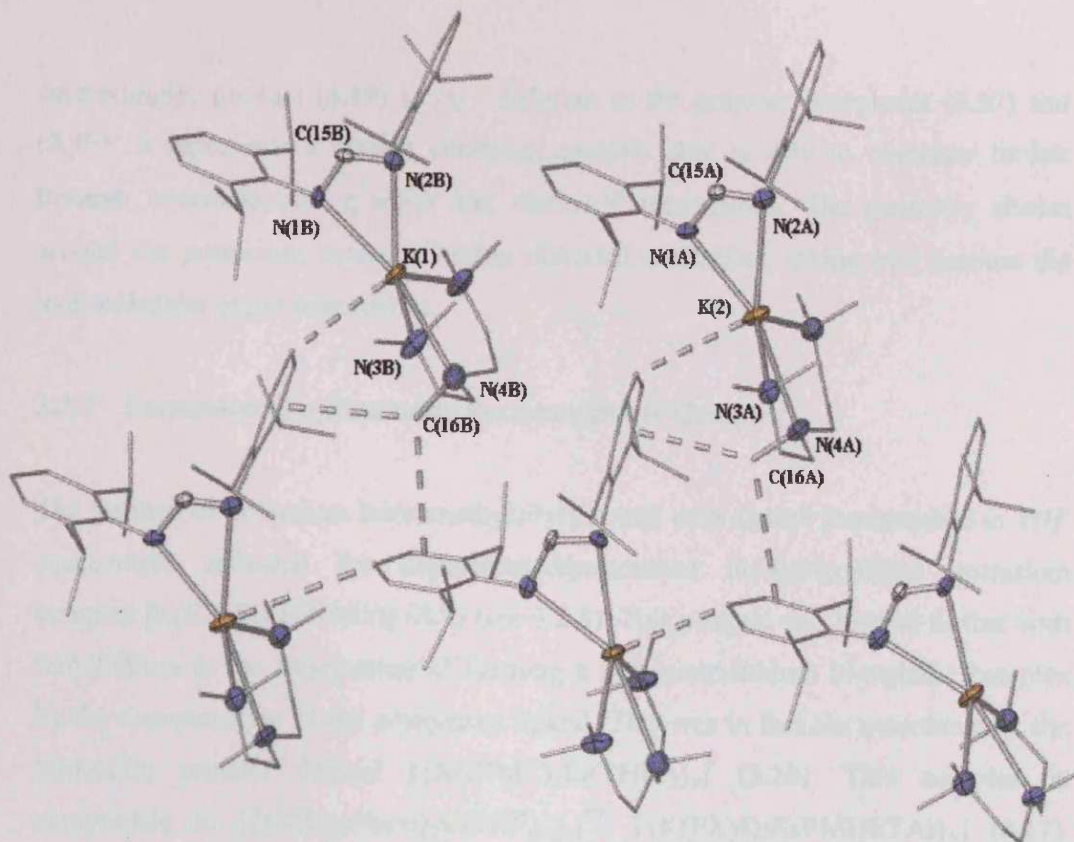


Figure 3.54 – Molecular Structure of [K(DippForm)(PMDETA)] (3.19)

Atoms	Distance	Atoms	Distance	Atoms	Distance
K(2)-N(1b)	2.753(5)	K(2)-N(3b)#	2.807(5)	C(17b)-C(18b)	1.473(9)
K(2)-N(2b)	2.740(5)	N(1b)-C(15b)	1.300(7)	C(17b)-N(4b)	1.489(9)
K(2)-N(3b)	2.807(5)	N(2b)-C(15b)	1.322(8)	N(4b)-C(17b)#	1.489(9)
K(2)-N(4b)	2.875(9)	N(3b)-C(18b)	1.362(8)		

Atoms	Angle	Atoms	Angle
N(1b)-C(15b)-N(2b)	124.7(6)	N(1b)-K(2)-N(3b)#	120.59(11)
C(15b)-N(1b)-K(2)	92.6(4)	N(2b)-K(2)-N(3b)	107.90(14)
C(15b)-N(2b)-K(2)	92.6(4)	N(2b)-K(2)-N(4b)	147.2(4)
N(1b)-K(2)-N(2b)	50.03(16)	N(2b)-K(2)-N(3b)#	107.90(14)
N(1b)-K(2)-N(3b)	120.59(11)	N(3b)-K(2)-N(4b)	61.41(13)
N(1b)-K(2)-N(4b)	162.8(4)	N(3b)-K(2)-N(3b)#	118.7(2)

Table 3.19 – Selected bond lengths (Å) and angles(°) for [K(DippForm)(PMDETA)] (3.19)

Interestingly, product (3.19) is very different to the polymer complexes (3.17) and (3.18). It represents a simple chelating complex that is able to associate further through intermolecular  $\eta^6$ arene and methyl-K interactions. The geometry shown around the potassium centre is highly distorted octahedral, taking into account the intermolecular arene interactions.

### 3.2.7 Formation of a Bimetallic Formamidinate Complex

The reaction of potassium bis(trimethylsilyl) amide with diethyl formamidine in THF successfully afforded the deprotonated/protonated bis-formamidine potassium complex  $[K(FPhEt)(HFPhEt)]$  (3.7) (see 3.2.3). This product was reacted further with butyllithium in the anticipation of forming a potassium-lithium bi-metallic complex by the deprotonation of the protonated ligand. This was in fact the outcome with the bimetallic product formed  $[ \{ K(FPhEt)_2Li(THF)_2 \}_n ]$  (3.20). This complex is comparable to  $[ \{ K(DippForm)_2K(THF)_2 \}_n ]$ <sup>87</sup>,  $[ \{ K(FXyl)_2K(PMDETA) \}_n ]$  (3.17), and  $[ \{ K(FPhEt)_2K(PMDETA) \}_n ]$  (3.18).

The  $[ \{ K(FPhEt)_2Li(THF)_2 \}_n ]$  (3.20) complex has two distinct metal co-ordination environments. The potassium environment, is very much the same as one of the potassium environments in the reported  $[ \{ K(DippForm)_2K(THF)_2 \}_n ]$ <sup>87</sup> and the discussed complexes (3.17 and 3.18). This sees a potassium coordination sphere satisfied by two bridging formamidinate ligands and two separate  $\eta^6$ arene interactions. The lithium environment mirrors the other potassium environment observed in these species with its co-ordination sphere satisfied by two bridging formamidinate ligands and two terminal THF molecules. One difference, however, is that the geometry around the lithium centre is distorted tetrahedral, rather than the distorted trigonal bipyramidal seen in (3.17) and (3.18), due to the lower ionic radius of lithium compared to potassium. It is worth remembering, however, that the THF coordinated potassium centre in  $[ \{ K(DippForm)_2K(THF)_2 \}_n ]$ <sup>87</sup> has a distorted tetrahedral geometry with only two THF molecules ligating to it. The amido-potassium distances in (3.20) are slightly longer at 2.804(8) Å and 2.783(8) Å than those for  $[ \{ K(FPhEt)_2K(PMDETA) \}_n ]$  (3.18) at 2.769(3) Å and 2.778(3) Å.



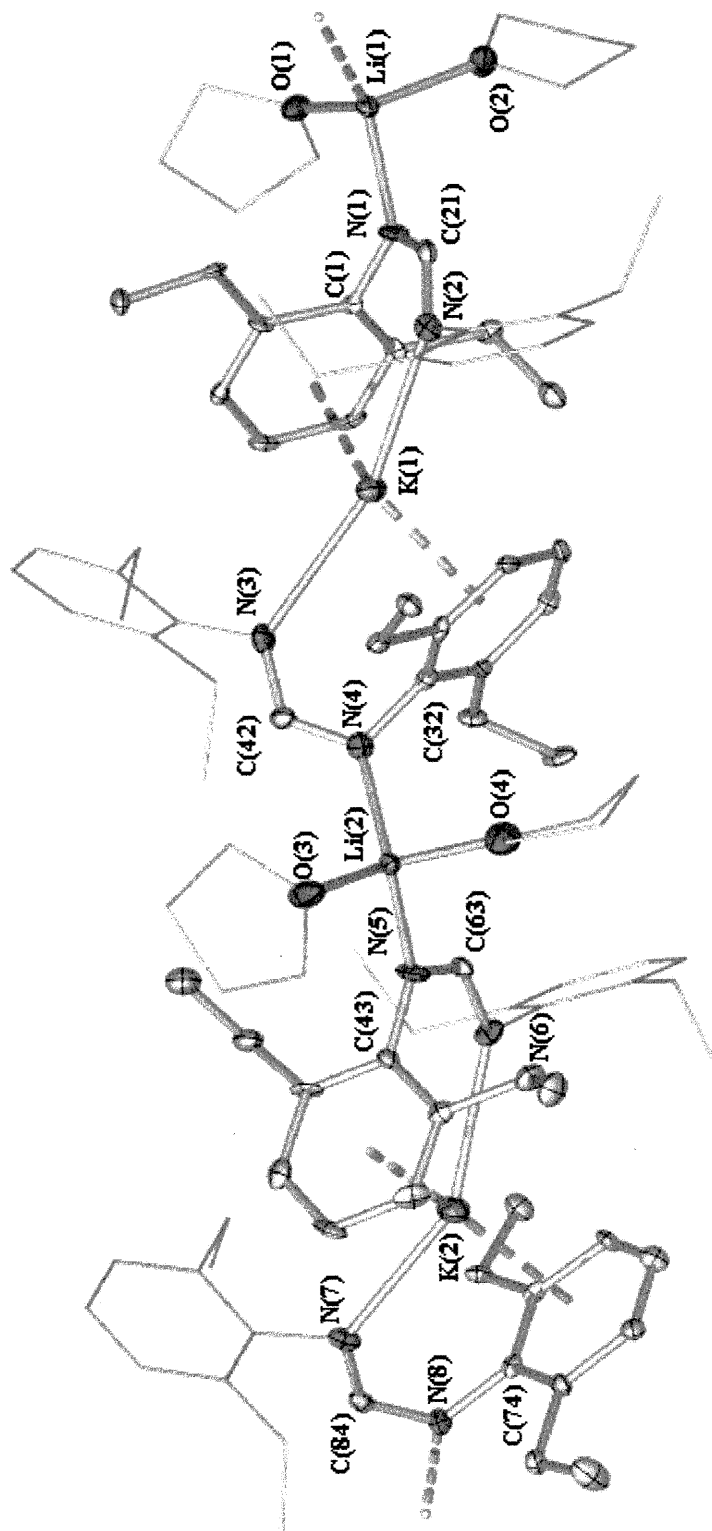


Figure 3.55 – Molecular Structure of  $[\{K(FPhEt)_2Li(THF)_2\}_n]$  (3.20)

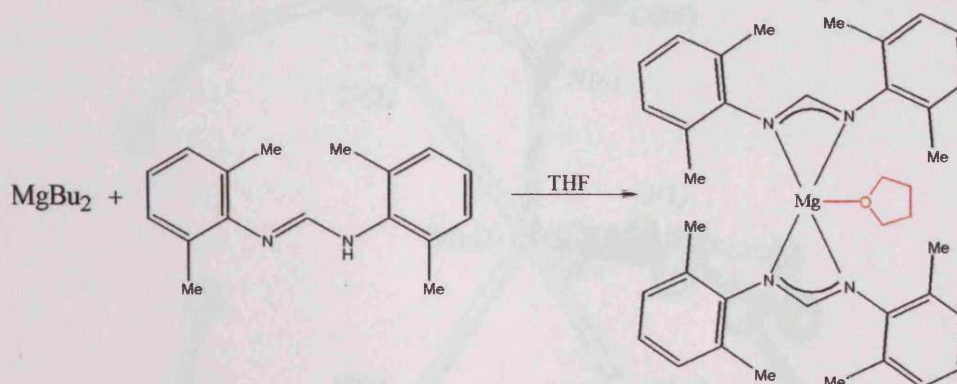
Atoms	Distance	Atoms	Distance	Atoms	Distance
K(1)-N(2)	2.804(8)	K(1)-C(1)	3.161(10)	N(1)-C(21)	1.319(10)
K(1)-N(3)	2.783(8)	K(1)-PhAve	3.207	N(2)-C(21)	1.312(10)
K(1)-C(37)	3.228(9)	N(4)-C(32)	1.419(10)	N(1)-Li(1)	2.017(16)
K(1)-C(32)	3.159(10)	N(4)-C(42)	1.315(10)	O(1)-Li(1)	1.975(14)
K(1)-PhAve	3.195	N(3)-C(42)	1.309(10)	O(2)-Li(1)	2.028(14)
K(1)-C(6)	3.232(9)	N(3)-C(22)	1.407(10)	Li(1)-N(8)#	2.081(15)
K(1)-cent(1)	2.901(17)	K(1)-cent(2)	2.871(17)		

Atoms	Angle	Atoms	Angle
N(4)-C(42)-N(3)	127.6(11)	N(2)-C(21)-N(1)	129.3(11)
C(42)-N(3)-K(1)	129.1(7)	C(21)-N(2)-K(1)	126.0(7)
C(42)-N(4)-Li(2)	128.7(9)	C(21)-N(1)-Li(1)	120.7(9)
N(3)-K(1)-N(2)	151.3(2)	N(1)-Li(1)-N(8)#	121.1(7)
O(1)-Li(1)-O(2)	102.1(7)	centroid(1)-K(1)-N(4)	139.4(5)
centroid(1)-K(1)-N(2)	79.8(6)	centroid(2)-K(1)-N(4)	44.6(5)
centroid(2)-K(1)-N(2)	104.7(6)		

Table 3.20 – Selected bond lengths (Å) and angles (°) for [ $\{K(FPhEt)_2Li(THF)_2\}_n$ ] (3.20)

### 3.2.8 Synthesis of a Group 2 Formamidinate Complex

Group 2 amidinate complexes, like their group 1 counterparts, have potential use as precursors to other main group, transition and lanthanide metal amidinate complexes. The first group 2 formamidinate complex, a dinuclear magnesium species, [(THF)(DPhF)Mg( $\mu$ -Cl) $_2$ ( $\mu$ -THF)Mg(DPhF)(THF)] was reported in 1997<sup>88</sup>. In this complex the magnesium atoms are bridged via two chlorides and a THF molecule, rather than the amidinate ligands as we have come to expect in group 1 chemistry. Work by the Junk group has extended knowledge in this area with the formation of a variety of other magnesium formamidinate complexes<sup>89</sup>. The diversity of complexes formed in their studies was achieved by changing the solvent medium (THF, DME and TMEDA) and applying slightly different formamidinate ligands (*N,N'*-di(*para*-methylphenyl)formamidinate and *N,N'*-di(*ortho*-methylphenyl)formamidinate<sup>89</sup>. In the current study we were able to form a mononuclear magnesium bisformamidinate complex (3.21) with a trigonal bipyramidal magnesium geometry in the reaction of *N,N'*-di(2,6-dimethylphenyl)formamidine with butylmagnesium in THF.



Scheme 3.14 – Synthesis of a trigonal bipyramidal magnesium bis-di(dimethylphenyl)formamidinate complex with a solvated THF molecule (3.21)



The most significant difference between this complex and the other magnesium formamidinate complexes is the co-ordination number and hence geometry. This  $[\text{Mg}(\text{FXyl})_2(\text{THF})]$  (**3.21**) complex is the first five co-ordinate trigonal bipyramidal magnesium formamidinate complex, and can be compared to other four (tetrahedral)<sup>90</sup> and six co-ordinate (octahedral) complexes<sup>88, 89</sup>. The trigonal bipyramidal geometry is based around a N(3)-Mg(1)-N(2) axis ( $173.77(8)^\circ$ ) and complimented with a N(1), N(4), O(1) trigonal plane ( $\Sigma$  angles  $359.96^\circ$ ). We can compare these results to the octahedral magnesium bisformamidinate complex  $[\text{Mg}(\text{FTolP})_2(\text{THF})_2]$ <sup>90</sup>. The NCN angles of formamidinate ligands of both complexes are acute and very similar since both are chelating to the magnesium centres,  $116.9^\circ$  average in the referenced complex<sup>90</sup> compared to N(1)-C(17)-N(2)  $116.6(2)^\circ$ , N(3)-C(34)-N(4)  $117.0(2)^\circ$  in (**3.21**).

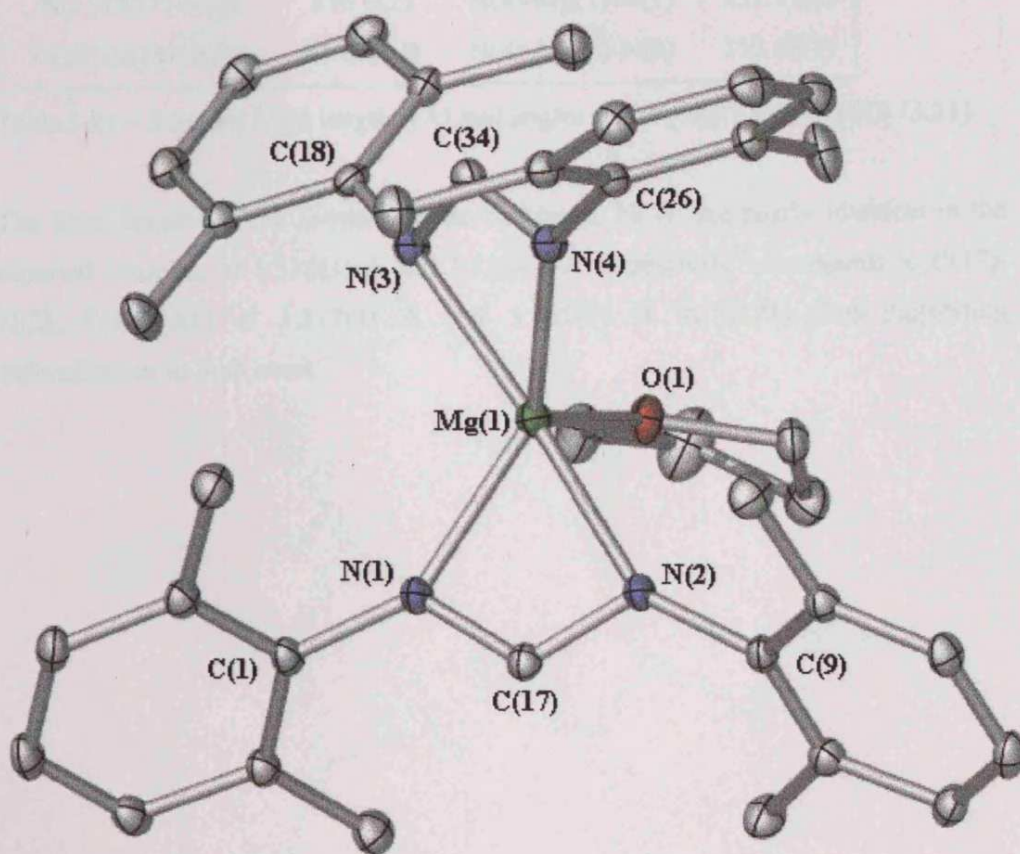


Figure 3.56 – Molecular Structure of  $[\text{Mg}(\text{FXyl})_2(\text{THF})]$  (**3.21**)

Atoms	Distance	Atoms	Distance	Atoms	Distance
Mg(1)-N(3)	2.169(2)	Mg(1)-N(2)	2.155(2)	N(4)-C(34)	1.322(3)
Mg(1)-N(4)	2.0876(19)	Mg(1)-O(1)	2.0576(17)	N(1)-C(17)	1.325(3)
Mg(1)-N(1)	2.0904(19)	N(3)-C(34)	1.321(3)	N(2)-C(17)	1.317(3)

Atoms	Angle	Atoms	Angle
N(3)-C(34)-N(4)	117.0(2)	C(17)-N(2)-Mg(1)	88.41(13)
C(34)-N(3)-Mg(1)	87.65(13)	N(1)-Mg(1)-N(2)	63.94(7)
C(34)-N(4)-Mg(2)	91.10(14)	N(1)-Mg(1)-O(1)	112.99(7)
N(3)-Mg(1)-N(4)	63.90(7)	N(2)-Mg(1)-O(1)	93.64(7)
N(3)-Mg(1)-O(1)	92.53(7)	N(3)-Mg(1)-N(1)	112.68(8)
N(4)-Mg(1)-O(1)	115.86(7)	N(3)-Mg(1)-N(2)	173.77(8)
N(1)-C(17)-N(2)	116.6(2)	N(4)-Mg(1)-N(1)	131.11(8)
C(17)-N(1)-Mg(1)	91.00(14)	N(4)-Mg(1)-N(2)	113.83(8)

Table 3.21 – Selected bond lengths (Å) and angles (°) for [Mg(FXyl)<sub>2</sub>(THF)] (**3.21**)

The bond lengths in the formamidinate backbone, NCN, are nearly identical in the reported complex, at 1.318(3) Å and 1.323(3) Å respectively<sup>90</sup>, compared to C(17)-N(2), C(17)-N(1) at 1.317(3) Å and 1.325(3) Å in (**3.21**) thus suggesting delocalisation in both cases.

### 3.2.9 Synthesis of Group 13 Formamidinate Complexes

Group 13 amidinate complexes have received considerable attention in recent years, particularly in studies by the Jordan group who have used some aluminium complexes as olefin polymerisation catalysts. The most important classes of these complexes are the mono(amidinato)  $[\{RC(NR^1)_2\}MX_2]$  species ( $X$  = halide or alkyl), adopting distorted tetrahedral geometries<sup>112, 98</sup> and the bis(amidinato)  $[\{RC(NR^1)_2\}_2MX]$  species ( $X$  = halide or alkyl), embracing distorted trigonal bipyramidal structures<sup>98, 99</sup>. We were interested in the synthesis of related group 13 formamidinate complexes, hence it was proposed that reaction of  $Li(FPhEt)(HPhEt)^{113}$  with aluminium trichloride would yield an aluminium formamidinate complex by metathesis. This proved to be the case with complex (3.22) being formed in high yields.

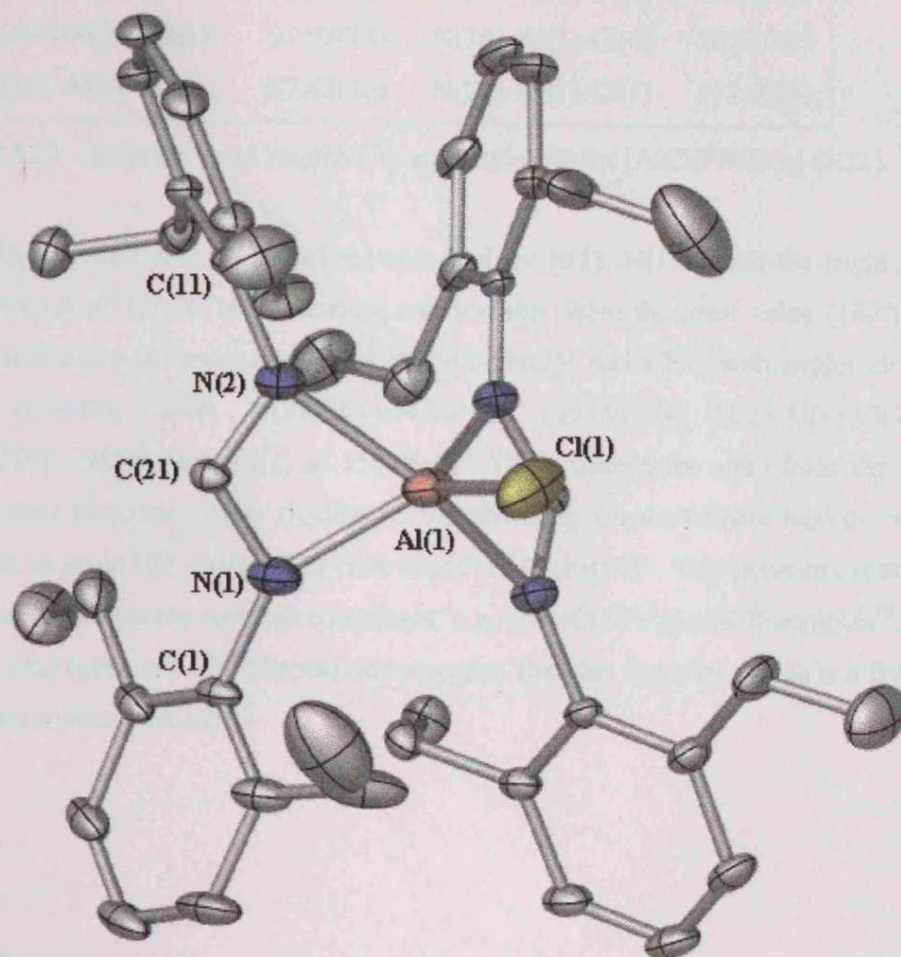


Figure 3.57 – Molecular Structure of  $[AlCl(FPhEt)_2]$  (3.22)

Atoms	Distance	Atoms	Distance	Atoms	Distance
Al(1)-N(1)	2.016(2)	Al(1)-N(2)#	1.921(3)	N(1)-C(1)	1.439(4)
Al(1)-N(1#)	2.016(2)	Al(1)-Cl(1)	2.1383(18)	C(21)-N(1)	1.304(4)
Al(1)-N(2)	1.921(3)	Al(1)-C(21#)	2.375(3)	N(2)-C(21)	1.334(4)

Atoms	Angle	Atoms	Angle
N(1)-C(21)-N(2)	112.0(3)	N(1)-Al(1)-N(1#)	155.20(16)
C(21)-N(1)-Al(1)	88.65(19)	N(1)-Al(1)-N(2#)	100.48(10)
C(21)-N(2)-Al(1)	91.93(18)	N(2)-Al(1)-N(1#)	100.48(10)
N(1)-Al(1)-N(2)	67.43(10)	N(2)-Al(1)-N(2#)	123.90(17)
N(1#)-C(21#)-N(2)#	112.0(3)	N(1)-Al(1)-Cl(1)	102.40(8)
C(21#)-N(1#)-Al(1)	88.65(19)	N(2)-Al(1)-Cl(1)	118.05(9)
C(21#)-N(2#)-Al(1)	91.93(18)	N(1#)-Al(1)-Cl(1)	102.40(8)
N(1#)-Al(1)-N(2#)	67.43(10)	N(2#)-Al(1)-Cl(1)	118.05(9)

Table 3.22 – Selected bond lengths (Å) and angles (°) for [AlCl(FPhEt)<sub>2</sub>] (**3.22**)

The pseudo-axial sites of (**3.22**) are occupied by N(1), N(1)#, with the angle N(1)-Al(1)-N(1)# of 155.20(16)° deviating considerably from the ideal value (180°). The equatorial plane is therefore defined by N(2), N(2)# and Cl(1) with angles close to their expected values, N(2)-Al(1)-N(2)# at 123.90(17)°, N(2)-Al(1)-Cl(1) at 118.05(9)°, N(2)#-Al(1)-Cl(1) at 118.05(9)°. These distortions arise from the steric constraints imposed by the rigidity of the chelating formamidinate ligands, which impose an acute N(1)-Al(1)-N(2) “bite angle” of 67.43(10)°. This geometry is similar to those in previously reported complexes, e.g. [{MeC(NPr<sup>i</sup>)<sub>2</sub>}<sub>2</sub>AlCl] complex<sup>99</sup>. <sup>27</sup>Al NMR data (peak at δ 63.951ppm) also suggests that this complex (**3.22**) is a five coordinate species in solution.



We have also prepared a closely related 5-coordinate complex,  $[\text{AlCl}(\text{DippForm})_2]$  (**3.23**) from the reaction of  $\text{Li}(\text{DippForm})(\text{HDippForm})^{113}$  with aluminium trichloride in THF. As was the case with (**3.22**), this appears to retain its solid state structure in solution as suggested from its  $^{27}\text{Al}$  NMR spectrum, peak at  $\delta$  67.863ppm.

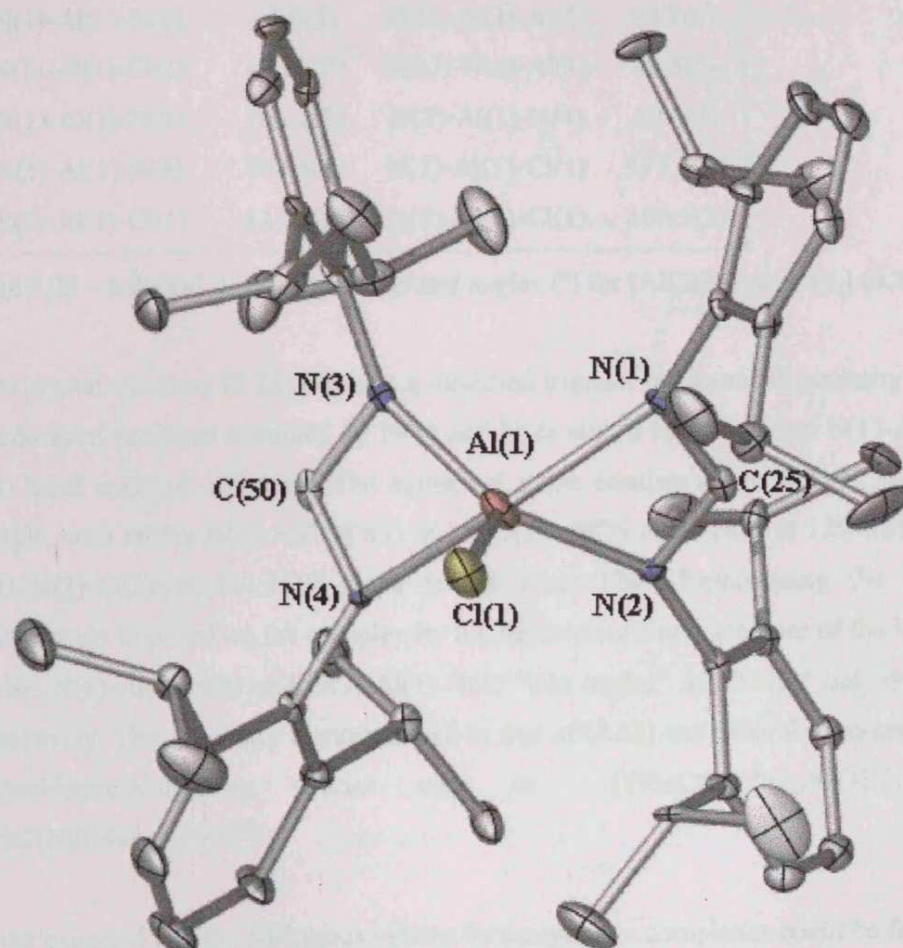


Figure 3.58 – Molecular Structure of  $[\text{AlCl}(\text{DippForm})_2]$  (**3.23**)

Atoms	Distance	Atoms	Distance	Atoms	Distance
Al(1)-N(1)	2.057(7)	Al(1)-Cl(1)	2.145(4)	N(2)-C(13)	1.447(11)
Al(1)-N(2)	1.943(8)	N(1)-C(1)	1.465(10)	N(3)-C(26)	1.428(11)
Al(1)-N(3)	1.901(8)	N(1)-C(25)	1.297(11)	N(3)-C(50)	1.340(10)
Al(1)-N(4)	2.013(7)	C(25)-N(2)	1.315(10)	C(50)-N(4)	1.293(10)

Atoms	Angle	Atoms	Angle
N(1)-C(25)-N(2)	115.8(8)	N(2)-Al(1)-N(3)	125.4(3)
C(25)-N(1)-Al(1)	86.1(5)	N(2)-Al(1)-N(4)	101.7(3)
C(25)-N(2)-Al(1)	90.5(6)	N(3)-C(50)-N(4)	115.8(8)
N(1)-Al(1)-N(2)	67.1(3)	C(50)-N(3)-Al(1)	88.7(6)
N(1)-Al(1)-Cl(1)	100.0(2)	C(50)-N(4)-Al(1)	85.3(5)
N(1)-Al(1)-N(3)	102.2(3)	N(3)-Al(1)-N(4)	69.4(3)
N(1)-Al(1)-N(4)	159.4(3)	N(3)-Al(1)-Cl(1)	117.3(3)
N(2)-Al(1)-Cl(1)	117.3(3)	N(4)-Al(1)-Cl(1)	100.5(2)

Table 3.23 – Selected bond lengths (Å) and angles (°) for [AlCl(DippForm)<sub>2</sub>] (3.23)

In its crystal structure (3.22) displays a distorted trigonal bipyramidal geometry with pseudo-axial positions occupied by N(1) and N(4) with a far from ideal N(1)-Al(1)-N(4) bond angle of 159.4(3)°. The equatorial plane consists of an N(2)-N(3)-Cl(1) triangle, with angles N(2)-Al(1)-Cl(1) at 117.3(3)°, N(2)-Al(1)-N(3) at 125.4(3)° and N(3)-Al(1)-Cl(1) at 117.3(3)° close to the ideal 120°. Emphasising the steric requirements imposed on the complex by the bidentate chelating nature of the ligand are the N(1)-Al(1)-N(2) and N(3)-Al(1)-N(4) “bite angles” at 67.1(3)° and 69.4(3)° respectively. This geometry compares well to that of (3.22) and other five co-ordinate bis(amidinato)aluminium species such as [<sup>t</sup>BuC(NPr)<sub>2</sub>]<sub>2</sub>AlCl]<sup>99</sup> and [PhC(NSiMe<sub>3</sub>)<sub>2</sub>]<sub>2</sub>AlH]<sup>96</sup>.

It was expected that the analogous indium formamidinate complexes could be formed in similar metathesis reactions with the lithium salts. However, in the reaction of Li(FPhEt)(HFPhEt)<sup>113</sup> with InCl<sub>3</sub> the unusual trigonal bipyramidal bis(formamidine) indium trichloride complex (3.24) was produced in a 29% yield. At this stage it is not known why a formamidinate complex could not be isolated from this reaction.

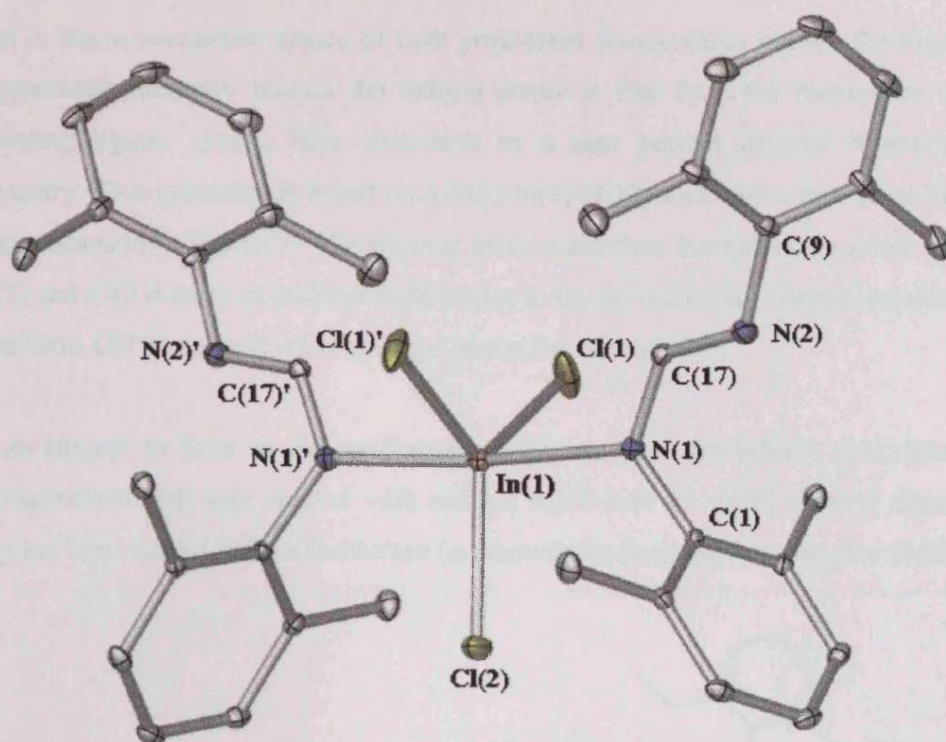


Figure 3.59 – Molecular Structure of  $[\text{InCl}_3(\text{HFXyl})_2]$  (3.24)

Atoms	Distance	Atoms	Distance	Atoms	Distance
In(1)-N(1)	2.2926(17)	In(1)-Cl(2)	2.3675(8)	N(1)-C(17)	1.295(2)
In(1)-N(1#)	2.2926(17)	In(1)-Cl(1#)	2.4066(7)	C(17)-N(2)	1.332(2)
In(1)-Cl(1)	2.4066(7)	N(1)-C(1)	1.441(2)	N(2)-C(9)	1.439(2)

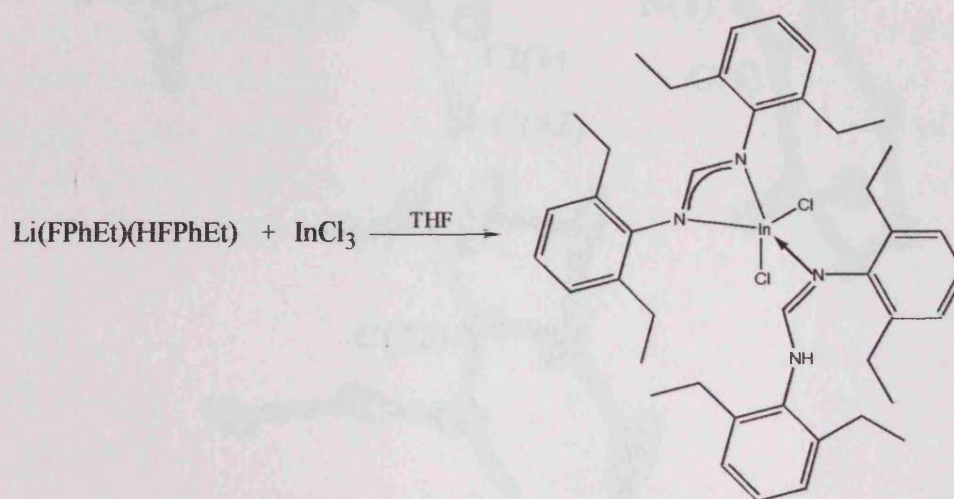
Atoms	Angle	Atoms	Angle
N(1)-C(17)-N(2)	126.05(16)	C(17#)-N(1#)-In(1)	117.45(12)
C(17)-N(1)-In(1)	117.45(12)	N(1)-In(1)-Cl(1)	89.19(4)
N(1)-In(1)-N(1#)	175.54(7)	N(1#)-In(1)-Cl(1#)	89.19(4)
N(1)-In(1)-Cl(1)	89.19(4)	N(1#)-In(1)-Cl(2)	92.23(3)
N(1)-In(1)-Cl(1#)	88.51(4)	Cl(1)-In(1)-Cl(1#)	118.00(4)
N(1)-In(1)-Cl(2)	92.23(3)	Cl(1)-In(1)-Cl(2)	120.998(19)
N(1#)-In(1)-Cl(1)	88.51(4)	Cl(1#)-In(1)-Cl(2)	120.998(19)
N(1#)-C(17)-N(2#)	126.05(16)	Cl(1#)-In(1)-Cl(2)	120.998(19)

Table 3.24 – Selected bond lengths (Å) and angles (°) for  $[\text{InCl}_3(\text{HFXyl})_2]$  (3.24)



Due to the monodentate nature of both protonated formamidine ligands the trigonal bipyramidal geometry around the indium centre is free from the restrictions of a chelating ligand, giving little distortion to a near perfect trigonal bipyramidal geometry. This geometry is based on a N(1)-In(1)-N(1#) axis with a near ideal linear angle measuring  $175.54(7)^\circ$ . The trigonal plane comprises three chloride atoms Cl(1), Cl(2) and Cl(1)# lying at uniform right angles to the co-ordinating nitrogen atoms and a uniform  $120^\circ$  from each other giving a triangular sum of  $360^\circ$ .

In an attempt to form an indium-formamidinate complex the lithium diethylphenyl formamidinate salt was reacted with indium trichloride to afford a novel distorted trigonal bipyramidal indium dichloride formamidinate formamidine complex (**3.25**).



*Scheme 3.15 – Preparation of a novel indium dichloride di(diethylphenyl)-formamidinate di(diethylphenyl)formamidine complex (**3.25**)*



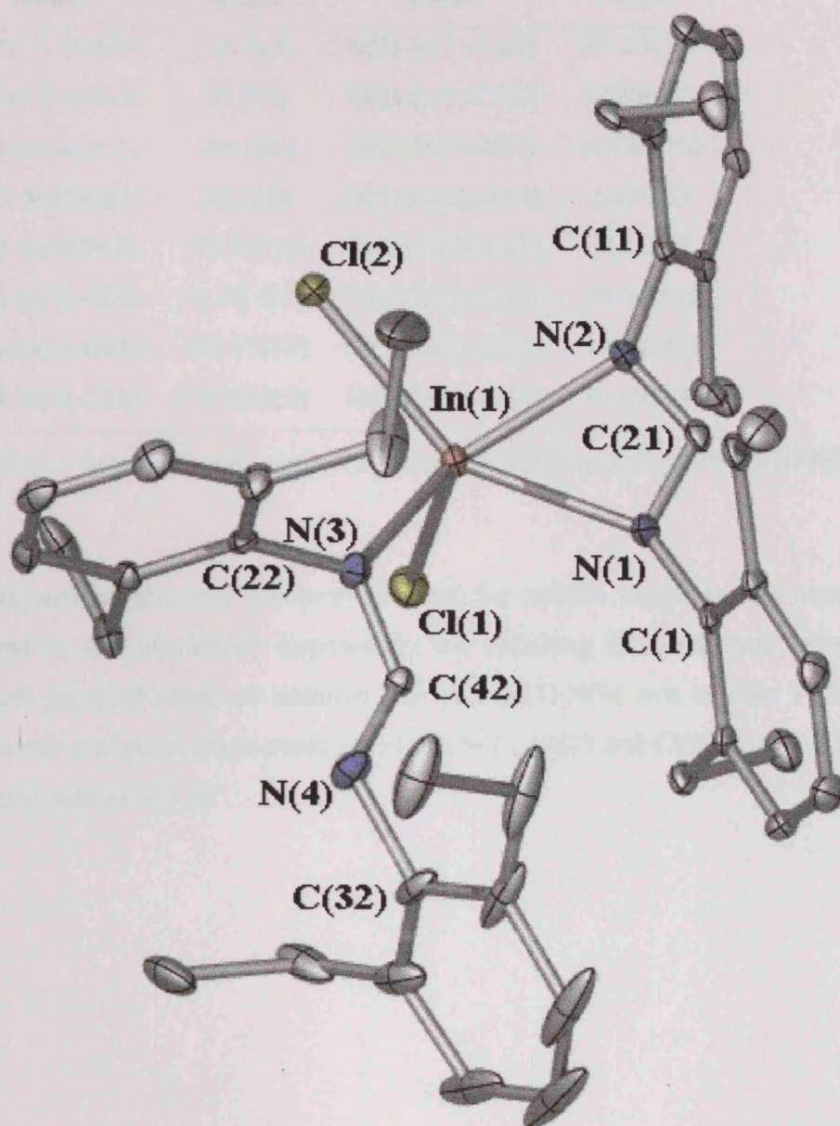


Figure 3.60 – Molecular Structure of  $[\text{InCl}_2(\text{FPhEt})(\text{HPhEt})]$  (3.25)

Atoms	Distance	Atoms	Distance	Atoms	Distance
In(1)-N(1)	2.296(4)	In(1)-Cl(2)	2.3895(16)	N(2)-C(11)	1.440(7)
In(1)-N(2)	2.194(4)	C(1)-N(1)	1.421(7)	N(3)-C(22)	1.450(7)
In(1)-N(3)	2.211(4)	N(1)-C(21)	1.311(7)	N(3)-C(42)	1.300(7)
In(1)-Cl(1)	2.3878(15)	C(21)-N(2)	1.302(7)	C(42)-N(4)	1.333(7)

Atoms	Angle	Atoms	Angle
N(1)-C(21)-N(2)	116.5(5)	N(2)-In(1)-Cl(1)	108.29(13)
C(21)-N(1)-In(1)	89.7(3)	N(2)-In(1)-Cl(2)	97.89(13)
C(1)-N(1)-In(1)	146.6(3)	N(2)-In(1)-N(3)	143.87(16)
C(21)-N(2)-In(1)	94.5(3)	N(3)-C(42)-N(4)	126.0(5)
N(1)-In(1)-N(2)	59.26(16)	C(42)-N(3)-In(1)	113.9(3)
N(1)-In(1)-N(3)	91.32 (16)	N(3)-In(1)-Cl(1)	98.44(12)
N(1)-In(1)-Cl(1)	104.17(13)	Cl(1)-In(1)-Cl(2)	110.87(6)
N(1)-In(1)-Cl(2)	143.08(12)	N(3)-In(1)-Cl(2)	94.67(12)

Table 3.25 – Selected bond lengths (Å) and angles (°) for [InCl<sub>2</sub>(FPhEt)(HFPhEt)] (3.25)

The trigonal bipyramidal geometry around the indium centre in this complex is distorted by the restrictions imposed by the chelating formamidinate ligand. This becomes apparent when we consider the N(2)-In(1)-N(3) axis of only 143.87(16)°. This leaves a trigonal plane made up of the N(1), Cl(1) and Cl(2) atoms with a near triangular sum of 357.62°.

### 3.3 Conclusions

We have shown that deprotonation of di-methyl, -ethyl and -isopropyl phenyl formamidine ligands with LiBu,  $[\text{Na}\{\text{N}(\text{SiMe}_3)_2\}]$  and  $[\text{K}\{\text{N}(\text{SiMe}_3)_2\}]$  in a variety of co-ordinating solvents yields the solvated alkali metal complexes with a diversity of bonding modes, that are dependant on the solvent and *N*-substituent. We have also been able to form the novel lithium-potassium, bimetallic formamidinate complex  $[\text{K}(\text{FPhEt})_2\text{Li}(\text{THF})_2]$  in the reaction of  $[\text{K}(\text{FPhEt})(\text{HFPhEt})]$  (3.7) with LiBu. In a similar vein the novel trigonal bipyramidal group 2 magnesium-formamidinate complex,  $[\text{Mg}(\text{FXyl})_2(\text{THF})]$  (3.21), has been prepared in high yield as have several novel group 13 formamidinate complexes.

### 3.4 Experimental

The lithium, sodium and potassium alkyl and amide reagents used were purchased from the Aldrich Chemical Company. Solvents were freshly purified using current literature methods<sup>114</sup> and stored in re-sealable greaseless flasks under an atmosphere of argon. All product complexes were sensitive to air and moisture, which meant that manipulations required the employment of Schlenk and glove box manipulation techniques. <sup>1</sup>H NMR spectra were recorded at 300.138 MHz and <sup>13</sup>C NMR spectra were recorded at 75.477 MHz using a Bruker BZH 300/52 NMR spectrometer with a Varian console. Chemical shifts were referenced to residual <sup>1</sup>H and <sup>13</sup>C resonances of the solvent used namely C<sub>6</sub>D<sub>6</sub> or D<sub>8</sub>-THF. IR spectra were recorded as Nujol mulls on NaCl plates using a Nicolet Nexus 670 FTIR spectrophotometer in the range 400 – 4000 cm<sup>-1</sup>. X-ray crystallography was carried out on crystals, which were sealed and mounted in 0.5 mm capillaries, with hemispheres of data collected at room temperature on a Bruker SMART CCD diffractometer using the omega scan mode with total reflections and unique data recorded with the complexes. Data sets were corrected for absorption using the SADABS<sup>115</sup> program. Structures were solved using SHELXL-97 and SHELXS-97<sup>116</sup>, utilising the graphical interface X-Seed<sup>117</sup>. All molecular structure figures were generated using POV-RAY<sup>118</sup>. All non-hydrogen atoms were located and refined with anisotropic thermal parameters. Hydrogen atoms were placed in calculated positions using the riding model and were not refined.

#### 3.4.1 Syntheses of Formamidine ligands

***N,N'*-Di(2,6-dimethylphenyl)formamidine, (HFXyl)**<sup>113</sup>. This synthesis followed a slight modification of a published procedure<sup>88, 119</sup>. Yield (90.3%).

***N,N'*-Di(2,6-diethylphenyl)formamidine, (HFPhEt)**<sup>113</sup>. This synthesis followed a slight modification of a published procedure<sup>88, 119</sup>. Yield (52.1%).

***N,N'*-Di(2,6-diisopropylphenyl)formamidine, (HDippForm)**<sup>113</sup>. This synthesis followed a slight modification of a published procedure<sup>88, 119</sup>. Yield (63.5%).

### 3.4.2 Synthesis of Lithium Formamidinate Complexes in DME

**[{Li(FPhEt)(DME)}<sub>2</sub>] (3.1).** HFPhEt (1.16 g, 3.8 mmol) was dissolved in DME (20 mls), and a solution of LiBu<sup>n</sup> (2.35 mls, 3.8 mmol as 1.6 M in hexanes) added drop-wise. The resulting golden reaction solution was concentrated *in vacuo* and cooled to -15 °C upon which clear orange crystals were produced. Yield 1.23 g (66%), mp = >350 °C. <sup>1</sup>H NMR (C<sub>6</sub>D<sub>6</sub>, δ/ppm) 1.09 (broadened multiplet, 12H, CH<sub>3</sub> ethyl), 2.63 (broadened multiplet, 8H, CH<sub>2</sub> ethyl), 2.68 (s, 8H, O-CH<sub>2</sub> DME), 2.78 (s, 12H, O-CH<sub>3</sub> DME), 6.88-6.97 (multiplet, 6H, aromatics), 7.49 (s, 1H, NC(H)N backbone proton). <sup>13</sup>C NMR (C<sub>6</sub>D<sub>6</sub>, δ/ppm) 15.58 (FPhEt CH<sub>3</sub>), 25.94 (FPhEt CH<sub>2</sub>), 58.94 (O-CH<sub>2</sub> DME), 70.88 (O-CH<sub>3</sub> DME), 122.72, 126.14, 138.46, 149.94 (aromatic carbons), 167.98 (NCN backbone carbon). IR (Nujol, NaCl plates) 2096.0(m,shp), 2015.6(w,shp), 1952.6(str,shp), 1892.3(str,shp), 1842.1(str,shp), 1781.9(m,shp), 1741.7(str,shp), 1596.1(str,br), 1545.8(str,br), 1189.3(str), 1028.9(str), 918.2(str,shp), 962.9(str,shp), 802.7(str,shp), 762.5(str,shp) cm<sup>-1</sup>.

**[Li(DippForm)(DME)] (3.2).** HDippForm (1.03 g, 2.8 mmol) was dissolved in DME (20 mls), and a solution of LiBu<sup>n</sup> (1.8 mls, 2.8 mmol as 1.6M in hexanes) added drop-wise. The reaction mixture was concentrated *in vacuo* and cooled to -15 °C upon which colourless crystals were produced. Isolated Yield 0.90 g (69%), mp = 340-353°C. <sup>1</sup>H NMR (C<sub>6</sub>D<sub>6</sub>, δ/ppm) 1.33 (d, 24H, Pr<sup>i</sup> CH<sub>3</sub>), 2.76 (s, 4H, O-CH<sub>2</sub> DME), 3.00 (s, 6H, O-CH<sub>3</sub> DME), 3.75 (sept, 4H, Pr<sup>i</sup> CHMe<sub>2</sub>), 7.10-7.25 (multiplet, 6H, aromatics), 7.96 (s, 1H, NC(H)N backbone proton). <sup>13</sup>C NMR (C<sub>6</sub>D<sub>6</sub>, δ/ppm) 23.10 (Pr<sup>i</sup> CH<sub>3</sub>), 26.97 (Pr<sup>i</sup> CH), 57.67 (O-CH<sub>2</sub> DME), 69.00 (O-CH<sub>3</sub> DME), 120.84, 121.82, 141.35, 148.25 (aromatic carbons), 164.54 (NCN, backbone carbon). IR (Nujol, NaCl plates) 3177.8(w), 2719.1(w,shp), 1922.2(w,shp), 1890.0(w,shp), 1858.7(w,shp), 1844.4(w,shp), 1772.0(w,shp), 1750.0(w,shp), 1666.5(m,shp), 1552.1(w,shp), 1533.0(m,br), 1316.7(m,br), 1233.9(m,br), 1188.9(str), 1113.9(str), 933.8(str,shp), 872.2(str,shp), 823.7(w,shp), 802.3(str,shp), 760.8(str,shp), 716.7(w,shp) cm<sup>-1</sup>.

### 3.4.3 Synthesis of Sodium Formamidinate Complexes in DME

**[Na(FXyl)(DME)<sub>2</sub>] (3.3).** HFXyl (1.04 g, 4.1 mmol) was dissolved in THF (20 mls), and a solution of NaN(SiMe<sub>3</sub>)<sub>2</sub> (4.1 mls, 4.1 mmol as 1M in THF) added drop-wise. The reaction mixture was dried to a powder and the residue extracted in DME (4 mls) then cooled to -15 °C upon which colourless crystals were produced. Isolated Yield 1.35 g (72%), mp = 58-62 °C. <sup>1</sup>H NMR (C<sub>6</sub>D<sub>6</sub>, δ/ppm) 2.36 (s, 12H, FXyl CH<sub>3</sub>), 3.03 (s, 12H, O-CH<sub>3</sub> DME), 3.11 (s, 8H, O-CH<sub>2</sub> DME), 6.9-7.0 (multiplet, 2H, *p*-aromatics), 7.12-7.15 (m, 4H, *m*-aromatics), 7.67 (s, 1H, NC(H)N backbone proton). <sup>13</sup>C NMR (C<sub>6</sub>D<sub>6</sub>, δ/ppm) 18.40 (FXyl CH<sub>3</sub>), 57.38 (O-CH<sub>2</sub> DME), 70.48 (O-CH<sub>3</sub> DME), 120.65, 121.89, 125.06, 130.56 (aromatic carbons), 144.864 (NCN backbone carbon). IR (Nujol, NaCl plates) 2104.0(w,shp), 2050.5(w,shp), 1946.0(w,shp), 1886.7(m,shp), 1824.6(m,shp), 1765.8(m,shp), 1651.3(m,shp), 1589.9(m,shp), 1537.8(w,shp), 1247.2(m,br), 1199.1(str), 1114.3(str,br), 1032.0(str), 944.2(m,shp), 859.0(w,shp), 758.8(str,shp), 666.6(w,shp) cm<sup>-1</sup>.

**[{Na(FPhEt)(DME)}<sub>2</sub>] (3.4).** HFPhEt (0.96 g, 3.1 mmol) was dissolved in THF (20 mls), and a solution of NaN(SiMe<sub>3</sub>)<sub>2</sub> (3.1 mls, 3.1 mmol as 1M in THF) added drop-wise. The reaction mixture was dried to a powder and the residue extracted in DME (8 mls), concentrated *in vacuo* and cooled to -15 °C upon which colourless crystals were produced. Isolated Yield 0.80 g (61%), mp = 79-98 °C. <sup>1</sup>H NMR (C<sub>6</sub>D<sub>6</sub>, δ/ppm) 1.31 (t, 12H, CH<sub>3</sub> ethyl), 2.85 (q, 8H, CH<sub>2</sub> ethyl), 2.96 (s, 8H, O-CH<sub>2</sub> DME), 2.99 (s, 12H, O-CH<sub>3</sub> DME), 6.9-7.20 (multiplet, 6H, aromatics), 7.74 (s, 1H, NC(H)N backbone proton). <sup>13</sup>C NMR (C<sub>6</sub>D<sub>6</sub>, δ/ppm) 14.34 (FPhEt CH<sub>3</sub>), 24.24 (FPhEt CH<sub>2</sub>), 57.36 (O-CH<sub>2</sub> DME), 69.85 (O-CH<sub>3</sub> DME), 120.26, 124.86, 136.79, 150.02 (aromatic carbons), 162.52 (NCN backbone carbon). IR (Nujol, NaCl plates) 3157.7(m,br), 2257.3(w,shp), 2178.0(w,shp), 1910.8(w,shp), 1848.2(w), 1790.5(w,shp), 1743.1(w,shp), 1649.0(m,shp), 1587.8(m,shp), 1537.4(m), 1329.7(w,shp), 1254.0(w,shp), 1189.0(str,shp), 1102.7(w,shp), 1032.1(w,shp), 919.1(m,shp), 896.0(w,shp), 862.4(w,shp), 841.3(w,shp), 808.8(m), 757.1(str), 667.4(m,shp), 638.8(m,shp) cm<sup>-1</sup>.

**[Na(DippForm)(DME)<sub>2</sub>] (3.5).** HDippForm (1.04 g, 2.9 mmol) was dissolved in THF (20 mls), and a solution of NaN(SiMe<sub>3</sub>)<sub>2</sub> (2.9 mls, 2.9 mmol as 1M in THF) added drop-wise. The reaction mixture was dried to a powder and the residue extracted in DME (8 mls), concentrated *in vacuo* and cooled to -15 °C upon which colourless crystals were produced. Isolated Yield 1.30 g (80%), mp = 115-118 °C. <sup>1</sup>H NMR (C<sub>6</sub>D<sub>6</sub>, δ/ppm) 1.41 (d, 24H, Pr<sup>i</sup> CH<sub>3</sub>), 2.97 (s, 12H, O-CH<sub>3</sub> DME), 2.99 (s, 8H, O-CH<sub>2</sub> DME), 3.80 (sept, 4H, Pr<sup>i</sup> CHMe<sub>2</sub>), 7.10-7.27 (multiplet, 6H, aromatics), 7.85 (s, 1H, NC(H)N backbone proton). <sup>13</sup>C NMR (C<sub>6</sub>D<sub>6</sub>, δ/ppm) 23.28 (Pr<sup>i</sup> CH<sub>3</sub>), 26.78 (Pr<sup>i</sup> CH), 57.41 (O-CH<sub>2</sub> DME), 70.04 (O-CH<sub>3</sub> DME), 120.35, 121.75, 137.76, 141.28 (aromatic carbons), 162.26 (NCN, backbone carbon). IR (Nujol, NaCl plates) 3188.9(w,shp), 3055.6(w,shp), 2733.3(m,shp), 2600.0(w,shp), 1888.9(m,shp), 1838.9(m,shp), 1788.9(w,shp), 1738.9(w,shp), 1661.1(m,shp), 1588.9(m,shp), 1538.9(m,shp), 1322.2(w,shp), 1294.4(w,shp), 1244.4(m,shp), 1194.4(m,shp), 1111.1(m), 1066.7(w,shp), 1044.4(w,shp), 1022.2(m,shp), 983.3(m,shp), 933.3(m,shp), 855.6(str,shp), 794.4(m,shp), 755.6(str,shp), 722.2(w,shp) cm<sup>-1</sup>.

#### 3.4.4 Synthesis of Potassium Formamidinate Complexes in DME and THF

**[K<sub>3</sub>(FXyl)<sub>3</sub>(DME)<sub>3</sub>] (3.6).** HFXyl (1.02 g, 4 mmol) was dissolved in THF (20 mls), and a solution of KN(SiMe<sub>3</sub>)<sub>2</sub> (8.1 mls, 4 mmol as 0.5M in toluene) added drop-wise. The reaction mixture was dried to a powder and the residue extracted in DME (4 mls) cooled to -15 °C upon which colourless crystals were produced. Isolated Yield 1.24 g (81%), mp = 82-95 °C. <sup>1</sup>H NMR (C<sub>6</sub>D<sub>6</sub>, δ/ppm) 2.15 (s, 12H, FXyl CH<sub>3</sub>), 3.03 (s, 6H, O-CH<sub>3</sub> DME), 3.15 (s, 4H, O-CH<sub>2</sub> DME), 6.7 (multiplet, 2H, *p*-aromatics), 6.9 (m, 4H, *m*-aromatics), 7.45 (s, 1H, NC(H)N backbone proton). <sup>13</sup>C NMR (C<sub>6</sub>D<sub>6</sub>, δ/ppm) 57.33 (O-CH<sub>2</sub> DME), 70.73 (O-CH<sub>3</sub> DME). IR (Nujol, NaCl plates) 1897.1(m,shp), 1832.4(m,shp), 1774.5(m,shp), 1650.9(m,shp), 1247.9(str,shp), 1192.9(str), 1112.4(str,br), 1028.0(str,shp), 984.0(str,shp), 948.8(m,shp), 919.8(m,shp), 898.7(m,shp), 847.1(str,shp), 812.7(m,shp), 792.0(m,shp), 756.1(str,shp), 662.7(str,shp), 621.0(m,shp), 583.3(m,shp) cm<sup>-1</sup>.

**[{K(FPhEt)(HFPhEt).toluene}<sub>n</sub>] (3.7).** HFPhEt (1.02 g, 3.3 mmol) was dissolved in THF (20 mls), and a solution of KN(SiMe<sub>3</sub>)<sub>2</sub> (6.6 mls, 3.3 mmol as 0.5M in toluene) added drop-wise. The golden reaction mixture was left stirring overnight, filtered, concentrated *in vacuo* and cooled to -15 °C upon which colourless crystals were produced. Isolated Yield 0.92 g (43%), mp = 267 °C. <sup>1</sup>H NMR (D<sub>8</sub>-THF, δ/ppm) 1.15 (t, 24H, CH<sub>3</sub> ethyl), 2.65 (q, 16H, CH<sub>2</sub> ethyl), 5.0-6.6 (s, broad, 1H, NH), 6.75 (multiplet, 4H, *p*-aromatics), 6.91 (m, 8H, *m*-aromatics), 7.4 (s, 2H, NC(H)N backbone protons). <sup>13</sup>C NMR (D<sub>8</sub>-THF, δ/ppm) 15.59 (FPhEt CH<sub>3</sub>), 25.97 (FPhEt CH<sub>2</sub>), 126.53, (aromatic carbon). IR (Nujol, NaCl plates) 1627.0(m,shp), 1531.1(m), 1255.9(m,shp), 1190.0(str,shp), 1150.6(m,shp), 1101.3(m,shp), 1075.5(w,shp), 1030.7(w,shp), 959.6(m,shp), 918.1(str,shp), 870.1(m,shp), 786.5(w,shp), 757.7(str,shp), 728.0(str,shp), 694.3(str,shp), 662.0(m,shp) cm<sup>-1</sup>.

**[K(FPhEt)(HFPhEt)(THF)] (3.8).** HFPhEt (1.24 g, 4.0 mmol) was dissolved in THF (20 mls), and a solution of KN(SiMe<sub>3</sub>)<sub>2</sub> (4.0 mls, 2.0 mmol as 0.5M in toluene) added drop-wise. The reaction mixture was concentrated *in vacuo* and cooled to -15 °C upon which colourless crystals were produced. Isolated Yield 0.98 g (67%), mp = 250-260 °C. <sup>1</sup>H NMR (D<sub>8</sub>-THF, δ/ppm) 1.15 (t, 24H, CH<sub>3</sub> ethyl), 2.65 (q, 16H, CH<sub>2</sub> ethyl), 5.0-6.6 (s, broad, 1H, NH), 6.75 (multiplet, 4H, *p*-aromatics), 6.91 (m, 8H, *m*-aromatics), 7.4 (s, 2H, NC(H)N backbone protons). <sup>13</sup>C NMR (D<sub>8</sub>-THF, δ/ppm) 15.59 (FPhEt CH<sub>3</sub>), 25.97 (FPhEt CH<sub>2</sub>), 126.53, (aromatic carbon). IR (Nujol, NaCl plates) 3144.4(m,br), 2632.6(w), 2544.4(w,shp), 2344.4(w,shp), 2011.1(w,shp), 1900.0(w), 1838.9(w,shp), 1783.3(m,shp), 1622.2(m), 1366.7(str), 1344.4(str), 1250.0(str,shp), 1227.8(m,shp), 1188.9(str,shp), 1155.6(m,shp), 1100.0(m,shp), 1055.6(str,shp), 1016.7(m,shp), 988.9(w,shp), 911.1(str,shp), 866.7(m,shp), 788.9(str), 755.6(m,shp), 722.2(m,shp), 661.1(m,shp) cm<sup>-1</sup>.

**[K(DippForm)(DME)<sub>n</sub>] (3a).** HDippForm (1.182 g, 3.24 mmol) was dissolved in THF (20 mls), and a solution of KN(SiMe<sub>3</sub>)<sub>2</sub> (6.48 mls, 3.24 mmol as 0.5M in toluene) added drop-wise. The reaction mixture was dried to a powder and the residue extracted in DME (4 mls) cooled to -15 °C upon which colourless crystals were produced. Isolated Yield 0.841 g (53%), mp = 85 °C. <sup>1</sup>H NMR (C<sub>6</sub>D<sub>6</sub>, δ/ppm) 1.33 (d,



24H, Pr<sup>i</sup> CH<sub>3</sub>), 3.11 (s, 6H, O-CH<sub>3</sub> DME), 3.30 (s, 4H, O-CH<sub>2</sub> DME), 3.70 (sept, 4H, Pr<sup>i</sup> CHMe<sub>2</sub>), 7.07-7.28 (multiplet, 6H, aromatics), 7.85 (s, 1H, NC(H)N backbone proton). <sup>13</sup>C NMR (C<sub>6</sub>D<sub>6</sub>, δ/ppm) 24.77 (Pr<sup>i</sup> CH<sub>3</sub>), 28.53 (Pr<sup>i</sup> CH), 58.90 (O-CH<sub>2</sub> DME), 72.52 (O-CH<sub>3</sub> DME), 122.23, 123.42, 127.52, 142.79 (aromatic carbons), 161.48 (NCN, backbone carbon). IR (Nujol, NaCl plates) 2052.0(w,shp), 1892.4(w,shp), 1839.9(w,shp), 1733.0(w,shp), 1671.9(m,shp), 1594.4(str,shp), 1573.8(str), 1324.9(str), 1242.8(str), 1192.7(m,shp), 1112.9(m,br), 1030.3(m,shp), 934.5(m,shp), 912.8(m,shp), 857.7(str,shp), 820.3(w,shp), 798.0(str,shp), 753.3(str,shp), 721.3(w,shp), 670.0(w,shp) cm<sup>-1</sup>.

### 3.4.5 Synthesis of Lithium Formamidinate Complexes in TMEDA

**[Li(FXyl)(TMEDA)] (3.9).** HFXyl (1.05 g, 4.2 mmol) was dissolved in hexane (35 mls) and TMEDA (4 mls), and a solution of LiBu<sup>n</sup> (2.6 mls, 4.2 mmol as 1.6M in hexanes) added drop-wise. The reaction mixture was concentrated *in vacuo*, filtered giving a blue solution. This was slowly cooled to -15 °C upon which colourless crystals were produced. Isolated Yield 1.15 g (74%), mp = >355 °C. <sup>1</sup>H NMR (C<sub>6</sub>D<sub>6</sub>, δ/ppm) 1.73 (s, 4H, 2CH<sub>2</sub> TMEDA), 1.87 (s, 12H, 4CH<sub>3</sub> TMEDA), 2.34 (s, 12H, FXyl CH<sub>3</sub>), 6.92 (multiplet, 2H, *p*-aromatics), 7.16 (multiplet, 4H, *m*-aromatics), 7.74 (s, 1H, NC(H)N backbone proton). <sup>13</sup>C NMR (C<sub>6</sub>D<sub>6</sub>, δ/ppm) 20.28 (FXyl CH<sub>3</sub>), 45.52 (4CH<sub>3</sub> TMEDA), 56.65 (2CH<sub>2</sub> TMEDA), 121.79, 129.05, 132.26, 152.19 (aromatic carbons), 166.84 (NCN backbone carbon). IR (Nujol, NaCl plates) 1908.9(w,shp), 1888.1(w,shp), 1847.5(w,shp), 1776.1(w,shp), 1651.6(str,shp), 1600.2(m,shp), 1537.9(m,shp), 1293.9(m,shp), 1249.5(m,shp), 1199.5(m,br), 1112.8(str,br), 1030.8(str,shp), 981.4(m,shp), 940.7(m,shp), 893.7(w,shp), 869.3(m,shp), 824.6(w,shp), 791.9(w,shp), 759.0(str,shp), 733.5(m,shp) cm<sup>-1</sup>.

**[Li(FPhEt)(TMEDA)] (3.10).** HFPhEt (0.88 g, 2.9 mmol) was dissolved in hexane (30 mls) and TMEDA (0.9 mls, 5.8 mmol), and a solution of LiBu<sup>n</sup> (1.78 mls, 2.9 mmol as 1.6M in hexanes) added drop-wise. The reaction mixture was concentrated *in vacuo* and cooled to -15 °C upon which clear crystals were produced. Isolated Yield 0.83 g (68%), mp = 121-126 °C. <sup>1</sup>H NMR (C<sub>6</sub>D<sub>6</sub>, δ/ppm) 1.09 (broadened multiplet,

12H, CH<sub>3</sub> ethyl), 2.63 (broadened multiplet, 8H, CH<sub>2</sub> ethyl), 2.68 (s, 8H, O-CH<sub>2</sub> DME), 2.78 (s, 12H, O-CH<sub>3</sub> DME), 6.88-6.97 (multiplet, 6H, aromatics), 7.49 (s, 1H, NC(H)N backbone proton). IR (Nujol, NaCl plates) 2795.9(m,shp), 2720.9(w,shp), 1896.0(w,shp), 1833.4(w,shp), 1666.6(w,shp), 1596.4(m,shp), 1531.3(str,shp), 1291.3(str,shp), 1255.1(w,shp), 1194.9(str,shp), 1157.4(w,shp), 1129.3 (w,shp), 1100.0 (m,shp), 1066.1(w,shp), 1037.2(w,shp), 999.6(m,shp), 942.4(m,shp) 872.3(w,shp), 828.0(w,shp), 793.4(m,shp), 756.0(str,shp), 731.8(w,shp) cm<sup>-1</sup>.

**[Li(DippForm)(TMEDA)] (3.11).** HDippForm (1.02 g, 2.8 mmol) was dissolved in toluene (20 mls) and TMEDA (0.9 mls, 5.6 mmol), and a solution of LiBu<sup>n</sup> (1.8 mls, 2.8 mmol as 1.6M in hexanes) added drop-wise. The reaction mixture was concentrated *in vacuo* and cooled to -15 °C upon which clear crystals were produced. Isolated Yield 1.05 g (77%), mp = 240 °C (Decomp.). <sup>1</sup>H NMR (CDCl<sub>3</sub>, δ/ppm) 1.28 (d, 24H, Pr<sup>i</sup> CH<sub>3</sub>), 1.68 (s, 4H, 2CH<sub>2</sub> TMEDA), 1.89 (s, 12H, 4CH<sub>3</sub> TMEDA), 3.68 (sept, 4H, Pr<sup>i</sup> CHMe<sub>2</sub>), 7.01-7.19 (multiplet, 6H, aromatics), 7.88 (s, 1H, NC(H)N backbone proton). <sup>13</sup>C NMR (CDCl<sub>3</sub>, δ/ppm) 23.32 (Pr<sup>i</sup> CH<sub>3</sub>), 26.84 (Pr<sup>i</sup> CH), 43.73 (4CH<sub>3</sub> TMEDA), 54.96 (2CH<sub>2</sub> TMEDA), 120.51, 121.78, 141.20, 148.51 (aromatic carbons), 164.21 (NCN, backbone carbon). IR (Nujol, NaCl plates) 2718.2(w,shp), 2056.7(w,shp), 1925.4(m,shp), 1895.6(w,shp), 1860.4(w,shp), 1841.4(w,shp), 1796.5(w,shp), 1748.2(w,shp), 1731.9(w,shp), 1666.7(m,shp), 1651.6(w,shp), 1592.2(m,shp), 1537.8(w,shp), 1284.2(m,br), 1187.7(m), 1129.1(w,shp), 1096.9(str,shp), 1038.6(w,shp), 1017.3(w,shp), 937.7(str,shp), 898.1(w,shp), 882.7(w,shp), 800.9(m,shp), 756.5(m,shp) cm<sup>-1</sup>.

### 3.4.6 Synthesis of Lithium Formamidinate Complexes in PMDETA

**[Li(FXyl)(PMDETA)] (3.12).** HFXyl (0.93 g, 3.7 mmol) was dissolved in THF (20 mls) and PMDETA (3 mls), and a solution of LiBu<sup>n</sup> (2.3 mls, 3.7 mmol as 1.6M in hexanes) added drop-wise. The reaction mixture was concentrated *in vacuo*, filtered giving a pale blue solution. This was slowly cooled to -15 °C upon which pale blue translucent crystals were produced. Isolated Yield 1.31 g (82%), mp = 125-135 °C. <sup>1</sup>H NMR (C<sub>6</sub>D<sub>6</sub>, δ/ppm) 1.87 (s, 12H, 4CH<sub>3</sub> PMDETA), 2.02 (multiplet, 8H, 4CH<sub>2</sub>

PMDETA), 2.14 (s, 3H, CH<sub>3</sub> PMDETA), 2.38 (s, 12H, FXyl CH<sub>3</sub>), 6.90 (multiplet, 2H, *p*-aromatics), 7.15 (multiplet, 4H, *m*-aromatics), 7.78 (s, 1H, NC(H)N backbone proton). <sup>13</sup>C NMR (C<sub>6</sub>D<sub>6</sub>, δ/ppm) 19.02 (FXyl CH<sub>3</sub>), 42.86 (2CH<sub>2</sub> PMDETA), 44.43 (4CH<sub>3</sub> PMDETA), 53.85 (2CH<sub>2</sub> PMDETA), 56.46 (CH<sub>3</sub> PMDETA), 119.27, 127.46, 130.13, 152.83 (aromatic carbons), 162.63 (NCN backbone carbon). IR (Nujol, NaCl plates) 2016.0(w,shp), 1912.5(m,shp), 1883.5(w,shp), 1849.3(w,shp), 1821.7(w,shp), 1787.8(w,shp), 1761.9(w,shp), 1727.1(w,shp), 1648.5(w,shp), 1601.0(str,shp), 1548.6(str), 1330.8(m,shp), 1301.5(m,shp), 1250.0(str,shp), 1193.9(m), 1168.6(w,br), 1155.6(m,shp), 1112.0(m,shp), 1092.8(str,shp), 1060.0(w,shp), 1033.2(str), 999.5(w,shp), 982.9(m,shp), 932.2(m,shp), 920.8(w,shp), 903.4(m,shp), 821.6(w,shp), 788.5(w,shp), 768.0(m,shp), 755.1(m,shp), 729.9(w,shp), 670.1(w,shp), 591.4(w,shp) cm<sup>-1</sup>.

**[Li(FPhEt)(PMDETA)] (3.13).** HFPhEt (0.99 g, 3.2 mmol) was dissolved in THF (20 mls) and PMDETA (3 mls), and a solution of LiBu<sup>n</sup> (2.0 mls, 3.2 mmol as 1.6M in hexanes) added drop-wise. The reaction mixture was concentrated *in vacuo* and cooled to -15 °C upon which clear crystals were produced. Isolated Yield 1.16 g (74%), mp = 69-75 °C. <sup>1</sup>H NMR (C<sub>6</sub>D<sub>6</sub>, δ/ppm) 1.04 (broadened multiplet, 12H, CH<sub>3</sub> ethyl), 1.79 (multiplet, 8H, 4CH<sub>2</sub> PMDETA), 1.89 (s, 12H, 4CH<sub>3</sub> PMDETA), 2.05 (s, 3H, CH<sub>3</sub> PMDETA), 2.66 (broadened multiplet, 8H, CH<sub>2</sub> ethyl), 6.73-6.99 (multiplet, 6H, aromatics), 7.63 (s, 1H, NC(H)N backbone proton). <sup>13</sup>C NMR (C<sub>6</sub>D<sub>6</sub>, δ/ppm) 14.97 (FPhEt CH<sub>3</sub>), 24.28 (FPhEt CH<sub>2</sub>), 41.90 (2CH<sub>2</sub> PMDETA), 44.50 (4CH<sub>3</sub> PMDETA), 52.71 (2CH<sub>2</sub> PMDETA), 56.86 (CH<sub>3</sub> PMDETA), 119.23, 125.04, 136.33, 151.62 (aromatic carbons), 163.74 (NCN backbone carbon). IR (Nujol, NaCl plates) 3176.5(w,shp), 2493.6(w), 2363.0(w,shp), 1905.3(w,shp), 1885.3(w,shp), 1835.0(w,shp), 1784.8(w,shp), 1734.6(w,shp), 1654.3(str,shp), 1589.0(str,shp), 1538.8(str,shp), 1332.9(w), 1292.7(m,shp), 1262.6(m,shp), 1192.3(m,shp), 1147.1(m,shp), 1122.0(m,shp), 1096.9(m,shp), 1031.6(str,shp), 936.2(m,shp), 891.0(w,shp), 860.9(m,shp), 795.6(str), 755.4(m,shp), 720.3(w,shp) cm<sup>-1</sup>.

**[Li(DippForm)(PMDETA)] (3.14).** HDippForm (1.05 g, 2.9 mmol) was dissolved in THF (20 mls) and PMDETA (3 mls), and a solution of LiBu<sup>n</sup> (1.8 mls, 2.9 mmol as 1.6M in hexanes) added drop-wise. The reaction mixture was concentrated *in vacuo* and cooled to -15 °C upon which clear crystals were produced. Isolated Yield 1.05 g (67%), mp = 134-149 °C. <sup>1</sup>H NMR (C<sub>6</sub>D<sub>6</sub>, δ/ppm) 1.40 (d, 24H, Pr<sup>i</sup> CH<sub>3</sub>), 1.87 (multiplet, 8H, 4CH<sub>2</sub> PMDETA), 2.02 (s, 12H, 4CH<sub>3</sub> PMDETA), 2.09 (s, 3H, CH<sub>3</sub> PMDETA), 3.87 (sept, 4H, Pr<sup>i</sup> CHMe<sub>2</sub>), 7.14 (multiplet, 2H, *p*-aromatics), 7.31 (multiplet, 4H, *m*-aromatics), 7.97 (s, 1H, NC(H)N backbone proton). <sup>13</sup>C NMR (C<sub>6</sub>D<sub>6</sub>, δ/ppm) 23.83 (Pr<sup>i</sup> CH<sub>3</sub>), 26.50 (Pr<sup>i</sup> CH), 42.73 (2CH<sub>2</sub> PMDETA), 44.22 (4CH<sub>3</sub> PMDETA), 53.09 (2CH<sub>2</sub> PMDETA), 55.87 (CH<sub>3</sub> PMDETA), 120.16, 121.89, 141.29, 149.54 (aromatic carbons), 164.11 (NCN, backbone carbon). IR (Nujol, NaCl plates) 1897.3(m,shp), 1842.9(m,shp), 1787.4(w,shp), 1664.4(str,shp), 1596.0(str,shp), 1537.6(str), 1300.4(str), 1255.3(m,shp), 1228.2(m,shp), 1173.8(m,shp), 1098.8(m,shp), 1071.7(w,shp), 1054.1(w,shp), 1032.2(str), 989.7(m,shp), 935.3(str,shp), 916.9(m,shp), 896.8(w,shp), 818.6(w,shp), 800.4(str,shp), 790.2(w,shp), 778.3(w,shp), 765.9(w,shp), 755.7(str,shp), 721.7(w,shp), 671.6(w,shp) cm<sup>-1</sup>.

### 3.4.7 Synthesis of Sodium Formamidinate Complexes in TMEDA

**[Na(FXyl)(TMEDA)] (3b).** HFXyl (0.98 g, 3.9 mmol) was dissolved in toluene (20 mls) and TMEDA (1.17 mls, 7.8 mmol), and a solution of NaN(SiMe<sub>3</sub>)<sub>2</sub> (3.9 mls, 3.9 mmol as 1M in THF) added drop-wise. The golden reaction mixture was concentrated *in vacuo* and cooled to -15 °C upon which clear crystals were produced. Isolated Yield 1.34 g (89%), mp = 119-138 °C. <sup>1</sup>H NMR (CDCl<sub>3</sub>, δ/ppm) 1.72 (s, 4H, 2CH<sub>2</sub> TMEDA), 2.12 (s, 12H, 4CH<sub>3</sub> TMEDA), 2.16 (s, 12H, FXyl CH<sub>3</sub>), 6.99-7.03 (multiplet, 2H, *p*-aromatics), 7.10-7.16 (m, 4H, *m*-aromatics), 7.42 (s, 1H, NC(H)N backbone proton). <sup>13</sup>C NMR (CDCl<sub>3</sub>, δ/ppm) 20.14 (FXyl CH<sub>3</sub>), 44.17 (4CH<sub>3</sub> TMEDA), 55.91 (2CH<sub>2</sub> TMEDA), 120.02, 124.45, 128.05, 130.35 (aromatic carbons), 156.58 (NCN backbone carbon). IR (Nujol, NaCl plates) 2720.8(w,shp), 2022.4(m,shp), 1891.9(w,shp), 1870.4(w,shp), 1651.3(m,shp), 12499.2(m,shp), 1203.8(m,shp), 1155.6(w,shp), 1133.8(w,shp), 1091.0(m,shp), 1024.1(str),

981.9(m,shp), 946.8(str,shp), 906.6(m,shp), 817.7(str,shp), 793.9(m,shp), 757.7(m,shp), 728.8(m,shp), 695.6(str,shp), 667.9(m,shp), 583.6(m,shp)  $\text{cm}^{-1}$ .

### 3.4.8 Synthesis of Sodium Formamidinate Complexes in PMDETA

[Na(FXyl)(PMDETA)] (3.15). HFXyl (1.00 g, 4.0 mmol) was dissolved in THF (20 mls) and PMDETA (3 mls), and a solution of  $\text{NaN}(\text{SiMe}_3)_2$  (4.0 mls, 4.0 mmol as 1M in THF) added drop-wise. The reaction mixture was concentrated *in vacuo* and cooled to  $-15^\circ\text{C}$  upon which colourless crystals were produced. Isolated Yield 1.32 g (74%), mp =  $107\text{--}125^\circ\text{C}$ .  $^1\text{H}$  NMR ( $\text{C}_6\text{D}_6$ ,  $\delta/\text{ppm}$ ) 1.97 (s, 3H,  $\text{CH}_3$  PMDETA), 2.01 (multiplet, 8H,  $4\text{CH}_2$  PMDETA), 2.06 (s, 12H,  $4\text{CH}_3$  PMDETA), 2.50 (s, 12H, FXyl  $\text{CH}_3$ ), 6.98–7.01 (multiplet, 2H, *p*-aromatics), 7.23–7.30 (m, 4H, *m*-aromatics), 8.06 (s, 1H, NC(H)N backbone proton).  $^{13}\text{C}$  NMR ( $\text{C}_6\text{D}_6$ ,  $\delta/\text{ppm}$ ) 18.95 (FXyl  $\text{CH}_3$ ), 41.73 ( $2\text{CH}_2$  PMDETA), 44.07 ( $4\text{CH}_3$  PMDETA), 53.73 ( $2\text{CH}_2$  PMDETA), 56.04 ( $\text{CH}_3$  PMDETA), 118.62, 127.09, 129.69 (aromatic carbons), 162.63 (NCN backbone carbon). IR (Nujol, NaCl plates) 2764.7(w,shp), 1911.1(w,shp), 1838.9(w,shp), 1651.4(m,shp), 1589.7(w,shp), 1534.3(w,shp), 1261.0(m,br), 1149.4(w,shp), 1090.7(w,shp), 1030.8(str,shp), 932.5(w,shp), 893.8(w,shp), 789.1(m,shp)  $\text{cm}^{-1}$ .

[Na(FPhEt)(PMDETA)] (3c). HFPhEt (1.02 g, 3.3 mmol) was dissolved in THF (20 mls) and PMDETA (3 mls), and a solution of  $\text{NaN}(\text{SiMe}_3)_2$  (3.3 mls, 3.3 mmol as 1M in THF) added drop-wise. The reaction mixture was concentrated *in vacuo* and cooled to  $-15^\circ\text{C}$  upon which colourless crystals were produced. Isolated Yield 1.51 g (91%), mp =  $228^\circ\text{C}$  (decomp).  $^1\text{H}$  NMR ( $\text{C}_6\text{D}_6$ ,  $\delta/\text{ppm}$ ) 1.34 (t, 12H,  $\text{CH}_3$  ethyl), 2.13 (s, 12H,  $4\text{CH}_3$  PMDETA), 2.15 (s, 3H,  $\text{CH}_3$  PMDETA), 2.33 (multiplet, 8H,  $4\text{CH}_2$  PMDETA), 2.86 (q, 8H,  $\text{CH}_2$  ethyl), 7.05–7.22 (multiplet, 6H, aromatics), 7.65 (s, 1H, NC(H)N backbone proton).  $^{13}\text{C}$  NMR ( $\text{C}_6\text{D}_6$ ,  $\delta/\text{ppm}$ ) 14.39 (FPhEt  $\text{CH}_3$ ), 24.36 (FPhEt  $\text{CH}_2$ ), 41.91 ( $\text{CH}_3$  PMDETA), 44.60 ( $4\text{CH}_3$  PMDETA), 55.19 ( $2\text{CH}_2$  PMDETA), 56.87 ( $2\text{CH}_2$  PMDETA), 120.91, 126.44, 136.64, 139.49 (aromatic carbons), 145.01 (NCN backbone carbon). IR (Nujol, NaCl plates) 1912.4(m,br), 1891.8(w,shp), 1836.8(m,shp), 1785.8(m,shp), 1747.3(m,shp), 1657.3(str,shp), 1596.0(m,shp), 1537.5(str), 1305.2(m), 1253.3(m), 1184.4(m,shp), 1150.1(w,shp),

1100.4(m), 1061.8(m), 1031.9(m), 984.2(m,shp), 931.5(m,shp), 892.7(w,shp), 870.9(m,shp), 826.2(w,shp), 754.5(str), 728.7(w,shp)  $\text{cm}^{-1}$ .

**[Na(DippForm)(PMDETA)] (3.16).** HDippForm (1.01 g, 2.8 mmol) was dissolved in THF (20 mls) and PMDETA (3 mls), and a solution of  $\text{NaN}(\text{SiMe}_3)_2$  (2.8 mls, 2.8 mmol as 1M in THF) added drop-wise. The reaction mixture was concentrated *in vacuo* and cooled to  $-15\text{ }^\circ\text{C}$  upon which clear crystals were produced. Isolated Yield 1.00 g (64%), mp =  $179\text{ }^\circ\text{C}$  (decomp.).  $^1\text{H}$  NMR ( $\text{C}_6\text{D}_6$ ,  $\delta/\text{ppm}$ ) 1.41 (d, 24H,  $\text{Pr}^i\text{CH}_3$ ), 1.85 (multiplet, 8H,  $4\text{CH}_2$  PMDETA), 1.9 (s, 3H,  $\text{CH}_3$  PMDETA), 2.03 (s, 12H,  $4\text{CH}_3$  PMDETA), 3.90 (sept, 4H,  $\text{Pr}^i\text{CHMe}_2$ ), 7.10-7.31 (multiplet, 6H, aromatics), 7.95 (s, 1H,  $\text{NC(H)N}$  backbone proton).  $^{13}\text{C}$  NMR ( $\text{C}_6\text{D}_6$ ,  $\delta/\text{ppm}$ ) 25.24 ( $\text{Pr}^i\text{CH}_3$ ), 28.21 ( $\text{Pr}^i\text{CH}$ ), 43.49 ( $2\text{CH}_2$  PMDETA), 45.44 ( $4\text{CH}_3$  PMDETA), 54.68 ( $2\text{CH}_2$  PMDETA), 57.46 ( $\text{CH}_3$  PMDETA), 121.28, 123.28, 142.64, 152.18 (aromatic carbons), 164.71 ( $\text{NCN}$ , backbone carbon). IR (Nujol, NaCl plates) 2493.3(w,shp), 2353.8(w,shp), 2275.6(m,shp), 2055.8(w,shp), 1897.6(str,shp), 1841.8(str,shp), 1787.7(m,shp), 1741.9(m,shp), 1663.8(str,shp), 1594.3(m,shp), 1537.3(m,shp), 1355.7(m,shp), 1303.4(m), 1255.4(m,shp), 1176.9(m,shp), 1112.0(m), 1054.4(m,shp), 1033.1(m), 979.2(m,shp), 894.2(m,shp), 820.0(w,shp), 808.8(str,shp), 785.0(w,shp), 755.1(str,shp), 720.4(w,shp), 671.1(w,shp), 590.0(w,shp)  $\text{cm}^{-1}$ .

### 3.4.9 Synthesis of Potassium Formamidinate Complexes in TMEDA

**[K(FXyl)(TMEDA)] (3d).** HFXyl (0.95 g, 3.8 mmol) was dissolved in toluene (20 mls), and a solution of  $\text{KN}(\text{SiMe}_3)_2$  (7.53 mls, 3.8 mmol as 0.5M in toluene) added drop-wise. The reaction mixture was concentrated *in vacuo* and cooled to  $-15\text{ }^\circ\text{C}$  upon which clear crystals were produced. Isolated Yield 1.07 g (70%).  $^1\text{H}$  NMR ( $\text{C}_6\text{D}_6$ ,  $\delta/\text{ppm}$ ) 2.16 (s, 4H,  $2\text{CH}_2$  TMEDA), 2.20 (s, 12H, FXyl  $\text{CH}_3$ ), 2.39 (s, 12H,  $4\text{CH}_3$  TMEDA), 7.06 (multiplet, 2H, *p*-aromatics), 7.08 (m, 4H, *m*-aromatics), 7.46 (s, 1H,  $\text{NC(H)N}$  backbone proton).  $^{13}\text{C}$  NMR ( $\text{C}_6\text{D}_6$ ,  $\delta/\text{ppm}$ ) 18.34 (FXyl  $\text{CH}_3$ ), 44.69 ( $4\text{CH}_3$  TMEDA), 57.10 ( $2\text{CH}_2$  TMEDA), 121.51, 124.41, 127.37, 128.05 (aromatic carbons), 144.48 ( $\text{NCN}$  backbone carbon).

**[K(DippForm)<sub>2</sub>] (3e).** HDippForm (1.01 g, 2.8 mmol) was dissolved in toluene (20 mls) and TMEDA (0.84 mls/5.5 mmols), and a solution of KN(SiMe<sub>3</sub>)<sub>2</sub> (5.5 mls, 2.8 mmol as 0.5M in toluene) added drop-wise. The reaction mixture was concentrated *in vacuo* and cooled to -15 °C upon which colourless crystals were produced. Isolated Yield 0.58 g (27% based on K), mp = 196-202 °C. <sup>1</sup>H NMR (C<sub>6</sub>D<sub>6</sub>, δ/ppm) 1.24 (d, 24H, Pr<sup>i</sup> CH<sub>3</sub>), 3.53 (sept, 4H, Pr<sup>i</sup> CHMe<sub>2</sub>), 7.06-7.26 (multiplet, 6H, aromatics), 10.75 (s, 1H, NH). <sup>13</sup>C NMR (C<sub>6</sub>D<sub>6</sub>, δ/ppm) 22.47 (Pr<sup>i</sup> CH<sub>3</sub>), 27.05 (Pr<sup>i</sup> CH), 122.17, 124.54, 139.47, 142.56 (aromatic carbons), 154.04 (NCN, backbone carbon). IR (Nujol, NaCl plates) 1663.3(str,shp), 1587.7(m,shp), 1331.9(w,shp), 1286.9(str,shp), 1257.7(w,shp), 1234.0(w,shp), 1180.5(m,shp), 1098.6(w,shp), 1058.5(w,shp), 1000.3(w,shp), 935.6(w,shp), 821.0(w,shp), 799.7(m,shp), 767.6(w,shp), 753.4(m,shp), 722.2(w,shp) cm<sup>-1</sup>.

#### 3.4.10 Synthesis of Potassium Formamidinate Complexes in PMDETA

**[[K(FXyl)<sub>2</sub>K(PMDETA)]<sub>n</sub>] (3.17).** HFXyl (1.02 g, 4 mmol) was dissolved in THF (20 mls) and PMDETA (2 mls), and a solution of KN(SiMe<sub>3</sub>)<sub>2</sub> (8.1 mls, 4 mmol as 0.5M in toluene) added drop-wise. The reaction mixture was concentrated *in vacuo* and layered with hexane (2 mls) upon which colourless crystals were produced. Isolated Yield 1.33 g (87%), mp = 137-148 °C. <sup>1</sup>H NMR (C<sub>6</sub>D<sub>6</sub>, δ/ppm) 1.88 (s, 3H, CH<sub>3</sub> PMDETA), 1.99 (s, 12H, FXyl CH<sub>3</sub>), 2.01 (multiplet, 8H, 4CH<sub>2</sub> PMDETA), 2.27 (s, 12H, 4CH<sub>3</sub> PMDETA), 6.69 (multiplet, 2H, *p*-aromatics), 6.93 (m, 4H, *m*-aromatics), 7.38 (s, 1H, NC(H)N backbone proton). <sup>13</sup>C NMR (C<sub>6</sub>D<sub>6</sub>, δ/ppm) 19.06 (FXyl CH<sub>3</sub>), 40.16 (CH<sub>3</sub> PMDETA), 43.97 (4CH<sub>3</sub> PMDETA), 54.90 (2CH<sub>2</sub> PMDETA), 56.16 (2CH<sub>2</sub> PMDETA), 118.91, 124.09, 130.24, 136.67 (aromatic carbons), 154.92 (NCN backbone carbon). IR (Nujol, NaCl plates) 3500.0(w,shp), 2533.3(w,shp), 2366.7(w,shp), 2011.1(w,shp), 1911.1(w,shp), 1888.9(w,shp), 1861.1(w), 1822.2(w,shp), 1788.9(w,shp), 1722.2(w,shp), 1694.4(w,shp), 1650.0(str,shp), 1588.9(m), 1533.3(str,br), 1305.6(m,shp), 1238.9(str,shp), 1194.4(str,shp), 1166.7(m,shp), 1122.2(m), 1088.9(str,shp), 1027.8(str), 977.8(str,shp), 927.6(m,shp), 900.0(str,shp), 761.1(str), 722.2(w,shp), 661.1(m,shp) cm<sup>-1</sup>.

**[{K(FPhEt)<sub>2</sub>K(PMDETA)}<sub>n</sub>] (3.18).** HFPhEt (0.91 g, 3.0 mmol) was dissolved in THF (20 mls) and PMDETA (3 mls), and a solution of KN(SiMe<sub>3</sub>)<sub>2</sub> (5.9 mls, 3.0 mmol as 0.5M in toluene) added drop-wise. The reaction mixture was concentrated *in vacuo* and cooled to -15 °C upon which colourless crystals were produced. Isolated Yield 0.92 g (72%), mp = 84-102 °C. <sup>1</sup>H NMR (C<sub>6</sub>D<sub>6</sub>, δ/ppm) 1.40 (t, 24H, CH<sub>3</sub> ethyl), 1.82 (s, 3H, CH<sub>3</sub> PMDETA), 2.05 (s, 12H, 4CH<sub>3</sub> PMDETA), 2.20 (multiplet, 8H, 4CH<sub>2</sub> PMDETA), 2.92 (q, 16H, CH<sub>2</sub> ethyl), 6.95-7.22 (multiplet, 12H, aromatics), 7.87 (s, 2H, NC(H)N backbone protons). <sup>13</sup>C NMR (C<sub>6</sub>D<sub>6</sub>, δ/ppm) 14.40 (FPhEt CH<sub>3</sub>), 24.63 (FPhEt CH<sub>2</sub>), 41.04 (CH<sub>3</sub> PMDETA), 44.28 (4CH<sub>3</sub> PMDETA), 55.03 (2CH<sub>2</sub> PMDETA), 56.53 (2CH<sub>2</sub> PMDETA), 125.14, 126.45, 127.28, 128.05 (aromatic carbons), 153.88 (NCN backbone carbon). IR (Nujol, NaCl plates) 3503.3(w,shp), 3055.9(w,shp), 2350.4(w,shp), 1892.8(w,shp), 1860.2(w,shp), 1836.4(w,shp), 1649.6(m), 1592.2(str,shp), 1532.3(str,shp), 1495.6(w,shp), 1341.4(m,shp), 1308.1(w,shp), 1255.6(m,shp), 1227.7(m,shp), 1189.3(str,shp), 1162.7(w,shp), 1118.1(w,shp), 1102.9(m,shp), 1081.0(w,shp), 1032.1(str,shp), 965.7(w,shp), 947.3(w,shp), 931.6(w,shp), 910.8(m,shp), 860.8(m,shp), 810.8(str,shp), 787.0(str,shp), 757.5(str,shp), 730.6(str,shp), 695.0(str,shp), 673.4(w,shp) cm<sup>-1</sup>.

**[K(DippForm)(PMDETA)] (3.19).** HDippForm (1.03 g, 2.8 mmol) was dissolved in THF (20 mls) and PMDETA (3 mls), and a solution of KN(SiMe<sub>3</sub>)<sub>2</sub> (5.65 mls, 2.8 mmol as 0.5M in toluene) added drop-wise. The reaction mixture was concentrated *in vacuo* and cooled to -15 °C upon which colourless crystals were produced. Isolated Yield 1.51 g (93%), mp = 104-115 °C. <sup>1</sup>H NMR (D<sub>8</sub>-THF, δ/ppm) 1.16 (d, 24H, Pr<sup>i</sup> CH<sub>3</sub>), 2.04 (s, 12H, 4CH<sub>3</sub> PMDETA), 2.17 (s, 3H, CH<sub>3</sub> PMDETA), 2.33 (multiplet, 4H, 2CH<sub>2</sub> PMDETA), 2.44 (multiplet, 4H, 2CH<sub>2</sub> PMDETA), 3.50 (sept, 4H, Pr<sup>i</sup> CHMe<sub>2</sub>), 6.89-7.19 (multiplet, 6H, aromatics), 7.36 (s, 1H, NC(H)N backbone proton). <sup>13</sup>C NMR (D<sub>8</sub>-THF, δ/ppm) 20.57 (Pr<sup>i</sup> CH<sub>3</sub>), 24.70 (Pr<sup>i</sup> CH), 39.52 (CH<sub>3</sub> PMDETA), 42.42 (4CH<sub>3</sub> PMDETA), 53.57 (2CH<sub>2</sub> PMDETA), 55.03 (2CH<sub>2</sub> PMDETA), 119.37, 122.21, 125.07, 125.83 (aromatic carbons), 139.73 (NCN, backbone carbon). IR (Nujol, NaCl plates) 3502.9(w,shp), 2255.6(w), 1914.8(w,shp), 1787.0(w,shp), 1664.0(str,shp), 1592.4(str,shp), 1534.7(str), 1353.9(str),



1310.2(str,shp), 1257.4(m,shp), 1233.8(str,br), 1178.1(str,shp), 1129.2(m,shp), 1099.0(m,shp), 1079.9(w,shp), 1033.5(str), 932.7(m,shp), 914.5(m,shp), 898.1(w,shp), 838.3(w,shp), 803.8(str,shp), 772.6(str,shp), 760.5(str,shp), 728.1(m,shp), 694.1(w,shp)  $\text{cm}^{-1}$ .

#### 3.4.11 Synthesis of a Bimetallic Potassium-Lithium Formamidinate Complex in THF

**[{K(FPhEt)<sub>2</sub>Li(THF)<sub>2</sub>}]<sub>n</sub> (3.20).** HFPhEt (1.18 g, 3.8 mmol) was dissolved in THF (20 mls), and a solution of KN(SiMe<sub>3</sub>)<sub>2</sub> (3.8 mls, 1.9 mmol as 0.5M in toluene) added drop-wise. This was left stirring overnight before the addition of LiBu<sup>n</sup> (1.2 mls, 1.9 mmol as 1.6M in hexanes) added drop-wise. The reaction mixture concentrated *in vacuo* and cooled to -15 °C upon which colourless crystals were produced. Isolated Yield 1.11 g (72%), mp = 329-335 °C. <sup>1</sup>H NMR (D<sub>8</sub>-THF,  $\delta$ /ppm) 1.16 (t, 24H, CH<sub>3</sub> ethyl), 1.76 7(m, 8H, 2CH<sub>2</sub> THF), 2.65 (q, 16H, CH<sub>2</sub> ethyl), 3.61 (m, 8H, 2CH<sub>2</sub> THF), 6.80 (multiplet, 4H, *p*-aromatics), 6.93 (m, 8H, *m*-aromatics), 7.39 (s, 2H, NC(H)N backbone protons). <sup>13</sup>C NMR (D<sub>8</sub>-THF,  $\delta$ /ppm) 11.58 (FPhEt CH<sub>3</sub>), 21.84 (2CH<sub>2</sub> THF) 22.52 (FPhEt CH<sub>2</sub>), 64.350 (2CH<sub>2</sub> THF), 119.03 (ortho), 122.76 (meta), 134.58 (para), 144.93 (ipso aromatic carbon), 153.15 (NCN backbone carbon). IR (Nujol, NaCl plates) 2355.6(w,shp), 1920.2(w,shp), 1860.5(w,shp), 1801.0(w,shp), 1744.8(w,shp), 1661.1(m,shp), 1593.2(str,shp), 1228.1(m,shp), 1189.4(str), 1103.0(m,shp), 1072.3(str), 987.4(w,shp), 960.7(m,shp), 916.4(m), 865.8(m,shp), 811.8(m,shp), 788.8(m,shp), 756.9(m,shp), 728.6(str,shp), 694.5(m,shp), 671.1(str,shp)  $\text{cm}^{-1}$ .

#### 3.4.12 Synthesis of a Magnesium Formamidinate Complex in THF

**[Mg(FXyl)<sub>2</sub>(THF)] (3.21).** HFXyl (1.07 g, 4.2 mmol) was dissolved in THF (20 mls), and a solution of Mg(Bu)<sub>2</sub> (2.1 mls, 2.1 mmol as 1M in heptane) added drop-wise. The reaction mixture was filtered and concentrated. The filtrate was cooled to -15 °C upon which colourless crystals were produced. Isolated Yield 1.07 g (85%), mp = 259-274 °C. <sup>1</sup>H NMR (C<sub>6</sub>D<sub>6</sub>,  $\delta$ /ppm) 1.2 (m, 2CH<sub>2</sub> THF), 2.1 (s, 12H, FXyl CH<sub>3</sub>), 3.5

(m, 2CH<sub>2</sub> THF), 6.8-6.99 (multiplet, 2H, *para* and *meta* aromatic protons), 7.7 (s, 1H, NC(H)N backbone proton). <sup>13</sup>C NMR (C<sub>6</sub>D<sub>6</sub>, δ/ppm) 19.90 (FXyl CH<sub>3</sub>), 25.82 (2CH<sub>2</sub> THF), 69.04 (2CH<sub>2</sub> THF), 123.06, 129.71, 132.71, 148.46 (aromatic carbons), 168.97 (NCN backbone carbon). IR (Nujol, NaCl plates) 2727.4(m,shp), 1913.8(m,shp), 1842.4(m,shp), 1776.2(w,shp), 1651.7(w,shp), 1278.0(m), 1092.5(m,shp), 1026.4(m,shp), 981.7(w,shp), 954.9(w,shp), 916.9(w,shp), 885.3(w,shp), 769.1(m), 735.7(m,shp), 676.1(w,shp) cm<sup>-1</sup>.

### 3.4.13 Synthesis of Aluminium Formamidinate Complexes in THF

[AlCl(FPhEt)<sub>2</sub>] (3.22). HFPhEt (2.12 g, 6.9 mmol) was dissolved in THF (20 mls), and a solution of LiBu<sup>n</sup> (2.2 mls, 3.4 mmol as 1.6M in hexanes) added drop-wise. This was left stirring for two hours before being added drop-wise to a solution of AlCl<sub>3</sub> (0.458 g, 3.4 mmol) in THF (25 mls). The reaction mixture was concentrated *in vacuo* and cooled to -15 °C upon which colourless crystals were produced. Isolated Yield 0.99 g (42%), mp = 259-264 °C. <sup>1</sup>H NMR (C<sub>6</sub>D<sub>6</sub>, δ/ppm) 1.12 (t, 12H, 4CH<sub>3</sub> ethyl), 2.59 (q, 8H, CH<sub>2</sub> ethyl), 6.91-7.16 (multiplet, 6H, aromatics), 7.26 (s, 1H, NC(H)N backbone proton). <sup>13</sup>C NMR (C<sub>6</sub>D<sub>6</sub>, δ/ppm) 14.11 (FPhEt CH<sub>3</sub>), 23.71 (FPhEt CH<sub>2</sub>), 124.55, 125.01, 138.51, 139.35 (aromatic carbons), 168.49 (NCN backbone carbon). <sup>27</sup>Al NMR (C<sub>6</sub>D<sub>6</sub>, δ/ppm) 63.951. IR (Nujol, NaCl plates) 2302.7(w,br), 1933.8(w,shp), 1866.7(w,shp), 1800.0(w,shp), 1666.7(m,shp), 1644.5(m,shp), 1594.4(w,shp), 1548.4(m), 1322.2(m,shp), 1260.6(str,shp), 1209.5(str,shp), 1161.1(w,shp), 1105.6(w,shp), 1072.2(w,shp), 1033.3(w,shp), 1014.5(w,shp), 989.1(str,shp), 916.7(w,shp), 867.2(m,shp), 802.4(m,shp), 764.5(m,shp), 688.9(w,shp), 567.7(w,shp) cm<sup>-1</sup>.

[AlCl(DippForm)<sub>2</sub>] (3.23). HDippForm (2.00 g, 5.5 mmol) was dissolved in THF (20 mls), and a solution of LiBu<sup>n</sup> (1.7 mls, 2.7 mmol as 1.6M in hexanes) added drop-wise. This was left stirring for two hours before being added drop-wise to a solution of AlCl<sub>3</sub> (0.366 g, 2.7 mmol) in THF (25 mls). The reaction mixture was concentrated *in vacuo* and cooled to -15 °C upon which clear crystals were produced. Isolated Yield 0.956 g (44%), mp = 250-267 °C. <sup>1</sup>H NMR (C<sub>6</sub>D<sub>6</sub>, δ/ppm) 1.39 (d, 24H, Pr<sup>i</sup>

CH<sub>3</sub>), 3.58 (sept, 4H, Pr<sup>i</sup> CHMe<sub>2</sub>), 7.0-7.16 (multiplet, 6H, aromatics), 7.72 (s, 1H, NC(H)N backbone proton). <sup>13</sup>C NMR (C<sub>6</sub>D<sub>6</sub>, δ/ppm) 26.06 (Pr<sup>i</sup> CH<sub>3</sub>), 28.72 (Pr<sup>i</sup> CH), 124.16, 126.53, 139.55, 145.88 (aromatic carbons), 170.39 (NCN, backbone carbon). <sup>27</sup>Al NMR (C<sub>6</sub>D<sub>6</sub>, δ/ppm) 67.863 (5-coord Al found around 50ppm). IR (Nujol, NaCl plates) 1941.6(w,shp), 1865.9(w,shp), 1804.7(w,shp), 1666.0(str,shp), 1548.8(m,shp), 1325.7(m,shp), 1256.2(w,shp), 1738.9(w,shp), 1179.9(m,shp), 1072.6(str), 1003.0(m,shp), 977.5(m,shp), 914.4(str), 802.5(str,shp), 771.4(m,shp), 755.3(str,shp), 726.8(w,shp), 681.9(m,shp), 617.2(m,shp), 575.0(w,shp), 557.2(w,shp) cm<sup>-1</sup>.

#### 3.4.14 Synthesis of Indium Formamidinate and Formamidine Complexes in THF

[InCl<sub>3</sub>(HFXyl)<sub>2</sub>] (3.24). HFXyl (2.06 g, 8.2 mmol) was dissolved in THF (20 mls), and a solution of LiBu<sup>n</sup> (2.6 mls, 4.1 mmol as 1.6M in hexanes) added drop-wise. This was left stirring overnight before the drop-wise addition of InCl<sub>3</sub> (0.907 g, 4.1 mmol) slurry in THF (20 mls). The reaction mixture was filtered, leaving a white insoluble residue, concentrated *in vacuo* and cooled to -15 °C upon which red crystals were produced. Isolated Yield 0.86 g (29%), mp = 142 °C decomp). <sup>1</sup>H NMR (C<sub>6</sub>D<sub>6</sub>, δ/ppm) 1.80 (s, 12H, FXyl CH<sub>3</sub>), 6.59 (multiplet, 2H, *p*-aromatics), 6.84 (m, 4H, *m*-aromatics), 7.82 (s, 1H, NC(H)N backbone proton). <sup>13</sup>C NMR (C<sub>6</sub>D<sub>6</sub>, δ/ppm) 17.11 (FXyl CH<sub>3</sub>), 125.62, 126.65, 131.81, 133.56 (aromatic carbons), 155.53 (NCN backbone carbon). IR (Nujol, NaCl plates) 3340.8(m,shp), 3161.9(str,br), 1634.1(str,shp), 1587.8(m,shp), 1555.5(m), 1312.3(m,shp), 1250.4(m,shp), 1201.5(str,shp), 1162.6(w,shp), 1147.4(m,shp), 1071.6(str,shp), 1048.4(w,shp), 985.7(w,shp), 957.7(w,shp), 910.7(str), 821.7(w,shp), 783.7(m,shp), 771.8(m,shp), 759.7(str,shp), 714.3(w,shp), 662.1(w,shp), 620.5(w,shp) cm<sup>-1</sup>.

[InCl<sub>2</sub>(FPhEt)(HFPhEt)] (3.25). HFPhEt (2.24 g, 7.3 mmol) was dissolved in THF (20 mls), and a solution of LiBu<sup>n</sup> (2.3 mls, 3.6 mmol as 1.6M in hexanes) added drop-wise. This was left stirring overnight before the drop-wise addition of InCl<sub>3</sub> (0.803 g, 3.6 mmol) slurry in THF (20 mls). The reaction mixture was filtered, leaving a white insoluble residue, concentrated *in vacuo* and cooled to -15 °C upon which colourless

crystals were produced. Isolated Yield 0.78 g (26%), mp = 142 °C (decomp).  $^1\text{H}$  NMR ( $\text{C}_6\text{D}_6$ ,  $\delta/\text{ppm}$ ) 0.97 (t, 6H,  $2\text{CH}_3$  ethyl), 1.12 (t, 12H,  $4\text{CH}_3$  ethyl), 1.35 (t, 6H,  $2\text{CH}_3$  ethyl), 2.21 (q, 4H,  $\text{CH}_2$  ethyl), 2.74 (q, 8H,  $\text{CH}_2$  ethyl), 3.08 (q, 4H,  $\text{CH}_2$  ethyl), 6.68-7.16 (multiplet, 12H, aromatics), 7.29 (s, 1H, NC(H)N backbone proton), 7.84 (s, 1H, NC(H)N backbone proton).  $^{13}\text{C}$  NMR ( $\text{C}_6\text{D}_6$ ,  $\delta/\text{ppm}$ ) 13.62 (FPhEt  $\text{CH}_2$ ), 13.80 (FPhEt  $\text{CH}_2$ ), 13.99 (FPhEt  $\text{CH}_3$ ), 22.97 (FPhEt  $\text{CH}_3$ ), 23.69 (FPhEt  $\text{CH}_3$ ), 24.01 (FPhEt  $\text{CH}_3$ ), 124.396, 125.03, 125.25, 125.66, 132.47, 136.464, 138.304, 138.978, 139.898, 163.48, 163.92 (NCN backbone carbons). IR (Nujol, NaCl plates) 3331.7(m), 1634.3(str), 1586.3(m,shp), 1547.7(m,shp), 1310.2(m,shp), 1260.4(str,shp), 1192.0(w,shp), 1158.3(w,shp), 1020.4(str), 918.2(w,shp), 868.9(w,shp), 801.7(str), 677.5(w,shp)  $\text{cm}^{-1}$ .

### 3.5 References

- <sup>1</sup> R.W. Chamber, P.C. Scherer, *J. Am. Chem. Soc.*, **1926**, 48, 1054.
- <sup>2</sup> G. Brauer, *Handbook of Preparative Inorg. Chem.*, 2nd Ed., Vol 1, pg 464, Academic Press, **1963**.
- <sup>3</sup> G.W. Watt, W.C Fernelius, *J. Am. Chem. Soc.*, **1939**, 61, 1692.
- <sup>4</sup> D.D. Humphreys, *US Patent*, **1954**, 2,685,604.
- <sup>5</sup> P.C. Jones, *US Patent*, **1935**, 2,046,876.
- <sup>6</sup> U. Wannagat, H. Burger, M.E. Peach, K. Hensen, K.H. Lebert, *Z. Anorg. Chem.*, **1965**, 336, 129.
- <sup>7</sup> K. Ziegler, H. Eberle, H. Ohlinger, *Ann.*, **1933**, 504, 94.
- <sup>8</sup> D.H. Harris, M.F. Lappert, *J. Organomet. Chem.*, **1976**, 2, 13.
- <sup>9</sup> D.O. DePree, *US Patent*, **1957**, 2,799,705; *Chem. Abstr.*, **1958**, 52, 1202.
- <sup>10</sup> K. Ziegler, *Ger. Patent*, **1935**, 615,468; *Chem. Abstr.*, **1935**, 29, 6250.
- <sup>11</sup> M. Picon, *Compt. Rend.*, **1930**, 175C, 5267.
- <sup>12</sup> Deutsche Gold und Silber-Scheideanstalt, *Brit. Patent*, 293,040; *Chem. Abstr.*, **1929**, 23, 1418.
- <sup>13</sup> U. Wannagat, H. Niederprum, *Chem. Ber.*, **1961**, 94, 1540.
- <sup>14</sup> J.L. Atwood, *J. Organomet. Chem.*, **1978**, 157, 229.
- <sup>15</sup> Mulvey, *J. Chem. Soc., Chem. Comm.*, **1986**, 869.
- <sup>16</sup> R.E. Mulvey, *Chem Soc. Rev.*, **1991**, 20, 167.
- <sup>17</sup> N.D.R. Barnett, W. Clegg, L. Horsburgh, D.M. Lindsay, Q-Y. Liu, F.M. Mackenzie, R.E. Mulvey, P.G. Willard, *Chem Commun.*, **1996**, 2321.
- <sup>18</sup> H. Burger, H. Seyffert, *Angew. Chem. Int. Ed.*, **1964**, 3, 646.
- <sup>19</sup> M.H. Chisholm, M.W. Extine, *J. Am. Chem. Soc.*, **1975**, 97, 1623.
- <sup>20</sup> R.H. Neilson, R.L. Wells, *Inorg. Chem.*, **1974**, 13, 480.
- <sup>21</sup> W.H. Puterbaugh, C.R. Hauser, *J. Org. Chem.*, **1959**, 24, 416.
- <sup>22</sup> E.R. Biehl, S.M. Smith, P.C. Reeves, *J. Org. Chem.*, **1971**, 36, 1841.
- <sup>23</sup> M.F. Lappert, P.P. Power, A.R. Sanger, R.C. Srivastava, *Metal and Metalloid Amides*, Ellis Horwood Ltd., Chichester, England, **1980**.
- <sup>24</sup> F.W. Bergstrom, W.C. Fernelius, *Chem. Rev.*, **1937**, 20, 413.
- <sup>25</sup> H.G. Viehe, *Angew. Chem. Int. Ed.*, **1967**, 6, 767.
- <sup>26</sup> B. Martel, E. Aly, *J. Organomet. Chem.*, **1971**, 29, 61.

- 
- <sup>27</sup> B. Martel, J.M. Hiriart, *Tet. Let.*, **1971**, 2737.
- <sup>28</sup> A.A. Petrov, V.A. Kromer, *Zh. Obshch. Khim.*, **1964**, 34, 1868 & 3284.
- <sup>29</sup> K. Ruhlmann, G. Kuhrt, *Angew Chem. Int. Ed.*, **1968**, 7, 809.
- <sup>30</sup> C. Kruger, E.G. Rochow, U. Wannagat, *Chem. Ber.*, **1963**, 96, 2132.
- <sup>31</sup> G. Wittig, G. Haeusler, *Ann.*, **1971**, 746, 185.
- <sup>32</sup> M. Hammell, R. Levine, *J. Org. Chem.*, **1950**, 15, 162.
- <sup>33</sup> N. Wiberg, G. Fisher, H. Bachhuber, *Angew. Chem. Int. Ed.*, **1972**, 11, 829.
- <sup>34</sup> A.R. Sanger, *Inorg. Nucl. Chem. Let.*, **1973**, 9, 351.
- <sup>35</sup> A. Tzschach, E. Reiss, *J. Organomet. Chem.*, **1967**, 8, 255.
- <sup>36</sup> J.J. Sanderson, C.R. Hauser, *J. Am. Chem. Soc.*, **1949**, 71, 1595.
- <sup>37</sup> H. Jacobs, R. Juza, *Z. Anorg. Chem.*, **1970**, 370, 248 & 254.
- <sup>38</sup> N.A. Bell, *J. Chem. Soc. (A)*, **1966**, 542.
- <sup>39</sup> G.E. Coates, M.L.H. Green, K. Wade, *Organomet. Comp.*, Methuen, 1, II, **1967**.
- <sup>40</sup> H. Burger, C. Forker, J. Goubeau, *Monatsh.*, **1965**, 96, 597.
- <sup>41</sup> G.E. Coates, D. Ridley, *J. Chem. Soc. (A)*, **1967**, 56.
- <sup>42</sup> E. Lorz, R. Baltzly, *J. Am. Chem. Soc. (A)*, **1967**, 56.
- <sup>43</sup> C. Beis, *Compt. Rend.*, **1903**, 137C, 575.
- <sup>44</sup> N.A. Bell, G.E. Coates, *J. Chem. Soc. (A)*, **1966**, 1069.
- <sup>45</sup> A. Terent'ev, *Bull. Soc. Chim. Fr.*, **1924**, 35, 1164.
- <sup>46</sup> H. Gurien, *J. Org. Chem.*, **1963**, 28, 878.
- <sup>47</sup> G.E. Coates, M. Trarah, *J. Chem. Soc. (A)*, **1967**, 236.
- <sup>48</sup> G.E. Coates, A.H. Fishwick, *J. Chem. Soc. (A)*, **1967**, 1199.
- <sup>49</sup> G.E. Coates, P.D. Roberts, *J. Chem. Soc. (A)*, **1968**, 2651.
- <sup>50</sup> J.L. Atwood, G.D. Stucky, *J. Am. Chem. Soc.*, **1969**, 91, 4426.
- <sup>51</sup> V.R. Magnusson, G.D. Stucky, *Inorg. Chem.*, **1969**, 8, 1427.
- <sup>52</sup> A. Petyunin, *Russ. Chem. Rev.*, **1962**, 31, 100.
- <sup>53</sup> S. Birtwell, F.H.S. Curd, F.L. Rose, *J. Chem. Soc.*, **1949**, 2556.
- <sup>54</sup> R. Fetter, *Organomet. Chem. Rev. (A)*, **1968**, 3, 1.
- <sup>55</sup> W. Bergstrom, *J. Am. Chem. Soc.*, **1928**, 50, 652.
- <sup>56</sup> K. Niedenzu, J.W. Dawson, *Boron-Nitrogen Compounds*, Springer, Berlin, **1964**.
- <sup>57</sup> E. Wiberg, *Naturwiss.*, **1948**, 35, 182, 212.

- <sup>58</sup> G.E. Coates, M.L.H. Green, K. Wade, *Organomet. Comp.*, Meuthuen, London, 1, III, 1967.
- <sup>59</sup> M. Cohen, J.K. Gilbert, J.D. Smith, *J. Chem. Soc.*, 1965, 1092.
- <sup>60</sup> N. Davidson, H.C. Brown, *J. Am. Chem. Soc.*, 1942, 64, 316.
- <sup>61</sup> K. Gosling, J.D. Smith, D.H.W. Wharmby, *J. Chem. Soc. (A)*, 1969, 1738.
- <sup>62</sup> A.W. Laubengayer, J.D. Smith, G.G. Ehrlich, *J. Am. Chem. Soc.*, 1961, 83, 542.
- <sup>63</sup> J.K. Gilbert, J.D. Smith, *J. Chem. Soc. (A)*, 1968, 233.
- <sup>64</sup> E.C. Ashby, R.A. Kovar, *J. Organomet. Chem.*, 1970, 22, C34.
- <sup>65</sup> J.K. Ruff, *J. Am. Chem. Soc.*, 1961, 83, 2835.
- <sup>66</sup> J.K. Ruff, M.F. Hawthorne, *J. Am. Chem. Soc.*, 1960, 82, 2141.
- <sup>67</sup> E.C. Ashby, R.A. Kovar, *Inorg. Chem.*, 1971, 10, 893.
- <sup>68</sup> E. Wiberg, A. May, *Z. Naturforsch.*, 1955, 106, 234.
- <sup>69</sup> J.L. Atwood, G.D. Stucky, *J. Am. Chem. Soc.*, 1970, 92, 285.
- <sup>70</sup> W. Harris, A. Storr, J. Trotter, *J. Chem. Soc., Chem. Comm.*, 1971, 1101.
- <sup>71</sup> K.N. Semenko, E.B. Lobkowski, A.L. Dorosinskii, *J. Struct. Chem.*, 1972, 13, 696.
- <sup>72</sup> T.R.R. McDonald, W.S. McDonald, *Acta Cryst.*, 1972, B28, 1619.
- <sup>73</sup> K. Mertz, W. Schwartz, B. Eberwein, J. Weidlein, H. Hess, H.D. Hausen, *Z. Anorg. Chem.*, 1977, 429, 102.
- <sup>74</sup> S. Cucinella, T. Salvatori, C. Busetto, G. Perego, A. Mazzei, *J. Organomet. Chem.*, 1974, 78, 185.
- <sup>75</sup> G. Del Piero, M. Cesari, G. Perego, S. Cucinella, E. Cernia, *J. Organomet. Chem.*, 1977, 129, 289.
- <sup>76</sup> S. Cucinella, T. Salvatori, C. Busetto, A. Mazzei, *J. Organomet. Chem.*, 1976, 108, 13.
- <sup>77</sup> M. Wedler, F. Knösel, M. Noltemeyer, F.T. Edelmann, *J. Organomet. Chem.*, 1990, 388, 21.
- <sup>78</sup> R. Duchateau, C.T. van Wee, A. Meetsma, J.H. Teuben, *J. Am. Chem. Soc.*, 1993, 115, 4931.
- <sup>79</sup> F.A. Cotton, T. Inglis, M. Kilner, T.R. Webb, *Inorg. Chem.*, 1975, 14, 2023.
- <sup>80</sup> J. Barker, M. Kilner, *Coord. Chem. Rev.*, 1994, 133, 219.
- <sup>81</sup> I. Cragg-Hine, M.G. Davidson, F.S. Mair, P.R. Raithby, R. Snaith, *J. Chem. Soc., Dalton Trans.*, 1993, 2423.

- 
- <sup>82</sup> J.A.R. Schmidt, J. Arnold, *Chem. Comm.*, **1999**, 2149.
- <sup>83</sup> G.R. Giesbrecht, A. Shafir, J. Arnold, *J. Chem. Soc., Dalton Trans.*, **1999**, 3601.
- <sup>84</sup> M.L. Cole, P.C. Junk, L.M. Louis, *J. Chem. Soc., Dalton Trans.*, **2002**, 3906.
- <sup>85</sup> J. Baldmus, C. Berghof, M.L. Cole, D.J. Evans, E. Hey-Hawkins, P.C. Junk, *J. Chem. Soc., Dalton Trans.*, **2002**, 2802.
- <sup>86</sup> J. Baldmus, C. Berghof, M.L. Cole, D.J. Evans, E. Hey-Hawkins, P.C. Junk, *J. Chem. Soc., Dalton Trans.*, **2002**, 4185.
- <sup>87</sup> M.L. Cole, P.C. Junk, *J. Organomet. Chem.*, **2003**, 666, 55.
- <sup>88</sup> F.A. Cotton, S.C. Haefer, J.H. Matonic, X. Wang, C.A. Murillo, *Polyhedron*, **1997**, 16, 541.
- <sup>89</sup> M.L. Cole, D.J. Evans, P.C. Junk, L.M. Louis, *New. J. Chem.*, **2002**, 26, 1015.
- <sup>90</sup> A.R. Sadique, M.J. Heeg, C.H. Winter, *Inorg. Chem.*, **2001**, 40, 6349.
- <sup>91</sup> B. Srinvas, C.-C. Chang, C.-H. Chen, M.Y. Chiang, I.-T. Chen, Y. Wang, G.H. Lee, *J. Chem. Soc., Dalton Trans.*, **1997**, 957.
- <sup>92</sup> J.A.R. Schmidt, J. Arnold, *J. Chem. Soc., Dalton Trans.*, **2002**, 2890.
- <sup>93</sup> M.P. Coles, D.C. Swenson, R.F. Jordan, V.G. Young Jr., *Organomet.*, **1997**, 16, 5183.
- <sup>94</sup> M.P. Coles, S. Dagorne, A. Guzei, R.F. Jordan, *J. Am. Chem. Soc.*, **2000**, 122, 274.
- <sup>95</sup> G. Talarico, P.H.M. Budzelaar, *Organomet.*, **2000**, 19, 5691.
- <sup>96</sup> R. Duchateau, A. Meetsma, J.H. Teuben, *Chem. Commun.*, **1996**, 223.
- <sup>97</sup> S. Dagorne, R.F. Jordan, V.G. Young Jr., *Organomet.*, **1999**, 18, 4619.
- <sup>98</sup> J. Baker, N.C. Blacker, P.R. Phillips, N.W. Alcock, W. Errington, M.G.H. Wallbridge, *J. Chem. Soc., Dalton Trans.*, **1996**, 431.
- <sup>99</sup> M.P. Coles, D.C. Swenson, R.F. Jordan, *Organomet.*, **1997**, 16, 5183.
- <sup>100</sup> M.P. Coles, R.F. Jordan, *J. Am. Chem. Soc.*, **1997**, 119, 8125.
- <sup>101</sup> H.D. Hausen, F. Gerstner, W. Schwarz, *J. Organomet. Chem.*, **1978**, 145, 277.
- <sup>102</sup> Y. Zhou, D.S. Richeson, *Inorg. Chem.*, **1996**, 35, 1423.
- <sup>103</sup> S.L. Aeilts, M.P. Coles, D.C. Swenson, R.F. Jordan, *Organomet.*, **1998**, 17, 3265.
- <sup>104</sup> J. Barker, M. Kilner, *Coord. Chem. Rev.*, **1994**, 133, 219.
- <sup>105</sup> F.A. Cotton, L.M. Daniels, C.A. Murillo, *Inorg. Chem.*, **1993**, 32, 2881.
- <sup>106</sup> F.J. Lahoz, A. Tiripichio, M.T. Camellini, L.A. Oro, M.T. Pinillos, *J. Chem. Soc., Dalton Trans.*, **1985**, 1487.



- 
- <sup>107</sup> K. Gregory, P.vR. Schleyer, R. Snaith, *Adv. Inorg. Chem.*, **1991**, 47.
- <sup>108</sup> P.C. Andrews, D.R. Baker, R.E. Mulvey, W. Clegg, P.A. O'Neil, *Polyhedron*, **1991**, 10, 1839.
- <sup>109</sup> P.B. Hitchcock, M.F. Lappert, M. D-S Liu, *J. Organomet. Chem.*, **1995**, 488, 241.
- <sup>110</sup> P.B. Hitchcock, M.F. Lappert, M. Layh, *J. Chem. Soc., Dalton Trans.*, **1998**, 3113.
- <sup>111</sup> Value reported with reference to a survey of the Cambridge Crystallographic Database.
- <sup>112</sup> R. Lechler, H.-D. Hausen, J. Weidlein, *J. Organomet. Chem.*, **1989**, 359, 1.
- <sup>113</sup> M.L. Cole, P.C. Junk, *Unpublished Results*.
- <sup>114</sup> W. L. F. Armarego, D. D. Perrin, *Purification of Laboratory Chemicals*, Butterworth-Heinemann, Oxford, **1999**.
- <sup>115</sup> R. H. Blessing, *Acta Crystallogr., Sect. A*, **1995**, 51, 33.
- <sup>116</sup> G. M. Sheldrick, SHELXL-97 & SHELXS-97, University of Göttingen, Germany, **1997**.
- <sup>117</sup> L. J. Barbour, *X-Seed*, Crystallographic Interface, University of Missouri-Columbia, USA, **1999**.
- <sup>118</sup> POV-RAY, Ray Tracing Program, [www.povray.org](http://www.povray.org).
- <sup>119</sup> R.M. Roberts, *J. Org. Chem.*, **1949**, 14, 277.

## Appendix

### Publications in Support of this Thesis

- (i) Synthesis and characteristics of the first carbene-thallium complexes: Molecular structure of  $[\text{TlCl}_3\{\text{CN}(\text{Mes})\text{C}_2\text{H}_2\text{N}(\text{Mes})\}]$ , Mes =  $\text{C}_6\text{H}_2\text{Me}_{3-2,4,6}$ , Marcus L. Cole, Aaron J. Davies and Cameron Jones, *J. Chem. Soc., Dalton Trans.*, **2001**, 2451.
- (ii) Structural and spectroscopic studies of carbene and N-donor ligand complexes of group 13 hydrides and halides, Robert J. Baker, Aaron J. Davies, Cameron Jones and Marc Kloth, *J. Organomet. Chem.*, **2002**, 656, 203.
- (iii) Lithium and sodium *N,N'*-di(2,6-dialkylphenyl)formamidinate complexes: A study of the perturbation of amidinate binding with increasing steric bulk, Marcus L. Cole, Aaron J. Davies, Cameron Jones and Peter. C. Junk, *J. Organomet. Chem.*, in press.

### Oral Presentations in Support of this Thesis

- (iv) "Aryl Ring Allyl Coupling Reactions Mediated by Gallium (I) Iodide", Monash University, Melbourne, Australia, August 2002.
- (v) "Synthesis of Group 1 and 13 metal Formamidinate Complexes", Cardiff University, February 2003.

### Conference Paper in Support of this Thesis

- (vi) "Synthesis of Group 1 and 13 metal Formamidinate Complexes", Cardiff University, March 2003 and Bristol University, April 2003.

